URL. : http://ijrar.com **ISSN 2349 - 5138** **E - ISSN 2348 - 1269**

An open Access, peer reviewed, refereed, online and print research journal

International Journal of Research and Analytical Reviews

UGC Approved Research Journal

Periodicity - Quarterly

Atman Publishing Academy

International Journal of Research and Analytical Reviews
Atman Publishing Academy
2061-C/2/B, Nr. Adhyatma Vidya Mandir, Sanskar Mandal, Bhavnagar-364002.
Contact : 9427903033 E mail : **editorsijrar@gmail.com**, **ijrar1@gmail.com**

International Journal of Research and Analytical Reviews

ijrar.com

© IJRAR - All rights reserved. Reproduction in any form is strictly prohibited.
This work is licenced under Creative Commons International Licence Attribution 4.0 E-version.

Rs. 900

Subscription	1 year	2 years	5 years
Individual	3,000	6,000	15,000
Institutional	4,000	8,000	40,000
Advertisement	1000/Black	3000/colour	Per Page

Send your Paper(s)/Article(s) and Contact us on any one of following

E mail: (1) editorsijrar@gmail.com (2) ijrar1@gmail.com (3) drrbjoshi@ijrar.com

Contect No.: +91 9427903033

---

1. Thoughts, language vision and example in published research paper are entirely of author of research paper. It is not necessary that both editor and editorial board are satisfied by the research paper. The responsibility of the matter of research paper/article is entirely of author.
2. Editing of the IJRAR is processed without any remittance. The selection and publication is done after recommendations of at least two subject expert referees.
3. In any condition if any National/International University denies accepting the research paper/article published in IJRAR, than it is not the responsibility of Editor, Publisher and Management.
4. Only the first author is entitle to receive the copies of all co-author.
5. Before re-use of published research paper in any manner, it is compulsory to take written permission from the Editor – IJRAR, unless it will be assumed as disobedience of copyright rules.
6. All the legal undertakings related to IJRAR is subject to Bhavnagar Jurisdiction.

Editor

International Journal of Research and Analytical Reviews

Atman Publishing Academy

2061-C/2/B, Nr. Adhyatma Vidya Mandir, Sanskar Mandal, Bhavnagar-364002.

Contact : 9427903033 E mail : **editorsijrar@gmail.com**, **ijrar1@gmail.com**

URL. : http://ijrar.com **ISSN 2349-5138** **E-ISSN 2348-1269**

An open Access, peer reviewed, refereed, online and print research journal

Editor in chief

Dr. R. B. Joshi

Senior Advisory Board

Dr. H. O. Joshi Retd. Prof. & Head, Department of Education, Saurashtra University, Rajkot, Gujarat.	**Dr. Bhavesh Joshi** Associate Professor College of Food Processing Technology & Bioenergy, Agricultural University, Anand – 388110, Gujarat	**Vasantkumar Pathak** Director, Pathak Group of Schools & College, Rajkot.

Editorial Board

Prof. (Dr.) Ami Upadhyay Director, Department of Humanities And Social Sciences, Dr. Babasaheb Ambedkar Uni. A'Bad.	**Dr. Awa Shukla** Asst. Professor & Director, Social Sciences Dept. Babasaheb Ambedkar Open University, Ahmedabad.	**Dr. Dushyant Nimavat** Associate Professor Department of English, Gujarat Uniersity, Gujarat, India
Dr. A. Heidari Faculty of Chemistry California South University (CSU) Irvine, California, **U. S. A.**	**Dr. Bharat Ramanuj** Professor & Head, Department of Education, Saurashtra University, Rajkot.	**Dr. Nahla Mohammed Abd El-Aziz** Assistant professor - Entomolog Department, Faculty of Science Cairo University, **Egypt.**
Dr. Manahar Thaker Principal G. H. Sanghavi college of Education, Bhavnagar, Gujarat.	**Dr. K. S. Meenakshisundaram** Director, C. A. A., Great Lakes Institute of Management, Chennai	**Dr. J. D. Dave** I/c Principal P.D. Malviya Graduate Teachers' College, Rajkot, Gujarat.
Dr. M. B. Gaijan Associate Professor, Shamaldas Arts College, Bhavnagar.	**Dr. A. K. Lodi** H.O.D. Faculty of Education, Integral University, Lucknow(UP)	**Dr. Trupti Pathak** Assistant Vice Precident(Tech.) Claris life Sciences, Ahmedabad. Gujarat.
Dr. K. Ramadevi Associate Professor Department of Civil Engineering Kumaraguru College of Technology, Coimbatore, Tamilnadu.	**Dr. Jayant Vyas** Professor & Head, Department of Education, M. K. Bhavnagar University, Bhavnagar	**Dr. Dilip D. Bhatt** Associate Prof. & Head, Department of English, V. D. K. Arts college, Savarkundla, Gujarat.
K. S. Dave Lecturer J. H. Bhalodia Women's College Rajkot, Gujarat.	**Dr. Anil Ambasana** Retd. Prof. & Head, Department of Education, Saurashtra University, Rajkot. Gujarat.	**Dr. Sandeep R. Sirsat** Associate Professor & Head, Department of Computer Science, Shri Shivaji Science & Arts College, Chikhli, Dist: Buldana (M.S.-India)

International Journal of Research and Analytical Reviews

URL. : http://ijrar.com **ISSN 2349-5138** **E-ISSN 2348-1269**

An open Access, peer reviewed, refereed, online and print research journal

Review Committee

Editor & Head of Review Committee

Dr. S. Chelliah
Professor & Head,
Dept. of English and Comparative Literature,
Madurai Kamraj University, Madurai-21, **India.**

Mr. Zeeshan Shah Senior Lecturer, Department of Multimedia and Communication, University College of Bahrain, **Kingdom of Bahrain**.	**Dr. Samira Shahbazi** Plant Protection & Biotechnology Research Group, Nuclear Agricultural Research School, Nuclear Science & Technology Research Institute (NSTRI), **Iran**	**Dr. Belal Mahmoud Al-Wadi** Lecturer, University of Dammam (Saudi Arabia), Founder & Vice President of the Jordanian Society for Business Entrepreneurship **(Jordan)**
Harish Mahuvakar Associate Professor & Head, Dept. of English, Sir P. P. Institute of Science, Bhavnagar, Gujarat, **India.**	**Dr. Mainu Devi** Assistant Professor (Sr. Grade) in Zoology, Diphu Govt. college, Karbi Anglong – Assam **India.**	**Asim Gokhan YETGIN** Assistant Professor, Faculty of Engineering, Dumlupinar University, Kutahya**,** **Turkey.**
Dr. A. Kusuma Assistant Professor, Department of Social Work, Vikramasimhapuri University, Nellore.(AP)	**Prof. Rajeshkumar N. Joshi** I/C Dean, Faculty of Arts & Humanities, C. U. Shah University, Gujarat, **India.**	**Sunita. B. Nimavat** Assistant Professor of English, N.P.College of Computer & Mgt., Kadi (North Gujarat).
Nahla Mohammed Abdelazez Assisstant Professor Faculty of Science, Cairo University, Giza Governorate, **Egypt.**	**Dr. Riyad Awad** Associate professor, Structural Engineering, An - Najah National University, Nablus, **Palestine.**	**Dr. Amer A. Taqa** Professor Dept. of Dental Basic Science, College of Dentistry, Mosul University, Masul, **Iraq.**

International Journal of Research and Analytical Reviews

Vol. 6 / I - 4 Jan. 2019

Contents

1	**Synthesis, Characterization and Antimicrobial studies of poly N-tert-amyl acrylamide (NTA) and 7-acryloyloxy-4-methylcoumarin (ACU) Copolymers** P.Vimala	01 - 06
2	**Adsorptive Removal of Cu (II) Using graft copolymer of Cellulose Nano Crystals (CNCs) extracted from banana fiber with butyl acrylate monomer** K.Rani, K. Sangeetha & P.N.Sudha	07 – 17
3	**SYNTHESIS, CHARACTERISATION AND ANTIBACTERIAL ACTIVITY OF Ni(II), Zn(II) COMPLEXES OF TETRADENTATE SCHIFF BASE LIGAND** K. DEEPA & RANGASWAMY VENKATESH	18 – 25
4	**NOVEL SYNTHESIS OFHYDROXYAPATITE NANOPARTICLESBY USING HYDROTHERMAL COUPLED SHOCK WAVE METHOD** I. Venda, V. Thamizharasi, E. Sathya & V. Collins Arun Prakash	26 – 30
5	**SYNTHESIS, CHARACTERIZATION AND ANTIMICROBIAL STUDIES OF POLY N-TERT-AMYLACRYLAMIDE (NTA) AND (PA) COPOLYMERS** P. Vimala	31 – 36
6	**STUDY OF INHIBITION OF MILD STEEL CORROSION IN MINERAL ACID BY AQUEOUS EXTRACT OF PISONIA ALBA** N. Sridevi & S. Rani	37 – 47
7	**GREEN SYNTHESIS OF ZINC OXIDE NANOPARTICLES USING PEEL EXTRACT OF CARICA PAPAYA AND THEIR BIOLOGICAL ACTIVITY** M.Bharathi, S.Shree devi & CT. Ravichandran	48 – 56
8	**Hydrothermal assisted synthesis of Graphene oxide doped Nickel oxide – a material for supercapacitor** G. Manikandan[1,2] , H.A. Arjun[1] & N. Saradhadevi[1,3]	57 – 68
9	**A Study on Synthesis and Characterization of garnet based solid electrolytes for Batteries applications** Leo Edward M & Jaisankar V	69 – 73
10	**The First Recyclable, Eco-benign Liquid Resin Mediated Synthesis of Hantzsch 1, 4 Dihyropyridines, 1, 8-Dioxodecahydroacridine and polyhydroquinolines derivatives** K. Venkatapthy, G. Lavanya, C. J. Magesh, P. Amudha & S. Prema	74 – 85
11	**SYNTHESIS AND CHARACTERIZATION OF HYDROGEL BEADS BY USING SODIUM ALGINATE** Bhavani Perumal, CT.Ravichandran, G. Saranya & Bama Perumal	86 – 92
12	**DNA binding and biological activity of cobalt(III) complex containing 2, 2'-bipyridyl and Schiff base** S. Dhakshanamoorthy, N. Sri Gayathrai Devi, M. Murali Krishnan & M.N. Arumugham	93 – 102
13	**Adsorption, biosorption and discolouration on tannery effluents using Ferrous chloride and Ferric chloride Nano particles by using rose petal extract form collected near tannery industry** E. Revathi, A. Thaminum Ansari, S. Ulaganathan & CT. Ravichandran	103 – 107

14	**Adsorption, biosorption and discolouration on Vat dye effluents using Ferrous chloride and Ferric chloride Nano particles by using rose petal extract form collected near textile dye industry** S. Ulaganathan, A. Thaminum Ansari, E. Revathi & CT. Ravichandran	108 – 112
15	**ELECTROCHEMICAL DETERMINATION OF CEFTRIAXONE ON GRAPHENE OXIDE MODIFIED GLASSY CARBON ELECTRODE USING DIFFERENTIAL PULSE VOLTAMMETRY** K. Boobalan, S. Nithya, S. Shreedevi & CT Ravichandran	113 – 120
16	**MICROWAVE-ASSISTED SYNTHESIS OF HETEROCYCLIC COMPOUNDS BINDING WITH CHALCONE NUCLUES CONTAINING THIAZOLE MOIETY** R. SUMATHI	121 - 126

NATIONAL SEMINAR ON

RECENT ADVANCES IN CHEMICAL SCIENCES

(RACS – 2018)

5th & 6th September 2018

Organized by

PG & RESEARCH DEPARTMENT OF CHEMISTRY

ARIGNAR ANNA GOVERNMENT ARTS COLLEGE

CHEYYAR - 604 407, THIRUVANNAMALAI DISTRICT

TAMILNADU, INDIA.

Website: www.aagaccheyyar.com

National Seminar on

RECENT ADVANCES IN CHEMICAL SCIENCES

(RACS – 2018)

5th & 6th September 2018

ORGANIZING COMMITTEE

Chief Patron

Dr. G. Ezhilan
Principal
Arignar Anna Govt. Arts College
Cheyyar - 604 407

Organizing Secretary

Dr. CT. RAVICHANDRAN
Associate Professor & Head
Department of Chemistry
Arignar Anna Govt. Arts College
Cheyyar – 604 407
Email id : *ctrchem@yahoo.com*

Committee Members

Dr. S. Rani
Dr. S. Sreedevi
Dr. C. J. Magesh
Prof. D. Parthiban
Dr. K. Rajesh
Dr. N. Senthilkumar
Dr. P. Bhavani
Dr. N. Saradha Devi

International Journal of Research and Analytical Reviews

Special Issue : (RACS – 2018)

Organized by

PG & RESEARCH DEPARTMENT OF CHEMISTRY
ARIGNAR ANNA GOVERNMENT ARTS COLLEGE
CHEYYAR - 604 407, THIRUVANNAMALAI DISTRICT
TAMILNADU, INDIA.
Website: www.aagaccheyyar.com

Synthesis, Characterization and Antimicrobial studies of poly N-tert-amyl acrylamide (NTA) and 7-acryloyloxy-4-methylcoumarin (ACU) Copolymers

P.Vimala
Assistant Professor of chemistry, Muthurangam Govt. Arts College (Autonomous), Vellore, India

ABSTRACT: *Copolymers of N-tert-amyl acrylamide (NTA) and copolymerized with 7-acryloyloxy-4-methylcoumarin (ACU). Copolymers of N-tert-amyl acrylamide (NTA) and 7-acryloyloxy-4-methylcoumarin (ACU) were prepared by free radical polymerization in DMF at 60^{0}C using AIBN as an initiator. (Scheme 1)*
The copolymer composition were determined by 1H-NMR analysis. The reactivity ratios of monomers were determined by Fineman-Ross (FR) (r1 = 0.58 and r_2 = 1.11), Kelen-Tudos (KT) (r1 = 0.58and r_2 = 1.11). The $r_1.r_2$ = 0.64 indicated the formation of random copolymers.T_g found to increasing feed content of ACU. The antimicrobial studies showed that the copolymers are active against both Bacteria and Fungi.

Keywords: *N-tert-amyl acrylamide, 7-acryloyloxy-4-methylcoumarin (ACU) reactivity ratios, copolymer composition.*

Introduction

The determination of copolymer composition and reactivity ratios of the monomers is important in evaluating the specific application of copolymer[1]. The monomer reactivity ratios determined by conventional linearization methods are not always accurate and several non-linear methods have been attempted to determine their [2-4]. [1] H-NMR spectroscopic analysis has been established as a powerful tool for the estimation of copolymer composition[5, 6]. Knowledge of the copolymer composition is an important step in the evaluation of its utility. Copolymer composition and monomer distribution in the copolymer are dependent on the reactivity ratios. The most common mathematical model of copolymerization is based on finding the relationship between the composition of copolymers and the composition of the monomer feed in which the monomer reactivity ratios are the parameters to be determined[7]. The accurate estimation of copolymer composition and determination of monomer reactivity ratios are significant for tailor-made copolymers with required physical and chemical properties and in evaluating the specific and application of the copolymers. The present article reports the synthesis and characterization of copolymers of N-tert-amyl acrylamide with 7-acryloyloxy-4-methylcoumarin.

The synthesis of antimicrobial polymers is one of the leading frontiers of research in polymer science. With this view our work N-tert-amyl acrylamide was copolymerized with 7-acryloyloxy-4-methylcoumarin with different feed ratio were prepared and characterized by **^{1}H-NMR** spectroscopy. The reactivity ratios of monomers were determined by Fineman-Ross (FR), Kelen-Tudos (KT) methods. The r_1 - r_2 value indicates the formation of random copolymers.

Experimental

Preparation of N-tert-amyl acrylamide (NTA)

The monomer N-tert-amyl acrylamide was prepared by the reaction of tert-amyl alcohol with acrylonitrile. N-tert-amyl acrylamide was recrystallized in warm dry benzene. The white crystals have amp.91° C (Lit.91-92° C) and the yield was -87%. The monomer was confirmed by both 1H- NMR and ^{13C}-NMR.

Copolymerization of NTA and ACU

Copolymers of N-tert-amyl acrylamide (NTA) and 7-acryloyloxy-4-methylcoumarin (ACU) were prepared by free radical polymerization in DMF at 60°C using AIBN as initiator (scheme-1).

Characterization of copolymer spectra of Poly (NTA-co-ACU)

The ^{1}H-NMR spectrum of copolymers, poly (NTA-co-ACU) is shown in Figure1. The following peaks appear in the copolymer spectra : at 1.14 -2.96 ppm for CH_3, CH_2, of ACU group, at 3.08 ppm for backbone CH_2 , at 6.8-7.8 ppm due to ACU aromatic protons and 8.1 ppm for NH proton.

Determination of copolymer composition of Poly (NTA-co-ACU)

The copolymer composition was determined by ^{1}H-NMR spectral analysis of the copolymer. The Coumarin acrylate area is used to determine the copolymer composition. Resonance signal at 7.0-7.8 ppm

corresponds to aromatic proton, and their integrated intensity of this peak is compared to the total intensities of all the peaks in the copolymer spectrum, which is a measure of their relative areas.
The copolymer compositions can be obtained using

$$X_{ACU} = \frac{15A(aryl)}{3A\ total + 5A(aryl)} \quad \text{— — — — — —} \quad (1)$$

Where X= mole fraction and A= peak area.

Determination of Reactivity ratios

The value of r_1 is less than 1 and r_2 is greater than 1 indicates the formation of random copolymers. The r1. r_2 = 0 .64 which is closer to unity than zero confirms that the sequence of both monomeric units in copolymer. The monomer reactivity ratios of monomer 1 (NTA) and monomer 2 (ACU) were estimated by the methods of Fineman-Ross (FR) (Figure 2), Kelen-Tudos(KT) (Figure 3) . The significant parameters of F-R and K-T and equation are presented in Table-2.The reactivity ratios for NTA (r_1) and ACU (r_2) are given in Table-3 are at random in nature.

Thermal studies of Poly (NTA-co-ACU)

TGA curves could be seen from the Figure 4, have three stage decomposition regions for Poly (NTA-co-ACU). The initial weight loss is due to moisture content. Weight loss at stage 2 is associated with the dehydration of partially degraded amide groups; Maximum weight loss occurs at stage 3 around 300-400˚C indicates the main chain degradation and degradation of the polymer backbone. When the concentration of ACU is higher, stability of the polymer is found to be more. The T_g values of copolymers are higher than homo polymer of NTA.

Antimicrobial Activity of Poly (NTA-co-ACU)

The prepared polymers were tested against the various fungi and bacteria. DMSO was used as solvent control. Ciprofloxacin was used as reference antibacterial agent. Amphotericin B was used as reference antifungal agent. The tests were carried out in triplicates and the plates are shown in Figure 6. The Zone of inhibition values are presented in Table 5 and 6. From the table it is noticed that the increase in the mole fraction of NTA the activity is also increases. The copolymers are more active against E.coli and staphylococcus aureus Bacillus cereus. For antifungal studies, these copolymers are active against Aspergillus flavus, Aspergillus niger .
At higher feed composition of ACU showed higher zone of inhibition than the standard drug.

Scheme 1: Copolymerization of NTA and ACU

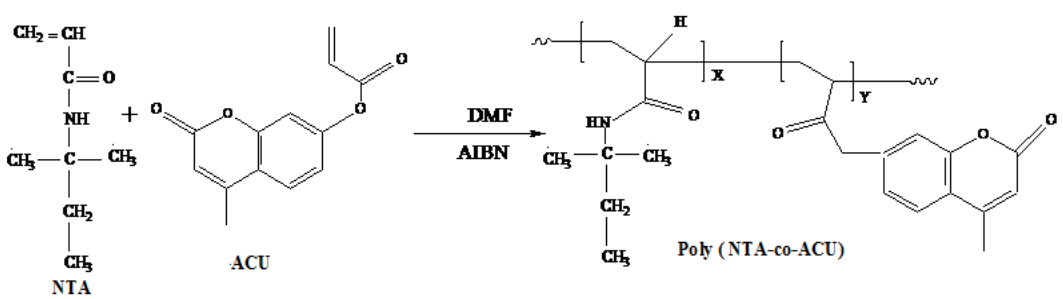

Figure 1:^{1}H-NMR spectrum of poly (NTA-co- ACU) (a) 0.5:0.5

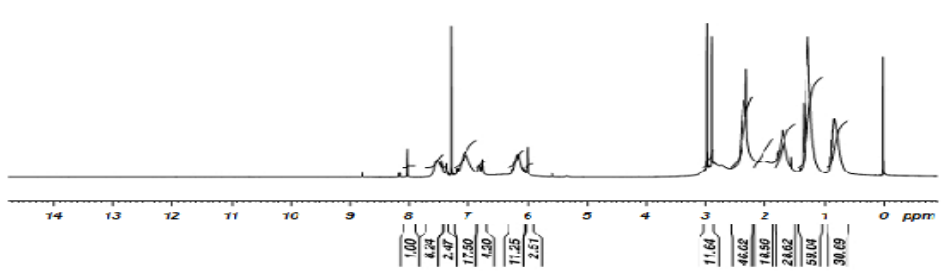

Figure 2: Fineman-Ross plot for Poly (NTA-co-ACU)

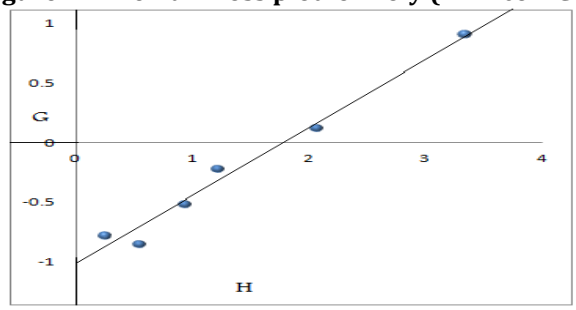

Figure 3: Kelen-Tudos plot for Poly (NTA-co-ACU)

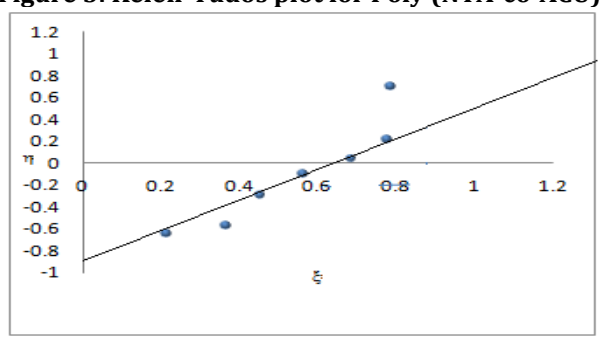

Table 1: Mole fractions of the copolymers of N-tert-amyl acrylamide (NTA) and 7-acryloyloxy-4-methylcoumarin (ACU)

Mole fraction of NTA in feed , M_1	Mole fraction of ACU in feed M_2	Mole fraction of NTA in copolymer, m_1	Mole fraction of ACU in copolymer , m_2	$F=M_1/M_2$	$f=m_1/m_2$
0.2	0.8	0.1949	0.8051	0.250	0.2421
0.3	0.7	0.2500	0.7500	0.427	0.3333
0.4	0.6	0.3600	0.6400	0.667	0.5625
0.5	0.5	0.4520	0.5501	1.000	0.8182
0.6	0.4	0.5215	0.4800	1.500	1.0865
0.7	0.3	0.6200	0.3803	2.333	1.316
0.8	0.2	0.8200	0.1800	4.000	4.5556

Table 2: Fineman-Ross and Kelen – Tudos parameters for the Copolymers of NTA and ACU

$G = F(f-1)/f$	$H=F^2/f$	$\eta=G/(\alpha+H)$	$\xi=H/(\alpha+H)$
-0.7831	0.2583	-0.6460	0.2131
-0.8581	0.5522	-0.5698	0.3666
-0.5188	0.7909	-0.2973	0.4533
-0.2222	1.2222	-0.1021	0.5616
0.1194	2.0709	0.0395	0.6846
0.9031	3.3359	0.2105	0.7776
3.12	3.5100	0.6989	0.7863

$\alpha = \sqrt{H_{min} \, . H_{max}} = 1.5754$

Table 3 : Reactivity ratios of NTA (r_1) and ACU (r_2)

Methods	r_1	r_2	$r_1.r_2$
Fineman-Ross (FR)	0.58	1.11	0.64
Kelen-Tudos (KT)	0.58	1.11	0.64

Table 4: TGA data for Poly (NTA-co-ACU)

Copolymer	Mole fraction of NTA in feed	Mole fraction of ACU, in feed	Mole fraction of ACU,in copolymer	IDT (°C)	T_{50} (°C)	T_f (°C)	T_g (°C)
NTA-ACU	0.70	0.30	0.2500	230	320	580	120
NTA-ACU	0.50	0.50	0.4200	250	320	610	111
NTA-ACU	0.30	0.70	0.6010	270	345	640	150
Poly-NTA		-	-	-	-		86.2

IDT: Initial Decomposition Temperature
T_{50} : decomposition temperature at 50% weight loss
T_f : final decomposition temperature
T_g : glass transition temperature

Table 5: Anti-bacterial activity of Poly (NTA-co-ACU)

S.No	Copolymers	Escherichia coli (mm) A	Staphylococcus aureus (mm) B	Bacillus Cereus (mm) C
1	0.3 NTA : 0.7 ACU	22	12	No zone
2	0.5 NTA : 0.5 ACU	20	12	No zone
3	0.7 NTA : 0.3 ACU	14	No zone	No zone
4	Ciprofloxacin	21	24	No zone

Table 6: Anti-fungal activity of Poly (NTA-co-ACU)

S.No	Copolymers	Aspergillus niger (mm) A	Aspergillus Flavus (mm) B	Candida albicans (mm) C
1	0.3 NTA : 0.7 ACU	24	26	15
2	0.5 NTA : 0.5 ACU	24	26	15
3	0.7 NTA : 0.3 ACU	13	13	6
4	Amphotericin B	12	12	13

Figure 4: Comparison of Zone of inhibition of Poly (NTA-co- ACU) with bacteria.

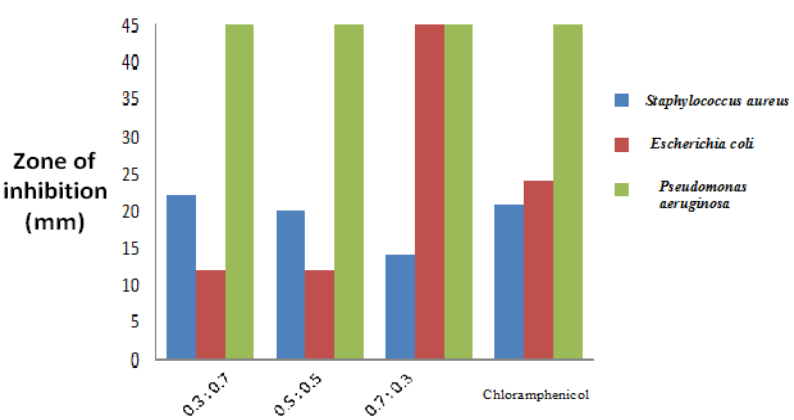

Figure 5: Comparison of Zone of inhibition of Poly (NTA-co-ACU) with fungi

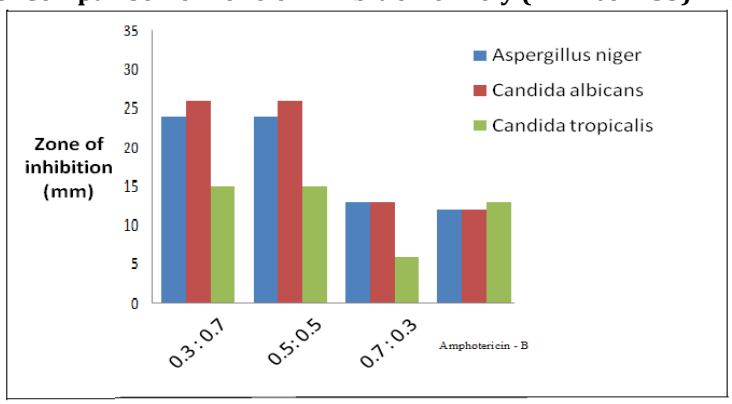

Figure 6: Antimicrobial studies of Poly (NTA-co-ACU)

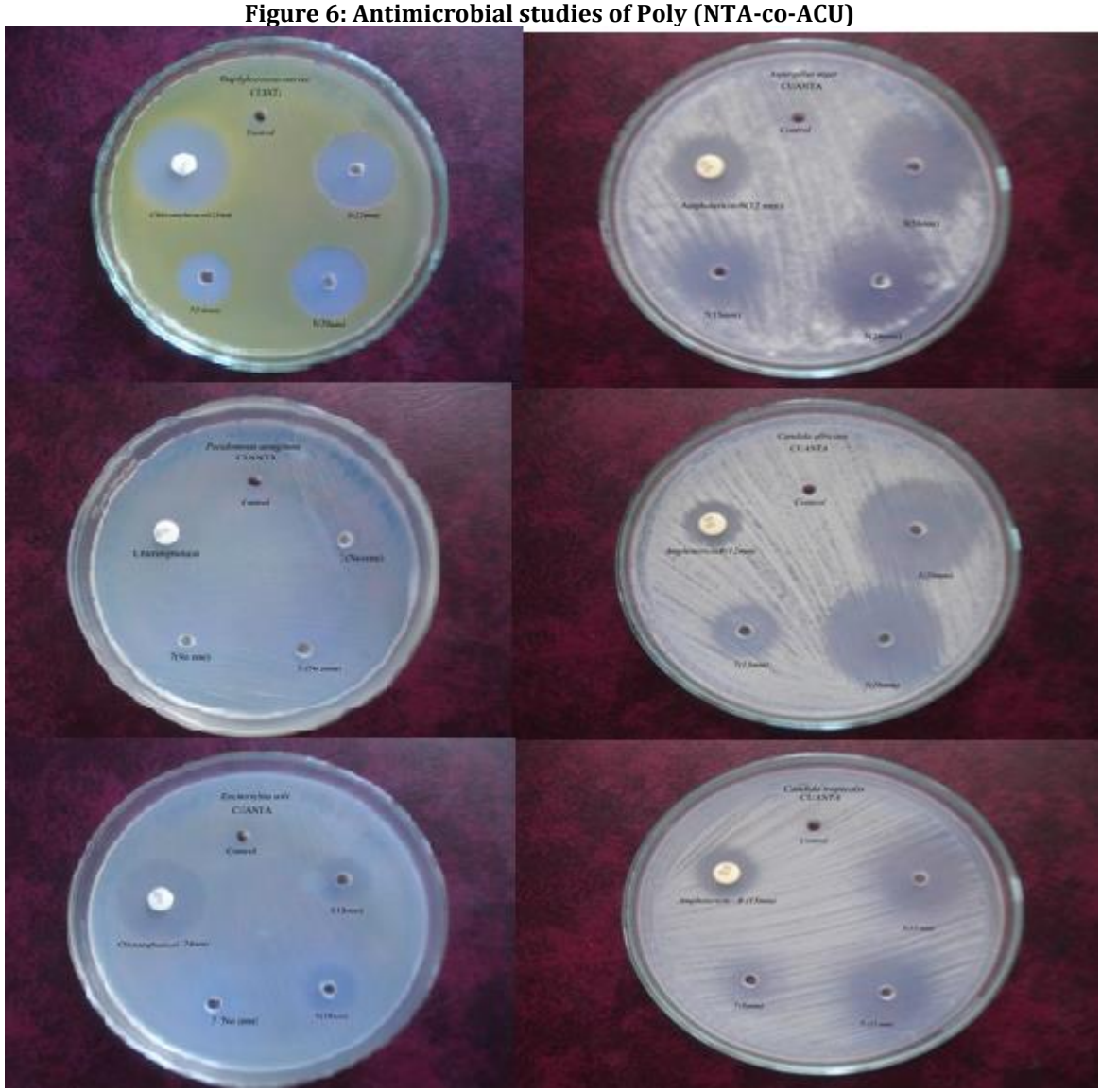

REFERENCES

1. S.pitchumani, B.S.Rami Reddy and C. Rajadurai, Journal of Polymer Science: Polymer Chemistry Edition, 20,277(1982).
2. M. Dube, R.A. Sanayei, A. Penlids, K.F. O' Driscoll and P.M. Reilly, Journal of Polymer Science, 29, 703(1991).
3. A. L. Polic, T.A Duever and A. Penlidis, Journal of Polymer Science Part A: PolymerChemistry, 36, 813 (1998).
4. C. Hagiopol, O. Frangu and L. Dumitru, Journal of Macromolecular Science Chemistry Edition, 26, 1363 (1989).
5. P. Pazhanisamy , M. Ariff and Q. Anwaruddin , Journal of Macromolecular Science: Pure and Applied Chemistry, 34, 1045 (1997).
6. P. Pazhanisamy, P. Sulochana, Q. Anwaruddin and M. Ariff, Journal of Polymer Science PartA: Polymer Chemistry, 35, 193 (1997).
7. R. Arshady, G. W. Kenner and A. W. Led, Journal of Polymer Science Polymer Chemistry Edition, 12 (9), 2017 (1974)

Adsorptive Removal of Cu (II) Using graft copolymer of Cellulose Nano Crystals (CNCs) extracted from banana fiber with butyl acrylate monomer

K.Rani[1], K. Sangeetha[2] & P.N.Sudha[3]
[1, 2, 3]Biomaterials Research Lab, Department of Chemistry,
DKM College for Women (Autonomous), Vellore, India

ABSTRACT: *The extraction of Cellulose Nano Crystals (CNCs) from banana fiber was done initially using steam explosion method. Extracted CNCs grafted with butyl acrylate monomer and ceric ammonium nitrate as initiator, was used. The prepared graft copolymer was used as adsorbent for the removal of Cu (II) from the aqueous solution.To evaluate the adsorption potential of the synthesized composite, the parameters such as pH, adsorbent dosage, contact time and initial Cu (II) ion concentration were investigated. From the observed results, it was evident that the adsorption of metal ions increased with the increase in contact time and adsorbent dosage. The optimum pH was found to be 5.0 for the removal of Cu (II) for CNCs-g-butyl acrylate copolymer. The adsorption isotherms of Cu (II) could be described very well by Freundlich model and the kinetic results revealed that pseudo second order kinetics shows a better fit. The characterization studies were carried out using FTIR and SEM-EDAX.*

Keywords: *Cellulose Nano Crystals (CNCs), Butyl acrylate, FT-IR, SEM-EDAX, Adsorption isotherm.*

1. INTRODUCTION

Water pollution caused due to addition of heavy metals resulting from the industrial activities is increasing tremendously and continues to be a great concern worldwide. As these heavy metals are non-biodegradable and will persistent in the environment may cause serious health problems such as brain damage, heart, kidney, and liver damage and various neurological malfunctions [1]. Some of the common toxic metals discharged from industrial wastewater include nickel, chromium, lead, cadmium, copper and so on. Among these heavy metals, copper causes serious hazards to living organisms as they enter the food chain and may accumulate in the human body. If copper is ingested beyond the permitted concentration, they can cause serious health disorders. Hence it is necessary to remediate this heavy metal copper from industrial wastewater to convert them to potable form.

There is a lot of existing data in the literature for removing heavy metals from industrial wastewaters. Common methods such as chemical precipitation, ion-exchange, membrane filtration, electrochemical technologies etc. were employed for removing various heavy metal ions from wastewater or aqueous solution [2, 3]. However, these methods are very expensive and very difficult to afford in small-scale industrial concerns. Among the various available techniques for water and wastewater treatment for heavy metal removal, adsorption is considered as the most attractive technique as it was of low cost, simple design and ease of operation [4].

Cellulose, a principal constituent in natural fibres is composed of β-(1, 4)-d-glucose polymeric chain units in a linear manner [5]. Native form of cellulose is semi-crystalline in nature i.e. comprised of crystalline and amorphous regions. This amorphous part in cellulose was vulnerable to acid attack and releases individual short monocrystalline nano-sized "Cellulose Nano Crystals (CNCs)" [6].

Cellulose Nano Crystals have gained substantial consideration for the role of an innovative material due to its significant characteristics like rod shape, tunable surface chemistry, high mechanical strength and sustainable nature [7]. As this nano-sized cellulose possesses high aspect ratio and numerous reactive hydroxyl groups which allow for easier chemical modifications. Graft polymerization was proven to be a robust approach through which physical and chemical properties of cellulose Nano Crystals can be tailored [8]. Grafting of polymer chains can be performed by several different methods, either by "grafting from", "grafting to" or "grafting through" [9].

In the present work the extracted cellulose Nano Crystals from banana fibre by steam explosion method was grafted with butyl acrylate monomer and the end product was used to remove heavy metal copper from aqueous solution. The adsorption capacity and efficiency of the grafted cellulose Nano Crystals

were investigated by varying the parameters such as adsorbent dose, contact time, pH and initial metal ion concentration. The data's obtained were interpreted and discussed below.

2. MATERIALS AND METHODS

2.1 MATERIALS

The materials used for the study includes banana fibers (collected from local farms), NaOH (commercial grade), acetic acid (commercial grade), sodium hypochlorite (commercial grade), oxalic acid (commercial grade). Analytical grade butyl acrylate, Ceric ammonium nitrate were used.

2.2 Preparation of Steam Exploded Banana Fibers. (Stage-1)

30 gms of Banana fibers were chopped into uniform size of approximately 10 cm. The fibers were treated with 2% NaOH (fiber to liquor ratio 1:10) in an autoclave and kept under 20 lb. pressure for a period of 1h. Pressure was released immediately. The fibers were removed from the autoclave, and the fibers were washed in water till they were rid of alkali. The washed fibers were allowed to drain off free flowing water.

2.3 Preparation of Steam Exploded Bleached Banana Fibers. (Stage-2)

The steam exploded fibers were bleached using a mixture of NaOH and acetic acid (27 and 78.8 g, respectively) and a mixture of 1:3 sodium hypochlorite solution. The bleaching was repeated six times. After bleaching, the fibers were thoroughly washed in distilled water and dried.

2.4 Preparation of Steam Exploded Fibers in Acidic Medium. (Stage-3)

The steam exploded bleached fibers were treated with oxalic acid (9%) in an autoclave till it attained a pressure of 20 lb. The pressure was released immediately. The autoclave was again set to reach a pressure of 20 lb., and the fibers were kept under that pressure for 15 min. The pressure was released and the process repeated 8 times. The fibers were taken out, washed till the washings no longer decolorized $KMnO_4$ solution to make sure that the washings were free from acid.

2.5 Mechanical Treatment of the Processed Banana Fibers (Stage-4)

The fibers were suspended in water and under continuous stirring with a mechanical stirrer of type RQ – 1.27 A and 8000 R.P.M. for 4 h. The suspension was kept in an oven at 90°C till it was dry.

Stage-1 **Stage-2** **Stage-3** **Stage-4**

Photograph of steam exploded banana fibers at various stages

2.6 Preparation of grafted co-polymer

A required amount of cellulose (0.5g) was dispersed in water (100ml) with constant stirring forming a homogeneous solution. 1mL of butyl acrylate monomer dissolved in 10 ml of ethanol was then added to that homogenous solution. To initiate the polymerization process, the initiator ceric ammonium nitrate (10 ml) was added.

After all the addition was over the above mixture was heated to 70°C simultaneously the stirring of that mixture was performed using a magnetic stirrer. This solution was then poured into excess sodium hydroxide solution to precipitate the graft copolymer. It was then filtered, dried and weighed.

2.7 Adsorption Experiment

Batch adsorption process was implemented to examine the applicability of CNCs-g-Butyl acrylate grafted copolymer for the uptake of Cu(II) from aqueous solution by varying different parameters such as pH, adsorbent dose, contact time and initial metal ion concentration. The Copper(II) solution (200mg/L) was initially prepared by dissolving 0.7858g of Copper Sulphate in 1000ml of deionised water. The metal ion adsorption experiments was carried out by soaking 1g of CNCs-g-Butyl acrylate copolymer in 100 ml of the above prepared specified Copper(II) solution (200mg/L). The adjustment of the initial pH of the sample solutions was accomplished with 2N HCl and 2NNaOH. This solution mixture was then equilibrated in

orbital shaker at a speed of 200 rpm for about 60 minutes at 30ºC. After the shaking process is over, the solution mixture was filtered using Whattmann filter paper and the supernatant was taken for AAS analysis of metal ion concentration. A similar procedure was carried out by varying the adsorbent dose, pH and time of contact. The metal ion removal percentage (%) and the adsorption capacity (mg/g) was calculated based on the following equations

$$Removal\ (\%) = \frac{\text{Initial metal conc} - \text{Final metal conc}}{\text{Initial metal conc}} \times 100$$

$$\text{Adsorption Capacity (qe)} = \frac{Co - Ce \times V}{\text{m}}$$

Where Ce (mg/L) is the liquid phase concentrations of metal ion at equilibrium, C_o (mg/L) is the initial concentration of the metal ion in solution, V is the volume of the solution (L) and m is the mass of dry adsorbent (g).

2.8. Desorption or Regeneration studies

Regeneration of the adsorbent from the Copper(II) ions loaded grafted copolymer is very important factor for adsorption process. The desorption of Copper(II) ions was conducted by the following process;For adsorption 1g of CNCs-g-BA was added to 100ml of Cu(II) solution (200mg/L) at room temperature and pH – 5 in a conical flask. The adsorption process was carried out for one hour. Afterwards, the metal loaded adsorbent was treated with 100ml of 0.1N HCl and 0.1M EDTA as desorbing agents. This solution mixture was then equilibrated in orbital shaker at a speed of 200 rpm for about 60 minutes, 120minutes and 180 minutes at 30ºC. After the shaking process is over, the solution mixture was filtered using Whattmann filter paper and the supernatant was taken for AAS analysis. Desorption ratio was calculated from the amount of metal ions adsorbed and the final metal ion concentration in desorption medium.

$$Desorption\ Ratio = \frac{Amount\ of\ metal\ ions\ desorbed}{\text{Amount of metal ions adsorbed}} \times 100$$

3. Results and Discussion

3.1 BATCH ADSORPTION STUDIES

3.1.1 EFFECT OF pH

The pH of a solution is an important factor affecting metal ions removal. The effect of pH Copper(II) ions using Cellulose Nano Crystals-g-n-butyl acrylate was investigated in the pH range 4-9 shows in **Fig-1.**

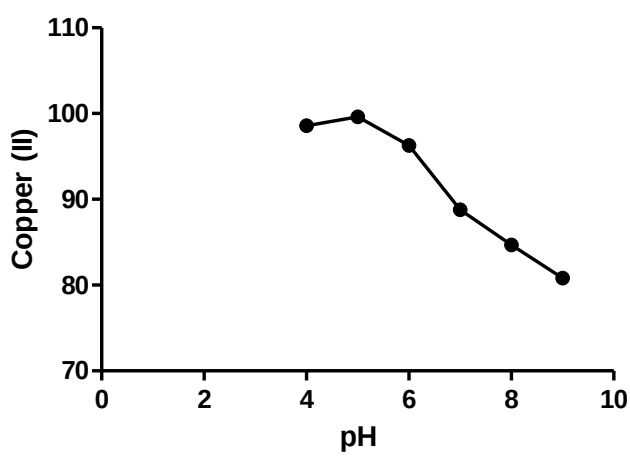

Figure-1 Effect of pH on the removal of Cu^{2+}- ions using CNCs-g-BA copolymer.

The present study at low pH very strong acidic mediumextra vacant protons and thus, give rise to electrostatic repulsion to metal cations. Moreover, these protons would compete with metal ions for binding sites on adsorbent, leading to a reduction of metal ionsAdsorption [10]. At pH increased to 4 - 5 repulsive forces decreased and increasing metal ions adsorption. So, the maximum adsorption capacity of pH-5 onto

CNCs-g-nBA [11]. Two types of interactions Chelation between hydroxyl groups and metal ions, electrostatic interaction between carboxylate and metal ions. The higher pH metal adsorption decreases due to precipitation of insoluble metal hydroxides [12].From the above results, it was concluded that Cellulose Nano Crystals-g-butyl acrylate copolymer maximum removal efficiencies was 99.6% at pH-5 respectively.

3.1.2 Effect of Adsorbent Dose

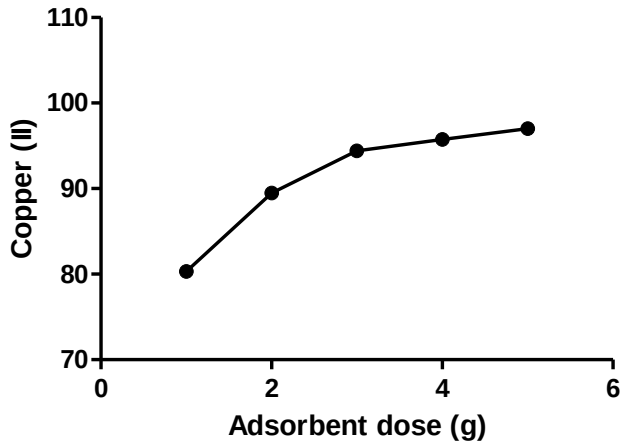

Figure-2 Effect of Adsorbent dose on the removal of Cu^{2+}- ions using CNCs-g-nBA copolymer.

The dependence of Cu(II) onto Cellulose Nano Crystals-g- n-butyl acrylate copolymer was studied by varying the adsorbent dose from 1 to 5g while keeping the other parameters pH and contact time as constant. **Fig-2** shows Effect of adsorbent dose of Cu^{2+} metal ions. The obtained results, the higher removal efficiency of increases with adsorbent dose due to active site on the adsorbent and which makes penetration of metal ions. Also attractive interaction between Cellulose Nano Crystals-g-n-butyl acrylate adsorbent and Cu(II) metal ions. Once the adsorbent reached equilibrium further addition of adsorbent dose due to saturation of active sites [13]. The maximum adsorbent dose 5g for Cu(II) ions.

3.1.3 Effect of Contact time

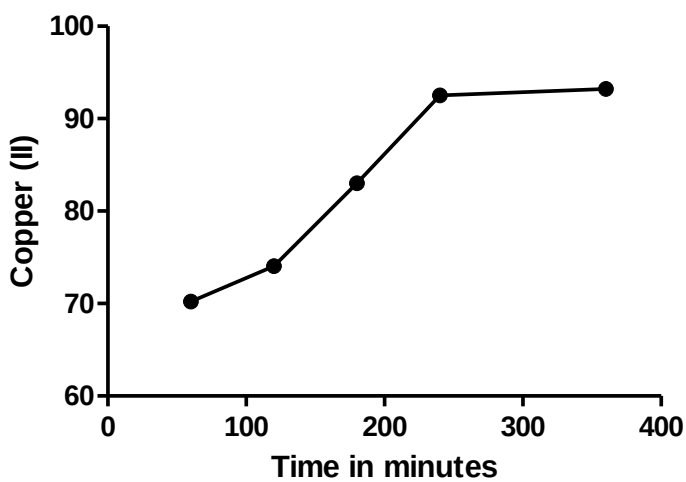

Figure-3Effect of Contact time on the removal of Cu^{2+}- ions using CNCs-g-nBA copolymer.

The **Fig-3** shows effect of contact time on metal ions removal by Cellulose-g-n-butyl acrylate varying contact time 60-300 minutes, while keeping others parameters pH, adsorbent dose and temperature constant. The adsorption increases with increasing contact time the adsorption sites reached at equilibrium [14] due to the complete saturation of the adsorbent active sites in the metal ions. Therefore 300 minutes maximum removal of contact time at the Copper(II) ions by using Cellulose Nano Crystals-g-n-butyl acrylate copolymer as adsorbent.

3.1.4 Effect of initial metal ion removal

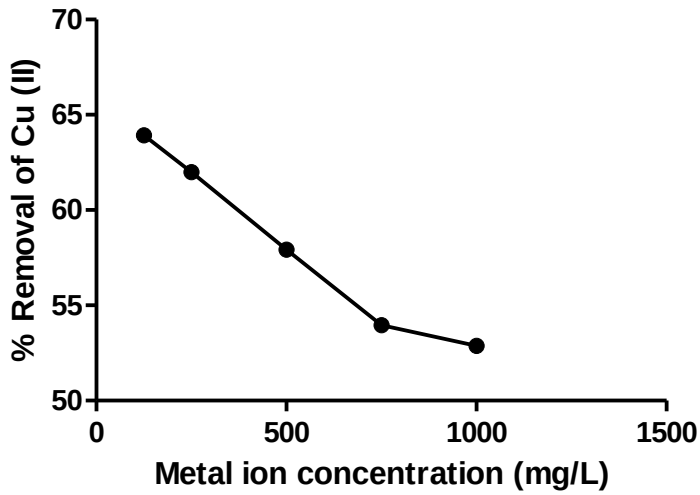

Figure-4 Effect of Initial metal ion concentration on the removal of Cu^{2+}- ions using CNCs-g-nBAcopolymer.

Effect of initial metal ion concentration by varying metal ion concentration 125, 250,500,750 and 1000 mg/L using an adsorbent Cellulose Nano Crystals-g-n-butyl acrylate grafted copolymer shows in **Fig-4**, while keeping other parameters pH, adsorbent dose and contact time as constant. In **Fig – 4** showsthe percent adsorption descended with increase in initial Copper(II) ion concentration. At lower metal ion concentration, the available binding sites is low and hence it shows an increased percentage removal [15]. At higher metal ion concentration, the number of binding sites less due to saturation and hence it shows a decreased percentage removal [16].

3.2.Adsorption isotherms

The adsorption isotherm indicates the certain relation between the concentration of adsorbate and its degree of accumulation onto the adsorbent surface at constanttemperature [17]. Various isotherm models were used to adsorption process like Langmuir, Freundlich, Temkin and Dubinin-Radushkevich model. Among the various models, in the present study two adsorption isotherm models namely Langmuir and Freundlich model were studied and investigated extensively the Copper(II) ions with Cellulose Nano Crystals-g-n-butyl acrylate grafted copolymer.

3.2.1 Langmuir Adsorption Isotherm

In Langmuir isotherm model the adsorption sites are “equally active” the surface is homogeneous, and a monolayer surface is formed without any interaction between the adsorbed molecules [18]. Moreover, there is a free-energy change for all adsorption sites considering no adsorbent–adsorbate interaction [19].The linearised form of Langmuir adsorption isotherm model is expressed as follows

$Ceq/Cads = bCeq/K_L+1/K_L$
$Cmax= KL/b$
where,
Cads = amount of metal ion adsorbed ($mg.g^{-1}$)
Ceq= equilibrium concentration of remaining metal ion in solution ($mg.dm^{-3}$)
K_L= Langmuir constant ($dm^3.g^{-1}$)
b = Langmuir constant ($dm^3.mg^{-1}$)
Cmax= Maximum metal ion to adsorb onto 1g adsorbent ($mg.g^{-1}$)

The Langmuir adsorption isotherm plot of Ceq/Cads Vs. Ceqfor Cu(II) ions onto CNCs-g-nBA grafted copolymer was represented in **Fig.5.**

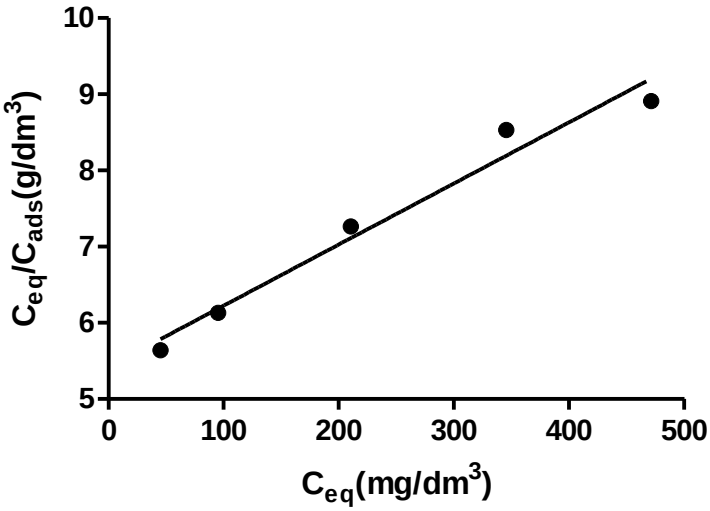

Figure-5 Langmuir adsorption isotherm plot for Cu(II)

The obtained results of adsorption of Cu (II) ions onto Cellulose Nano Crystals-g-n-butyl acrylate graft copolymer relates with the Langmuir equation and also the degree of suitability was estimated by dimensionless constant separation factor or equilibrium parameter, RL which can be calculated from the equation for different initial concentrations of Cu(II).

$RL = 1/1+bCf$
Where, $C_f$is the final concentration (mg/dm^3) of Cu(II)
b is the Langmuir constant (dm3 /mg)

The above calculated RL values used to predict whether an adsorption system is favourable or Unfavourable. If the obtained RL> 1, unfavourable isotherm; RL= 1, linear isotherm; RL= 0, irreversible isotherm; and 0 < RL< 1 favourable isotherm. The calculated RL values was represented in **Table – 1.**

Table-1: Calculated R_L values

Metal ion	Initial concentration (Ci) (mg/L)	Final concentration (Cf) (mg/L)	R_L Values
Cu(II)	1000	471.24	0.5893
	750	345.34	0.6619
	500	210.40	0.7626
	250	95.02	0.8767
	125	45.09	0.9374

From the above obtained values, it was evident that the calculated RL falls within the range of 0 <RL< 1. Hence from the obtained results it was concluded that the adsorption of Cu (II) on Cellulose Nano Crystals-g-n-butyl acrylate was found to be favourable.

3.2.2 Freundlich isotherm model

The another model give the details about the adsorptionparameters was Freundlich adsorption isotherm presented in the year 1906 [20]. The empiricalFreundlich equation for a heterogenous surface is

$q_e = K_F C_e^{1/n}$
The linearized form of Freundlich equation is represented as follows
$\log qe = \log KF + 1/n \log Ce$

Where qe is the amount of metal ion adsorbed (mg/g) and Ceis the equilibrium concentration (mg/L) and also KF and n are adsorption isotherm constants that is adsorption capacity and intensity of adsorption.
The Freundlich adsorption isotherm plot of log qeversus log Cepresented in**Fig-6** a straight line for the adsorption of Cu (II) and which gives the values of KF and 1/n from the slope and intercept of the above plot.

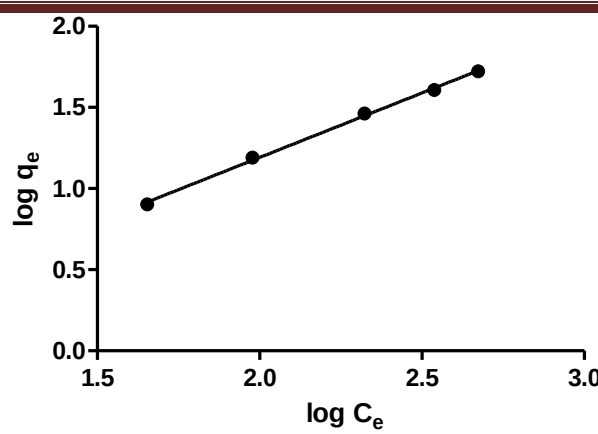

Figure-6Freundlich adsorption isotherm plot for Cu(II)

Table-2: Comparison between Langmuir and Freundlich constants

Langmuir Constants				Freundlich Constants		
K_L(dm^3/g)	b (dm^3/mg)	C_{max} (mg/g)	R^2	K_f	n	R^2
0.1843	0.001479	124.611	0.9698	2.4997	1.2583	0.9982

Table – 2 shows the comparison was made between Freundlich and Langmuir adsorption isotherm. The observed values concluded that Freundlich adsorption isotherm was the best fit, since the R^2= 0.9982 higher value for Freundlich adsorption isotherm. Based on the results cellulose Nano Crystals (CNCs)-graft/n-butyl acrylate grafted copolymer suggesting that the multilayer process takes place effectively.

3.3 Adsorption kinetics

Adsorption kinetics dependent on adsorbent and adsorbate relationship at different time intervals. The adsorption of Cu (II) onto Cellulose Nano Crystals-g-n-butyl acrylate were determined using Pseudo first order kinetics, Pseudo second order kinetics and intra particle diffusion method.

3.3.1 Pseudo first order kinetics

The linearized form of pseudo first order equation is [21]

$\log (qe - qt) = \log qe - K_1 t/2.303$

Where qe and qt are the amount of metal adsorbed on adsorbent (mg/g) at equilibrium andtime t. k1 is the rate constant with min-1. It yields a straight line when it is plotted with log (qe– qt) versus t and also the rate constant value k1 and qe is calculated from the slope and the intercept of the plot respectively. The pseudo first order kinetic plot for the adsorption of Cu (II) onto Cellulose Nano Crystals-g-n-butyl acrylate was given in the **Fig.7.**

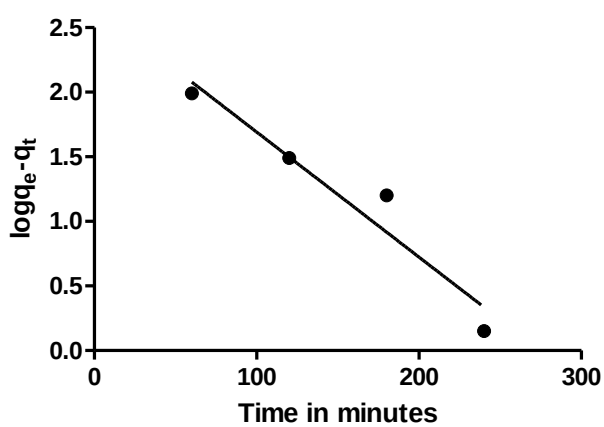

Figure -7 Pseudo first order kinetic plot for Cu(II) adsorption

3.3.2 Pseudo second order kinetics

The pseudo second order equation is expressed as follows [22]

$t/q_t = 1/K_2q_e^2 + t/q_e$

where qe and qt are the amount of metal adsorbed on adsorbent (mg/g) at equilibrium and time t. $K_2$is the rate constant with $gmg^{-1}min^{-1}$. It yields a straight line when it is plotted with t/qtversust and also qeand the rate constant value $K_2$is calculated from the slope and the intercept of the plotrespectively. The Pseudo second order kinetic plot for the adsorption of Cu (II) ontoCellulose Nano Crystals-g-n-butyl acrylate was given in the **Fig-8.**

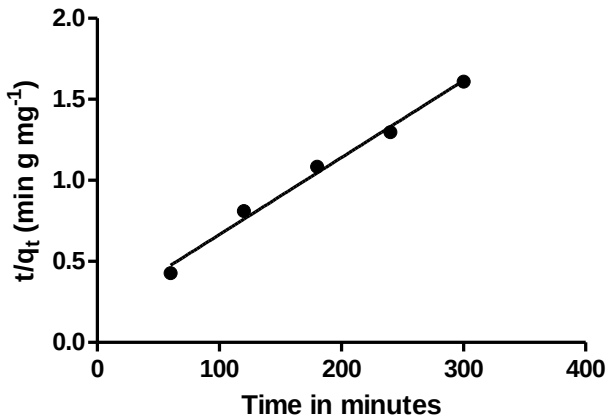

Figure -8 Pseudo second order kinetic plot for Cu(II) adsorption

3.3.3 Intra particle diffusion method

Intra particle diffusion method equation as follows [23]

$q_t = k_{id}\, t^{1/2} + C$

K_{id}= intraparticle diffusion rate constant ($mg/g\ min^{1/2}$)

C = Intercept

The intraparticle diffusion method the plots against q_t versus $t^{1/2}$. Theintraparticle diffusion kinetic plot for the removal of Copper(II) ions by Cellulose Nano Crystals-g-n-butyl acrylate grafted copolymerwas represented in **Fig.9.**

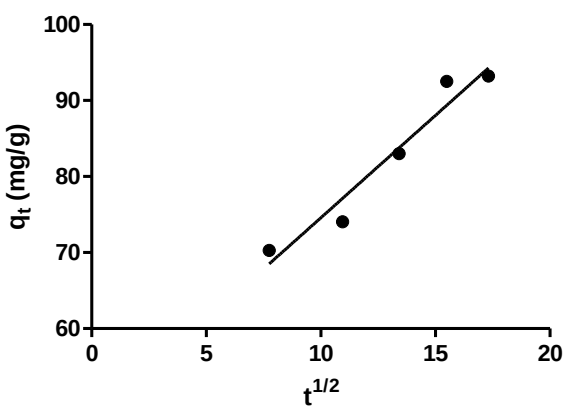

Figure-9 Intraparticle diffusion kinetic plot for Cu(II)

Comparison between Pseudo-first order and Pseudo-second order kinetics and Intra particle diffusion model for Copper(II) adsorption by CNCs-g-nBA copolymer were represented by Table – 3.

Table – 3: The Kinetic parameters of the adsorption by CNCs-g-nBA copolymer

Pseudo-first order Kinetic Model			Exp Value	Pseudo-second Order Kinetic Model			Intra Particle diffusion model		
q_e (mg/g)	k_1 (min^{-1})	R^2	qe (mg/g)	q (mg/g)	k_2 ($g\ mg^{-1}\ min^{-1}$)	R^2	K_{id}	I	R^2
457.08	0.02229	0.9322	127.85	210.43	0.0001187	0.9909	2.693	47.65	0.9441

Table – 3 shows, based on the results R^2 values Pseudo-second order kinetics model was better fit. Therefore the adsorption of Copper(II) ions onto Cellulose Nano Crystals-g-n-butyl acrylate follow pseudo-second order kinetics.

3.4 Characterization Study

3.4.1 FTIR ANALYSIS

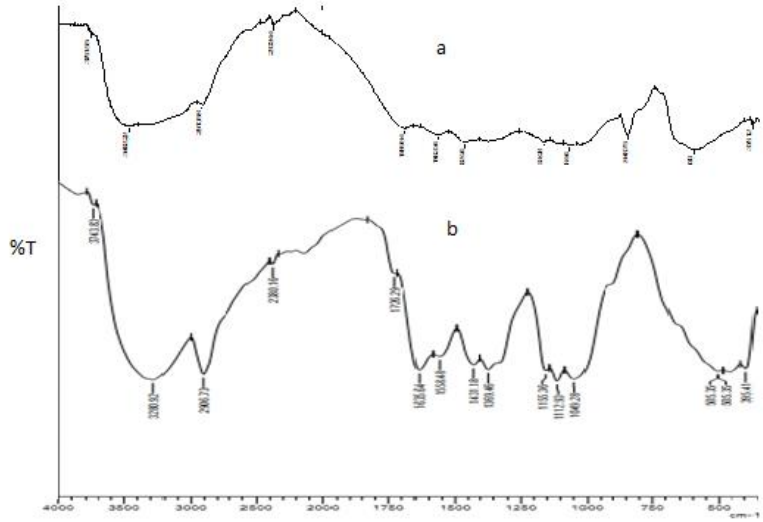

Figure-10 FTIR Spectra of Cellulose Nano Crystals grafted n-butyl acrylate before (a) and after adsorption (b) with Copper(II) ions.

The functional groups present in the adsorbent and interaction with Copper(II) ions was confirmed by FTIR analysis. The FTIR spectra of Cellulose Nano Crystals grafted n-butyl acrylate before and after adsorption shows in **Figure-10.**

Based on **Fig.10**a broadand strong adsorption band observed at 3462cm^{-1}corresponds to OH the stretching vibration [24]. The peak at 2910cm^{-1} due to asymmetric and symmetric vibrations of methyl (CH_2) groups, 1689cm^{-1} and 1635cm^{-1} the presence of C=C stretching vibrations [25]. A band at 1462$cm^{-1}$and 1431cm^{-1} were due to C-O stretching. The formation of new peaks observed at wave numbers1049cm^{-1} and 505cm^{-1} the after adsorption of Cellulose Nano Crystals-g-n-butyl acrylate after interaction with Cu(II) ions **(Fig.b).**

It is evident thatthe formation of new adsorption peaks, the changein adsorption intensity and the shift in wave number of the functional groups could be due to interaction of metal ions with active sites of Cellulose Nano Crystals-g-n-butyl acrylate through Copper(II) ions composite formation.

3.4.2 SEM-EDAX ANALYSIS

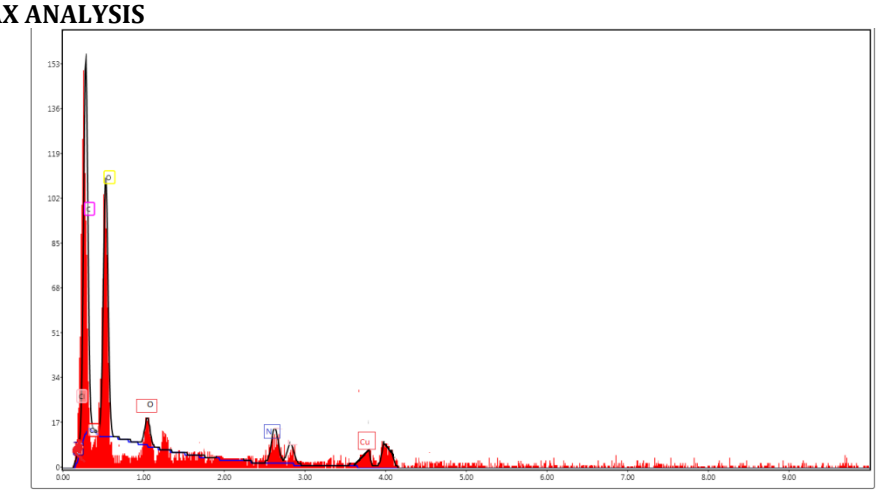

Figure-11 EDX spectrum of CNCs-g-butyl acrylate copolymer after interaction Cu(II) ions.

The adsorption of copper on the grafted adsorbentCNCs-g-butyl acrylate copolymer was evident from the EDX spectrum given **(Figure-11).** We suppose that the distribution of copper on the surface of adsorbent is caused due to chelating the copper ions through hydrogen bonding and the metal ion copper get adsorbed on the reactive sites, resulting in effective removal of copper. Thus the EDX spectrum corroborates the presence of copper in the Cellulose Nano Crystals-g-n-butyl acrylate copolymer has effectively formed. Overall the appearance of Cu on the surface of adsorbent indicates that the adsorbent was able to bind metal ions.

3.5 Desorption or Regeneration Studies

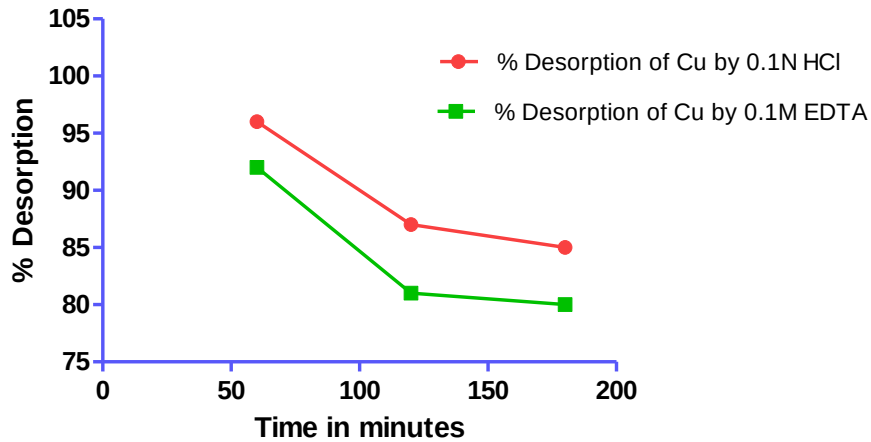

Figure – 12 Desorption of Cu(II) ions by 0.1N HCl and 0.1M EDTA

The regeneration or desorption of metal ions were examined by using 0.1N HCl and 0.1M EDTA the initial removal rate for 96% and 92%. The percentage removal was high in 0.1N HCl than 0.1M EDTA. The reason might be that EDTA desorbed metal ions by powerful chelating and HCl by electrostatic interaction. After the second hour, the removal rate became stable. So, the observed results showed thatthe adsorbent Cellulose Nano Crystals-g-n-butyl acrylate reached equilibrium at first one hour. The CNCs-g-n-BA shows wonderful reusability is one of the essential factors for evaluating its potentialcommercial applications. Based on the results, 0.1N HCl solution was selected for better regeneration of reagent CNCs-g-n-BA.

4. CONCLUSIONS

In the present study highlights potential of Cellulose Nano Crystals-g-n-butyl acrylate, a low cost material, as an alternative biosorbent to treat waste water treatment. It consists of a hydroxyl and carbonyl groups that favour metal ion binding through composite formation. The results showed that several experimentalparameters such as optimum pH-5, contact time-300 Minutes, adsorbent dosage-5g/100mL and initial metalconcentration-125mg/L. The adsorption isotherms such as Langmuir and Freundlich and kinetic models were investigated. The obtained results shows Freundlich model and kinetic studies of Copper(II) was found to be pseudo-second order model was better fit.The desorption studies 0.1N HCl followed by 0.1M EDTA were used to better desorping agents after three cycles.

5. REFERENCES

1. Asubiojo, O. I., & Ajelabi, O. B. (2009). Removal of heavy metals from industrial wastewaters using natural adsorbents. *Toxicological & Environmental Chemistry*, 91(5), 883–890.
2. Fu F. Wang Q. (2011) Removal of heavy metal ions from wastewaters: a review. *Journal of Environmental Management* 92 (3), 407–418.
3. Bernardo G R and Rene R M(2009) Chromium (III) uptake by agro-waste biosorbents: Chemical characterization, sorption–desorption studies, and mechanism. *Journal of Hazardous Materials* 170, 845–854.
4. Javadian H, (2014)Application of kinetic, isotherm and thermodynamic models for the adsorption of Co(II) ions on polyaniline/polypyrrole copolymer nanofibers from aqueous solution. *Journal of Industrial and Engineering Chemistry*, Vol.20, No.6, 4233-4241.
5. L. Brinchi, F. Cotano, E. Fortunati, J.M. Kenny.(2013) Production of nanocrystalline cellulose from lignocelulosic biomass: Technology and applications. *Carbohydr. Polym*. 94,154-169.

6. Yu, X., Tong, S., Ge, M., Wu, L., Zuo, J., Cao, C., & Song, W. (2013). Adsorption of heavy metal ions from aqueous solution by carboxylated cellulose nanocrystals. *Journal of Environmental Sciences*, 25(5), 933–943.
7. RaghvendraKumarMishra., ArjunSabu., Santosh K.Tiwari (2018, February, 23) Materials chemistry and the futurist eco-friendly applications of nanocellulose: Status and prospect. *Journal of Saudi Chemical Society*. (In press)
8. Wohlhauser, GwendolineDelepierre, Marianne Labet, GaelleMorandi, WimThielemans, ChristophWeder, and Justin O. Zoppe (2018) Grafting Polymers from Cellulose Nanocrystals: Synthesis, Properties, and Applications Sandra *Macromolecules*,*51* (16), pp 6157–6189.
9. D. Roy, M. Semsarilar, J.T. Guthrie, S. Perrier. (2009). Cellulose modification by polymer grafting: A review. *Chem. Soc. Rev*. 38(7), 2046-2064.
10. K.B. Girma, V. Lorenz, S. Blaurock, F.T. Edelmann,(2005) Coordination chemistry of acrylamide, Coord. *Chem. Rev*. 249, 1283–1293.
11. E. Igberase, P. Osifo, A. Ofomaja, (2014) The adsorption of copper(II) ions by polyaniline graft chitosan beads from aqueous solution: Equilibrium, kinetic and desorption studies, *J. Environ. Chem. Engin*. 2 362–369.
12. Zetty Azalea Sutirman, MohdMarsinSanagi, KhairilJuhanniAbd Karim, Wan Aini WanIbrahim, BintaHadiJume(2017) Equilibrium, kinetic andmechanism studies of Cu(II) and Cd(II)ions adsorption by modified chitosan beads. *Biological macromolecules*, doi:10.1016/j.ijbiomac.2018.05.031.
13. T. Hajeeth, P.N. Sudha, K. Vijayalakshmi, T. Gomathi, (2014) Sorption studies on Cr(VI) removal from aqueous solution using cellulose grafted with acrylonitrile monomer, Int. J. *Biol.Macromol*. 66 295–301.
14. R. Lavanya, T. Gomathi, K. Vijayalakshmi, M.Saranya, P.N. Sudha, Sukumaran Anil (2017) Adsorptive removal of copper (II) and lead (II) using chitosan-g-maleic anhydride-g-methacrylic acid copolymer, *International Journal of Biological Macromolecules.*04.116.
15. M. Thenkuzhali and S. Thillainatarajan, (2016) Adsorption of the copper ion by Phoenix sylvestris leaves *J. Chem.Pharm. Res*. 8 155-164.
16. P. Ajitha, K. Vijayalakshmi, M. Saranya, T. Gomathi, K. Rani, P.N. Sudha, Sukumaran Anil, (2017) Removal of toxic heavy metal lead (II) using chitosan oligosaccharide-graft-maleic anhydride/polyvinyl alcohol/silk fibroin composite, *International Journal of Biological Macromolecules*http://dx.doi.org/10.1016/j.ijbiomac.05.111.
17. Cleide S.T. Araújo, Ione L.S. Almeida, Hélen C. Rezende, SuzanaM.L.O. Marcionilio, José J.L. Léon, Túlio N. de Matos(2017) Elucidation of mechanism involved in adsorption of Pb(II) ontolobeira fruit (Solanumlycocarpum) using Langmuir, Freundlichand Temkin isotherms *Microc*, doi:10.1016/j.microc.2017.11.009.
18. M.Y. Abdelnaeim, I.Y. El Sherif, A.A. Attia, N.A. Fathy, M.F. El-Shahat, Impact of chemical activation on the adsorption performance of common reed towards Cu(II) and Cd(II), *Int. J. Miner. Process*. 157 (2016) 80–88.
19. M.R. Malekbala, M.A. Khan, S. Hosseini, L.C. Abdullah, T.S.Y. Choong, (2015) Adsorption/desorption of cationic dye on surfactant modified mesoporous carbon coated monolith: Equilibrium, kinetic and thermodynamic studies, *J. Ind. Engin. Chem*. 21 369–377.
20. H.M.F. Freundlich, (1906) Over the adsorption in solution, *J. Phys. Chem*. 57, 385–470.
21. S. Lagergren, (1898) Zurtheorie der sogenannten adsorption gelösterstoffe, K. Sven. Vetenskapsakad. Handl. 24, 1–39.
22. Y.S. Ho, G. McKay,(2000) The kinetics of sorption of divalent metal ions onto Sphagnum moss peat, *Water Res.* 34, 735–742. doi:http://dx.doi.org/ 1 0.1016/S0043- 1354(99)00232-8.
23. W.J. Weber, J.C. Morris,(1963) Kinetics of adsorption of carbon from solution, *J. Sanitary Eng.* Div. 89 31–59.
24. Azlan Kamari, SitiNajiahMohdYusoff, Fadhilah Abdullah, WiwidPranata Putra(2014), Biosorptive removal of Cu(II), Ni(II) and Pb(II) ions from aqueous solutions using coconut dregs residue: Adsorption and characterisation studies *J.Environ.Chem.Eng.* http://dx.doi.org/10.1016/j.jece.2014.08.014
25. Hisham A. Essawy, Magdy F. Mohamed, Nabila S.Ammar, Hanan S. Ibrahim (2017), The promise of a specially-designed graft copolymer of acrylic acid onto cellulose as selective sorbent for heavy metal ions, *International Journal of Biological Macromolecules* http://dx.doi.org/10.1016/j.ijbiomac.2017.05.052

SYNTHESIS, CHARACTERISATION AND ANTIBACTERIAL ACTIVITY OF Ni(II), Zn(II) COMPLEXES OF TETRADENTATE SCHIFF BASE LIGAND

K. DEEPA & RANGASWAMY VENKATESH
PG & Research Department of chemistry,
Muthurangam Government Arts College(Autonomous), Vellore-2, Tamilnadu, India

ABSTRACT: *Two different chloro substituted nickel(II), zinc(II) complexes were synthesized by the reaction of corresponding precursor with Tetradentate Schiff base ligand. The ligand was characterised by UV-Visible, FT-IR, H^1NMR Spectral studies. The synthesized complexes were characterised by molar conductance, UV- Visible, FT-IR spectral studies. The ligand and its complexes screened for antibacterial activity.*

Keywords: *Tetra-dentate Schiff base ligand. Nickel (II) complexes, Zinc (II) complexes antibacterial activity.*

Introduction:

The scope of coordination chemistry is indeed very broad and interdisciplinary. Some of the important types of coordination compounds occur in biological system. The coordination compounds is that coordinate bonds from between electron pair donors, known as the ligand, and electron pair acceptors, the metal atoms or ions. During recent years there has been considerable interest in the chemistry of transition metal complexes of Schiff base[1-3] . This is due to fact that Schiff base offer opportunities for substrate chirality, tuning the metal centered electronic factor, enhancing the solubility and stability of either homogeneous or heterogeneous catalysts[4-9]. The complexes containing O, N donor atoms are very important owing their significant antibacterial and anticancer activity[10] .

EXPERIMENTAL :

Materials and methods:

All chemicals and solvents used were of AR grade. IR spectra were recorded on a IR- Affinity-I Spectrometer using KBr pellets in the range 4000-400 cm^{-1}. Molar conductance of the ligand and complexes were measured in ethanol (10^{-3}M) solutions using a digital conductivity meter. UV-Visible spectra were recorded using Systronics spectrophotometer operating in the range of 200-800 nm with quartz. Antibacterial activities were done at Micro Labs, Vellore, Tamilnadu, India.

SYNTHESIS OF SCHIFF BASE LIGAND:

The schiff base ligand were prepared by initially 5-chloro-2-hydroxy acetophenone (14 mmol) in ethanol was kept under magnetic stirring. To this ethanolic solution of 4-nitro-o-phenylenediamine (7 mmol) was added in the reaction mixture. The mixture was refluxed for 8 hours. The precipitate was filtered and washed with hot water and ethanol. The purified product was kept under oven at 60°C for 2 hours.

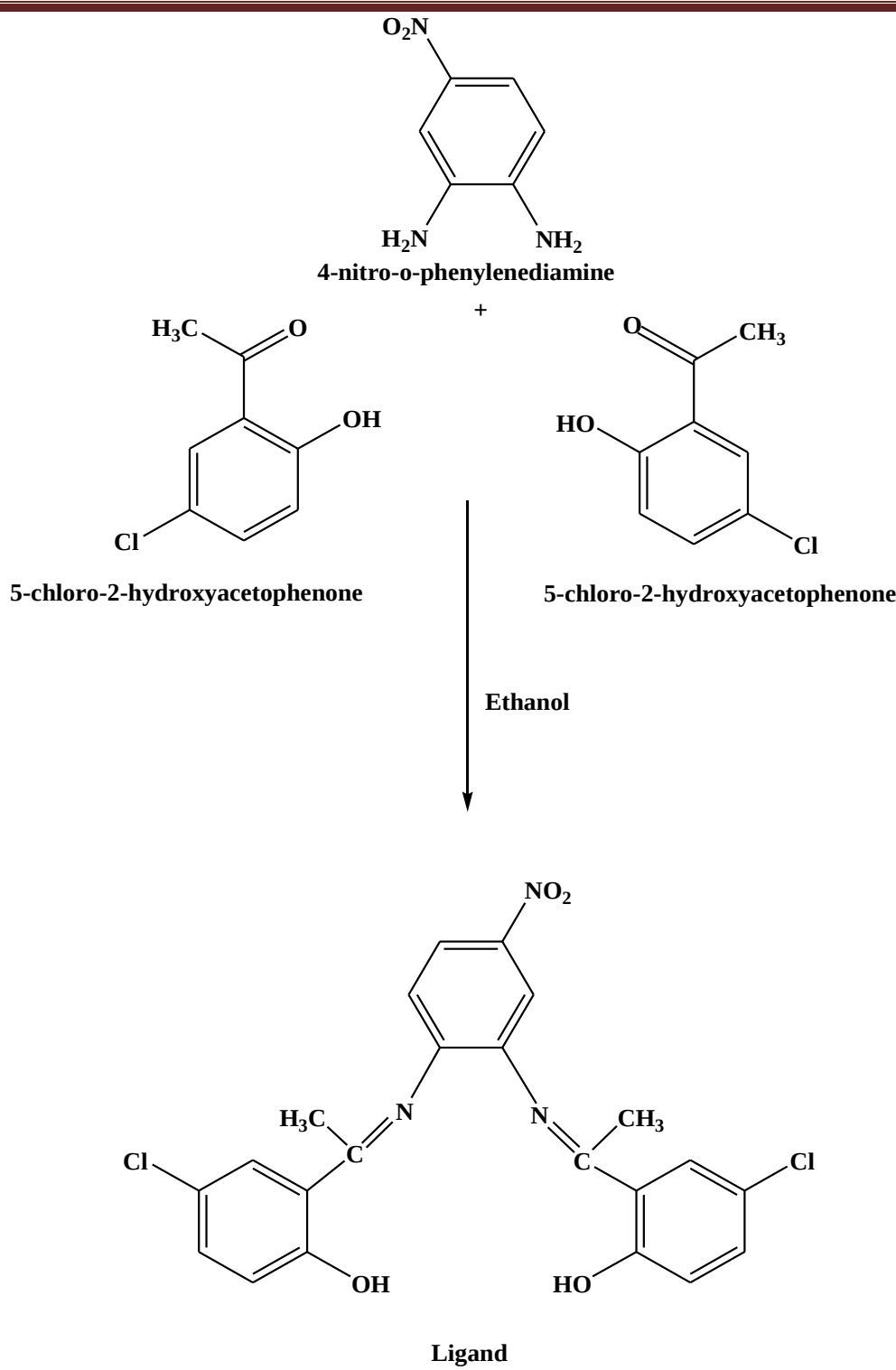

Ligand

SYNTHESIS OF NICKEL (II) COMPLEX:

The schiff base ligand (3 mmol) dissolved in ethanol was kept under magnetic stirring. To this ethanolic solution of Ni (II) acetate tetrahydrate (3 mmol) was added in the reaction mixture. The mixture was refluxed for 8 hours. The precipitate was filtered and washed with hot water and ethanol. The purified product was kept under oven at 60°C for 2 hours.

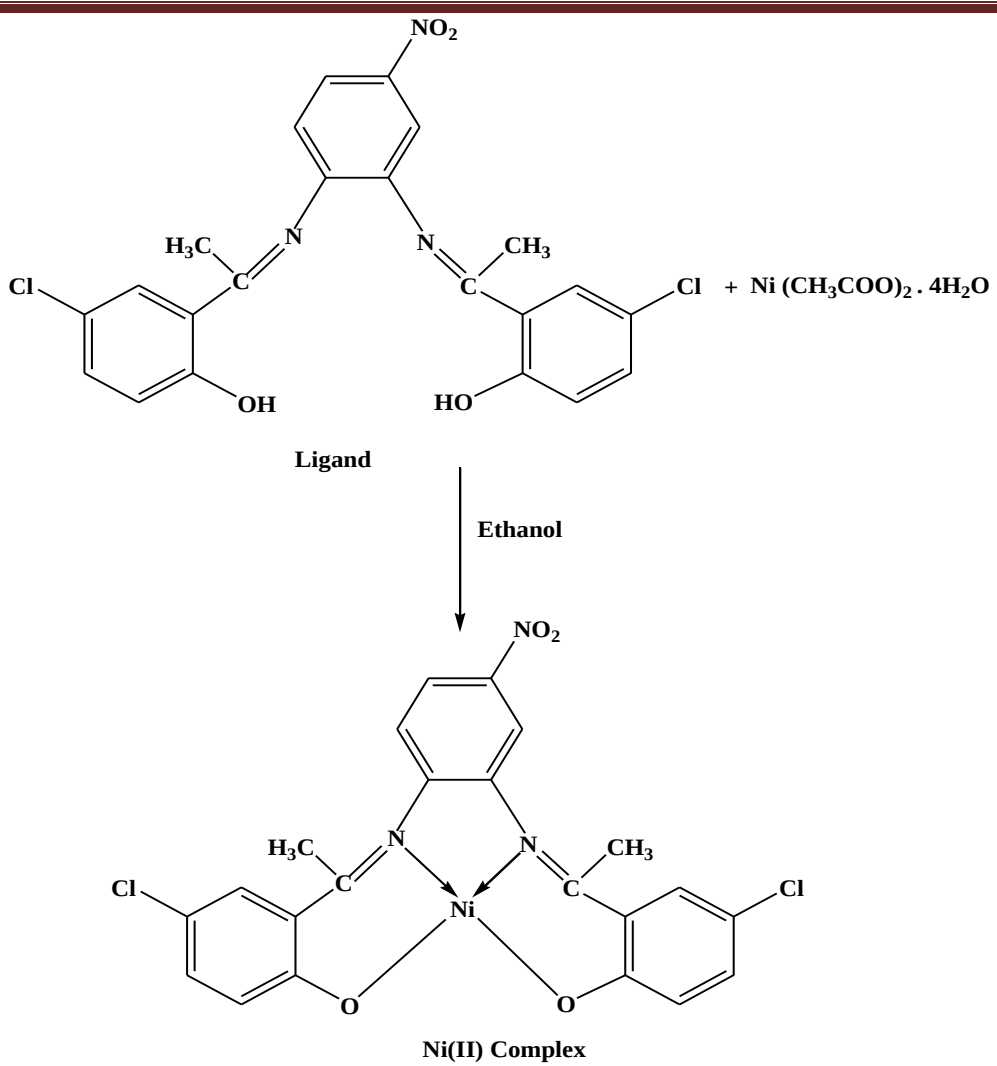

SYNTHESIS OF ZINC (II) COMPLEX:

The schiff base ligand (1 mmol) dissolved in ethanol was kept under magnetic stirring. To this ethanolic solution of Zn (II) acetate dihydrate (1 mmol) was added in the reaction mixture. The mixture was refluxed for 8 hours. The precipitate was filtered and washed with hot water and ethanol. The purified product was kept under oven at 60°C for 2 hours.

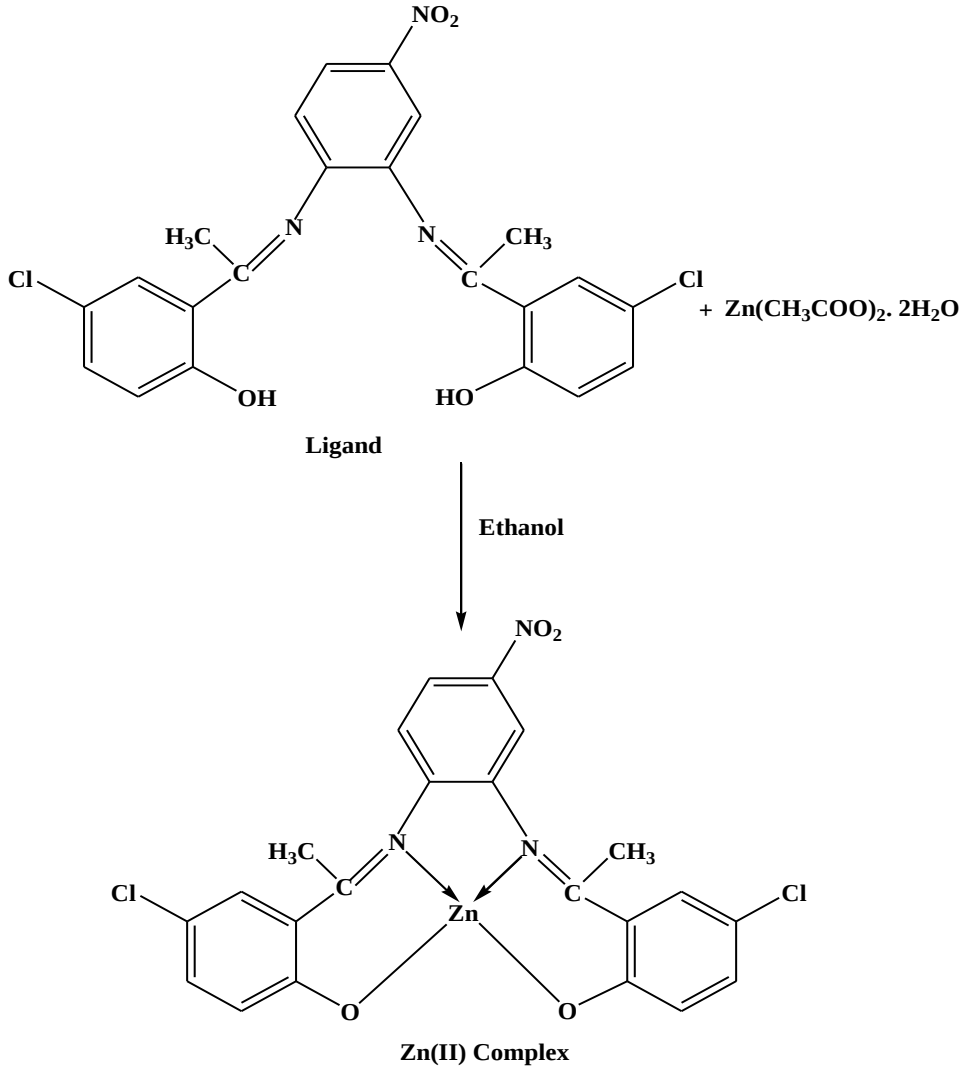

Results and Discussion:

Conductance Measurements:

The molar conductance of Ligand and metal (II) complexes are listed in the Table-1. The molar conductance values show that the complexes are non-electrolyte in nature[11]. The solvent used in molar conductance is ethanol.

Table.1: Analytical data of ligand and metal (II) complexes:

S.NO	Compound	Molecular formula	Molecular weight	Molar conductance (ohm^{-1} cm^2 mol)
1	Ligand	$C_{22}H_{17}N_3O_4Cl_2$	457.06	-
2	Ni(II) Complex	$C_{22}H_{15}N_3O_4Cl_2Ni$	513.74	45
3	Zn(II) Complex	$C_{22}H_{15}N_3O_4Cl_2Zn$	520.45	47

UV-VISIBLE SPECTROSCOPIC ANALYSIS:

UV-Visible spectra of ligand and all the complexes were recorded using ethanol and the spectral data are listed in Table-2. The absorption band observed in the region of 247 nm was due to π-π* transition of the benzene ring present in the ligand. The band at 367 nm was due to π-π* transition of the azomethine group (-HC=N) present in the ligand. The band at 413 nm was due to n –π* transition of the ligand. The band observed in the region of 241-246 nm was due to π-π* transition of the benzene ring present in the complexes. The band at 365-366 nm was due to π-π* transition of the azomethine group (-HC=N) present in

the complexes [12]. The band at 416-419 nm was due to n –π* transition. A new characteristic band observed in the region of 565- 567 nm was assigned to d-d transition of the complexes.

Table-2 : UV-Visible Spectral data of Ligand and metal (II) complexes.

Compounds	Wavelength (nm)			
	π -π*(nm) (benzene)	π -π*(nm) (-HC=N)	n – π*(nm)	d-d(nm)
Ligand	247	367	413	-
Complex-I	241	365	416	567
Complex-II	246	366	419	-

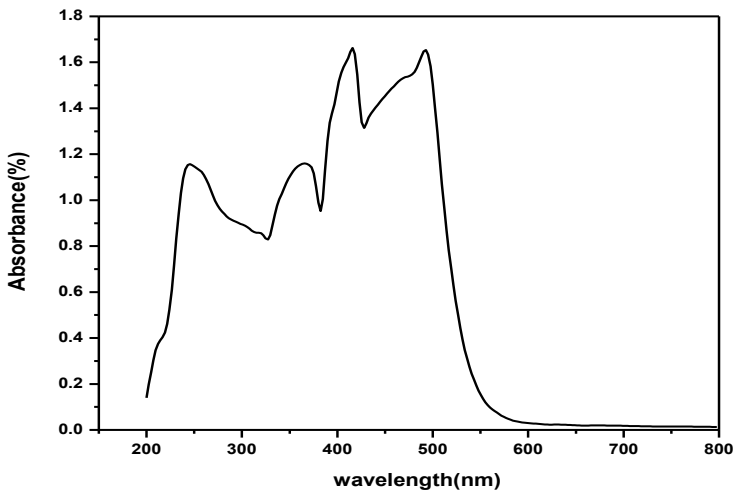

Figure 1: UV-Visible spectrum of Schiff base Ligand

FT-IR SPECTROSCOPIC ANALYSIS:

The FT-IR spectrum of Ligand and metal (II) complexes are recorded using KBr technique. The peak at 1639 cm^{-1} was due to the stretching frequency of the azomethine group (-HC=N) in the ligand. The peak appeared at 1296cm^{-1}were assigned to C-O stretching vibration of the ligand. The peak at 3338 cm^{-1} have been assigned to the -OH stretching vibration of the ligand. The peak at 1616-1639 cm^{-1} was observed due to the stretching frequency of the azomethine group (-HC=N) in the complexes. The peak 1639cm^{-1} was due to azomethine group of the ligand and it was shifted to lower frequency after complexation. This shows the co-ordination of metal with azomethine nitrogen[13]. The peak appeared at 1292-1305 cm^{-1}were assigned to C-O stretching vibration. The bands presence at 3340-3383 cm^{-1} have been assigned to the -OH stretching vibrations. The peak at 439-459 cm^{-1} was observed due to M-O stretching vibrations. The peak at 513-514 cm^{-1} was observed due to M-N stretching vibrations.

Table-3: FT-IR Spectral data of Ligand and metal (II) complexes:

Compounds	υ(-C=N) cm^{-1}	υ(-C-O) cm^{-1}	υ(-OH) cm^{-1}	υ(M-O) cm^{-1}	υ(M-N) cm^{-1}
Ligand-I	1639	1296	3338	_	_
Complex-I	1595	1292	3340	459	514
Complex-II	1616	1305	3383	439	513

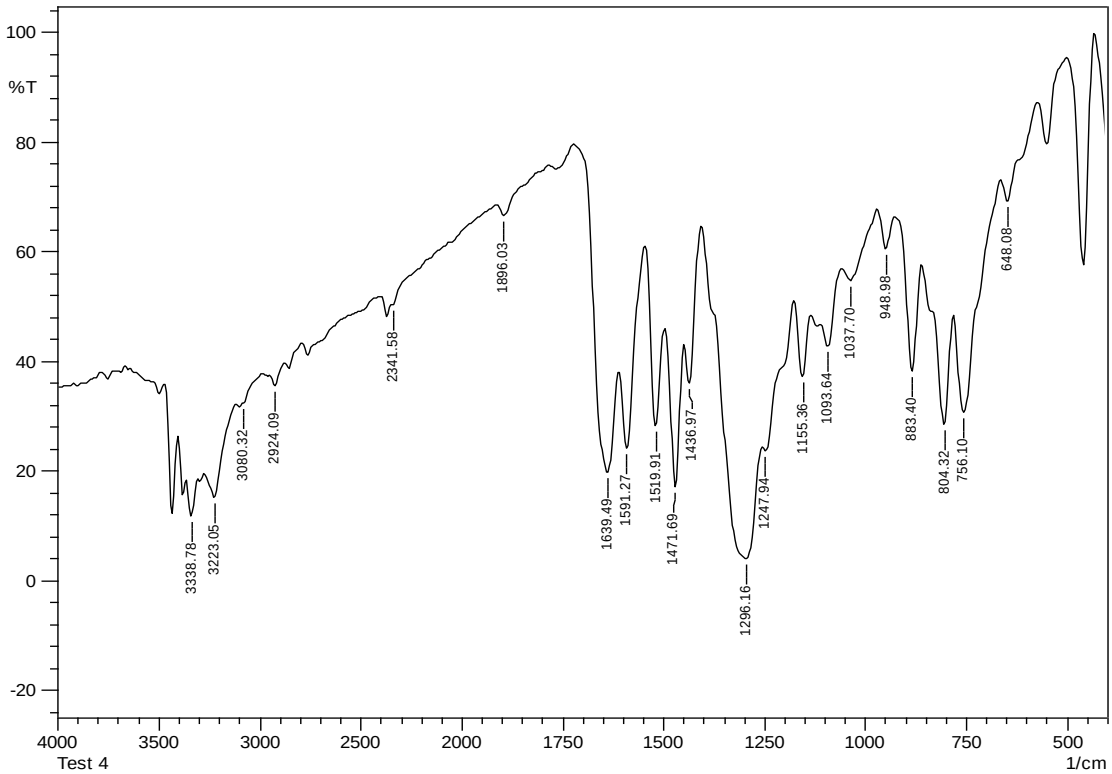

Figure 2: FT-IR Spectrum of the Schiff base Ligand

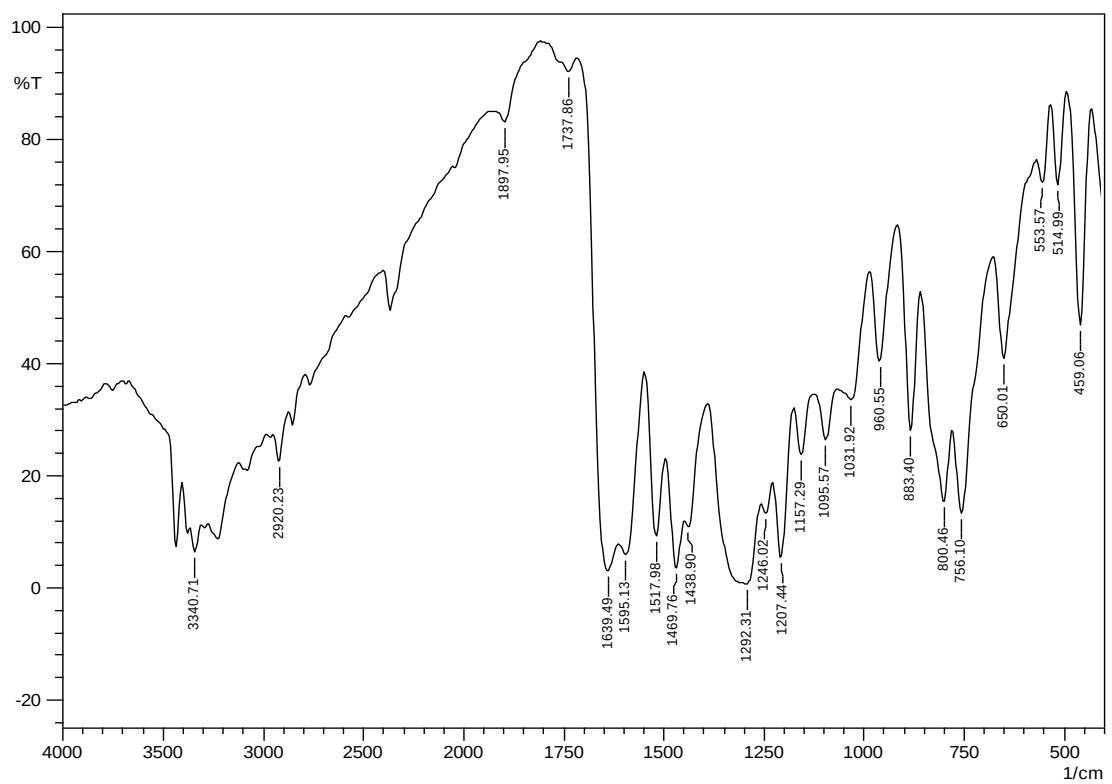

Figure 3: FT-IR Spectrum of Ni(II) Complex

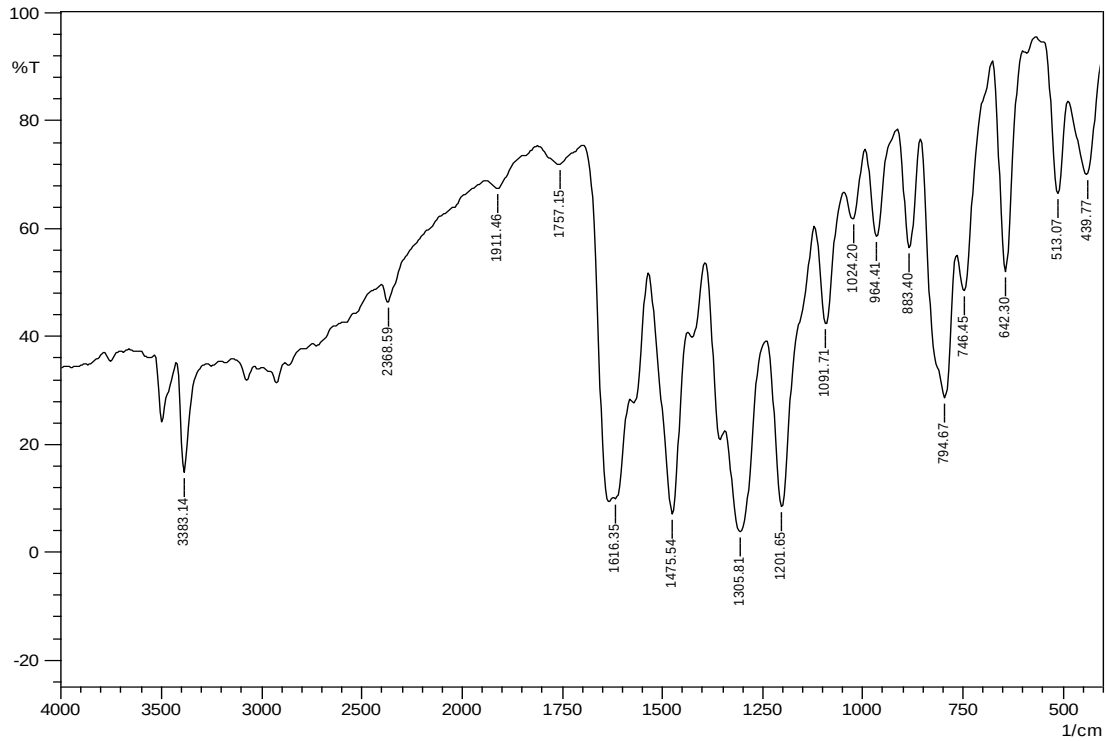

Figure 4: FT-IR Spectrum of Zn(II) Complex

^{1}H NMR SPECTROSCOPIC ANALYSIS OF LIGAND:

The ^{1}H NMR spectra of Schiff base ligand are recorded using CDCl3 as solvent, tetramethylsilane (TMS) as internal standard. The ^{1}H-NMR spectral data of Schiff base ligand and its spectrum is shown in Figure: 5. The multiplet signal observed at 7.52-7.72 ppm was due to the aromatic protons. The signal appeared at 6.65- 6.99 ppm was due to the protons of the azomethine group (-HC=N). The signal observed at 4.35 ppm was due to the protons of aromatic alcohol. The signal observed at 3.37 ppm is due to methyl group.

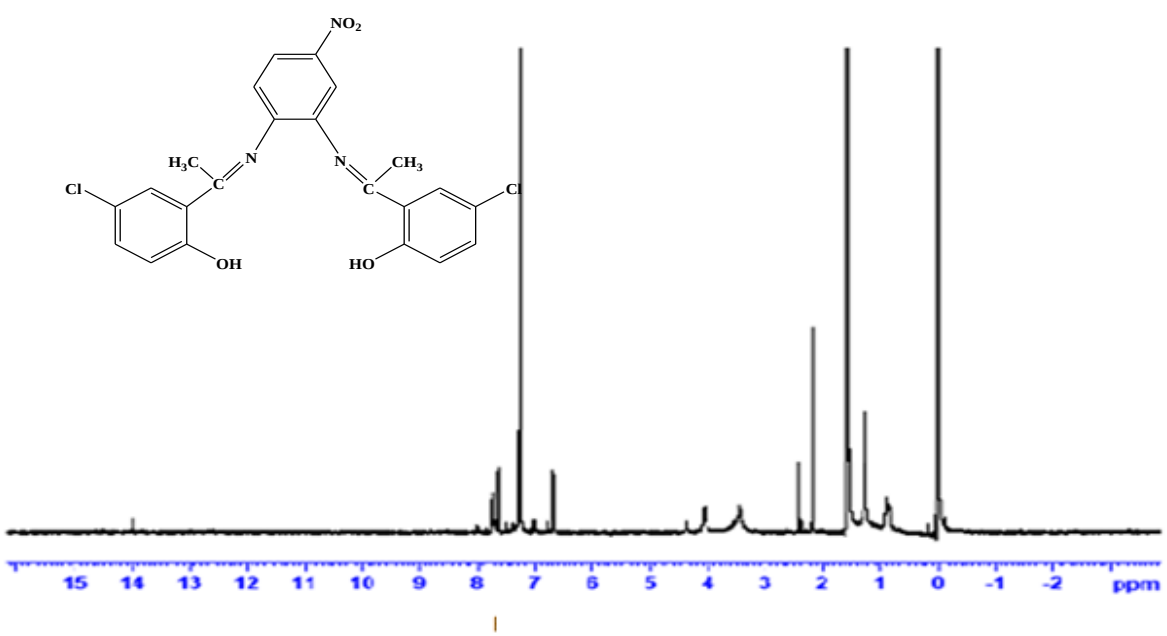

Figure 5: ^{1}H NMR SPECTRUM OF SCHIFF BASE LIGAND

BIOLOGICAL ACTIVITY:

The ligands and the complexes were screened for *in-vitro* antibacterial activity against *Enterococcus faecalis, Staphylococcus aureus, Salmonella typhi, Escherichia coli*. Ciprofloxacin was used as standard drug and DMSO as control. The antibacterial data summarized in table 4:

Table 4: Zone of inhibition of Ligand and Metal (II) complexes:

S.No	Microorganisms	L1	L1C1(Ni(II)	L1C2(Zn(II)	Ciprofloxacin
1	**Enterococcus faecalis**	-	-	-	30
2	**Staphylococcus aureus**	13	15	18	32
3	**Salmonella typhi**	07	06	05	33
4	**Escherichia coli**	10	8	12	20

The ligand and Ni(II)complex and Zn(II)complex exhibits good inhibition against Staphylococcus aureus.

CONCLUSION:

Tetradentate Schiff base ligand were synthesized using 4-nitro-o-phenylenediamine and 5-chloro-2-hydroxyacetophenone. The Synthesized transition metal [Ni(II), Zn(II)] complexes were characterized by using various analytical techniques Such as UV-Visible, FT-IR, Conductivity measurement. The Synthesized transition metal [Ni(II), Zn(II)] complexes were Screened for their antibacterial activity against *Staphylococcus aureus, Enterococcus faecalis, Salmonella typhi, Escherichia coli*. The ligand and complexes were found to inhibition to all selected micro organisms except Enterococcus faecalis.

References:

1. K. S. Murray, *Aust. J. Chem*., 1978; 58, 203.
2. H. Doine, Bull. *Chem. Soc. Jpn*., 1985; 58, 1387.
3. K. Nakajima, Y. Ando, H. Mano and M. Kojimai, *Inorg. Chim. Acta*, 1998; 274, 184.
4. B. De Clercq and F. Verpoort*, Macromolecules,* 2002; 42, 2876.
5. T. Opstal and F. Verpoort, Angew, Chem. Int. Ed., 2003; 42, 2876.
6. T. Opstal and F. Verpoort, Synth lett, 2002; 40, 4807.
7. S. N. Pal and S. Pal*, Inorg. Chem.,* 2001; 40, 4807.
8. B. De Clercq and F. Verpoot, *Adv. Synth. Catal*., 2002; 34, 639.
9. B. De Clercq, F. Lefebure and F. Verpoot*, Appt. Cata. Commun*., 2004; 7(2), 247.
10. D. Dhivyapriya, E.Akila, M. Usharani and R. Rajavel, *Int. J. Pharm. Tech*., 2012; 4(1), 4067.
11. Geary W.J., *Coord chem. Rev* 1971; 7: 81-122.
12. Nevin Turan and Memet Sekerci*, J.Chem. Soc. Pak* 2009; 31: 564-568.
13. Andruh, M.Kahn. O.Sainton, J.Dromzee, Y.Jeanin, S. *Inorg. Chem* 1993; 32: 1623- 1628.

NOVEL SYNTHESIS OF HYDROXYAPATITE NANOPARTICLES BY USING HYDROTHERMAL COUPLED SHOCK WAVE METHOD

I. Venda[1], V. Thamizharasi[2], E. Sathya[3] & V. Collins Arun Prakash[4*]
[1,2,3,4]Department of Chemistry, Sacred Heart College (Autonomous), Tirupattur, Vellore Dist. 635 601

ABSTRACT: *Hydroxyapatite (HA) is one of the most extensively studied calcium phosphates, is the most important inorganic constituent of bones and teeth of human body with molecular formula $Ca_{10}(PO_4)_6(OH)_2$ and it is used as a biomaterial for the regeneration of bone tissue because of its chemical composition similar to natural bone. Particularly this material is employed in orthopaedic and dental applications due to its excellent biocompatibility, bioactivity, and also osteoconductive properties. So, in this work, HAP powders were formed by Synthesis and characterization of hydroxyapatite nanoparticlesr using hydrothermal coupled shock wave method. Synthetic HAP powder were characterized by X-ray powder diffraction (XRD), Fourier transform infrared spectroscopy (FTIR) and scanning electron microscopy (SEM). FTIR spectroscopy confirms the presence of hydroxyapatite by observing hydroxyl groups, and phosphate groups. XRD technique confirms the high purity Nano hydroxyapatite crystals by viewing high intense peak. SEM technique reveals that the morphology and smaller particle size distribution hydroxyapatite powders are not as much agglomerated. The as synthesised powder is to be tested further for its biocompatibility.*

Keywords: *Biomaterials, Hydroxyapatite, Ultrasound, and Shock wave*

INTRODUCTION

Hydroxyapatite (HAP) is chemically represented as $Ca_{10}(PO_4)_6(OH)_2$ which was one of the most important inorganic bio ceramic material [1]. It is well recognized that, hydroxyapatite is the primary constituent of bones and tooth materials and has been extensively used as an artificial bone substituent because of its chemical and crystallographic similar to natural bone [2,3]. This material is currently used in various forms as a bone substitute due to exceptional properties such as biocompatibility, bioactivity, osteoconductivity, nontoxicity, [4-6] noninflammatory behaviour, non-immunogenicity [7,8] and also easy synthesizability [9-12]. In medical field hap have been widely used as an orthopaedic implant, dental implants and artificial joints applications due to their unique properties. HAP compatibly finds numerous applications in other fields of industrial or technological interest. For instance, catalyst in chromatography or gas sensor [13,14], fertilizers production, drug carrier [15] and water purification. The almost common method used to synthesise nanohydroxyapatite includes wet chemical, precipitation, sol-gel, microwave assisted technique etc., However more elevated processing conditions such as, temperature, microwave irradiation time, low quality control, long time consuming etc., [16,17] One approach to get over these drawbacks is shockwave route, which enables to synthesize the ultrafine, uniformsized and uniform shaped particles. The coupled hydrothermal, ultrasound and shockwave path permits many advantages such as, fast reaction, good yield, combined moderate temperature with high pressure, short time, high degree of crystallinity and excellent reproducibility.

In this report, the surface morphology and crystal structure of hydroxyapatite nano particles are synthesized by using coupled pre-and post-loaded shock wave with ultrasound and hydrothermal method. The results showed that the applied synthesis procedure offers, resourceful and inexpensive route to achieve high superiority nano-sized products with suitable size and high level of crystallinity. The as synthesised powder is to be tested further for its biocompatibility.

2. MATERIALS AND METHODS

2.1 Chemicals and Reagents

Chemicals like calcium nitrate $Ca(NO_3)_2.4H_2O$, Diammonium hydrogen phosphate $(NH_3)_2HPO_4$ and aqueous ammonium hydroxide (NH_4OH) solution were purchased from Merck. All the received chemicals were of analyte grade (AR) and deionized water was used throughout the synthesis process.

2.2 Synthesis of Hydroxyapatite nanoparticles

In this typical experimental procedure for the synthesis of Hydroxyapatite, $Ca(NO_3)_2.4H_2O$ and $(NH_3)_2HPO_4$ were taken as Ca and P precursors with a stoichiometric ratio (1.67). 0.05M of aqueous $Ca(NO_3)_2$ was dissolved in 50 ml de-ionized water and stirred for 15 min using magnetic stirrer. 0.03M of

$(NH_3)_2HPO_4$ was dissolved in 50 ml of de-ionized water. Subsequently, 0.03 M of phosphate solution was added dropwise into the above mixed solution under vigorous stirring for 1 h. The pH of the above suspension was maintained as 10.5 by using ammonia solution and then stirred for1 h. Then the obtained milky white precipitate was kept in an ultrasound for 40 min at 60 ^oC. Now the sample is loaded at shock wave like 100 with Mach number 2.0 at applied pressure (2.367MPa) and temperature (896k). The above solution was transferred into Teflon lined autoclave maintained at 100^oC for 4 h in a hot air oven. The resultant product was washed with ethanol and double distilled water for several times, filtered and dried at 100 °C for about 4h. The dried powder was calcinated in an electric burner at 4h and to obtain pure HAP. The obtained powder was further characterized with different analytical techniques.

2.3CHARACTERIZATION

Fourier transform infrared spectroscopy (Perkin- Elmer) is a spectroscopic technique which is used to identify the functional groups especially phosphate and hydroxyl groups in calcium phosphate. The spectrum was recorded in the wave number region of 4000-400 cm^{-1}.The crystallinity and phase analysis of the sample were carried out using XRD. The size of the crystal is calculated using Scherrer formula. The surface morphology of the sample was investigated using scanning electron microscopic technique.

3. RESULTS AND DISCUSSION

3.1 FTIR analysis of pure HAP powder

Fig.1(a) shows the FT-IR spectra of HAP powder synthesized by pre-shock wave loaded hydroxyapatite shock wave. The result of FT-IR (a) & (b) confirm the formation of hydroxyapatite without any trace of other calcium phosphate phases. In this spectrum a sharp peak situated at 3572 cm^{-1} are assigned to the stretching vibration mode of OH group. The broad peak found at 3431 cm^{-1}corresponds to hydroxyl groups of bending mode, while the peak observed at 630 cm^{-1} is due to bending vibrational mode of hydroxyl group. The peak observed at 469 cm^{-1} is assigned to be ν_2 modes of phosphate mode, 604 cm^{-1} and 567 cm^{-1} are assigned for ν_4 is due to bending mode of phosphate groups, ν_1 symmetric P-O stretching vibration is observed at 962 cm^{-1}, The doubly degenerate bands situated at 1094 $cm^{-1}$and 1028 cm^{-1} indicates ν_3 mode of P-O stretching vibration of phosphate groups.

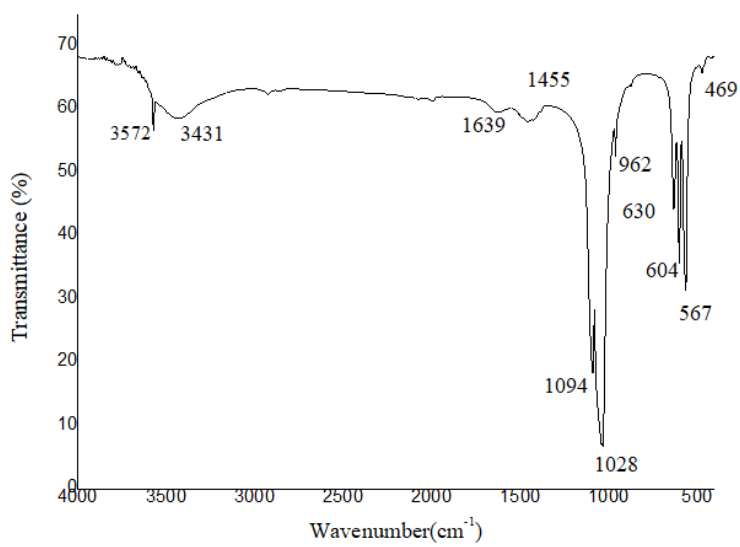

Fig.1(a) FTIR of HAP powder synthesized shock without wave.

The HAP structure contains OH and PO_4 group. In **Fig.1 (b)**. In this spectrumThe HAP structure contains OH and PO_4 group. In **Fig.3.1 (a)** The sharp band situated at 3571 cm^{-1}, and 627 $cm^{-1}$the indicates O-H functional group, and the broad peak at 3453cm^{-1} corresponds to hydroxyl group.The peak observed at 469 is assigned to the ν_2 modes of phosphate mode, 599 cm^{-1} and 567 cm^{-1} are assigned for $\nu_4$is due to bending mode of phosphate groups, ν_1 symmetric P-O stretching vibration is observed at 965, The doubly degenerate bands situated at 1091 & 1031 cm^{-1} indicates ν_3 mode of P-O stretching vibration of phosphate groups.

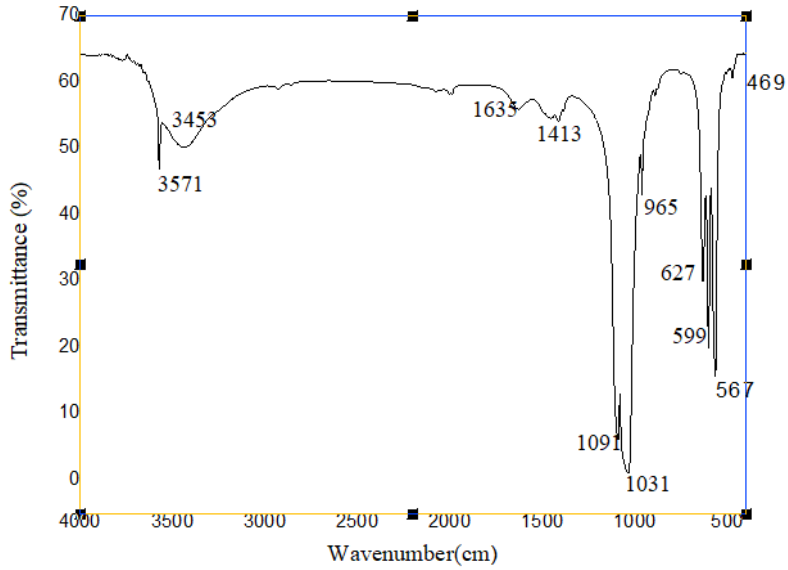

Fig. 1(b) FTIR of HAP powder synthesized by SW (100)

3.2. XRD CHARACTERISATION OF HYDROXYAPATITE POWDER

The phase composition, crystallinity, and purity of the as-synthesized hydroxyapatite powder were studied by XRD. Fig.3 illustrates the XRD pattern of synthesized sample of HAP powder reached by using both ultrasound and shockwave method. This sample confirmed the presence of hexagonal structure. In **Fig. 2(a)** shows the peak that are attributed to the HAP are found in the XRD pattern. The 2θ value for the pre-shock wave loaded hap peak were found to be 25.84, 28.87, 31.86, 32.95, 34.17, 39.87, 42.10, 46.81, 49.59, 50.45, 52.06, and 53.30 respectively, and the plan corresponding to the 2θ values were 002, 102, 211, 300, 202, 310, 131, 222, 213, 312, 321 and 402. In **Fig .2 (b)**, the 2θ value for the 100-shock number loaded HAP, peaks appeared at 25.84, 28.94, 31.86, 32.16, 32.95, 34.17,39.87, 41.88,46.81, 50.74, 52.29 and 53.13 respectively, and the plan corresponding to the 2θ values were 002, 102, 211, 112, 300, 202, 310, 131, 222, 213, 321, 402 and 004. This peak was well matched with the International Centre for Diffraction Data No. 09-0432 (ICDD) for HAP which indicated that the crystal structure of HAP sample is similar to the pure hydroxyapatite. The particle dimensions showed a steady decrease when compared with pre-shock and post shock wave loaded HAP. The pre-shock wave HAP showed lower crystallinity when compared to shock loaded HAP. The crystallinity size of the sample was calculated from XRD peaks by using Scherrer's equation. Shockwave assisted HAP nanoparticles (±51nm) is lower than, pre-shockwave (±53nm) HAP nanoparticles.

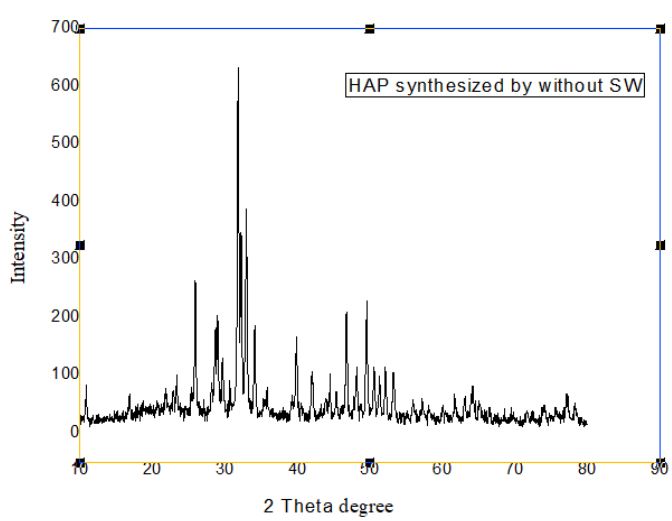

Fig.2 (a)XRD pattern of powder HAP synthesized by without SW.

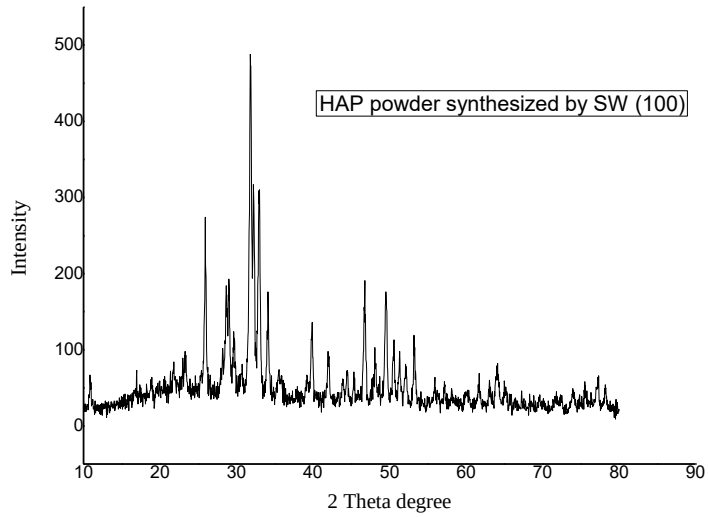

Fig. 2 (b) XRD pattern of HAP powder synthesized by SW (100)

3.3 SCANNING ELECTRON MICROSCOPIC STUDIES

The surface morphology, size and the crystallinity of the synthesized HAP powder were investigated by using scanning electron microscope.

SEM micrograph of pre- shock wave and shock wave assisted- calcinated sample were given in **Fig.3 (a) & (b).** The obtained powders showed a significant level of agglomerated and amorphous properties without shock wave. However, shock-wave assisted powders have a very fine particle size when compared to pre- shock wave. On the other hand, shock wave samples had more regular array and rod like structure unlike pre-shock wave powder.

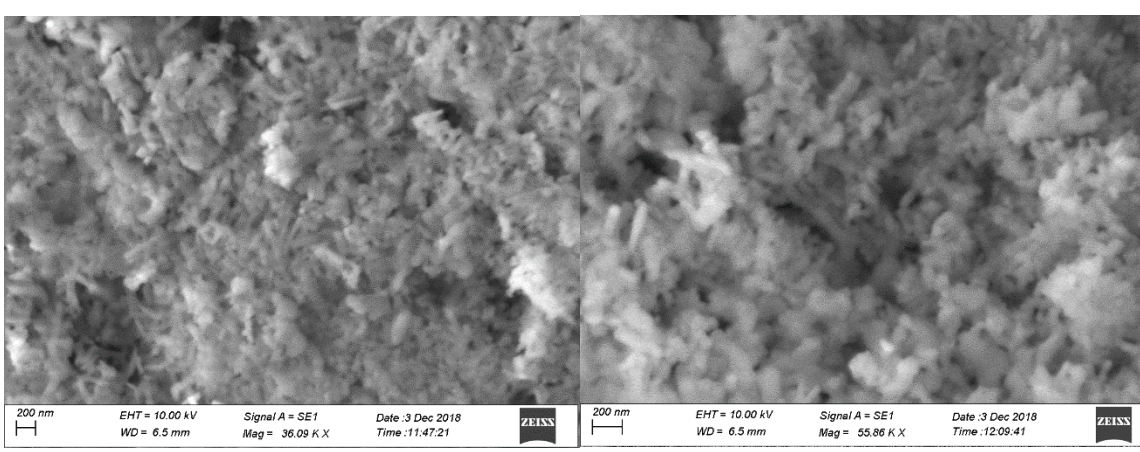

Fig. 3(a) & (b) SEM micrograph of HAP powder synthesized without and with SW (100).

CONCLUSION

In the present work, the hydroxyapatite nanoparticles were successfully prepared by ultrasound coupled shock wave method from calcium ion [Ca $(NO_3)_2$] and phosphate ion source [$(NH_3)_2HPO_4$] as starting materials. The FT-IR results have exposed that obtained HAP powder contain presence of characteristic peaks of the phosphate and OH groups and the XRD data found all confirmed the formation of nano hydroxyapatite powders. As the shock wave number is increased, the crystallinity and size of the particles decreases as a result of cavitation like process and was apparent from the XRD and SEM findings. Consequently, this method conveys a simple and cost-effective route to produce calcium deficient hydroxyapatite with controlled particle size, high purity, and minor level of impurities nearer to those of living hard tissues like teeth and bone, hence it could be decided that this type of synthesis would always

offer useful insights for designing good bioactive nano-HAP powder with improved performance for the orthopaedic implants.

ACKNOWLEDGEMENT

One of the authors (Dr. V. Collins Arun Prakash) thank the Abraham Panampara Research centre (APRC), Sacred Heart College (Autonomous) Tirupattur, for the financial assistance through received under "Don Bosco grant" scheme.

REFERENCES

1. L.L. Hench, J. Am. Ceram. Soc., 74, (1991), 1487.
2. Ciobanu, C.S.; Popa, C.L.; Predoi, D. Sm:HAp Nano powders Present Antibacterial Activity against Enterococcus faecalis. J. Nanomater. (2014), 1.
3. Suchanek, W.; Yoshimura, M. Processing and properties of hydroxyapatite-based biomaterials for use as hard tissue replacement implants. J. Mater. Res. 13, (1998), 94.
4. M. Sivakumar, K.P. Rao, Preparation, characterization and in vitro release of gentamicin from coralline hydroxyapatite-gelatin composite microspheres, Biomaterials 23 (2002) 3175-3181.
5. Y. Zhang, M. Zhang, Calcium phosphate/Chitosan composite scaffolds for controlled in vitro antibiotic drug release, J. Biomed. Mater. Res. 62 (2002) 378-386.
6. I. Yamaguchi, K. Tokuchi, H. Fukuzaki, Y. Koyama, K. Takakuda, H. Monma, J. Tanaka, Preparation and microstructure analysis of chitosan/hydroxyapatite nanocomposites, J. Biomed. Mater. Res. 55 (2001) 20-27.
7. K. Loku, S. Yamauchi, H. Fujimori, S. Goto, M. Yoshimura,Hydrothermal preparation of fibrous apatite and apatite sheet, Solid State Ionics 151 (2002) 147– 150.
8. J. Liu, X. Ye, H. Wang, M. Zhu, B. Wang, H. Yan, The influence of pH and temperature on the morphology of hydroxyapatite synthesis by hydrothermal method, Ceram. Int. 29 (2003) 629–633.
9. C. Zhou, Y. Hong, X. Zhang, Applications of nanostructured calcium phosphate in tissue engineering, Biomater. Sci. 1 (2013) 1012-1028.
10. R. Murugan, S. Ramakrishna, Bioresorbable composite bone paste using polysaccharide based nano hydroxyapatite, Biomaterials 25 (2004) 3829-3835.
11. C. Chai, B.B. Nissan, S. Pyke, L. Evans, Sol-gel derived hydroxylapatite coatings for biomedical applications, Mater. Manufac. Proc. 10 (1995) 205-216.
12. I. Mobasherpour, E. Salahi, M. Pazouki, Removal of nickel (II) from aqueous solutions by using nano-crystalline calcium hydroxyapatite, J. Saudi Chem. Soc. 15 (2011) 105-112.
13. R.Z. LeGeros, Calcium Phosphates in Oral Biology and Medicine. Karger, Basel, Switzerland, 1991.
14. J. Torrent-Burgues, J. Torrent-Burgues, T. Boix, J. Fraile, R. Rodriguez-Clemente, Cryst. Res. Tech. 36 (2001) 1075-1082.
15. J. Arensds, J. Chistoffersen, M.R. Chistoffersen, H. Eckert, J. Cryst. Growth 84(1987) 515523.
16. Y.J. Wang, S.H. Zhang, K. Wei, N.R. Zhao, J.D. Chen, X.D. Wang, Hydrothermal synthesis of hydroxyapatite nanopowders using cationic surfactant as a template, Mater. Lett. 60 (2006) 1484–1487.
17. Y. Fujishiro, H. Yabuki, K. Kawamura, T. Sato, A. Okuwaki, Preparation of needlelike hydroxyapatite by homogeneous precipitation under hydrothermal conditions, J. Chem. Technol. Biotechnol. 57 (1993) 349–353.

SYNTHESIS, CHARACTERIZATION AND ANTIMICROBIAL STUDIES OF POLY N-TERT-AMYLACRYLAMIDE (NTA) AND (PA) COPOLYMERS

P. Vimala
Assistant Professor of chemistry, Muthurangam Govt. Arts College (Autonomous), Vellore, India

ABSTRACT: *Copolymers of N-tert-amyl acrylamide (NTA) and copolymerized with Phenyl acrylate (PA). Copolymers of N-tert-amyl acrylamide (NTA) and Phenyl acrylate(PA) were prepared by free radical polymerization in DMF at 60^{0}C using AIBN as an initiator. (Scheme 1). The copolymer composition were determined by ^{1}H-NMR analysis. The reactivity ratios of monomers were determined by Fineman-Ross (FR) (r1 = 1.33 and r_2 = 0.60), Kelen-Tudos (KT) (r1 = 1.33and r_2 = 0.59). The $r_1.r_2$ = 0.798 indicated the formation of random copolymers. T_g found to increasing feed content of PA. The antimicrobial studies showed that the copolymers are active against both Bacteria and Fungi.*

Keywords: *N-tert-amyl acrylamide, Phenyl acrylate, reactivity ratios, copolymer composition.*

INTRODUCTION

The determination of copolymer composition and reactivity ratios of the monomers is important in evaluating the specific application of copolymer[1]. The monomer reactivity ratios determined by conventional linearization methods are not always accurate and several non-linear methods have been attempted to determine their [2-4] . ^{1}H-NMR spectroscopic analysis has been established as a powerful tool for the estimation of copolymer composition[5,6] . Knowledge of the copolymer composition is an important step in the evaluation of its utility. Copolymer composition and monomer distribution in the copolymer are dependent on the reactivity ratios. The most common mathematical model of copolymerization is based on finding the relationship between the composition of copolymers and the composition of the monomer feed in which the monomer reactivity ratios are the parameters to be determined[7]. The accurate estimation of copolymer composition and determination of monomer reactivity ratios are significant for tailor-made copolymers with required physical and chemical properties and in evaluating the specific and application of the copolymers. The present article reports the synthesis and characterization of copolymers of N-tert-amyl acrylamide with Phenyl acrylate.

Synthesis of antimicrobial polymers is one of the leading frontiers of research in polymer science. With this view our work N-tert-amyl acrylamide was copolymerized with Phenyl acrylate with different feed ratio were prepared and characterized by ^{1}H-NMR spectroscopy. The reactivity ratios of monomers were determined by Fineman-Ross (FR), Kelen-Tudos (KT) methods.

Experimental

Preparation of N-tert-amyl acrylamide (NTA)

The monomer N-tert-amyl acrylamide was prepared by the reaction of tert-amyl alcohol with acrylonitrile. N-tert-amyl acrylamide was recrystallized in warm dry benzene. The white crystals have amp.91° C (Lit.91-92° C) and the yield was -87%. The monomer was confirmed by both ^{1}H- NMR and ^{13}C-NMR.

Copolymerization of NTA and PA

Copolymers of N-tert-amyl acrylamide (NTA) and Phenyl acrylate (PA) were prepared by free radical polymerization in DMF at 60^{0}C using AIBN as an initiator.(Scheme 1).

Characterization of copolymer spectra of Poly (NTA-co- PA)

The ^{1}H-NMR spectra of copolymers, poly (NTA-co-PA) is shown in Figure 1. The following peaks appear in the copolymer spectrum : at 1.1 -2.9 ppm for CH_2 group , at 2.7 ppm for backbone CH_2 , at 6.8-7.4 ppm due to PA aromatic protons and 7.7 for NH proton of NTA.

Determination of copolymer composition of Poly (NTA-co- PA)

The phenyl acrylate area is used to determine the copolymer composition. Resonance signal at 6.8-7.4 ppm corresponds to aromatic proton, and their integrated intensity of this peak is compared to the total intensities of all the peaks in the copolymer spectrum, which is a measure of their relative areas.
The copolymer compositions can be obtained using

$$X_{PA} = \frac{15A\ (aryl)}{5A_{total} + 7A(aryl)} \quad \text{------ (1)}$$

Where X= mole fraction and A= peak area.

Determination of Reactivity ratios

The reactivity ratios value for NTA (r_1) and PA (r_2) from the F-R plot (Figure 2), K-T plot (Figure 3) are given in Table3. The value of r_1 is greater than1 and r_2 is less than1. The system is lying in the range $r_2 < 1$, $r_1 > 1$. As $r_1.r_2$ is towards unity, the sequence of both monomeric units in copolymer chain is at random.

Thermal studies of Poly (NTA-co- PA)

TGA curves shows two stage decomposition regions for Poly (NTA-co-PA). The initial weight loss region appears around -100˚C due to moisture content. Weight loss at stage 1 is associated with dehydration of partially degraded amide groups; Maximum weight loss occurs at stage 2 around 300-400˚C indicates the main chain degradation and degradation of the polymer backbone. The DSC analysis indicates that the T_g values increases with increasing the content of PA in feed are given in table 4.

Antimicrobial Activity of Poly (NTA-co- PA)

Antimicrobial analysis was followed using standard agar well diffusion method to study the antimicrobial activity of compounds antimicrobial activity was evaluated by measuring the diameter of the zone of inhibition against the test microorganisms. DMSO was used as solvent control. Chloramphenicol was used as reference antibacterial agent. Amphotericin - B was used as reference antifungal agent. The tests were carried out in triplicates. The results are shown in Figure 6, the values are given in Table 5 and 6. The antimicrobial studies showed that these polymers are active against both bacteria and Fungi. Copolymers showed more activity than the control.

Scheme 1: Copolymerization of NTA and PA

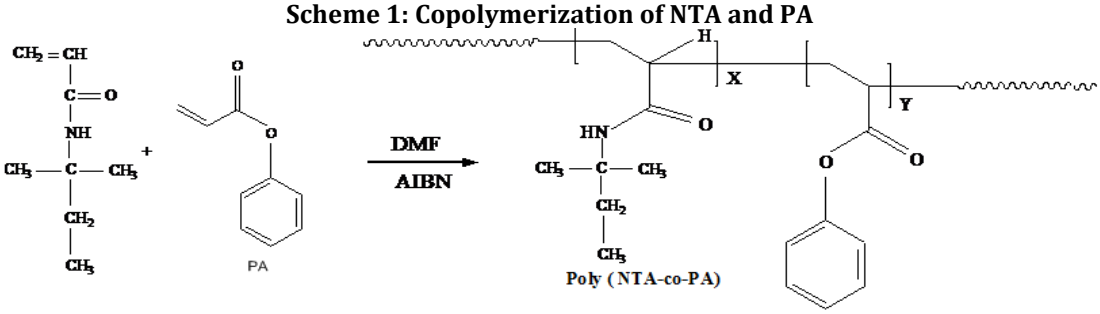

Figure 1:¹H-NMR spectrum of poly (NTA-co- PA) (a) 0.5:0.5

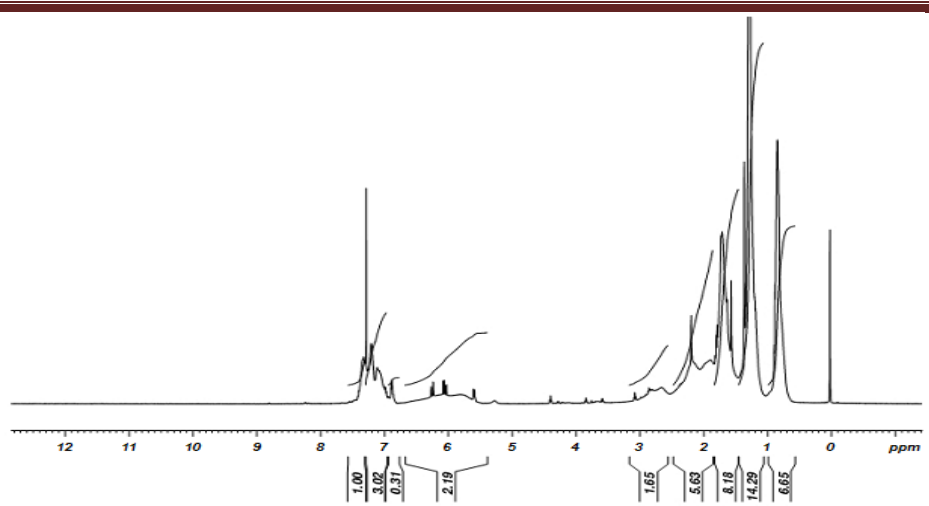

Figure 2 : Fineman-Ross plot for Poly (NTA-co- PA)

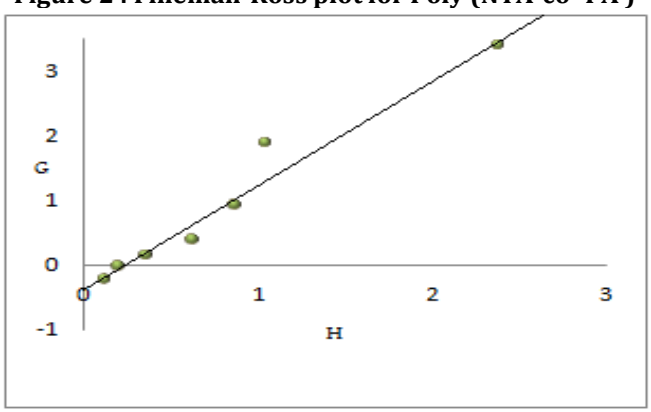

Figure 3: Kelen-Tudos plot for Poly (NTA-co- PA)

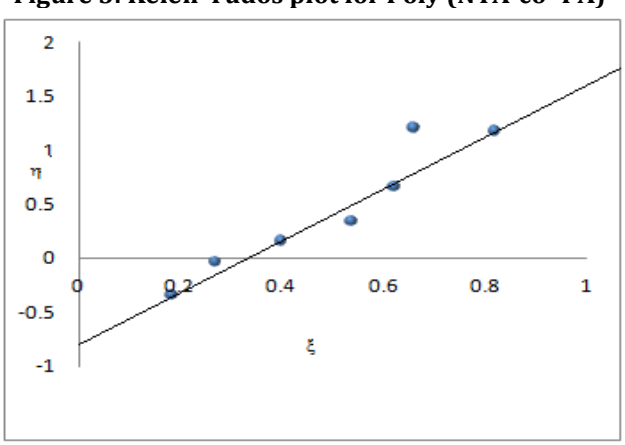

Table 1: Mole fractions of the copolymers of N-tert-amylylacrylamide (NTA) and (PA)

Mole fraction of NTA in feed, M_1	Mole fraction of PA in feed, M_2	Mole fraction of NTA in copolymer, m_1	Mole fraction of PA in copolymer, m_2	$F=M_1/M_2$	$f=m_1/m_2$
0.2	0.8	0.3450	0.6550	0.2500	0.5267
0.3	0.7	0.4850	0.5150	0.4286	0.9417
0.4	0.6	0.5588	0.4412	0.6667	1.2665

0.5	0.5	0.6200	0.3800	1.0000	1.6316
0.6	0.4	0.7224	0.2776	1.5000	2.6023
0.7	0.3	0.8398	0.1602	2.3333	5.2422
0.8	0.2	0.8708	0.1292	4.0000	6.7399

Table 2: Fineman-Ross and Kelen – Tudos parameters for the Copolymers of NTA and PA

G = F(f-1)/f	H=F²/f	η=G/(α+H)	ξ=H/(α+H)
-0.2247	0.1187	-0.3463	0.1829
-0.0266	0.1954	-0.0366	0.2694
0.1404	0.3513	0.1593	0.3986
0.3871	0.6129	0.3387	0.5363
0.9236	0.8646	0.6622	0.6200
1.8880	1.0383	1.2038	0.6621
3.4064	2.3746	1.1727	0.8175

α=0.53

Table 3: Reactivity ratios of NTA (r_1) and PA (r_2)

Methods	r_1	r_2	$r_1.r_2$
Fineman-Ross	1.60	0.41	0.65
Kelen-Tudos	1.55	0.41	0.64

Table 4: TGA data for Poly (NTA-co- PA)

Copolymers	Mole fraction of NTA, in feed	Mole fraction of PA, in feed	Mole fraction of PA, in copolymer	IDT (°C)	T_{50} (°C)	T_f (°C)	T_g (°C)
NTA-PA	0.70	0.30	0.1602	120	361	666	120
NTA-PA	0.50	0.50	0.3800	127	378	677	150
NTA-PA	0.30	0.70	0.5150	162	383	711	160
Poly-NTA		-	-	-	-		86.2

IDT: Initial Decomposition Temperature
T_{50} : decomposition temperature at 50% weight loss
T_f : final decomposition temperature
T_g : glass transition temperature

Table 5 : Anti bacterial activity of Poly (NTA-co- PA)

Sl. No	Copolymers	*Staphylococcus aureus(mm)*	*Escherichia coli (mm)*	*Pseudomonas aeruginosa (mm)*
1.	0.3 NTA:0.7 PA	14	No zone	17
2.	0.5 NTA:0.5PA	18	No zone	22
3.	0.7 NTA:0.3 PA	19	No zone	23
4.	Chloramphenicol	26	28	10

Table 6 : Anti fungal activity of Poly (NTA-co- PA)

Sl. No	Copolymers	*Aspergillus niger (mm)*	*Candida albicans (mm)*	*Candida tropicalis (mm)*
1.	0.3 NTA:0.7 PA	11	08	07
2.	0.5 NTA:0.5 PA	24	13	20
3.	0.7 NTA:0.3 PA	21	09	20
4.	Amphotericin - B	16	17	18

Figure 4 : Comparison of Zone of inhibition of Poly (NTA-co- PA)with bacteria

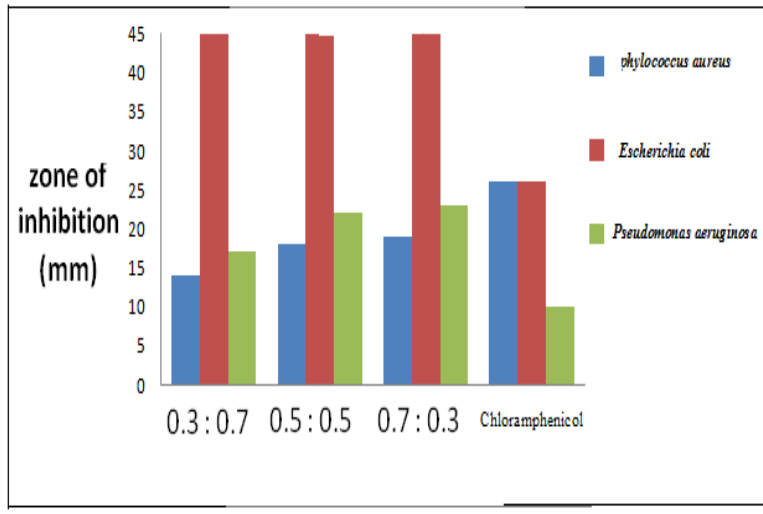

Figure 5 : Comparison of Zone of inhibition of Poly (NTA-co- PA)with fungi

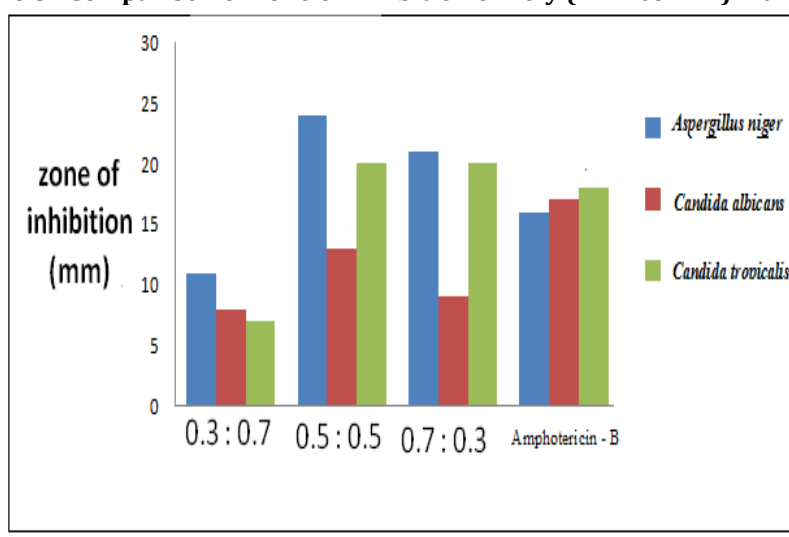

Figure 6: Antimicrobial studies of Poly (NTA-co- PA)

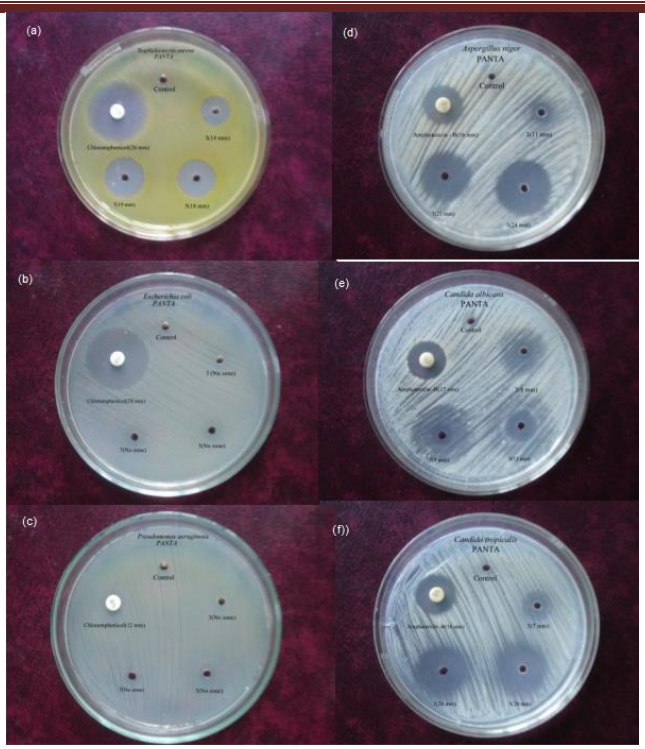

REFERENCES

1. S.Pitchumani, B.S.Rami Reddy and C. Rajadurai, Journal of Polymer Science: Polymer Chemistry Edition, 20,277(1982).
2. M. Dube, R.A. Sanayei, A. Penlids, K.F. O' Driscoll and P.M. Reilly, Journal of Polymer Science, 29, 703 (1991).
3. A.L.Polic, T.A Duever and A. Penlidis, Journal of Polymer Science Part A: polymer Chemistry,36, 813 (1998).
4. C. Hagiopol , O. Frangu and L. Dumitru , Journal of Macromolecular Science Chemistry Edition, 26, 1363 (1989).
5. P. Pazhanisamy , M. Ariff and Q. Anwaruddin , Journal of Macromolecular Science: Pure and Applied Chemistry, 34, 1045 (1997).
6. P. Pazhanisamy , P. Sulochana , Q. Anwaruddin and M. Ariff , Journal of Polymer Science parta: Polymer Chemistry, 35, 193 (1997).
7. R. Arshady, G.W.Kenner and A.W. Led, Journal of Polymer Science Polymer Chemistry Edition, 12 (9), 2017 (1974).

STUDY OF INHIBITION OF MILD STEEL CORROSION IN MINERAL ACID BY AQUEOUS EXTRACT OF PISONIA ALBA

N. Sridevi[1] & S. Rani[2]
[1]P.T. Lee CNCET, Oovery, Kanchipuram - 631 502
[2]Arignar Anna Govt. Arts College, Cheyyar - 604 407

ABSTRACT: *The corrosion of mild steel in 1N HCl is inhibited by Pisonia Alba extract have been studied using weight loss measurement, potentiodynamic polarization and electrochemical impedance spectroscopy(EIS). The inhibition effect increases with increase in concentration of Pisonia Alba extract and immersion period. The effect of temperature on mild steel corrosion in 1N HCl was studied at various temperatures from 298K to 343K. The corrosion is prevented by adsorption of inhibitor on mild steel obeys the Langmuir adsorption isotherm. The weight loss studies and polarization studies proved that the Pisonia Alba extract acted as a mixed type inhibitor. The FTIR and SEM analysis shows the corrosion inhibition property of the inhibitor.*

Keywords: *Corrosion inhibition, Pisonia Alba extract, Mild steel.*

1. Introduction:

Corrosion of metal and alloy structure causes major problem in industries. It results gradual decay of metallic parts of machines and engines, change of parts, damaging the products, breakdown of components, enhances the maintenance cost and also leads to environmental pollution [1]. Several protective measures are available to prevent corrosion; one of the best is by adding corrosion inhibitor to the corrosive environment [2-7]. Corrosion inhibitor is a substance which, when added in small concentration to an environment, minimizes or prevent corrosion [8]. Corrosion inhibitors prevent corrosion by forming various films at metal surfaces. The films are formed by adsorption, formation of bulky precipitate and / or formation of passive layer.

Various heterocyclic organic compounds [9-12] are studied as corrosion inhibitors. Although these compounds give good results, they are not environmentally safe, and also cause hazard to humans, aquatic life and other organisms in our earth.

To save the environment from pollution and hazard to living organisms, now-a-days many Eco-friendly corrosion inhibitors are developed from plants [13-23]. Also plants products are renewable resources, biodegradable, easily available and environmental safe.

Pisonia Alba (PS) commonly called the lettuce tree is erect shrub or small tree without spine. Leaves are alternate, opposite or clustered, blade mostly elliptic, 6-20 cm long, 4-10cm wide, soft hairless, leaf stalk 2-5 cm long. It origin at Andaman Islands and it moves to many parts of India. It belongs to family Nyctaginaceae (Bougainvillea family). Pisonia Alba has been used as medicinal plant for curing Arthristis/ Rheumatism, gastric problem, neck pain, obesity, back pain, algesia, ulcer and dysentery.

In this study Pisonia Alba extract was investigated as an eco-friendly corrosion inhibitor on mild steel in 1N HCl using weight loss method and electrochemical studies. The steel surface was analyzed by using SEM and FTIR spectroscopy.

2. Experiment:

2.1 Preparation of Pisonia Alba extract

Double distilled water, Analar grade Hydrochloric acid and ethanol are used for the present studies. The leaves of Pisonia Alba are washed and dried in shade. 50 g of dried leaves were refluxed in 1000ml of 1N HCl for 2 hrs. The refluxed solution was kept undisturbed overnight and filtered. The filtered solution was made up to 1000ml and used as 5% acid extract (stock solution). From this stock solution the various concentrations ranging from 0.05% to 1% extract have been prepared and all experiments were carried out.

2.2 Weight loss method

Mild steel samples with dimension of 5 x 2 x 0.2 cm and 0.2cm diameter hole near the top are used for the weight loss measurement. Each samples were rubbed with abraded paper for smooth surface, degreased with ethanol/ acetone and dried in desicator. Dried samples are dipped in 100ml of 1NHCl without and with inhibitors of different concentrations. Weight loss method has been carried out at different

temperatures via, 298K, 313K, 323K, 333K and 343K at 1hr immersion period. Each experiment was repeated thrice and the average was used. Inhibition efficiency was calculated by the following equation

$$I.E(\%) = \frac{W_1 - W_2}{W_1} \times 100$$

Where W_1 and W_2 are the weight loss in the absence and presence of inhibitor respectively.
Corrosion rate C_R (mg cm^{-2} h^{-1}) was calculated by following equation.

$$C_R = \frac{\Delta W}{St}$$

Where ΔW is weight loss (mg), t is the immersion time (h), S is surface area of specimen in (cm^2).

The relationship between the corrosion rate (C_R) and temperature (T) is given by Arrhenius equation.

$$C_R = K \exp(-E_a/RT)$$

Where E_a is the activation energy, K is the pre exponential factor, R is the gas constant and T is the absolute temperature.

The enthalpy and entropy of activation values are determined by following expressions

$$C_R = RT/Nh \exp(\Delta S^*/R) \exp(-\Delta H^*/R\,T)$$

By using the weight loss parameters, the mechanism of adsorption isotherm was studied. The surface coverage values are determined by using the expressions

$$\theta = (W_1 - W_2)/W_1$$

Where W_1 and W_2 are the weight loss in absence and presence of inhibitor respectively.

2.3 Electrochemical measurement

The electrochemical studies were made using three electrode cell system containing working electrode (mild steel) of $1cm^2$ exposed area, Ag-AgCl as reference electrode. The working electrode was abraded with different grades of emery paper, washed with water and degreased with acetone. Electrochemical analyzer, (CHI608E Instrument) was used to monitor the corrosion process. All electrochemical measurements were done in undisturbed condition at room temperature. EIS measurements were carried out in frequency range of 1Hz to 10^5Hz under potentiodynamic conditions with 0.01V amplitude. The charge transfer resistance (R_{ct}) values were obtained from diameter of the semicircle of Nyquistplotsand double capacitance were calculated by following equation

$$C_{dl} = \frac{1}{2\pi f_{max} R_{ct}}$$

Where f_{max} is the maximum frequency of Nyquist plot and R_{ct} is charge transfer resistance. The inhibition efficiency is calculated from charge transfer resistance values using the following equation. $R'_{ct} - R^{\circ}_{ct}$

$$\eta\% = \frac{R'_{ct} - R^{\circ}_{ct}}{R'_{ct}} \times 100$$

Where R°_{ct} and R'_{ct} are the charge transfer resistance in absence and presence of inhibitor respectively.

Tafel curves were obtained by changing the electrode potential from -200 to +200mV corrosion potential for different sweep rates. The corrosion current densities (I_{corr}) is obtained by extrapolation of Tafel anodic and cathodic curves. The inhibition efficiency is calculated by following equation.

$$\eta\% = \frac{I^{\circ}_{corr} - I_{corr}}{I^{\circ}_{corr}} \times 100$$

Where I°_{corr} and I_{corr} are corrosion current in absence and presence of inhibitor respectively.

2.4 Fourier Transform Infrared Spectroscopy

The mild steel specimen was dipped in inhibitor solution for one day. Then they were rinsed with distilled water, dried and scrapped. FTIR spectra were taken forscrapped rust power and dried inhibitor powder.

2.5 Scanning Electron Microscope

The mild steel specimens were dipped in presence and absence of inhibitor for 1hr. Then they were removed, rinsed with rectified sprit, dried and used for surface morphological analysis.

3. Result and discussions

3.1 Weight loss method

3.1.1 Effect of concentration

By weight loss method, the various parameters such as corrosion rate (CR), inhibition efficiency (IE) and surface coverage (θ) are calculated. Weight loss measurements were studied in 1N HCl in absence

and presence of inhibitor extract of various concentrations ranging from 0.05 to 0.1%. Inhibition efficiency rises with respect to raise in concentration of inhibitor up to 98.03%at a concentration of 0.8% inhibitor extract. This shows corrosion is prevented and inhibition efficiency enhances with rise of inhibitor concentration for mild steel in 1N HCl medium.

3.1.2 Effect of immersion time

To study the stability of inhibitor, weight loss method was carried out in presence and absences of extract for all concentration ranging from 0.05 to 0.1 % at immersion period of 0.5hrs to 72 hrs in 1N HCl medium. The effect of inhibition efficiency with time is shown in Figure 1. This shows that inhibition efficiency enhances with increase in time and reaches maximum value at 24 hrs and then almost stable. This indicate that good adsorption of inhibitor extract on mild steel surface occurs at 24 hrs.

3.1.3 Effect of temperature

To know the effective adsorption of inhibitor, weight loss measurements were carried out in the presence and absence of inhibitor extract on mild steel in 1N HCl at different temperature from 298K to 343K. Table 1 and 2, present inhibition efficiency and corrosion rate of inhibiton of mild steel in the presence of Pisonia Alba extract. It shows that rise in inhibition efficiency with rise in temperature. This indicates that increased rate of oxidation of mild steel and chemical adsorption of mild steel with temperature [23]. Table: 2 shows that the rate of corrosion raises with rise in temperature in the absence of inhibitor. It clearly indicates that the presence of inhibitor decreases the corrosion rate.

By Arrhenius equation [24, 25, 26] the corrosion rate of mild steel with temperature is known. Figure 2 shows the graph of $C_R \; vs \; 1/T$. The values of (E_a) Activation energy and K are computed from slopes and intercepts respectively and presented in Table 3. The activation energy falls with raise in concentration of inhibitor, indicates that the adsorption is chemisorption [27] and film formed by chemical process [23].

Figure 3 shows the graph of $\log(C_R/T) \;\; vs \; 1/T$. From the slopes and intercepts the values of ΔH^* and ΔS^* are determined respectively. Table: 3 shows activation parameters, i.e E_a, ΔH^* and ΔS^*. The ΔH^* value is positive for both presence and absence of inhibitor indicates that endothermic reaction of mild steel corrosion [28]. The ΔS^* value is negative for both presence and absence of inhibitor indicates that activation step in rate determining step represents an association rather than dissociation, randomness of system decreases by adsorption[29] and stable layer of inhibitor is formed on mild steel [30].

3.1.4 Adsorption isotherm:

The corrosion is prevented by adsorption of inhibitors on mild steel surface. Hence to know the mechanism of adsorption, weight loss parameters such as surface coverage (θ) are determined. Many attempts are made to find the adsorption isotherm, from that Langmuiradsorption isotherm was found to be the best isotherm. Hence θ, is related to concentration of inhibitor by Langmuir adsorption isotherm.

$$\frac{C}{\theta} = \frac{1}{K_{ads}} + C$$

Figure 4 shows the graph of $C/\theta \; vs \; C$, from the graph the slope of straight line is equal to unity. This indicates that adsorption of inhibitor extract on mild steel is Langmuir adsorption isotherm.

According to Langmuir adsorption isotherm, the solid surface adsorbed each one species at each fixed site. The adsorption species does not interact with each other and energy of adsorption is independent of degree of freedom.

By equation,

$$K_{ads} = \frac{1}{55.5} \exp\left(\frac{-\Delta G_{ads}}{RT}\right) \text{and}$$

$$\log K_{ads} = \log\left(\frac{1}{55.5}\right) - \frac{\Delta H_{ads}}{2.303RT} + \frac{\Delta S_{ads}}{2.303R}$$

The thermodynamic parameters such as ΔH_{ads}, ΔS_{ads} and ΔG_{ads} are calculated, Figure 5 shows the graph of $\log K_{ads} \; vs \; 1/T$,from graph, slope and intercept obtained is used to calculate ΔH_{ads} and ΔS_{ads}values respectively. Thermodynamic parameters are tabulated in Table: 4. it is evident that the values ΔG_{ads} around -20kJmol^{-1} indicates that electrostatic interaction between the inhibitor molecule and metal steel. The values of ΔG_{ads} confirm that adsorption is physisorption [31].

The negative values of ΔH_{ads} confirmed that the reaction was exothermic process. The positive values ΔS_{ads} indicates that the reaction was spontaneous and feasible [32].

3.2 Electrochemical studies

From the studies of electrochemical impedance the Nyquist plot obtained is shown in Figure 6. Various parameters are obtained namely the double layer capacitance (C_{dl}), charge transfer resistance (R_{ct}) and inhibition efficiency are computed from Nyquist plot and tabulated in Table 5.

In Nyquist plot the diameter of semi-circle raises with raised in inhibitor concentration, indicates that corrosion resistance of the mild steel in presence of inhibitor is increases with increased in concentration. From Table 5 it is evident that both charge transfer resistance and inhibition efficiency raises and fall in (C_{dl}) value with raised in inhibitor concentration indicates that inhibitor molecules act by adsorption mechanism at mild steel/acid interface and enhance the thickness of electric double layer [33]. Further, raised (R_{ct}) values indicates that formation of productive film at the mild steel surface.

From the study of potentiodynamic polarization, the Tafel plot obtained for sweep rate 10mVS^{-1} are shown in Figure 7. The various parameters are calculated and Tafel plots are tabulated in Table 6. It is evident that I_{corr} falls with raise of concentration of inhibitor, which indicates that corrosion inhibition effects on mild steel in the presence of inhibitor, is due to adsorption of inhibitor on mild steel surface. From the slope of polarization curve it has been noted that anodic and cathodic reactions are inhibited. The anodic Tafel slope is greater than cathodic slope indicates that anodic polarization is more pronounced than cathodic polarization. The change in anodic Tafel slope and cathodicTafel slope indicates that there is a change in anodic dissolution as well as cathodic hydrogen evolution respectively and inhibition action is mixed one.

Further, the E_{corr} values does not change significantly with current densities and only small shift towards cathodic region i.e.,$E_{corr} > 69mV$ indicates that Pisonia Alba inhibitor act as a mixed type inhibitor.

3.3 Fourier transform infrared spectroscopy

The type of bonding for organic inhibitors adsorbed on the metal surface was determined by powerful FTIR spectro photometer. In the present study FTIR spectra data's supports the fact that inhibition of mild steel in acid media is by adsorption of inhibitor molecules on metal surface. The prominent peaks are given in Table 7 and FTIR spectra obtained shown in Figure 8. It can be established that corrosion inhibition of mild steel in 1N HCl solution by Pisonia Alba extract was due to adsorption of inhibitor molecules on mild steel surface.

The main constituent present in the Pisonia Alba extract are Alkoloids, Flavonoids, Saponins and glycosides whose structuresare shown in Figure 9 having multiple bonds by which they adsorbed on mild steel surface. The good performance of Pisonia Alba extract is due to huge molecule constituent's which hide the mild steel surface and protect from corrosion [34].

3.4 Scanning Electron Microscope

The SEM images of mild steel in absence and presence of 1% of Pisonia Alba extract was shown in Figure 10 From the images, it was found that the surface of mild steel has pits, pores, grains and cracks, when exposed to the absence of inhibitor. In presence of inhibitor, the images was found that they are minimized on the mild steel surface, which confirmed that the formation of protective film over the surface of mild steel.

4. Conclusion

From the current work we obtained following conclusions.

- The inhibition efficiency of Pisonia Alba increases with increase in concentration of inhibitor.
- The maximum inhibition efficiency is 97% in HCl medium at 0.1%.
- The corrosion was inhibited by adsorption mechanism following Langmuir adsorption isotherm.
- The electrochemical studies have good agreement with weight loss method data.
- The potentiodynamic polarization studies prove that Pisonia Alba acts as mixed type inhibitor.
- From FTIR and SEM analysis the corrosion is prevented by adsorption of inhibitor on mild steel surface.

Reference:

1. Vasudha, V.G.,&ShanmugaPriya,K.(2013).PolyalthiaLongifolia as a Corrosion Inhibitor for Mild steel in HCl solution. Res. J. Chemical Sciences, 3(1), 21 – 26.
2. Bregman,J. I. (1963). Corrosion Inhibitor. London, Collier Mac Millan Co.
3. Eldredge,G.G., & WarnerJ.C. (1948).The Corrosion Hand book. New York, Wiley.
4. Nathan,C.C.(1973). Corrosion Inhibitors.Houstaon, Texas, Nationl Association of Corrosion Engineers (NACE).
5. Putilova, N., Balezin S.A., & Barannik V.P.(1966). Metallic Corrosion Inhibitor. London, Pergamon Press.
6. Brooke, M. (1962). chem. Eng 69 134.
7. Ranney, M.W.(1976). Inhibitors- Manufacture and Technology. New Jersey, Noyes Data Corp.
8. Riggs, O. L., Jr, in Nathan, C.C. (Ed).(1973). Corrosion Inhibitors.NACE, Houstan, Tx, P.11
9. Bentiss, F., & Traisnel, M., Lagrenee, M. (2000). Corros. Sci, 42 127.
10. Arab, S. T.,& Noor, E. A. (1993). Corrosion, 49 122.
11. Luo, H., Guan, Y. C., & Han, K.N.,(1988). Corrosion, 54 721.
12. Lagrenee, M., Mernari, B., Chaibi, N., Traisnel, M., Vezin H., & Bentiss ,F. (2001). Corros. Sci.43 951.
13. Kil bourn, B. T. (1985). Cer. Eng Sci. Proc. 6 1331.
14. Bethencourt, M., Botana, F.J. , Calvino, J. J. & Marcos, M. (1998). Corros. Sci. 40 1803.
15. Arenas, M. A., Onde, A. & Damborenea, J.de. (2002). Corros. Sci. 44 511.
16. El-Sawy, S. M., Abu – Ayana, Y. M. & Abdel – Mohdy F.A. (2001) Ant – Corros. Meth. Mat. 48 227.
17. Cano, E., Pinilla, P., Pollo J. L. & Bastidas, J.M. (2003). Mater. Corros.54 222.
18. Dong – Jin Choi, Yong – Wook Kim & Jung – Gu Kim. (2001). Mater. Corros.52 697.
19. Moretti, G., Guidi, F. & Grion, G. (2004). Corros. Sci. 49 387.
20. Sethuramaan, M. G., (2008). Materials Letters 62 113.
21. Sethuraman, M. G. & Bothi Raja, P. (2005). Pigment and Resin Technology, 34, 327.
22. Bothi Raja P. & Sethuraman, M.G. (2007). Surface Review and letters. 14 1157.
23. Schoor, M. & Yahalm, J. (1972). The significance of the energy of activation for the dissolution of reaction of metal in acids.Corros.Sci, 12 (11), 867-868.
24. Quraishi, M. A. and Khan, S. (2005). Thiadiazoles – A potential class of Hetercyclic inhibitors for prevention of mild steel corrosion in Hydrochloric acid solution. Ind. J. Chem. Technol, 12, (5), 576- 581.
25. Breslin, C. B. & Carrol, W.M.(1993) The activation of aluminium by indium ions in chloride, bromide and iodide solutions. Corros. Sci, 34 (2), 327-341.
26. Khedr, M. G. A & Lashien, M.S. (1992). The role of metal cations in the corrosion and corrosion inhibition of aluminium in aqueous solutions.Corros.sci, 33 (1), 137- 151.
27. Kasthuri, P.K &Arulnantham, A. (2001) Inhibition effect of eco-friendly extract of Euphorbia hirta on dissolution of mild steel.
28. Guan, N.M, Xuoming, L. & Fei, L. (2004). Synergistic inhibition between o-phenanthroline and chloride ion on cold rolled steel corrosion in phosphoric acid, Mater. Chem. Phys, 86, (1), 59-68.
29. Abd-El- Nabey, Khamis, E. Ramadan, M. and El-Guindy, A. (1996). Application of the Kinetic-Thermodynamic model for Inhibition of acid corrosionof steel by Inhibitors containing Sulfur and Nitrogen. Corrosion, 52, (9), 671 - 679.
30. Yurt, A., Balaban, A., Kandemir, S.U., Bereket, G., Erk, (2004). Investigation on some Schiff bases as HCl corrosion inhibitor for carbon steel. Mater. Chem. Phys., 85, (2-3), 420 – 426.
31. G. Moretti, F.Guidi, and G, Grion, (2004). Trptamine as a green iron corrosion inhibitor in 0.5M deaerated sulphhuricacd, Corrosion Science ,46(2), 387-403.
32. Bhajiwala, H. M. & Vashi, R.T. (2002). Ethylamines as corrosion inhibitors for zinc in HNO_3/HCl binary mixture. Bulletin of Electrochemistry, 18(6), 261-266.
33. Vashi, R.T & Champaneri, V. A. (1997). Electrochem, 13, 353-360.
34. Vashi, R.T & Champaneri, V. A. (1997). Electrochem, 13, 353-360.
35. Trabenelli, G&Mansfeld,F. (1987). Corrosion Mechanisms.109.

Table 1 : Inhibition efficiency of Pisonia Alba extract on mild steel with different temperature and concentration at 1h time.

Conc.,(%)	Inhibition efficiency (%)				
	298K	313K	323K	333K	343K
0	-	-	-	-	-
0.05	76.93	75.74	76.73	71.667	50.26
0.1	76.82	87.87	85.50	82.14	59.04
0.2	77.92	87.87	87.17	70.10	72.64
0.4	77.92	92.96	92.70	91.00	88.89
0.6	78.04	94.05	93.10	91.51	91.47
0.8	77.92	93.82	92.11	92.18	91.50
1.0	82.34	97.03	95.66	90.10	92.55

Table 2 : Corrosion rate of Pisonia Alba extract on mild steel with different temperature and concentration at 1h time.

Conc.,(%)	Corrosion rate (mg $cm^{-2}h^{-1}$)				
	298K	313K	323K	333K	343K
0	0.0505	0.2438	0.5658	1.0713	1.1239
0.05	0.0117	0.0591	0.1317	0.3035	0.9575
0.1	0.0184	0.03	0.082	0.1914	0.7884
0.2	0.0112	0.029	0.0725	0.3202	0.5267
0.4	0.0112	0.0173	0.0413	0.0965	0.2137
0.6	0.0110	0.0145	0.0391	0.0909	0.1640
0.8	0.0116	0.0150	0.0446	0.0837	0.1635
1.0	0.0089	0.0007	0.0246	0.0106	0.1434

Table 3 : Activation parameter for mild steel for different concentration of Pisonia Alba extract

Conc., (%)	Ea* KJ mol^{-1}	ΔH* KJ mol^{-1}	ΔS* KJ mol^{-1}
0	68.73	225.25	-196.90
0.05	80.77	273.54	-196.78
0.1	66.77	228.42	-196.93
0.2	60.46	211.65	-196.98
0.4	65.58	237.62	-196.93
0.6	52.29	190.34	-197.07
0.8	50.39	179.80	-197.11
1	56.90	202.12	-197.04

Table 4 : Thermodynamic parameter of Pisonia Alba extract from Langmuir adsorption isotherm.

Inhibitor	ΔH_{ads} KJ mol^{-1}	ΔS_{ads} KJ mol^{-1}	ΔG_{ads} KJ mol^{-1}
Pisonia Alba	*-16.074*	*14.014*	*-4.192*

Table 5 : Impedance parameters of mild steel in absence and presence of Pisonia Alba extract

Con (%)	Rct(Ωcm^2)	Cdl ($\mu F/cm^2$)	I.E (%)
0	6.247	9.911	--
0.05	8.078	7.003	22.67
0.1	76.392	0.0731	91.82
0.2	122.001	0.0281	94.88
0.4	65.50	0.0966	90.46
0.6	133.747	0.0241	95.31
0.8	98.53	0.044	93.66
1.0	153.632	0.065	95.93

Table 6 : Potentiodynamic polarization parameters of mild steel in absence and presence of Pisonia Alba extract for 10 mv sweep rate.

Con (%)	E_{corr} (mV)	I_{corr} mA/cm2	b_c	b_a	linear potential	IE %
0	-371	3.579	6.307	7.937	8.5	
0.05	-388	0.2103	9.33	10.428	104.6	94.12
0.1	-388	0.2582	8.7	12.134	80.8	92.79
0.2	-379	0.1393	8.801	12.0475	146.7	96.11
0.4	-390	0.1322	7.232	7.949	216.6	96.31
0.6	-389	0.1107	9.087	12.712	180.2	96.91
0.8	-385	0.1722	8.52	12.43	120.5	95.19
1	-394	0.1148	9.008	12.522	175.9	96.79

Table 7 Prominent peaks obtained from FTIR spectroscopy forPisonia Alba extract

Band assignment	wave number (cm^{-1})	
	Before inhibition	After inhibition
O-H stretching	3429	3356
C-H stretching	---	2924
C=O stretching	1629	1633
CH_3 asymmetric bending	1383	1383
C-N stretching	1316	
C-O-C asymmetric stretching	1113	1161
C-O stretching	---	1033
C-O stretching	780	---
C-C out of plane bending	665	676
	517	---
Fe - O stretching	---	479

Figure 1 : Inhibition efficiency of inhibitor vs time

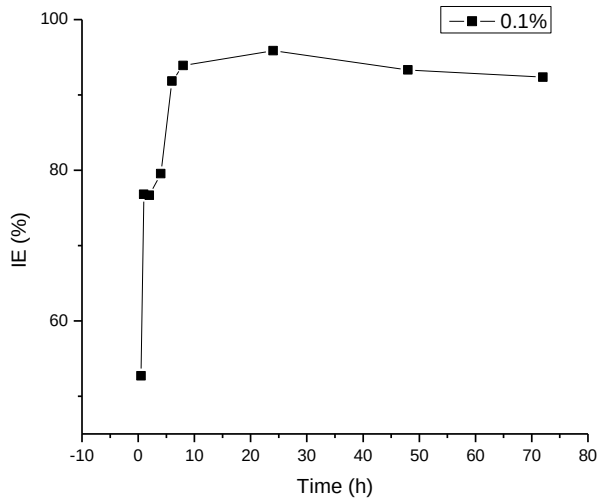

Figure 2 : $Log\ C_R\ vs\ 1/T$

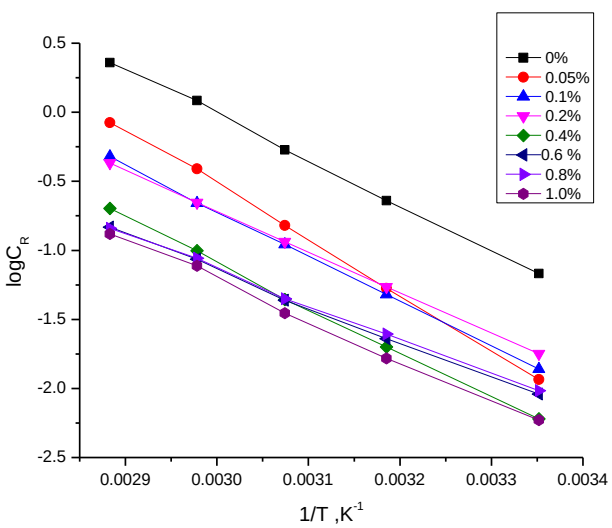

Figure 3 : $log\ C_R/T\ vs\ 1/T$

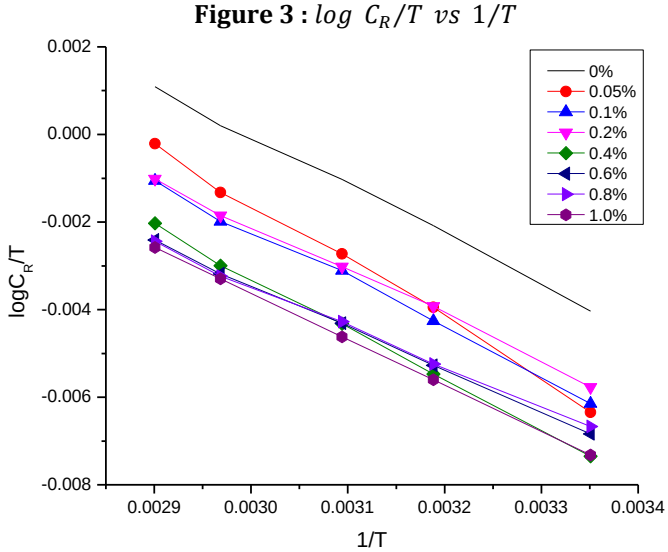

Figure 4 : $C/\theta \ vs \ C$

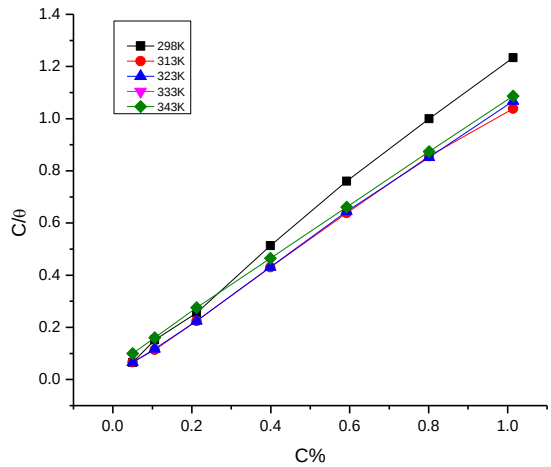

Figure 5 : $log \ K_{ads}/T \ vs \ 1/T$

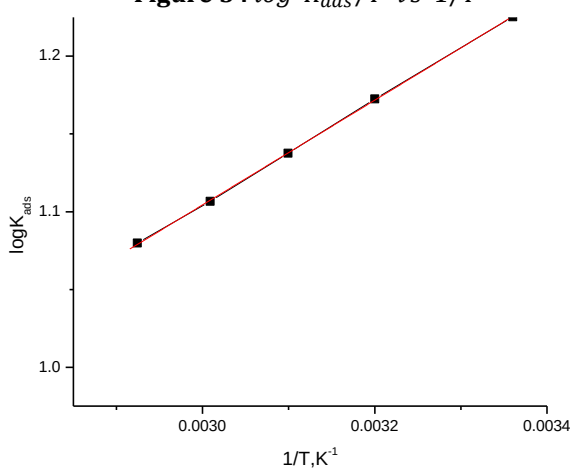

v

Figure 6 : Impedance diagaram of mild steel for various concentrations of Pisonia Alba extract

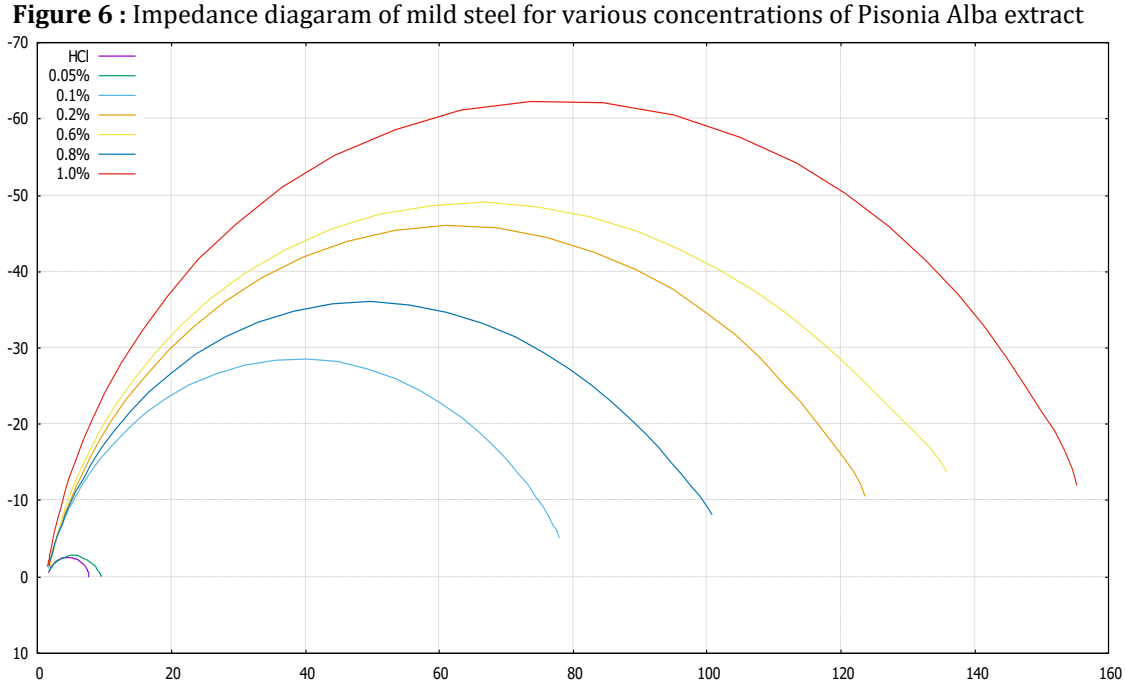

Figure 7 : Potentiodynamic polarization curves of mild steel for various concentrations of Pisonia Alba extract at sweep rate 10mV

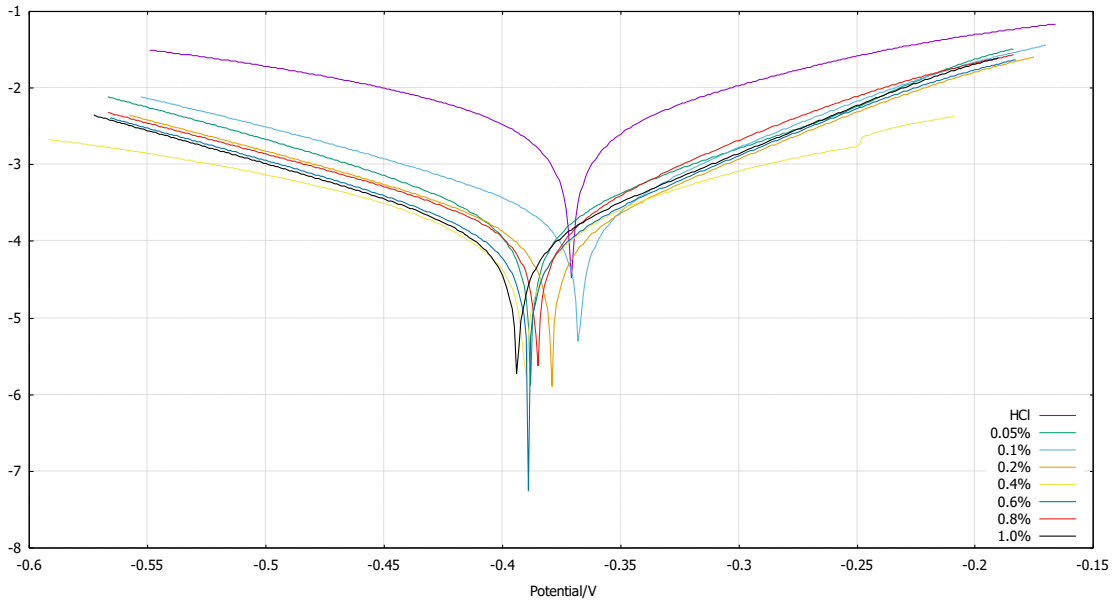

Figure 8 : FTIR spectra of Pisonia Alba Extract and Rust powder

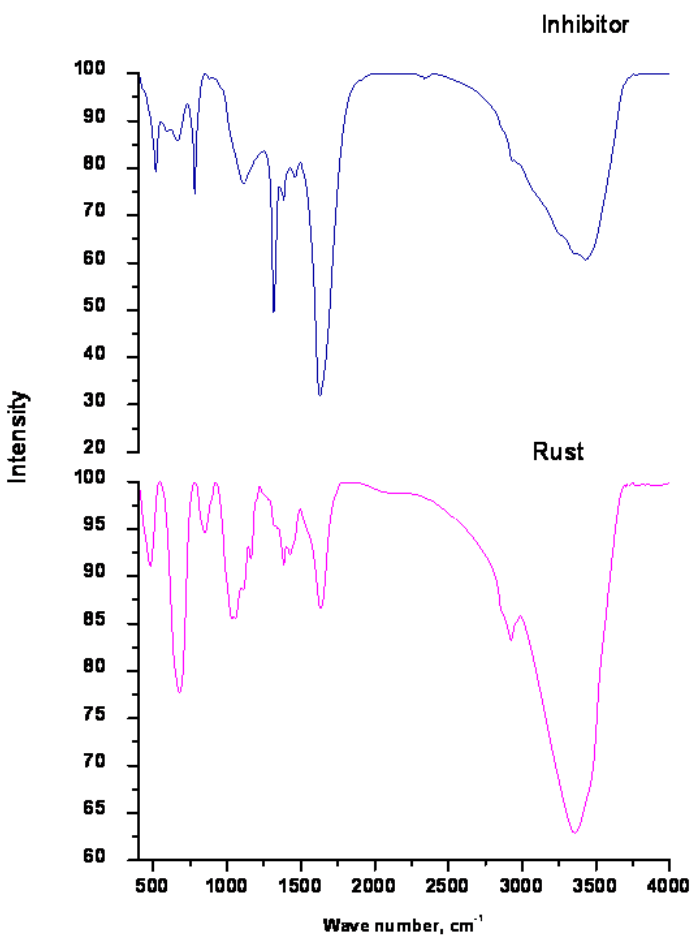

Figure 9 : Structure of main constituent of Pisonia Alba extract.

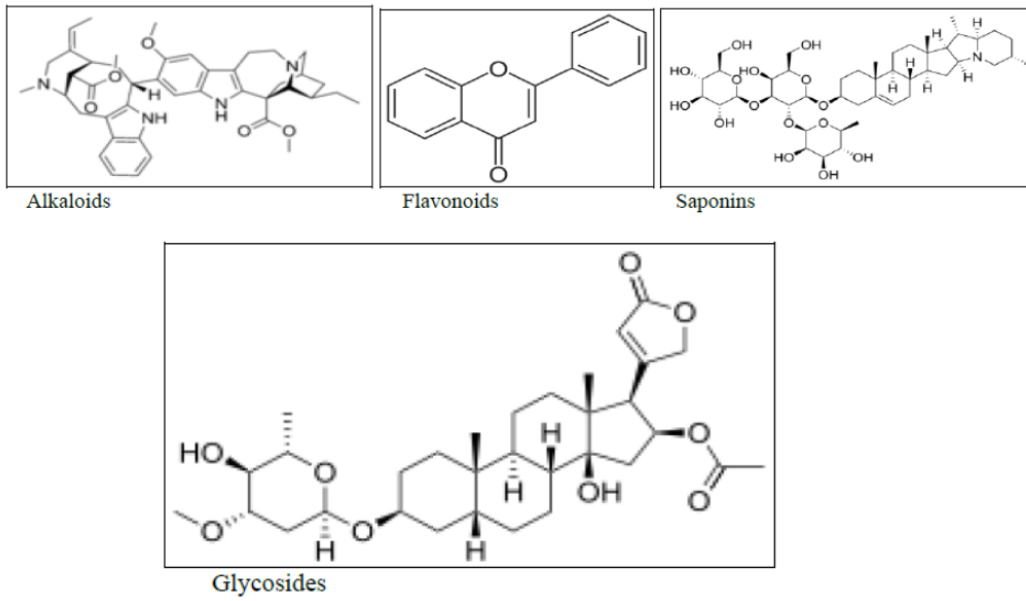

Figure 10 : Scanning electron micrograph of mild steel after exposure to (a) 1N HCl and (b) 0.1% Pisonia Alba extract.

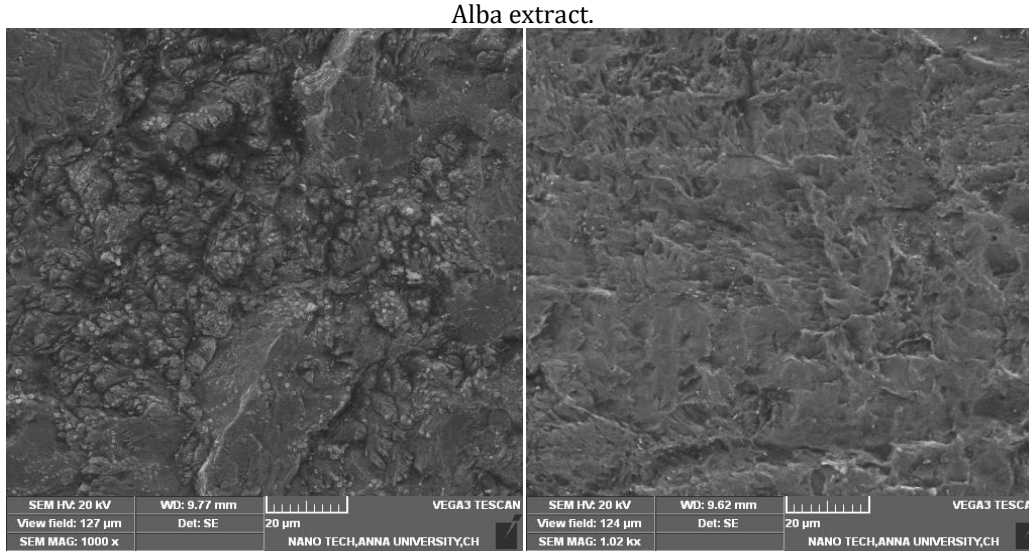

(a) (b)

GREEN SYNTHESIS OF ZINC OXIDE NANOPARTICLES USING PEEL EXTRACT OF CARICA PAPAYA AND THEIR BIOLOGICAL ACTIVITY

M.Bharathi, S.Shree devi & CT. Ravichandran
PG and Research Department of Chemistry,
Arignar Anna Government Arts College, Cheyyar – 604 407

ABSTRACT: *Nanotechnology, one of the scientific fields and direct most active area of research in all the branches of science. Generally it coalesce the information of chemistry, physics, biology and medicine. Nanotechnology deals productions and stabilizations of various nanoparticles having a size of 1 – 100 nm in one dimension acting a major role. Green synthesis of metal oxide nanoparticles is gaining considerable interest due to the use of environmentally friendly reactants and room temperature synthesis. This is the most preferred method of preparation as it makes use of pollution free chemicals and encourage the use of non-toxic solvents such as water and plant extracts. The present study is proposed with an objective to synthesize ZnO nanoparticles by the eco-friendly green synthesis using environmentally begin carica papaya peel extract. The obtained ZnO nanoparticles have been characterized by UV-vis spectrum, fourier transform infrared (FTIR), X-ray diffraction (XRD), and scanning electron microscopy (SEM) studies. The prepared nanoparticles were screened for In-vitro antibacterial, antifungal and antioxidant activity.*

Keywords: *Zinc Oxide Nanoparticles, Carica papaya peel extract, Green synthesis, X-ray diffraction. Scanning Electron Microscopy and Antimicrobial activity.*

INTRODUCTION

Nanotechnology is define as the treatment of matter through certain chemical, physical and biological processes to create materials with exact properties which can be used in several applications. The impact of nanotechnology extends from its medical, ethical, mental, legal and environmental applications to fields such as engineering, biology, chemistry, computing, materials science and communications. The major benefits of nanotechnology include improved manufacturing methods, physical enhancement, better food production methods, water purification systems, large scale infrastructure. Nanomedicine and nutrition [1].

Nanotechnology may be able to create many new materials and devices with a vast range of applications, such as in nanomedicine, nanoelectronics, biomaterials energy production, and consumer products [2].

The nanotechnology revolution is inevitably good. This misconception results from a preoccupation with the crucial contributions that technology makes to the comfort, security, healthfulness and longevity of people's lives in industrialized nations [3]. Hence they find a variety of applications in the areas of energy, agriculture, information, heavy industries and consumer goods. It is a very broad area comprising nanomaterials, nanotools and nanodevices [4]. The improvement of new chemical or physical methods has resulted in environmental contaminations, since the chemical process results in large amount of hazardous by products. So there is a need of "green synthesis" that they are safe, eco-friendly, and non-toxic to the environment. So there is no use of high pressure, temperature, and toxic materials[5].

Nanoparticles are microscopic particles and are extremely small of about 1-100 nanometres (nm) in size with a interfacial layer. A bulk materials should have constant physical properties regardless of its size but at nano-scale size dependent properties are often observed. In case of nanoparticles synthesis, bottom-up or self assembly procedures involve a homogeneous system wherein catalysts are producing nanostructures affected by catalyst properties, reaction medias and conditions (e.g. solvents, stabilizers, temperature)[6]. Engineered nanoparticles are intentionally designed and created with physical properties tailored to meet the needs of specific applications. In the case of quantum dots or pharmaceutical drugs they can be components later incorporated into separate end products, such as carbon black in rubber products Nonengineered nanoparticles, on the other hand, are unintentionally generated or naturally produced, such as atmospheric nanoparticles created during combustion. With nonengineered nanoparticles, physical properties also play an important role as they determine whether or not ill effects will occur as a result of the presence of these particles[7].

Nanoparticles can be in the form of nanocrystals, nanopowders or nanoclusters and the particles act as a bridge between bulk materials and atomic or molecular structures. Nanoparticles are with one half hydrophilic and other half hydrophobic which are termed as janus particles. Nanomaterials can be defined as the "materials with any external dimension in the nanoscale or surface structure or having internal

structure in the nanoscale". Nanomaterials research takes a materials science-based approach to nanotechnology, leveraging advances in materials metrology and synthesis which have been developed in support of microfabrication research.

ZnO nanoparticles have gathered the increasing interest of the scientific and industrial community due to diverse application in solar energy conversion, sensors, catalysis, cosmetics, paints, fibers, drug-delivery, antibacterial and luminescence properties[8].

The synthesis of zinc oxide nanoparticles (ZnO NPs) achieved by various methods such as reaction of hydrothermal synthesis, zinc with alcohol, precipitation method[9].

For example, nanoparticles can be induced to merge into a solid at relatively lower temperatures, often without melting, leading to improved and easy-to-create coatings for electronics applications (eg, capacitors). Typically, nanoparticles possess a wavelength below the critical wavelength of light. This renders them transparent, a property that makes them very useful for applications in cosmetics, coatings and packaging. Metallic nanoparticles can be attached to single strands of DNA non destructively. This opens upavenues for medical diagnostic applications metal oxides have also been employed as sorbents for environmental pollutant.

In the domain of nanotechnology, oxide nanoparticles can exhibit unique chemical properties owing to their limited size and high density of corner or edge surface sites. A number of physical and chemical preparative methods for accessing nanostructured oxides are on records among the metal oxides, nano ZnO exhibits wide band gap (-3.4eV) and large exciton binding energy (60 meV) and thus is considered most promising candidate for nano optoelectronics, sensors, transistors, nanopiezoelectronics and UV-detection[10].

MATERIALS AND METHODS

MATERIALS

All chemicals and reagents used as starting material for the research work were of analytical grade (AR) and of the highest purity available. Fresh Carica papaya fruits were collected locally in the market. *Culex, quinquefasciatus* larvae were produced from Zonal Entamological Unit, Villupuram. Bacteria and Fungi strains were received from Microlab Vellore.

Ultraviolet-Visible spectroscopy

The Ultraviolet-Visible spectra recorded on a SYSTRONICS 2201 spectrometer using DMSO in the wave length range of 800-200 nm.

FTIR Spectroscopy

The FTIR spectrum was taken using SHIMADZU spectrometer in 4000 - 400 cm-1 using KBr pellet.

X-Ray Diffraction analysis

X-ray diffractogram of samples were obtained using XRD-SHIMAZUXD-D1, Ni-filter and Cu Ka radiation source.

Scanning Microscopy Analysis (SEM Analysis)

SEM Analysis of ZnO Nanoparticles was done by using ISM-66101V Machine the scanning Electron Microscopic.

Preparation of the peel extract

The fresh Carica papaya peel was collected. The Carica Papaya peel were thoroughly washed several times using normal water and then followed by distilled water to remove impurities, the cleaned peel were subsequently dried under sunshade to remove moisture completely. Leaves were powdered by using mechanical grinder and then stored. 5 g of powdered leaves were taken in beaker along with 100 ml of double distilled water and allowed to boil at 60°C for 20 min, then it was cooled down to room temperature. The extract turned brown. The prepared solution was filtered through Whatman No.1 filter paper to get clear solution and filtrate was stored at 4°C for further works.

Preparation of Zinc sulphate solution

An accurate amount of 0.1 M zinc sulphate solution was prepared by dissolving 2.875 g of zinc sulphate in 100 mL of double distilled water.

Synthesis of Zinc oxide nanoparticles

As per the standard procedure[11-13] ZnO NPs were prepared. 80 mL of 0.1M zinc sulphate was mixed with 20 mL of leaves extract under continuous stirring. The colour of the solution changes from colourless to light yellow. Finally the reaction mixture was kept under stirring for about 3 hrs and colour change takes place from yellow to bright yellow colour. This solution was incubated for about 24 hrs at 4°C. The colourless residue was settled at the bottom of the beaker, it was carefully collected and dispersed in

double distilled water to eliminate unwanted material. The solution was filtered, dried and packed for characterization purpose.

Antimicrobial studies (*in vitro*)

In vitro antimicrobial studies against bacterial strains such as *Escherichia coli, Staphylococcus aureus* and fungal strains such as *Aspergillus niger, Rhizopus and Mucor Mycosis* were studied for the prepared nanoparticles by agar well diffusion method. The microorganisms were inoculated on Muller Hinton Agar and spread uniformly using sterile spreader in petri plates. 50 µL and 100 µL of the freshly prepared ZnO nanoparticles (1 mg / mL) in DMF were used as positive control and DMF alone taken as negative control. The plates were allowed to stand for 1 h at room temperature for the diffusion of the substances. Before the growth of organism commenced, the plates were incubated at 37°C for 4 h and inhibition of microbes was determined by measuring the diameter of zones.

Antioxidant activity

Oxidation is chemical reactions which produce free radicals results with many diseases. A substance that inhibits oxidation of other molecules is called antioxidant. Hydrogen peroxide scavenging activity is one of the best method to study the antioxidant property. [14,15] A solution of hydrogen peroxide (40 mM) was prepared in phosphate buffer (50 mM, pH 7.4). The concentration of hydrogen peroxide was determined by absorption at 230 nm using a spectrophotometer. 2 mg/mL in DMF of prepared CuO nanoparticles were added to hydrogen peroxide and absorbance at 230 nm was determined after 10 minutes against a blank solution containing phosphate buffer without hydrogen peroxide act as control. The percentage of hydrogen peroxide scavenging activity is calculated.

Scavenging activity = (Ac-As) / Ac x 100

Ac - absorbance of control, As - absorbance of sample.

RESULT AND DISCUSSION

UV- Visible spectra of Peel Extract

The UV-Visible spectra was taken for the freshly prepared Carica papaya peel extract. The UV-Visible spectra of the plant extract were studied at a wavelength range of 200 to 800 nm. The maximum absorption band obtained at 200 and 290 nm. The range 400 - 450 nm corresponding to phenolic acids and their derivatives (flavones, flavonols, phenylpropenes and quinones) [16]. The spectra for phenolic compounds (tannins) and flavonoids typically lie in the range of 200-290 nm [17] and the range 400 - 450 nm corresponding to phenolic acids and their derivatives (flavones, flavonols, phenylpropenes and quinones) [18]. Hence, the result of UV-Vis spectroscopic analysis confirms the presence of phenolic compounds and flavonoids in the aqueous peel extract of Carica Papaya peel which are capable of acting as reducing agent for the conversion of metallic state to nanoparticles.

UV-Visible Spectra of ZnO Nanoparticles

UV-Visible spectra for synthesized nanoparticles exhibit a strong absorbance between 224 nm to 550 nm confirms to formation of ZnO Nanoparticles.

Fig.1 Peel Extract

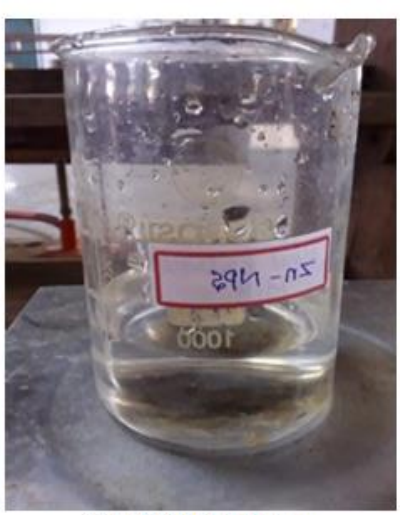

Fig.2 Zinc Sulphate

Fig.3 ZnO Nanoparticle

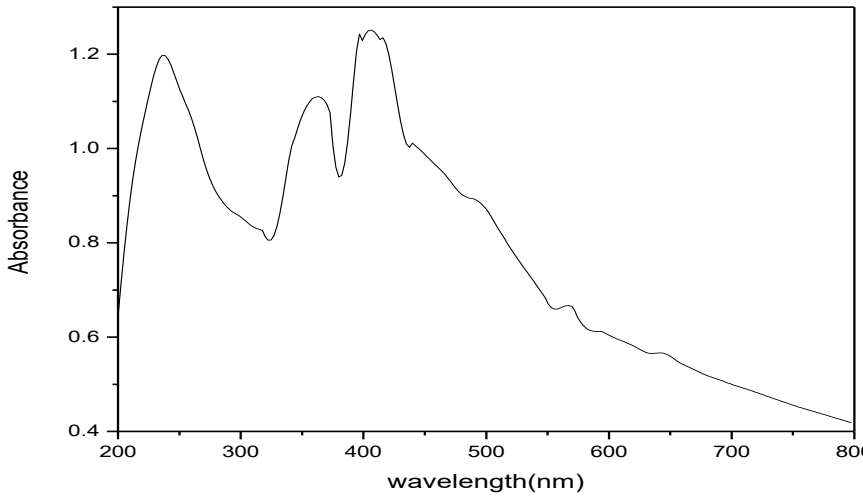

Fig. 4 UV- Visible Spectra for Zinc Oxide Nanoparticles

FT-IR Spectra

FT-IR Spectra of Peel Extract

The FTIR analysis was used to identify the capping, reducing and stabilizing capacity of the plant extract. The bioactive molecules present in Carica papaya peel extract was confirmed by FT-IR. The FTIR spectra of the Carica Papaya peel extract showed characteristics absorption bands.

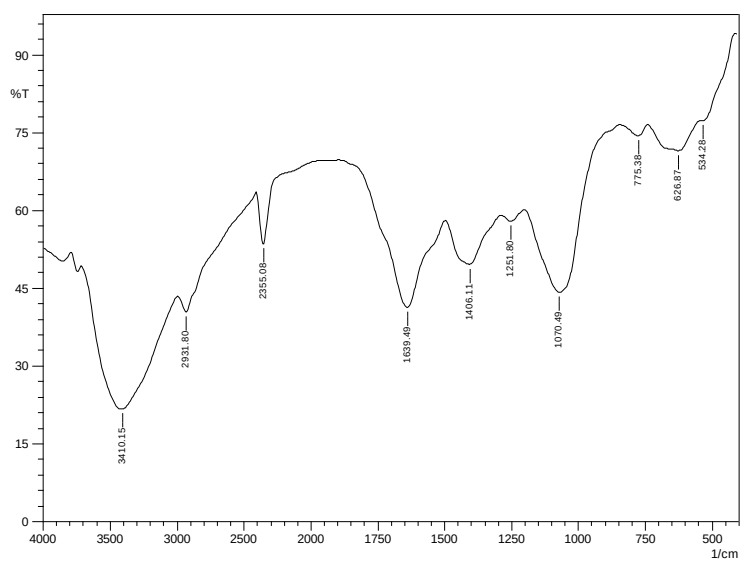

Fig. 5. FTIR spectra of Carica Papaya peel extract

Aqueous leaf extract showed the strong absorption band at 3410.15 cm^{-1} shows O-H stretching vibrations of the hydroxyl group, H-bonded alcohols and phenols. The strong band observed at 2931.80 cm^{-1} corresponds to C-H stretching of alkanes. The band at 2355.08 cm^{-1} was due to presence of C=O stretching, α, β - unsaturated aldehydes and ketones. The strong band observed at 1639.49 cm^{-1} corresponds to N-H bonding of primary amines. The absorption band observed at 1406.11 cm^{-1} assigned to O-H band indicates carboxylate, functionalized nanoparticle. The bands at 1251.80 cm^{-1} and 1070.49 cm^{-1} correspond to C-N stretching of amines. The peak at 775.38 cm^{-1}, 626.87 cm^{-1} and 534.25 cm^{-1} assigned to C-H stretching **[19]**.

FT-IR Spectra of ZnO Nanoparticles

The FTIR spectra was recorded for the synthesized Zn-O NPS in the range of 400 – 4000 cm^{-1}. The FT-IR analysis confirms the transformation from zinc sulphate to ZnO nanoparticles by the action of the different phytochemicals present in banana leave extract which was simultaneously act as stabilizing and capping agent.

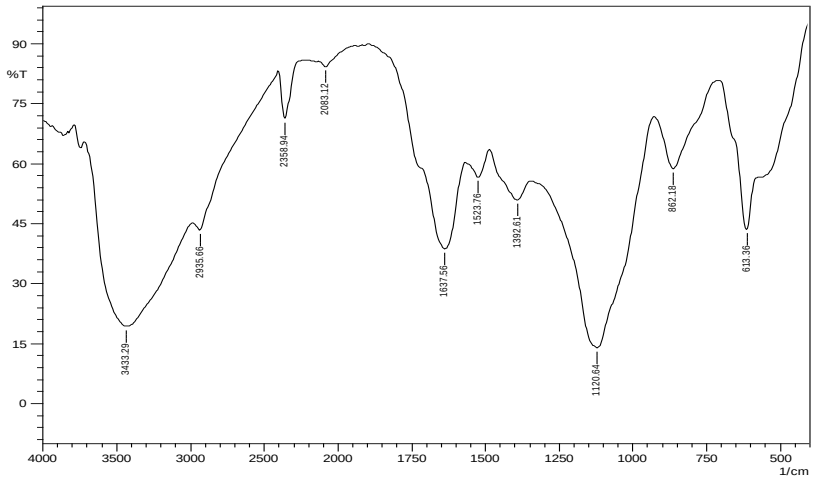

Fig. 6. FTIR spectra of ZnO nanoparticles

The few absorption band appeared at 3433.29 cm^{-1}, 2935.66 cm^{-1}, 2358.94 cm^{-1}, 2083.12 cm^{-1}, 1637.56 cm^{-1}, 1523.76 cm^{-1}, 1392.61 cm^{-1}, 1120.64 cm^{-1}, 862.18 cm^{-1}, the characteristic absorption band values at 460 cm^{-1} confirms presence of zinc oxide nanoparticles [20]. The band at 1120.64 and 1637.56 cm^{-1} may be ascribed to vibrational energy of aromatic hydrocarbons and amide linkage those have possessed their energy changed sue to interaction with nanoparticles[21]. The band at 1523.76 cm^{-1} and 3433.29 cm^{-1} originate from antisymmetric -C-O- vibration[22].Thus from analysis of the FTIR spectrum the formation of zinc oxide nanoparticles was confirmed and also we may conclude that the amide, phenols and carbohydrates present in leave extract stabilizes the zinc oxide nanoparticles.

X-Ray Diffraction analysis

X-Ray Diffraction analysis is the most useful method by which X-Rays of a known wavelength are passed through a sample to identify the crystalline structure. The average size of particle was calculated by applying full width at half maximum (FWHM) and the value of 2θ of characteristic peak of the experimental XRD powder pattern using the Debye–Scherer equation. $D = k\lambda / \beta \cos\theta$ (1) Where D is the average size, K is a constant (ca. 0.9), λ is the wavelength of Cu Kα, β is the full width at half maximum (FWHM) of the diffraction peak and θ is the Bragg's angle.

Exhibits XRD diffraction pattern of ZnO nanoparticles. The peaks are indexed as 18.230° (4.8624), 20.047° (4.42573), 25.886° (3.43917), 29.000° (3.07855), 35.487° (2.52757), 41.067° (2.19613), 49.890° (1.82645) and 54.626° (1.67876) respectively. Similar, X-ray diffraction pattern were reported 144,451. Average particle size of ZnO nanoparticles is found to be 9.55nm using[23] Diffraction pattern corresponding to impurities are found to be absent. This proves that pure ZnO nanoparticles were as synthesized.

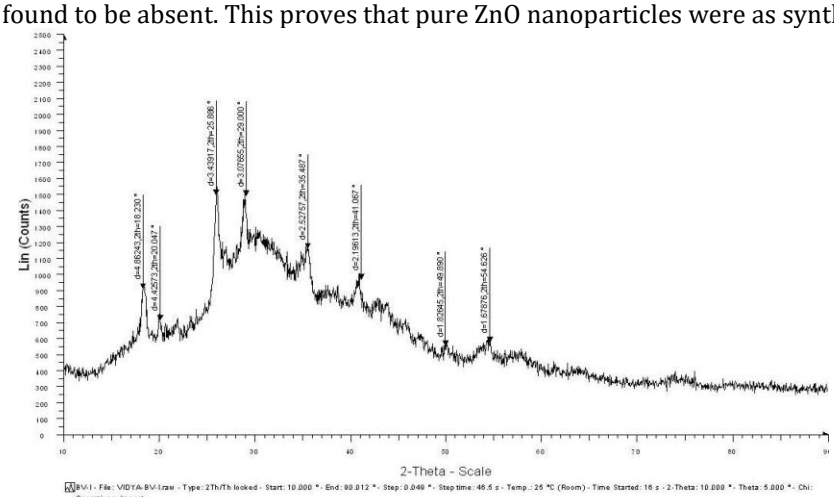

Fig. 7. XRD ZnO Nanoparticles

SEM Analysis

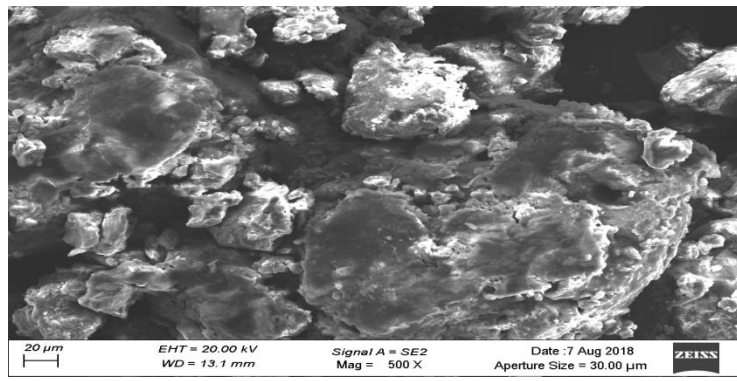

Fig. 8. SEM analysis ZnO nanoparticles

SEM analysis of Zinc oxide nanoparticles was done by using JSM- 66101 V Machine. The Scanning electron microscopic the synthesis ZnO nanoparticles were identified image of Morphology indicated the highly Agglomeration shape. The ZnO nanoparticles formed in the range of 20µm.

EDAX Analysis

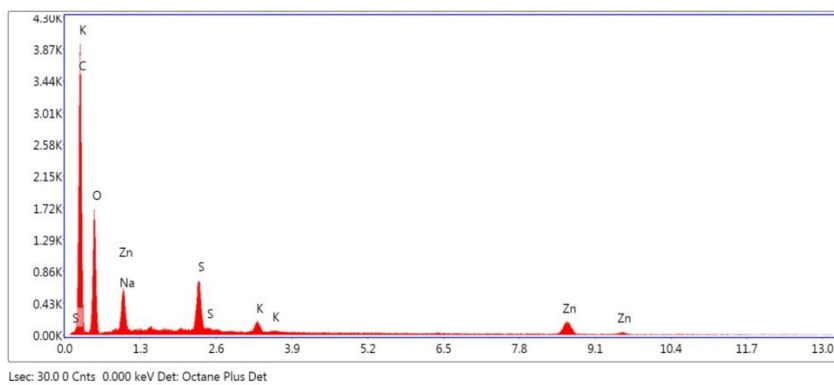

Fig. 9. EDAX analysis ZnO nanoparticles

Table 1. EDAX Analysis percentage of elemental table

Element	Weight %	Atomic Weight %
CK	58.99	69.32
OK	31.81	28.06
NaK	0.00	0.00
SK	2.37	1.04
KK	0.69	0.25
ZnK	6.14	1.33
Total	100	100

The EDAX element are present in ZnO Nps. In addition all the atomic percentage for **Table 1** C, O, Na, S, K. compare to all the metal (Na, S, K) are present in ZnO Nanoparticles. The addition atomic percentage for Elements (C, O, Na, S, K).

The Elemental composition of green synthesized in ZnO nanoparticles was analysis through EDAX. The EDAX spectrum confirms the formulation of C, O, Na, S, K, Zn. 0.000 KeV, which is in congruence with the major emission peaks specified for metallic element along with this small peaks of Na, S, K, Zn were also arisen due to the capping of ZnO Nanoparticles.

Biological properties of prepared ZnO nanoparticles

Antibacterial Activities

Antibacterial test was performed for aqueous peel extract and synthesized copper oxide nanoparticles. The zone of inhibition values are measured in mm. The zone of inhibition value less than 10 mm is considered as resistant towards the corresponding microorganism.

Table 2. Antibacterial activity data of prepared Zinc Oxide nanoparticles

Organism (bacteria)	Zone of inhibition (mm) ZnO nanoparticles	DMSO solvent (Negative control)
E-Coli	23	10
Staphylococcus aureus	20	10

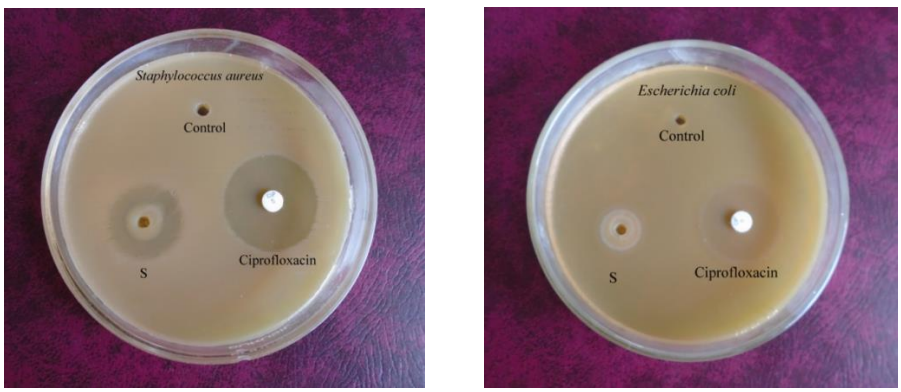

Fig. 10. Antibacterial activity data of prepared Zinc Oxide nanoparticles

Antifungal Activity

The prepared nanoparticles are assessed for their in vitro antifungal activity by well diffusion method against fungi such as Mucor mycosis, Rhizopu.s. and Aspergillus niger. The results with reference to in vitro antifungal activities of synthesized complexes are summarized in Table. The standard DMSO used as negative control. The photograph and graphical representation was given in the

Table 3: Antifungal activity of zinc oxide nanoparticle

Organism (bacteria)	Zone of inhibition (mm) ZnO nanoparticles	DMSO solvent (Negative control)
Rhizopus	22	11
Aspergillus Niger	19	10
Mucor Mycosis	20	11

Fig. 11. Antifungal activity of Zinc Oxide nanoparticle

The zone of inhibition values obtained for the synthesized nanoparticles reveals that the Rhizopus exhibiting the good antifungal activity against Aspergillus niger. The antibacterial and antifungal activity of the ZnO nanoparticle indicates that the nanoparticle possess higher growth inhibition potential. The antimicrobial activity of the zinc oxide nanoparticle increases with increase in concentration of the nanoparticles. It suggested that the synthesized ZnO nanoparticles having antibacterial and antifungal activities which inhibit multiplication process of the microbes by blocking their active sites.

Antioxidant activity

The antioxidant activity has mainly been designated as the peroxide value of oxidation products and the oxidation rate of co-existing lipids. To study the antioxidant potential through free radical

scavenging by the nanoparticles, the change in optical density of H_20_2 radicals is monitored. Prepared nanoparticles exhibits moderate antioxidant scavenging activity when compared with standard α-tocopherol.

Table 4: Antioxidant scavenging activity of Zinc Oxide nanoparticles

Concentrations	Zn-O NPS
Mg/200 ml	% of scavenging activity
4	35
2	22
1	08
0.5	04

CONCLUSION

In the present study ZnO nanoparticles has been synthesized using *Carica papaya* peel extract and characterized by spectral analyses like UV-Visible, FTIR, XRD and SEM. FTIR results shows that reduction of Zinc ions to stabilization of ZnO nanoparticles occur through possible. Participation of peel extracts and others. Metabolites present in the peel extracts X-ray diffraction (XRD) spectral results confirmed the particle size of prepared nps and it was found to be 9.55 nm of ZnO nanoparticles respectively. SEM analysis (Scanning Electronic Microscopic) Confirmed by agglomeration shape 20µm ZnO nanoparticles. The prepared ZnO nanoparticles were screened to study their biological properties like invitro antimicrobial, antibacterial and antifungal antioxidant activity[24].

REFERENCES

1. "About The Nanotechnology Initiative". United States National Nanotechnology Initiative. Retrieved 4 june 2016.
2. *Buzea C, Pacheco I, Robbie K. Nanomaterials and nanoparticles: Sources and toxicity. Biointerphases, 2007; 2: 17-71.*
3. Ronald Sandler. Nanotechnology: The social and ethical issues. Woodrow Wilson int center for scholars, 2009.
4. Panigrahi S, Kendu S, Ghosh SK, Nath S, Pal T. General methods of synthesis of metal nanoparticles. J Nanopart Res, 2004; 4: 411–414.
5. Parthasarathy G, Saroja M, Venkatachalam M, Evanjelene V.K. Biological Synthesis of Zinc Oxide Nanoparticles from Leaf Extract of *Curcuma neilgherrensis* Wight. Int J of Mat Sci, 2017; 12: 73-86.
6. Ana cauerhff , Guillermo R, Castro. Bionanoparticles, a green nanochemistry approach. Electronic J of Biotechnol, 2013; 16:
7. Jennifer scalf and Paul west. Pacific Nanotechnology. Introduction to nanoparticle characterization with AFM, 1 – 9.
8. Elizabeth Varghese, Mary George. Green synthesis of zinc oxide nanoparticles. Int J of Adv Res In Sci Eng, 2015; 4(1).
9. Pulit-Prociak J, Chwastowski J, Kucharski A, Banach M. Functionalization of textiles with silver and zinc oxide nanoparticles. App Surf Sci, 2016; 385: 543-553.
10. Deepali Sharma , Jaspreet Rajput., B.S. Kaith , Mohinder Kaur , Sapna Sharma Synthesis of ZnO nanoparticles and study of their antibacterial and antifungal properties. Thin Solid Films, 2010; 519: 1224-1229.
11. *Cedric Mims, Hazel Dockrell, Richard Goering, Ivan Roitt, Derek Wakelin, Zuckerman, Mark, eds. Medi Microbiol, 2004; 287.*
12. Siddiqui BS, Afshan F, Faizi GS, Naqui SNH, Tariq RM. Two insecticidal tetranortriterpenoids from Azadirachta indica. Phytochemistry, 2000; 53: 371–376.
13. Lalitha A, Subbaiya R, Ponmurugan P. Green synthesis of silver nanoparticles from leaf extract Azhadirachta indica and to study its anti-bacterial and antioxidant property. Int J Curr Microbiol App Sci, 2013; 2: 228–235.
14. Sreejayan N, Roa MNA. Nitric oxide scavenging by curcuminoids. J Pharm, 1997; 49: 105–107.
15. Cao G, Prior RL. Comparison of different analytical methods for assessing total antioxidant capacity of human serum. Clin Chem, 1998; 44: 309-1315.
16. Shankar SS, Raj A, colloid interface sci, 2004; 273: 496 -502.
17. Mulvaney P, Langmuir. Nanoscience properties Green chem text book, 1996; 788–800.
18. Shankar SS, Rai A, Ahmad AM, Sastry J**.** Colloid Interface Sci, 2004; 275: 496–502.
19. Ethiraj A S, Kang DJ. Nanoscale Res. Lett, 2012; 70.
20. Devasenan S, Hajara Beevi N, Jayanthi S S. Green Synthesis and Characterization of Zinc Nanoparticle Using *Andrographis paniculata* Leaf Extract. Int J Pharm Sci Rev Res, 2016; 39: 243-247.
21. Harish Kumar, Renu Rani. Structural and Optical Characterization of ZnO Nanoparticles Synthesized by Microemulsion Route. Int Letters Chem Physics Astronomy, 2013; 14: 26-36.

22. Yang G, Chai S, Xiong X, Zhang S, Zhang P. Preparation and tribological properties of surface modified Cu nanoparticles. Trans Nonferrous Met Soc China, 2012; 22(2): 366–372.
23. M.Bharathi and Saranya Jothiramalingam, Bio synthesis and characterization of CuO nanoparticles using carica papaya peel extract. WJPR volume 7, Issue 3, 2018.

Hydrothermal assisted synthesis of Graphene oxide doped Nickel oxide – a material for supercapacitor

G. Manikandan[1,2] , H.A. Arjun[1] & N. Saradhadevi[1,3]
[1]Department of Chemistry, Annamalai University, Annamalainagar 608002
[2]Government Arts College (Autonomous), Kumbakonam 612002
[3]Arignar Anna Government Arts College, Cheyyar 604407

ABSTRACT: *Graphene oxide (GO) is of great interest due to its low cost, easy access, and widespread ability to tuned. The nanoparticles insert between graphene layers and graphene nanosheets stack with each other, however, shows improved capacitance are interested in doing research on graphene/NiO nanocomposites. And of late, hydrothermal assisted synthesis has drawn much attention in the synthesis of NiO doped graphene oxide materials with uniform structures. The particulate nature of the synthesized materials is well imaged by SEM. XRD studies defended that the crystals are made of fcc in GO/NiO structure and the average size of NiO nanoparticles 14.49 nm. EDAX image confirmed the existence of Nickel oxide and graphene oxide. Further, the absorption behavior of the synthesized materials was well studied by FTIR spectra. CV and GCD reveal the electrochemical behavior of the synthesized material. Besides, symmetric supercapacitor cells were assembled and the specific capacitances of the symmetric cells of GO and GO/NiO are 46.55 and 13.08 Fg^{-1} respectively at scan rate of 2mVs^{-1}.*

Keywords: *graphene nanosheets, graphene/nickel oxide nano composites, hydrothermal, supercapacitor cells, specific capacitance*

1. Introduction

Nanoscience and nanotechnology primarily deal with the synthesis, characterization, exploration, and exploitation of nanomaterials. Carbon is a unique and versatile element in periodic table which is capable of forming different architectures at the nanoscale levels. Almost all carbon materials apart from diamonds are based on grapheme [1]. It is the basic building block of other important allotropes. Graphene is a new allotrope of carbon, which is a two dimensional crystalline form has going to be the future in electronics and materials science.

Graphene oxide is graphite that has been oxidized to intersperse the carbon layers with oxygen molecules and then reduced to separate the carbon layers completely into individual or few layer graphene. Graphene oxide is effectively a by-product of this oxidation as when the oxidizing agents react with graphite, the interplanar spacing between the layers of graphite is increased. The completely oxidized compound can then be dispersed in a base solution such as water, and graphene oxide is then produced [2,3].

Recently graphene has attracted tremendous attention because of its unique electronic, optical and chemical properties and many potential applications in nanomaterials and nanotechnology. It provides a large specific surface area for the immobilization of large amount of substances including a wide range of metals, nanoparticles, biomolecules, drugs, *etc [4].*

Functionalization of graphene oxide can fundamentally change the priority of graphene oxides. The resulting chemically modified graphene could then potentially become much more adaptable for a lot of applications. There are many ways in which graphene oxide can be functionalized, depending on the desired application such as optoelectronics, bio devices, as a drug-delivery material or energy storage devices etc.,[5].

Nickel oxide (NiO) is an important transition metal oxide with cubic lattice structure. It has attracted increasing attention owing to potential use in a variety of applications such as: catalysis, battery cathodes, supercapacitors, gas sensors, electrochromic films and magnetic materials. Also for low material cost as an ion storage material, NiO semiconductor becomes a motivating topic in the new area of research. Because of the volume effect, the quantum size effect, the surface effect and the macroscopic quantum tunnel effect, nano crystalline NiO is expected to possess many improved properties than those of micrometer-sized NiO particles [6].

With advancements in all areas of industry and technology, the interest has been focused on nano scale materials. Thus, many methods have been attempted to prepare nanosized nickel oxide, including nanoparticles [7], nanorings [8], nanosheets and nanoribbons [9]. However, a large specific volume change commonly occurs in the host matrix of the metal oxide during the cycling processes, thus leading to

pulverization of the electrodes and rapid capacity decay. Furthermore, high resistivity of NiO is another drawback for practical applications in ECs. Therefore, it is crucial to improve the capacity and conductivity of NiO in order to reinforce the energy density, power density and pseudo capacitive behaviour [10].

A number of synthetic methods have been developed to prepare NiO as well as NiO-based composites with tuneable surface morphologies and characteristic pseudo capacitance behaviour. Some of the reports emphasize the structure activity relationship of NiO material which accentuates the importance of surface properties on the charge storage performance. These studies show that, in addition to the parameters such as surface area and pore size, suitable surface morphology of NiO is also an essential parameter for exhibiting higher pseudo capacitance. Of late, microwave-mediated and hydrothermal assisted synthesis has drawn much attention in graphene oxide doped materials with uniform structures [11].

2. Experimental methods

The powder X-ray diffractograms (XRDs) of the synthesized oxides were recorded using a Bruker AXS D8 advanced diffractometer employing Cu K_α rays of wavelength 1.5406 Å with a tube current of 30 mA at 40 kV. The morphologies of the prepared oxides were examined with a JOEL JSM-5610 scanning electron microscope (SEM) equipped with BE detector. The samples were placed on an adhesive carbon slice supported on copper stubs and sputtered with 10 nm thick gold particles employing a JOEL JFC-1600 auto fine coater prior to measurement. A JOEL JSM-5610 SEM equipped with BE detector or a FEI Quanta 200 FEG HR-SEM under high vacuum mode was used to obtain the energy dispersive X-ray (EDX) spectra of the synthesized oxides. FTIR spectra was recorded for the samples in the middle IR region (400–4000 cm^{-1}) using a Avatar-330 FT-IR type instrument. The samples were introduced as pellets prepared with KBr powder. The cyclic voltammetry and galvanostatic charge/discharge studies of the samples were carried out using SP-150, Bio-Logic Science instruments in 1 M H_2SO_4 as an electrolyte at room temperature.

2.1 Synthesis of Graphene oxide

2.0 g of graphite powder was added to 300 mL of H_2SO_4 under stirring at 0 °C and then 3.0 g of $NaNO_3$ and 2.0 g of $KMnO_4$ were added gradually. Successively, the mixture was transferred to a water bath at 30 °C and stirred for 20 min to form a thick paste. Then, 250 mL of distilled water was slowly added and the temperature was increased to 98°C. After 30 min aging, another 500 mL of water was added and this was followed by a drop wise addition of 40 mL of H_2O_2 (30%). When the colour of the solution changed from dark brown to brilliant yellow, the mixture was filtered and washed using 10% HCl three times to remove metal ions and then washed with distilled water repeatedly until the pH became 7. Finally, the Graphene Oxide was obtained after drying in a vacuum oven at 60 °C for 6 hours.

2.2 Synthesis of Graphene oxide/ Nickel oxide composites

Graphene oxide is dispersed in water by ultrasonic agitation for 30 min before autoclave the mixture. An (0.58 g) Nickel carbonate and (0.1 g) graphene oxide was dispersed in 100 ml of water and then 2 mL of hydrazine monohydrate ($N_2H_4 \cdot H_2O$, 85%) was slowly added. The mixtures were then transferred to stainless steel autoclaves, kept at 160°C for 12 h. The resulting products (Graphene composites) were washed with acetone followed by water and then dried at 65°C in air.

2.3 Electrode and cell fabrication for supercapacitors

The working electrode has been fabricated using the prepared nanomaterials. The prepared material (40 mg, 80 wt%), carbon black (7.5 mg, 10 wt%) and PVDF (2.5 mg, 10 wt%) were dissolved in 0.2 mL of N-methyl 2-pyrrolidinone and made into slurry form. Then, 5 µL of slurry was placed on the pre-treated 304 grade stainless steel (SS) with an area of 1 cm^2 dried at 70 °C overnight. The cyclic voltammetric studies were performed with three electrode cell using the potential range between -0.5 and 0.5 V. An active material coated stainless steel sheet (area 1 cm^2), Pt wire and Ag/AgCl were used as the working, counter and reference electrodes respectively. The electrolyte used was a 1M H_2SO_4 aqueous solution.

Two electrodes each of 1 mg active material coated stainless steel with polypropylene sheet as separator. The cyclic voltmmetry study was carried out between the potential ranges of -1.0 to 1.0 V with different scan rates varied from 2 to 10 mV s^{-1} in 1M Na_2SO_4 electrolyte. The galvanostatic charge-discharge behaviour was studied using different current density ranges from 0.1 to 0.5 mA cm^2 at a constant pontential of 1 V with respect to Ag/AgCl.

3. Results and Discussion

The XRD patterns obtained for synthesized Graphene oxide nanoparticle is shown in Fig. 1. It shows diffraction peak at 2θ=9.7, which is mainly due to the oxidation of graphite. The peak at 10^0 shows that the

product is completely oxidised after the chemical oxidation and exfoliation, indicating a d-spacing of 21.5707nm. They are good agreement and also matches well with previous reports in the literature [12].

In the XRD pattern of the NiO/GO the clear diffraction bands centred at 2θ of 44.92°, 52.29° are corresponding to the (4 2 0) and (5 1 1) crystal planes respectively of the face-centred cubic (fcc) Ni (JCPDS 01-1239) shown in Fig. 2. A broad hump at 9.3° can be attributed to the (0 0 1) diffraction of GO, indicating the successfully reduction of GO by hydrazine hydrate [40]. In addition, the average size of Ni nanoparticles is 17.66 nm, which is calculated using Debye-Scherrer equation based on the full width at half-maximum of the diffraction peak [13].

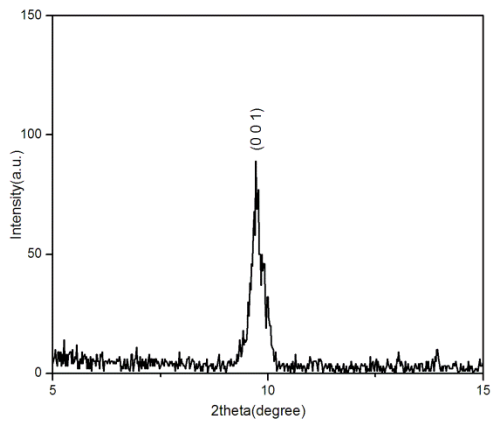

Fig. 1. PXRD pattern of Graphene Oxide

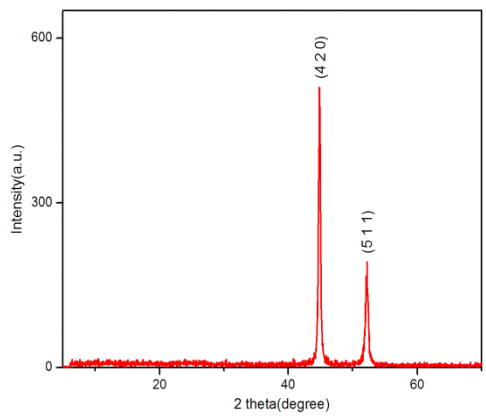

Fig. 2. PXRD pattern of NiO/GO

Table: 1

Materials	Pos. [°2Th.]	Height [cts]	FWHM [°2Th.]	d-spacing [Å]	Rel. Int. [%]	D (nm)
Graphene Oxide	9.7202	40.72	0.3699	16.9	36.67	**21.5707**
NiO/GO	44.9248	496.72	0.3542	2.01775	100.00	24.2886
	52.2950	157.15	0.4133	1.74941	31.64	21.4293
	76.7293	71.89	0.5040	1.24109	14.47	20.1185

SEM Images of GO is given in the Fig. 3. The grain size and surface morphology were observed by the scanning electron microscope.The SEM images of the Graphene Oxide (GO) have a well defined and interlinked three-dimensional graphene sheets forming a porous network that resembles a loose sponge like structure as shown in the figure which also matches well with previous reports in the literature [12]. The SEM images of GO/NiO were shown in Fig. 4, in which the NiO nanoparticles are clearly visible. Due to the corrugated nature of the disordered graphene oxide, the NiO nanoparticles are homogeneously distributed on the curly surface of the graphene oxide. The SEM images of monolayer GO/NiO suggest that nickel oxide particles grow on monolayer graphene densely and evenly with a size of about 17.66 nm.

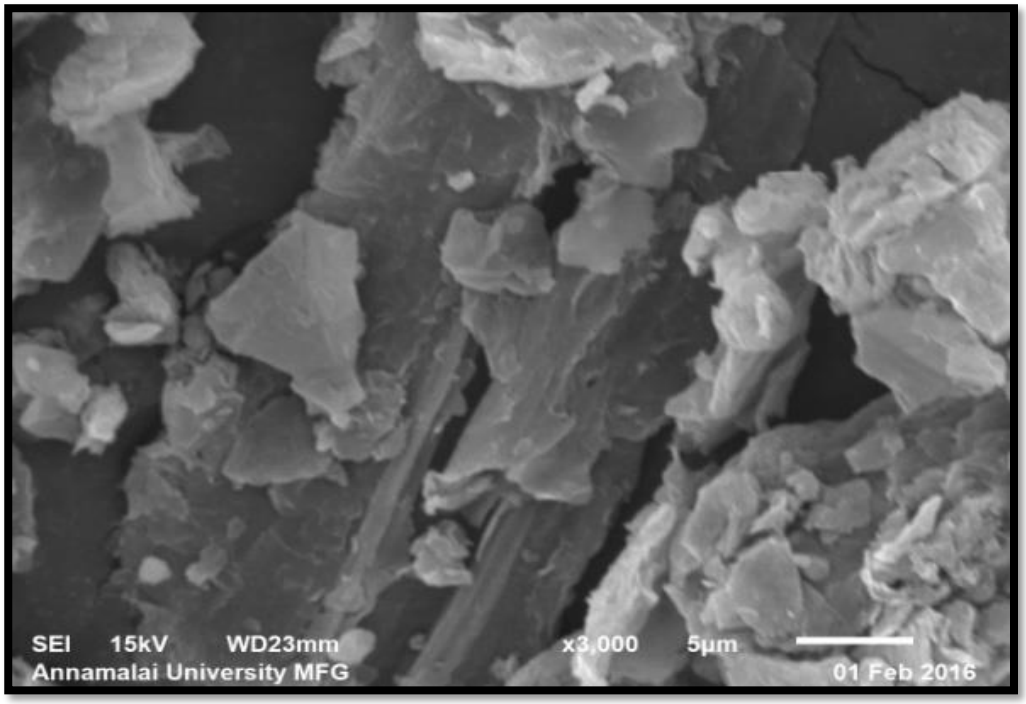

Fig. 3. SEM of Graphene Oxide

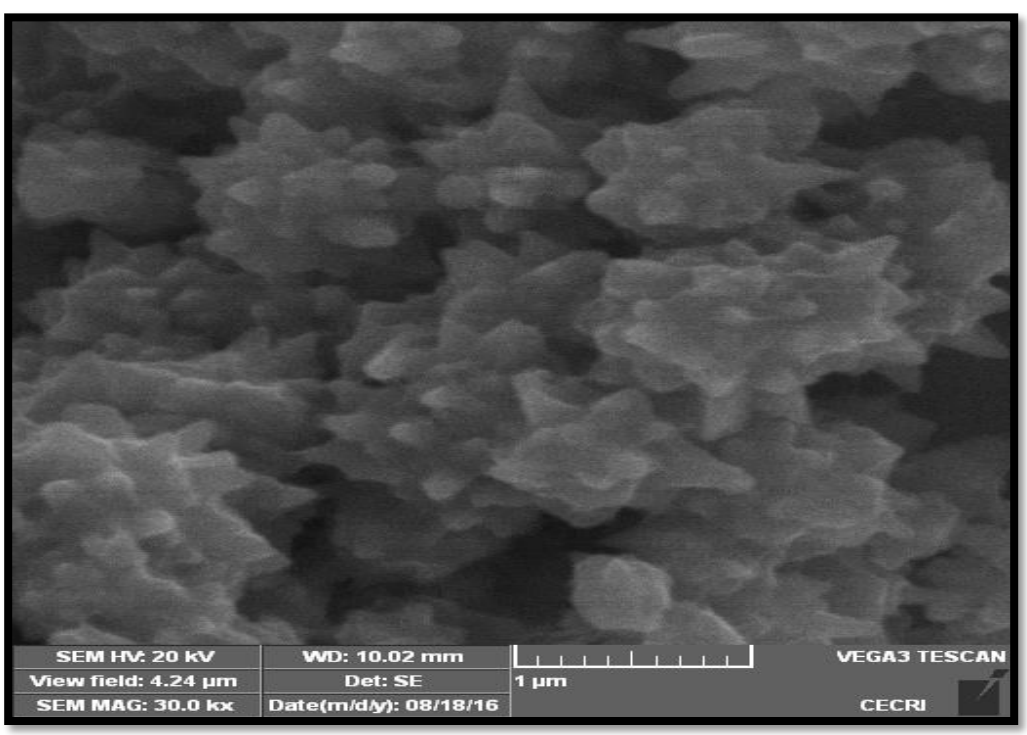

Fig. 4. SEM of NiO/GO

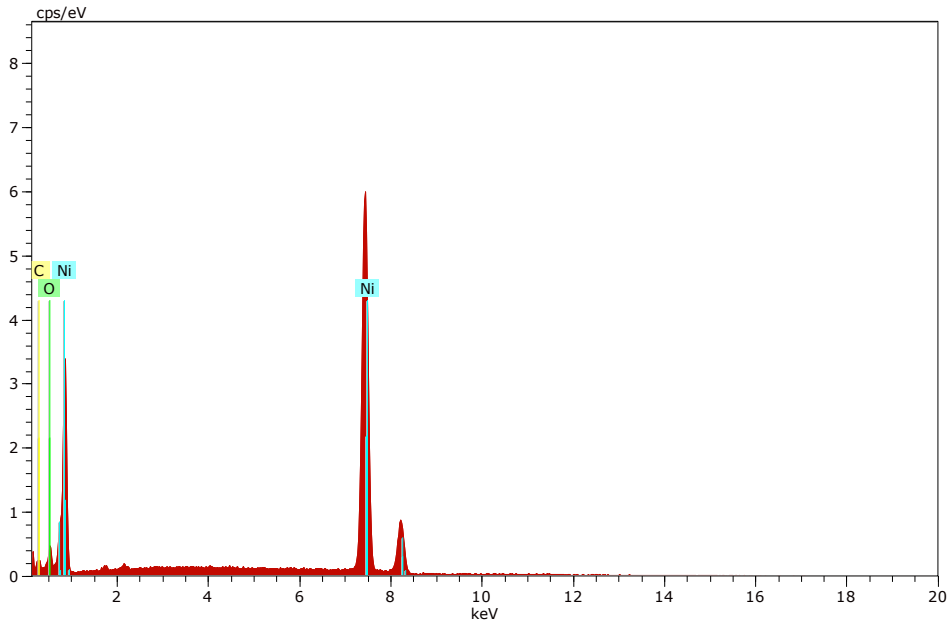

Fig. 5. EDAX pattern of GO/NiO

Table: 2

ELAN [wt.%]	Series[wt.%]	Unknown [at.%]	C[wt.%] norm	C Atom [wt.%]	(1Sigma)	K fact	Z Corr
Ni-28	K-Series	101.26	89.13	64.56	2.75	0.936	0.922
C-6	K-Series	8.45	7.43	26.31	1.84	0.282	0.263
O-8	K-Series	3.90	3.43	9.12	0.79	0.096	0.356
Total: 113.61 100.00 100.00							

The nature of the nickel oxide/ graphene oxide was further confirmed by EDAX analysis shown in Fig. 5. The peaks of Ni, O and C observed in the EDAX image confirmed the existence of nickel oxide and graphene oxide. The specific surface area is expected to become larger.

The FT-IR spectra of the as-prepared GO in Fig. 6. The broad absorptions at about 3,426 and 1,625 cm^{-1} are assigned to the hydroxyl groups of absorbed H_2O molecules, and the peaks around 2,970 and 2,900 cm^{-1} can be assigned to the asymmetric and symmetric vibrations of C-H, respectively. The absorption band at 1,085 cm^{-1} can be assigned to the stretching vibration of C-O. The C=O vibration band at 1,723 cm^{-1} disappears after hydrazine hydrate reduction of exfoliated GO, indicating that the reduction of GO to RGO is complete and also matches well with previous reports in the literature [14].

The FT-IR spectrum of GO/NiO is shown in Fig. 7. In the high frequency region, a broad band around 3421 cm^{-1} can be observed in two cases, and can be assigned to the bending vibrations of the adsorbed molecular water and stretching vibrations of the OH groups, the peaks around 2,923 cm^{-1}can be assigned to the asymmetric and symmetric vibrations of C-H. The intermediate of the composite is nickel hydroxide bonded to the graphene surface. As shown in Fig.7 the FT-IR spectrum showed vibrational bands at 34214, 1582, 1360, 1332, 1221, 645, and 484 cm^{-1}, which is typical for hydroxides [13]. In Fig.7 a new sharp peak is observed at 415 cm^{-1} in the low frequency region of the GO/NiO composite and can be ascribed to the Ni–O and Ni–O–Ni vibrations [15].

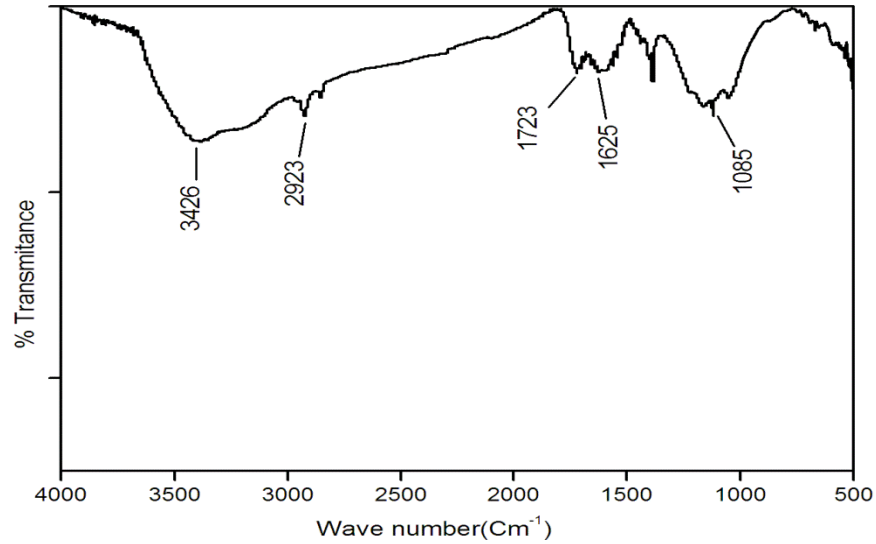

Fig. 6. FT-IR spectra of GO

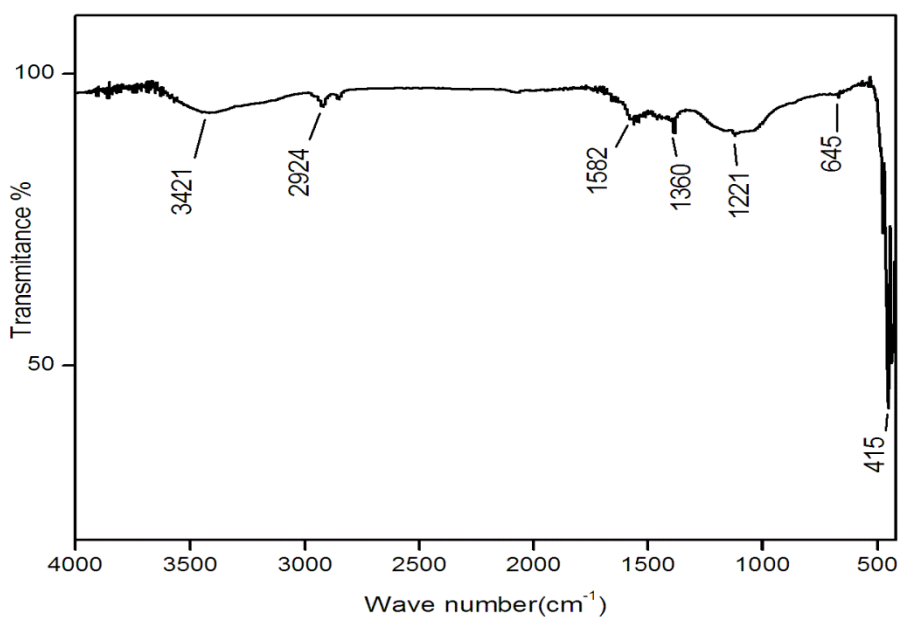

Fig. 7. FT-IR spectra of GO/Nio

The samples have been examined using various electrochemical techniques cyclic voltammetry (CV) and galvanostatic charge-discharge analysis (GCD) to know the capacitance behaviour of the electrode material. For CV studies a three electrode system with a potential range between -0.5 to 0.5 V in 1 M Na_2SO_4 electrolyte was employed. The specific capacitance of the electrode depends on the composites used, carbon coating and doping. The objective of present study is to know the behaviour of GO/NiO as supercapacitor. Fig.8 presents the comparitive CV curves of GO and GO/NiO nanoparticles. Generally, CV curves represent the specific capacitance of the electrode material. The specific capacitance of the GO is little higher than GO/NiO. Fig. 9 and Fig. 10 shows the CV curve of GO and GO/NiO at different scan rates from 2 to 5mV s^{-1}. It shows that the peak current is increased with increased scan rates. Therefore, the specific capacitance is decreased with increase of scan rate as shown in Fig.11. The GO possess the higher specific capacitance of 57.6 Fg^{-1} at low scan rate compared to GO/NiO which has specific capacitance of 25.85 Fg^{-1}. It is because of the fact that ions have enough time to access both inner and outer surface of the GO. But in GO/NiO, the NiO particles were well dispersed and adsorbed over the surface and have less

access to the ions. The specific capacitance of the electrode is low at high scan rates. This is because the ions have less accessible time in the electrode material which leads to storage of charge at the surface only.

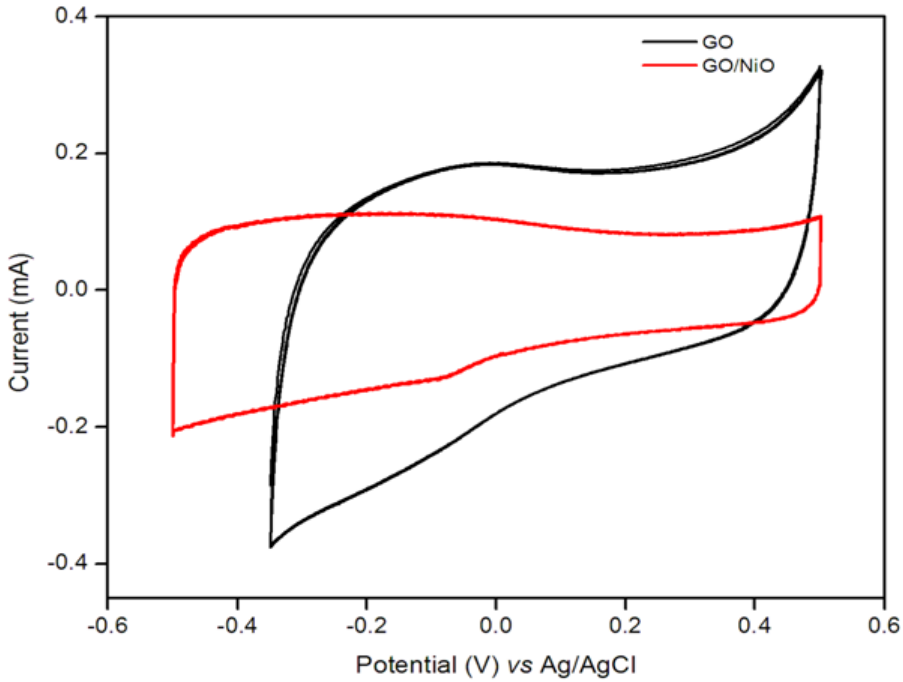

Fig. 8. Comparative CV graph of GO and GO/NiO at 3mV/s

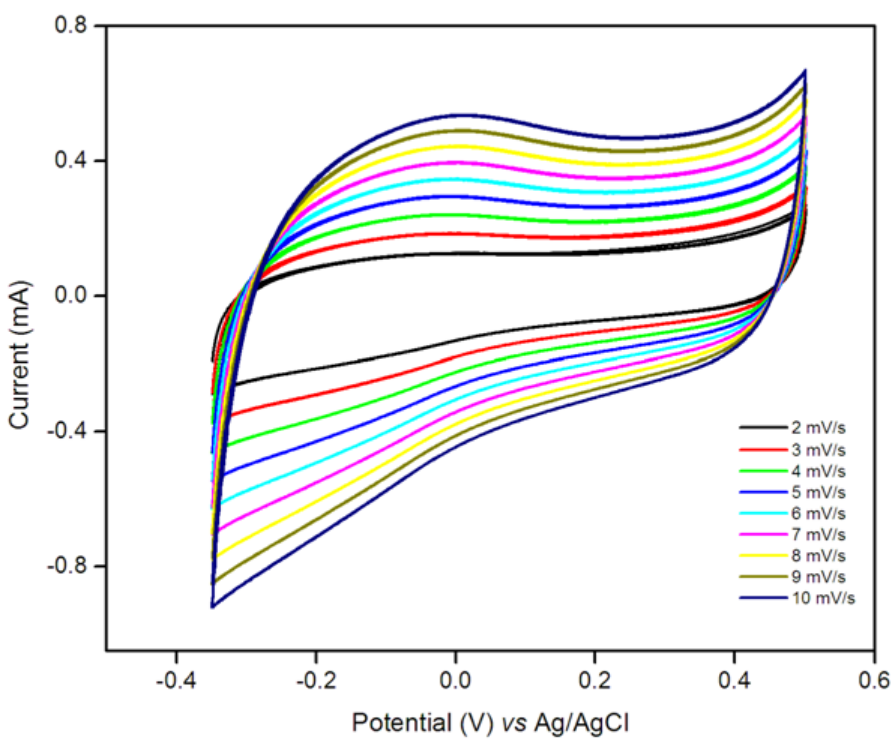

Fig. 9. CV graph of GO at different scan rates

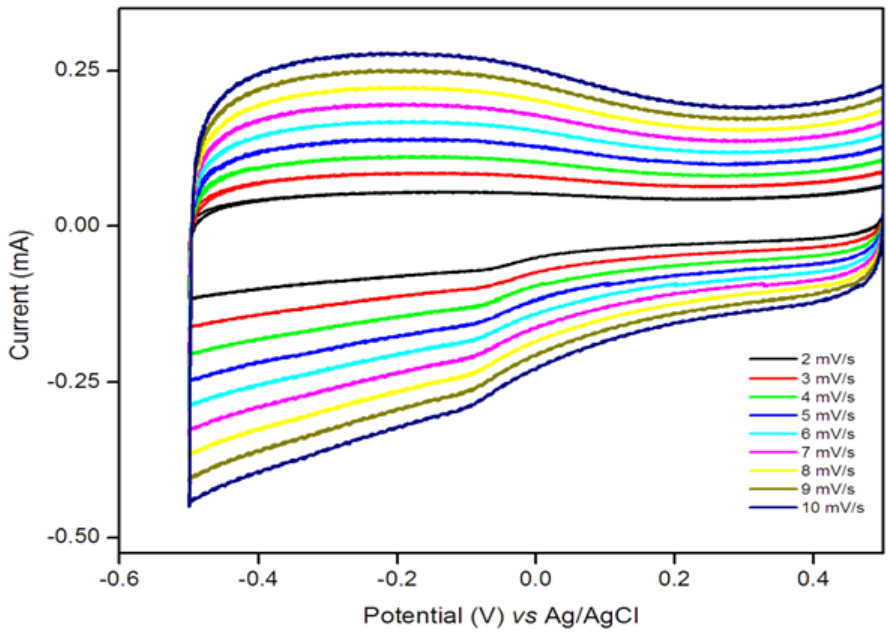

Fig. 10. CV graph of GO/NiO at different scan rates

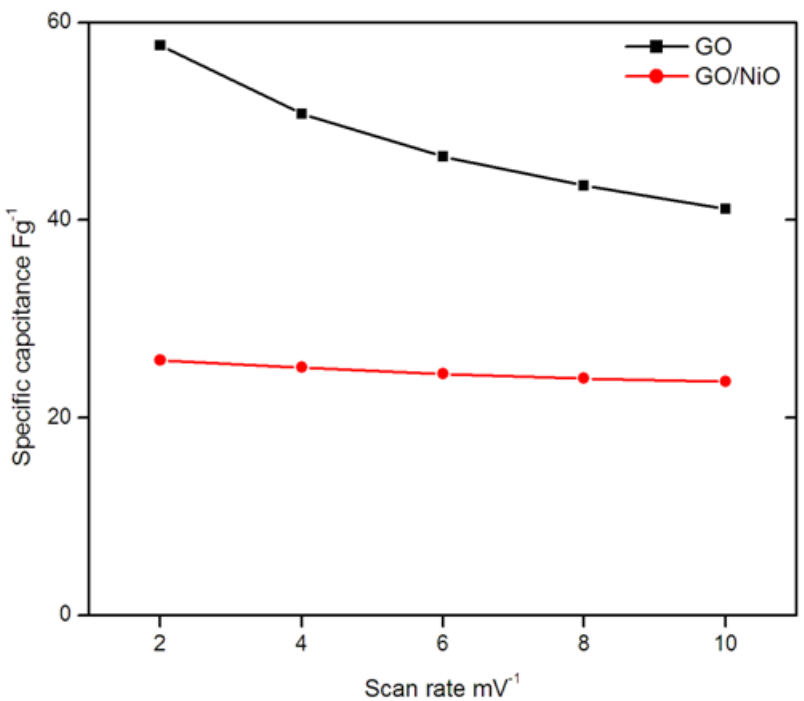

Fig. 11. Variation of specific capacitance with scan rates

To examine the capacitance behaviour of the nanocomposites, the GCD analysis is carried out at different current densities. Fig. 12 and Fig. 13 show the GCDs curve of GO and GO/NiO at different current densities. The charging time is different from discharge time. This non-linear property may be due to the presence of redox process in the electrode material. Fig. 14 shows the variation of specific capacitance with current density. GO shows the specific capacitance of 45.38 Fg^{-1} whereas GO/NiO shows 20.11 Fg^{-1} at scan rate of 0.2 mA cm^{-2}. At low current density, the electrodes possess maximum specific capacitance which is decreased with increasing current density. At high current density, the number of electroactive sites is decreased due to limited mobility of ions into the electrode material.

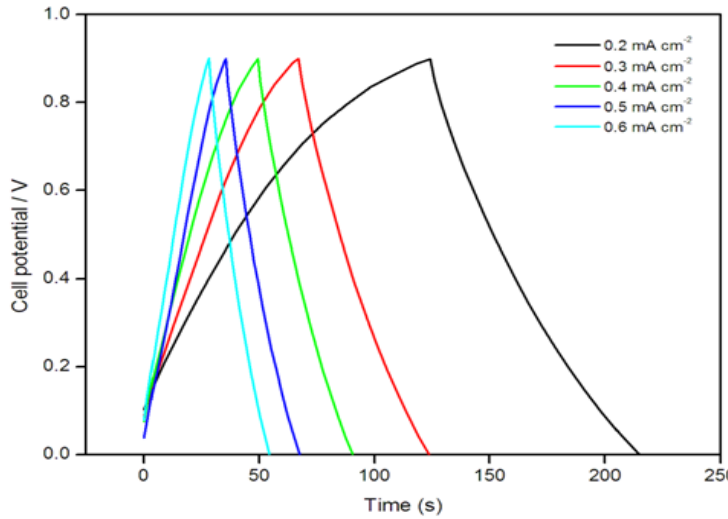

Fig. 12. GCD curves of GO at different current density

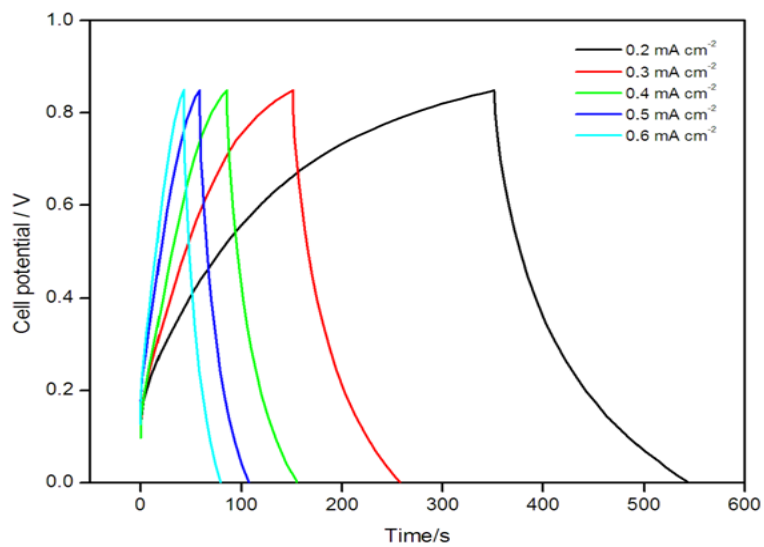

Fig. 13. GCD curves of GO/NiO at different current density

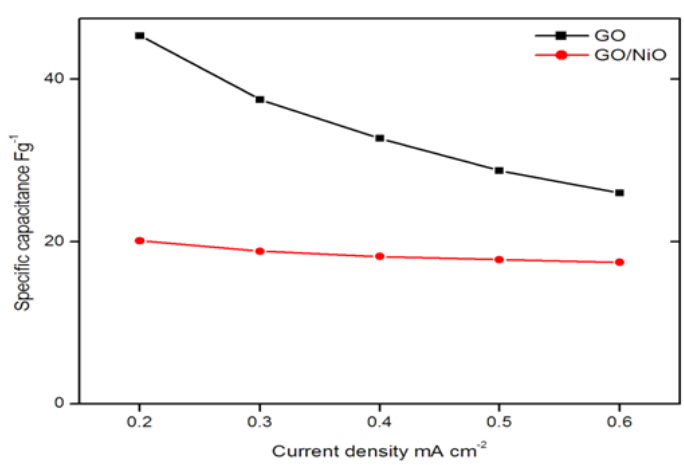

Fig. 14. Variation of specific capacitance with current density

The symmetric supercapacitor cell has been constructed and analyzed within the potential range of -1.0 to 1.0 V in 1M Na_2SO_4 electrolyte. The comparative CV curve of symmetric supercapacitor cells at scan rate of 3mV/s are shown in Fig 15. The CV curve of GO/NiO at different scan rate varying from 2 to 10mV/s was shown in Fig. 16. The CV curve display the ideal capacitance behaviour of the cell along with the oxidation and reduction peaks. The peak current is increased with increase of scan rate. The symmetric cell with good electrochemical reversibility even at high scan rate has been fabricated. The specific capacitances of the symmetric cells of GO and GO/NiO are 46.55 and 13.08 Fg^{-1} respectively at scan rate of 2mVs^{-1}. The effective scan rate on the specific capacitance of the symmetric cell is displayed in Fig 17. To examine the capacitance behaviour of the cell, the GCD analysis is carried out at different current densities. Fig. 18 shows the GCDs curve of supercapacitor cell at different current densities. The charging time is different from discharging time. This non-linear may be due to the presence of redox process in the electrode material. Fig 19 shows the variation of specific capacitance with current density. GO/NiO shows the specific capacitance of 17.82 Fg^{-1}, whereas GO shows only 16.76 Fg^{-1} at scan rate of 0.1 mA cm^{-1}. At low current density, the cells possess maximum specific capacitance which is decreased with increasing current density. At high current density, the number of electroactive sites is decreased due to limited mobility of ions into the electrode material. Hence, the symmetric cell gives maximum specific capacitance at low current density than high current density. From the GCD analysis, it has been clearly shown that GO/NiO has higher specific capacitance then bare GO. This may be attributed to the transition of Ni ions, which evidence that NiO stores the charge under surface redox reaction. It further substantiates the synthesized material is suitable for supercapacitor application.

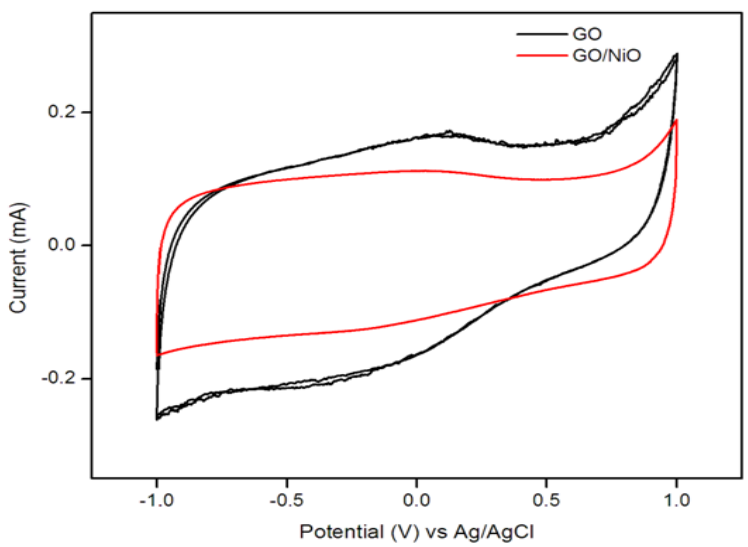

Fig. 15. Comparative CV graph of GO and GO/NiO supercapacitor at 3mV/s

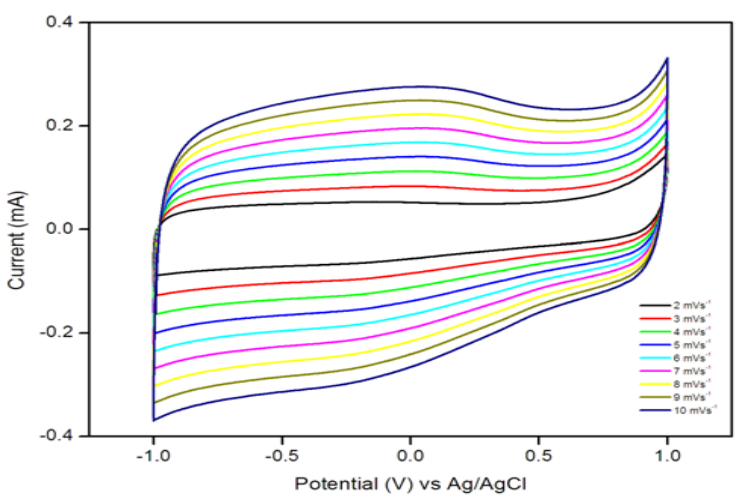

Fig. 16. CV of GO/NiO supercapacitor at different scan rates

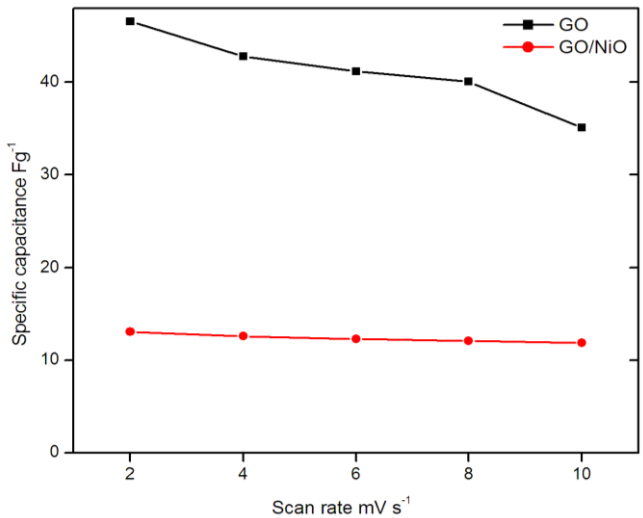

Fig. 17. Variation of Specific Capacitance with scan rate

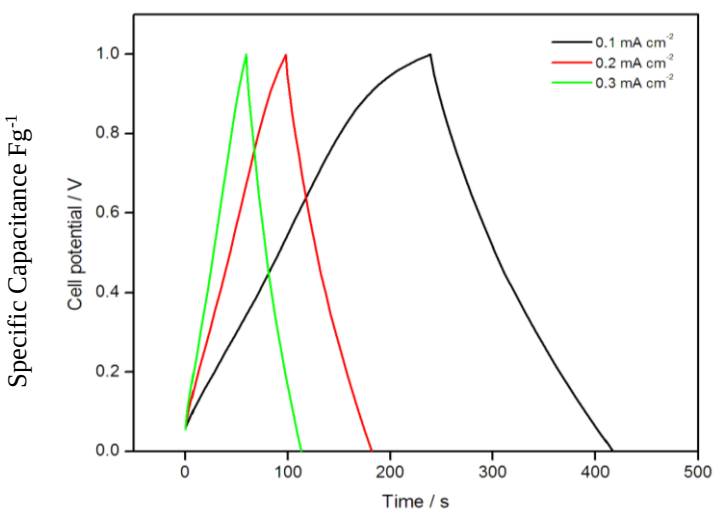

Fig. 18. GCD curves of GO/NiO at different current density

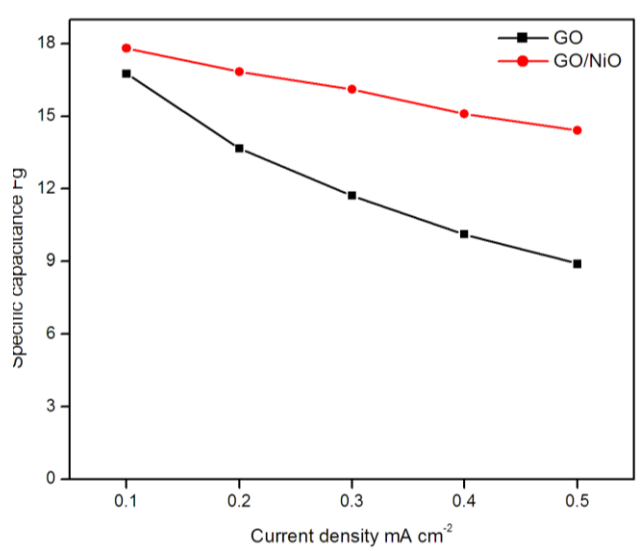

Fig. 19. Variation of Specific Capacitance with current density

4. Conclusion

GO and GO/NiO nanocomposites have been synthesized by hydrothermal method. The particulate nature of the synthesized materials is confirmed by SEM images. The XRDs of nanocomposites show the NiO is in cubic structure. Using scherrer equation the average particle size of 17.6635 nm was calculated for the hydrothermally synthesized nanocomposites. The EDX spectra of the synthesized nanocomposites show the purity and the percentage of the NiO on GO matrix. Further the FT-IR spectrum confirms the presence of doping NiO molecules on the GO matrix by the sharp peak at 645 cm^{-1}. However to explore the charge carrying capability of the hydrothermally synthesized GO and GO/NiO nanocomposites the electrochemical studies like Cyclic voltammetry, Galvanostatic charge-discharge has been studied. NiO doped on GO have some significant textural and good electrochemical property put forward to make it as a supercapacitor cell. CV and GCD reveal the electrochemical capacitive behavior of the synthesized material. The single electrodes made by GO/NiO have good rectangularity and reversibility and acquires high specific capacitance. But it was low when compare with bare GO. The symmetric supercapacitor cell assembled for the GO and GO/NiO shows good electrochemical behavior as substantiated by CV and GCD analysis. The specific capacitance from CV of the GO symmetric cell at a scan rate of 2 mV s^{-1} is 46.55 F g^{-1} and for GO/NiO synthesized by hydrothermal method has 13.08 F g^{-1}. The decrease in specific capacitance of GO/NiO is due to its high diffusive resistance. From GCD analysis the specific capacitance of both GO and GO/NiO was calculated as 17.82 and 16.76 Fg^{-1} respectively. It has been clearly shown that NiO doped GO shows higher specific capacitance than the undoped GO.

5. References

1. Novoselov KS, Geim AK, Morozov SV, Jiang D, Zhang Y, Bubonos SV, et al. Science., **2004**, 306(5696):666–9.
2. Balaprasad, Farah, Chemical Science., **2012**, 10: 500-507.
3. Ling S, Bunshi F, Journal of Nanomedicine & Nanotechnology., **2000,** 6(1):1000253
4. Li, Limiao, et al. Talanta 82.5., **2010,** 1637-1641.
5. Tian, Zhiting; Hu, Han; Sun, Ying. Int. J. Heat Mass Transfer., **2013,** 61: 577–582.
6. J. Liang, Y.D. Li, Chemistry Letters 32., **2003,** 1126–1127.
7. Zhao, Bing, et al. Journal of Materials Chemistry 21.46., **2011,** 18792-18798.
8. Meher, Sumanta Kumar, P. Justin, and G. Ranga Rao. ACS applied materials & interfaces 3.6., **2011,** 2063-2073.
9. B.J. Li, H.Q. Cao, J. Mater. Chem. 21., **2011,** 3346–3349.
10. J. Lin, M. Penchev, G.P. Wang, R.K. Paul, J.B. Zhang, X.Y. Jing, M. Ozkan, C.S. Ozkan, Material Research Express, 6., **2014,** 2448–2452.
11. O. Akhavan, ACS Nano 4., **2011,** 4174–4180.
12. Paulchamy B1, Arthi G2 and Lignesh BD., J Nanomed Nanotechnol, **2015**, 6-1-100253
13. Zhigang Wang, Yong Hu, Wenlong Yang, Sensors, **2012**, 12(4), 4860-4869
14. Zhangpeng Li, ab Yongjuan Mi, ab Xiaohong Liu, J. Mater. Chem., **2011**, 21, 14706-14711
15. Seung-Gi Hwang,Gyeong-OK Kim, Su-Ryeon Yun, Electrochimica Acta 78., **2012**, 406– 411

A Study on Synthesis and Characterization of garnet based solid electrolytes for Battery applications

Leo Edward M & Jaisankar V
PG and Research Department of Chemistry, Presidency College (A), Chennai-600005, India

ABSTRACT: *Designing of solid state batteries with good ionic conductivity, electrochemical stability, and scalable processing methodology is challenge for the recent years. Garnet solid electrolytes (GSE) plays a vital role in meeting needs of challenge. Garnet has revealed many potential properties novel structural applications. In this investigation, Garnet was synthesized using Lithium nitrate, Lanthanum nitrate, Zirconium oxy nitrate as precursors and acetic acid as a chelating agent by sol-gel method. Then, the cadmium nitrate was doped with the e synthesized garnet. The synthesized garnet and doped garnet nanopowders were calcinated at two different temperatures such as 600˚C and 800˚C. The synthesized materials were characterized using Fourier transform spectroscopy (FTIR), X-ray diffraction (XRD). The surface morphology of the synthesized garnet and doped garnet were observed using high resolution scanning electron microscopy (HRSEM). The thermal stability of Garnet and doped Garnet were analyzed by Thermogravimetric Analysis.*

Keywords: *Solid state batteries, Garnet, Sol-Gel method, nano powders, thermal stability.*

1. Introduction

High energy density lithium ion batteries are promising electrochemical energy storage devices and play an increasingly important role in the development of portable electronic devices as well as the electronic vehicles and smart grids (1). The investigation on crystalline lithium ionic conductors has been recently extended to a set of garnet-type $Li_5La_3M_2O_{12}$ (M = Nb, Ta, Ho) oxides. These compounds were found to exhibit pure lithium ionic conductivity and high chemical inertness versus Li, making them promising for application as electrolyte in all solid-state lithium secondary batteries [2-6].

In some cases, in which power sources are to be operated under extreme environmental conditions, such as at high temperature and pressure in the field of space, defence and oil and gas exploration, all-solid-state lithium-ion batteries are clearly the best choice [7]. Hence, great efforts have been taken to bridge the interfacial resistance between the garnet electrolyte and the electrode materials [8]. Amongst the oxide solid electrolytes, $Li_7La_3Zr_2O_{12}$ (LLZO) garnets are regarded as ideal candidates for lithium ion batteries [8-11]. There are various types of inorganic solid state electrolytes(SSEs) have been reported, including sulfide- type, oxide- type, and oxynitride-type materials [12]. Among different kinds of inorganic SSEs, garnet $Li_7La_3Zr_2O_{12}$ (LLZO) is a promising type of electrolyte for Li-metal batteries [13-16]. It has been suggested that supervalent cations can stabilize the cubic structure at room temperature by introducing Li vacancies and/or decreasing the Li content [17]. LLZO has been reported with two phases. The cubic phase shows two orders of higher conductivity compared to the tetragonal phase due to the lithium ion migration pathway and distribution in the structure of the LLZO [18-19]. Besides many researches focused on doping various cations (Fe^{3+}, Ga^{3+}, Nb^{4+}, Ta^{5+}, Te^{6+} etc) to stabilize cubic LLZO and obtained high ionic conductivities in the range of 1.37×10^{-2} to 10^{-4} S cm-1 at room temperature [20-24]. However, the majority of substitutions performed on the Zr4+ site in LLZO is made by high valence ions, which can decrease the lithium ion concentration and leads to produce impure phases easily. There are few reports on the substitution of Zr^{4+} by different ions of the same valence [13, 18]. Systematic research has been carried out on $Li_7La_3Zr_2{-}xCdxO_{12}$ lithium garnets to investigate the effect of Cadmium (Cd) ion substitution on the structure and electrochemical property.

2. Experimental details

2.1 Synthesis

The materials used for the synthesis are acetic acid as chelating agent and 1- propanol (IPA) surface active agent $LiNO_3$ (sigma Aldrich) $La(NO_3)_3$(sigma Aldrich) $ZrO(NO_3)_2$ (Merck) $Cd(NO_3)_2$ was obtained from(Alfa Aesar). All reagents used were of analytical grade and use directly without any purification.

In this work, synthesis garnet powders (LLZCO) were synthesized by sol-gel method. The appropriate amount of excess $LiNO_3$ excess (10 wt %) was added to compensate for expected Li loss. The

raw materials were mixed in a appropriate molar ratio based on the chemical formula of (LLZCO). La $(NO_3)_3 \cdot 6H_2O$, and $LiNO_3$ were dissolved into distilled water (A) and then $ZrO(NO_3)_2$ (A). , $Cd(NO_3)_2$ was separately dissolved in 1-propanol with1.0 M acetic acid and then added to (A) for doping. The solutions were magnetically stirred at 50 °C for 12 h. The solvent was then slowly evaporated and a transparent gel was obtained at 80 °C. The obtained gels were then dried for 12 hour in an oven at 100^0C, a light brown precursor powder was formed and then finely grounded well. The grounded powder was annealed at two kind of temperatures 600°C and 800 °C for 5 h for further characterization [25-26].

2.2 Schematic diagram for synthesis method

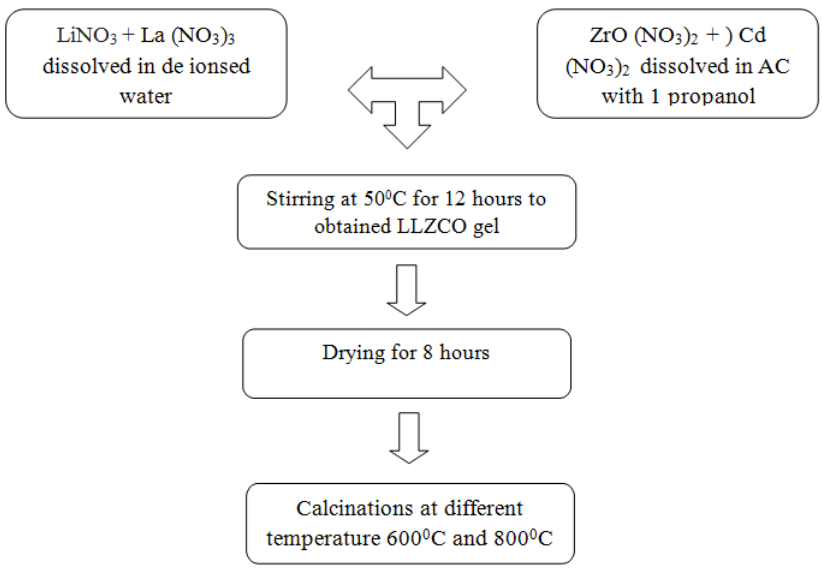

2.3 Characterization

FTIR spectra of synthesized garnet were recorded with a perkin Elmer FTIR spectrometer - spectrum. The surface morphology of the synthesized garnet powder were observed using HITACHI S-3000 high resolution scanning electron microscopy (HRSEM) . The phase composition of the synthesized garnet powder were characterized with X-ray diffraction with a Cu Kα radiation at 1.5406 A, scanned over 2ɵ range of 10-80º. Synthesized garnet powders thermal behaviors analysis by TG/DGA.

3. Results and discussion

3.1 Morphology analysis

Figure-1

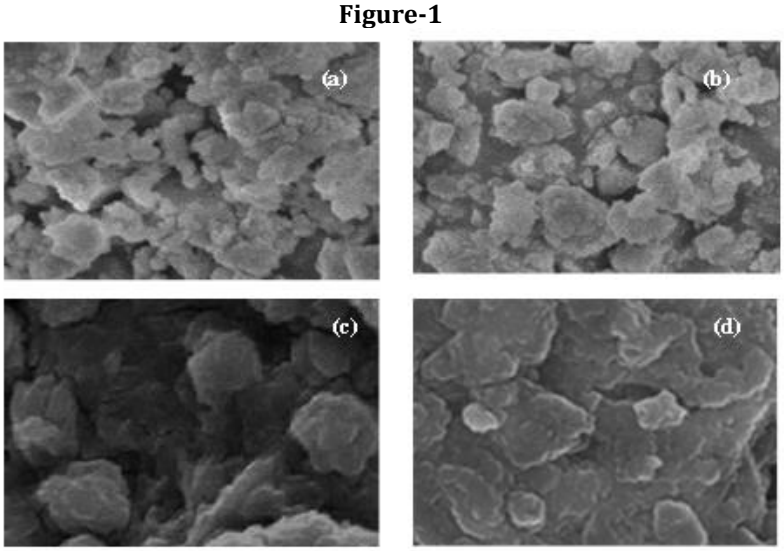

Fig.1 planer SEM images of the LLZCO powder prepared by sol-gel method using two different temperatures 600^0C and 800^0C images a and b 600^0C and images c and d 800^0C

Figure.1 shows SEM images of the surface of the LLZCO powders prepared by sol-gel methods and calcinated at two different temperature 600^0C and 800^0C image a and b calcinated at 600^0C and image c and d calcinated at 800^0c for 5 hours. This indicates that average particle sizes of the products also depend upon the surfactant agents used in sol-gel synthesis. The shape of the powder surface was found not to be significantly dependent on the synthesis method.

3.2. IR- Spectroscopy

The infrared spectra of the synthesized Li La Zr Cd-O garnet powders heat-treated at 600 C^o for 5 hours. The broad band in the region of 3500 cm^{-1} is related to the O-H group, which is associated with water molecules coordinated with the metal ions. The band positioned between 3200 and 2500 cm^{-1} was referred to the intramolecular hydrogen with C=O bond. A band observed at 1750 cm^{-1} is related to the C=O bond of acid with axial deformation. The bands observed between 1546 and 1362 cm^{-1} are ascribed to the stretching vibrations of the carboxilate (COO^-) groups, or C-H bonds (27).

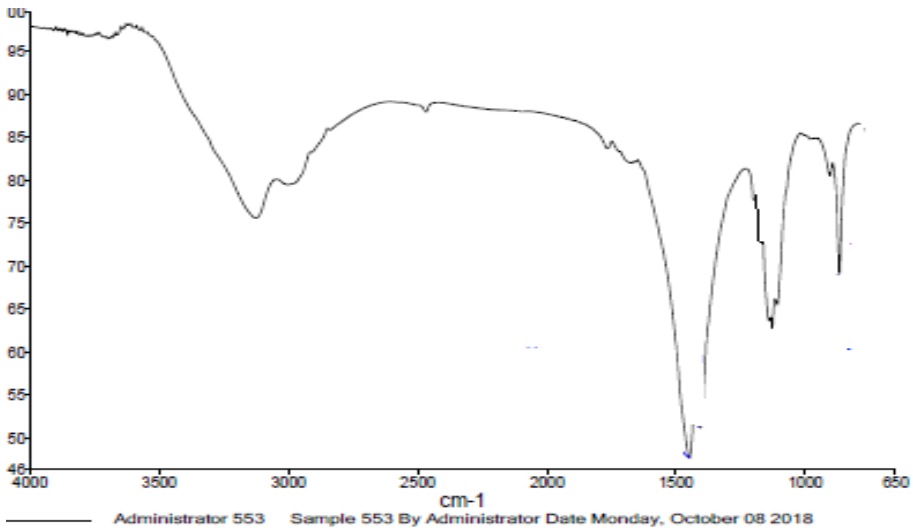

Figure.2 IR- spectrum the of synthesized Li,La,Zr-CdO_{12} garnet powder for 600°C

3.2. X-Ray Diffraction spectra

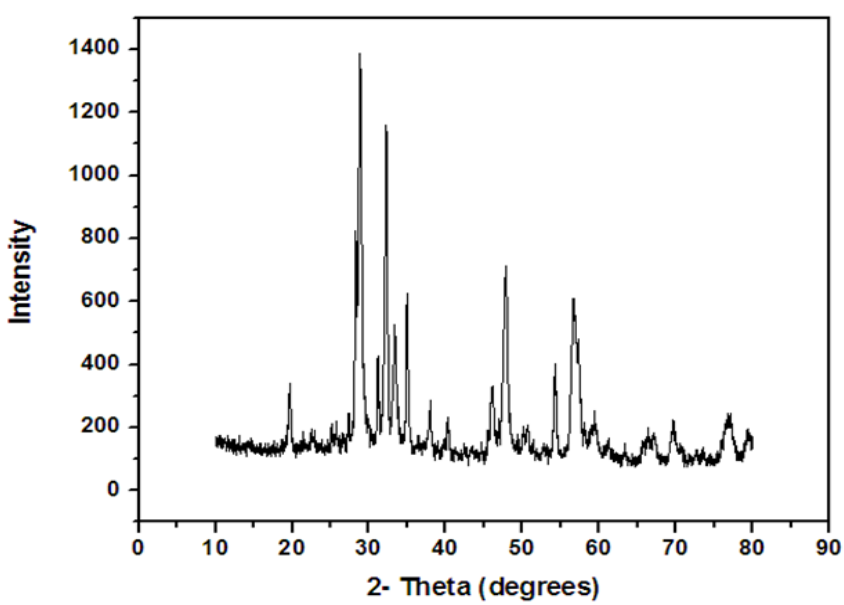

Figure.3 XRD patterns for the calcined Cd- LLZO garnet powder

The crystalline Structure of the synthesized garnet powder was analyzed by X- ray powder diffraction using a phillips X pert instrument with a Cu tube and K α radiation at 1.5406 A, scanned over 2ɵ range of 10-80° . The crystallite size was calculated using line broadening analysis based on the scherrer equation 28.

3.3. Thermal analysis

Thermogravimetric analysis / Differential thermal analysis (TG/DTA) was empolyed to narrow the proper temperature range for the synthesis. The decomposition behaviors of the garnet powder were also obtained by differential thermal analysis. TG/DTA curves of precursor calcinated at 600°C are presented in figure 4

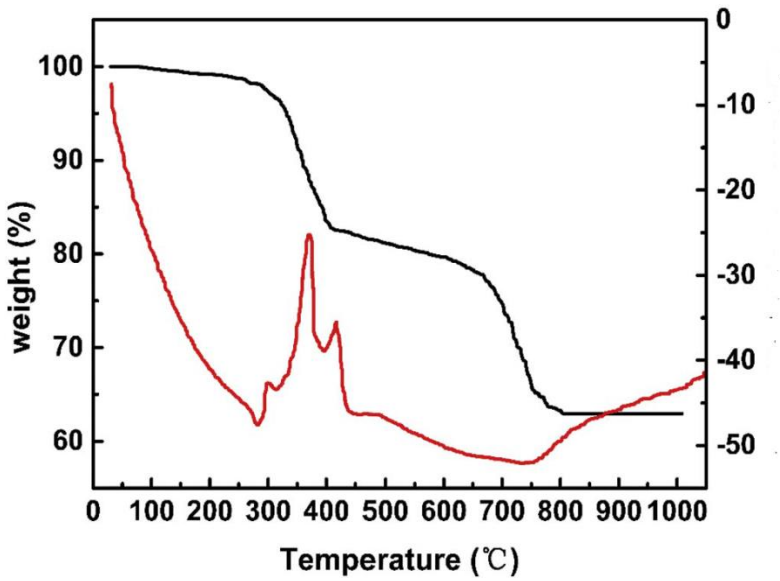

Figure-4 TG/DTA for the calcined Cd- LLZO garnet powder

4. Conclusion

In this present study ploy crystalline cubic LLZCO garnet type structure was synthesized at 600°C and 800°C by sol gel process in which acetic acid was used chelating agent and 1- propanol as surfactant, relatively good properties were obtained by first dissolving Li and La materials and Zr and Cd materials dissolving acetic acid alcohol mixture both solution together. SEM micrographs of LLZCO polycrystalline cubic with garnet related type structure has been synthesized at 600°C and 800°C, a slight amount of tetragonal phase was included because the driving energy of the transformation to the cubic phase was not sufficiently high.

References

1. Xiao Huang, Cai Liu, Yang Lu, Tongping Xiu, jun jin, Michael E Garnet Solid Electrolyte Protected Li-Metal Batteries, ACS Appl. Mater. Interfaces 2018, 10, 17147–17155.
2. Y.X. Gao, X.P. Wang, W.G. Wang,Q. F. Fang Sol–gel synthesis and transport property of nanocrystalline La2Mo2O9 thin films, J Sol-Gel Sci Technol (2008) 48:315–321.
3. V. Thangadurai, H. Kaack, W.J.F. Weppner, Novel Fast Lithium Ion Conduction in Garnet- Type Li5La3M2O12J, Journal of the American Ceramic Society, (2003) 86 [3] 437–40.
4. V. Thangadurai, W. Weppner, $Li_6ALa_2Nb_2O_{12}$ (A=Ca, Sr, Ba): A New Class of Fast Lithium Ion Conductors with Garnet-Like Structure J. Power Sources 142 (2005) 339.
5. V. Thangadurai, W. Wepper, Adv. Funct. Mater. 15 (2005) 107.
6. V. Thangadurai, S. Adams, W. Weppner, Crystal Structure Revision and Identification of Li+- Ion Migration Pathways in the Garnet-like Li5La3M2O12 (M) Nb, Ta) Oxides Chem. Mater (2004) . 16 2998
7. Kalaga, K. Rodrigues, M.-T. F. Gullapalli, H. Babu, G. Arava, L. M. R. Ajayan, P. M., Quasi-Solid Electrolytes for High Temperature Lithium Ion Batteries ACS Appl. Mater. Interfaces (2015),7, 25777-25783.
8. Thangadurai, V., Narayanan, S., Pinzaru, D., Garnet-type Solid-state Fast Li Ion Conductors for Li Batteries: Critical Review Chem. Soc. Rev. (2014), 43, 4714-4727.
9. Luo, W. Gong, Y.Zhu, Y. Fu, K. K. Dai, J. Lacey, S. D. Wang, C. Liu, B. Han, X Mo, Y.;Wachsman,E. D. Hu, L., Transition from Super-lithiophobicity to Super-lithiophilicity of Garnet 20Solid-state Electrolyte J. Am. Chem. Soc. (2016), 138, 12258–12262.

10. Fua, K. K.; Gonga, Y.; Daib, J.; Gong, A.; Han, X.; Yao, Y.; Wang, C.; Wang, Y.; Chen, Flexible, Solid-state, Ion-conducting Membrane with 3D Garnet Nanofiber Networks for Lithium Batteries, Natl. Acad. Sci. (2016), 113, 7094-7099.
11. Wu, J, Chen, E., Yu, Y., Liu, L., Wu, Y., Pang, W., Peterson, V. & Guo, X.. Gallium-Doped Li7La3Zr2O12 Garnet-Type Electrolytes with High Lithium-Ion Conductivity. ACS Applied Materials and Interfaces, (2017), 9 (2), 1542-1552.
12. Bernstein, N.; Johannes, M. D.; Hoang, K. Origin of the Structural Phase Transition inLi7La3Zr2O12. American Physical Society,*Phys. Rev.(* 2012), *109*, 205702
13. Boyang Liu, Yunhui Gong, Kun Fu, Xiaogang, Li7La3Zr2O12 Interface Modification for Li Dendrite Prevention ACS Appl. Mater. Interfaces (2017), 9, 18809−18815
14. Knauth, P. Inorganic Solid Li Ion Conductors, An Overview.Solid State Ionics (2009), 180, 911−916.
15. Afyon, S.; Krumeich, F.; Rupp, J. L. M. A Shortcut to Garnet-Type Fast Li-Ion Conductors for All-Solid State Batteries. J. Mater.Chem. (2015), 3, 18636−18648.
16. Zhu, Y. He, X. Mo, Y, Origin of Outstanding Stability in the Lithium Solid Electrolyte Materials: Insights from Thermodynamic Analyses Based on First-Principles Calculations. ACS Appl. Mater. Interfaces (2015), 7, 23685−23693.
17. J. Awaka, N. Kijima, H. Hayakawa, J. Akimoto, Synthesis and structure analysis of tetragonal Li7La3Zr2O12 with the garnet-related type structure, Solid State Chem. (2009) 182 2046–2052
18. Shuqiao Hu, You-Fen Li, Ru Yang, Zijian Yang, Lege Wang, Structure and ionic conductivity of Li7La3Zr2−xGexO12 garnet-like solid electrolyte for all solid state lithium ion batteries, Ceramics International, (2018) 44 6614–6618.
19. Rettenwander, D. Geiger, C. A. Amthauer, G. Synthesis and Crystal Chemistry of the Fast Li-Ion Conductor Li7La3Zr2O12 Doped with Fe, ACS Publication *Inorg. Chem.(*2013), *52*, 8005-8009.
20. Jalem, R.; Rushton, M. J. D. Manalastas, W. Nakayama, M. Kasuga, T. Kilner, J. A.;Grimes, R. W. Effects of Gallium Doping in Garnet-Type Li7La3Zr2O12 Solid Electrolytes ACS Publication *Chem. Mater. (*2015), *27*, 2821-2831.
21. Tong, X.; Thangadurai, V.; Wachsman, E. D. Highly Conductive Li Garnets by a Multielement Doping Strategy. ACS Publication *Inorg. Chem.(* 2015), *54*, 3600-3607.
22. Rettenwander, D. Geiger, C. A. Tribus, M.; Tropper, P. Amthauer, G. A Synthesis and Crystal Chemical Study of the Fast Ion Conductor Li7-3xGaxLa3Zr2O12 with x = 0.08 to 0.84.*Acs publication Inorg. Chem.* (2014) 16; 53(12): 6264–6269.
23. Deviannapoorani, C. Dhivya, L. Ramakumar, S. Murugan, R. Lithium Ion Transport Properties of High Conductive Tellurium Substituted Li7La3Zr2O12 Cubic Lithium Garnets. *J.Power Sources(* 2013), *240*, 18-25.
24. C. Shao, Z. Yu, H. Liu, Z. Zheng, N. Sun, C. Diao, Electrochim. Acta 225 (2017)345–349
25. Sang A Yoon, Nu Ri Oh, Ae Ri Yoo, Hee Gyun Lee, and Hee Chul Lee, Preparation and Characterization of Ta-substituted Li7La3Zr2-xO12 Garnet Solid Electrolyte by Sol-Gel Pro cessing, Journal of the Korean Ceramic Society, (2017) 54, No. 4, pp. 278~284.
26. N. Janani, S. Ramakumar, L. Dhivya, C. Deviannapoorani, K. Saranya, Ramaswamy Murugan, Synthesis of cubic Li7La3Zr2O12 by modified sol–gel process, Ionics, (2011) 17:575–580.
27. Adriano,Alves,Rabelo,Marfran,Cardosode,Macedo, Synthesis and Characterization of La1- xSrx MnO3±δ Powders Obtained by the Polymeric Precursor Route Materials Research. (2011) 14(1): 91-96.

The First Recyclable, Eco-benign Liquid Resin Mediated Synthesis of Hantzsch 1, 4 Dihyropyridines, 1, 8-Dioxodecahydroacridine and polyhydroquinolines derivatives

K. Venkatapthy, G. Lavanya, C. J. Magesh, P. Amudha & S. Prema
P.G. and Research Department of chemistry
Arignar Anna Govt. Arts and Science College, Cheyyar, Tamilnadu, India – 604 407

ABSTRACT: *In the present study, we report novel, eco-benign Phenol-formaldehyde liquid resin as a catalyst and medium for efficient one-pot three component synthesis of Hantzsch 1, 4 dihydropyridine in good Yields. The catalyst was also effective for the synthesis of polyhydroquinolines, acridine derivatives in good to excellent yields. The effect of temperature, substituents, catalyst loading and mole ratio on the reaction was also studied. All the product was thoroughly characterized by ^{1}H-NMR,^{13}C-NMR, FT-IR, Mass spectral and CHN analysis. A plausible mechanism for the synthesis was proposed and the catalyst could be successively reused without loss of activity atleast five times.*

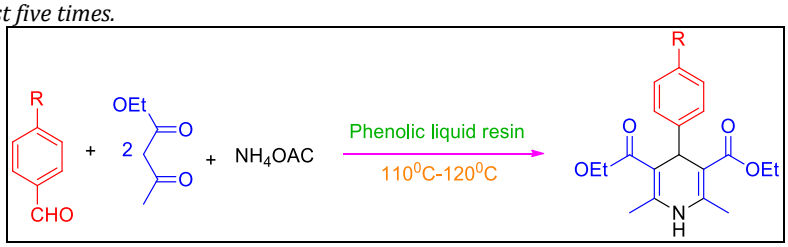

Keywords: *Phenol formaldehyde liquid resin, 1, 4 dihydropyridine, polyhydroxyquinoline, acridine, Multicomponent reaction, solvent free conditions.*

1. INTRODUCTION

Polyhydroquinolines, 1, 4 Dihydropyridines (1,4 DHP's) and Acridine derivatives are important class of heterocycles containing nitrogen atom. More recently much attention has been focused in the preparation of polyhydroquinoline, 1, 4 dihydropyridines and acridines because of their biological properties [1] such as vasodilator, antitumor, bronchodilator antiatherosclerotic, geroprotective and hepatoprotective activities [2]. In addition, these skeleton shows manifold therapatic utility such as platelet antiaggregatory activity and chemosensitizer acting in tumor treatment [3]. Acridine derivatives have been used as antimalarials [4,5] and some of the acridine compounds show good results in chemotherapy of cancer [6,7]. Acridine compounds are often used in the industry for the preparation of dyes (8). Therefore various methods have been developed for the synthesis of ploydroquinoline derivatives and 1,4 DHP and Acridine derivatives by using different catalyst containing molecular iodine [9], ionic liquid [10], rare earth metal triflates [11], $HClO_4 – SiO_2$ [12] Hy-zeolites [13], TMSCI – NaO [14], CAN [15], grinding techniques [16], *P*-TSA [17], Polymer catalysts [18], Organic catalysts [19], Solar heat [20], Triphenyl phosphine [21], Amberlyst [22], $H_3Pu_{12}O_{40}$ supported MCM-41 [23], LiBr [24], MCM – $4ISO_3H$ assisted by ultrasonics [25]. Inspite of the fact that processes offer many advantages, they are associated with some disadvantages such as unsatisfactory yields, low yield, extended reaction times, elevated temperatures, tedious work-up anhydrous organic solvents and high cost catalysts.

Because of its strength and stability phenol formaldehyde resin finds extensive application as fillers, electrical insulators, laminated plastics and as moulded parts for various application [26]. More recently we have reported the phenol formaldehyde liquid mediated synthesis of biginelli compounds [27]. In continuation of our search for effective utilisation of Phenol formaldehyde liquid resin as a medium and catalyst for organic synthesis, we now report an efficient, eco-benign synthesis of Hantzsch 1, 4 dihydropyridine, polyhydroxyquinoline and acridine derivatives mediated by phenol-formaldehyde liquid resin.

2. EXPERIMENTAL

2.1 A typical experimental procedure for novel liquid resin mediated synthesis of Hantzsch 1,4 Dihydropyridines (A).

A mixture of aromatic aldehyde (1a) (0.0045mol), ethylacetoacetate (2a) (0.0099 mol) and ammonium acetate (0.018 mol) was added to round bottom flask containing phenol-formaldehyde liquid resin (10g). The reaction mixture was stirred at 115-120°C for an appropriate time (Table 2). After complete conversion, as indicated by TLC, the reaction mixture was transferred to conical flask containing 50ml of 10% NaOH, stirred and ethylacetate (3×20ml) was added to it. The organic layer was separated, concentrated in vacuum. The crude product was purified by column chromatography on silica gel (Merck, 60–120 mesh, ethylacetate/petroleum ether, 1:4) to give the product (4a) in 94.0% yield.

2.2 A typical experimental procedure for novel liquid resin mediated synthesis of 1,8 dioxodecahydroacridine derivatives (B).

A mixture of aromatic aldehyde (1a) (0.0045 mol), 5,5-dimethylcyclohexane-1,3-dione (2a) (0.0099 mol) and ammonium acetate (0.0189 mol) was added into the round bottom flask containing phenol-formaldehyde liquid resin (10g). The reaction mixture was stirred at 115-120°C for an appropriate time (Table 2). After complete conversion, as indicated by TLC, the reaction mixture was transferred to conical flask containing 50ml of 10% NaOH, stirred and ethylacetate (3×20ml) was added to it. The organic layer was separated, concentrated in vacuum. The crude product was purified by column chromatography on silica gel (Merck, 60–120 mesh, ethylacetate/petroleum ether, 1:1) to give the product (6a) in 88.0% yield.

2.3 A typical experimental procedure for novel liquid resin mediated synthesis of polyhydroquinolines (C).

Aryl aldehyde (1mmol), Ethylaceto acetate (2mmol), ammonium acetate (2mmol) in the presence of phenolic liquid resin (10g) was taken in the RB flask and heated in a oil bath at 110° – 120°C. After complete conversion, as indicated by TLC, the reaction mixture was transferred to conical flask containing 50ml of 10% NaOH, stirred and ethylacetate (3×20ml) was added to it. The organic layer was separated, concentrated in vacuum. The crude product was purified by column chromatography on silica gel (Merck, 60–120 mesh, ethylacetate/petroleum ether, 1:1) to give the product (7a) in 87.0% yield.

2.4 Spectral Data

2.4.1. Diethyl 2,6-dimethyl-4-phenyl-1,4-dihydropyridine-3,5-dicarboxylate (4a)
FT- IR (KBr) V_{max} cm^{-1}: 3323, 1676, 1648, 1853, 1240, 1120, 631; **^{1}H NMR ($CDCl_3$, 300 MHz, ppm) δ:** 7.23 (m, 5H), 5.70 (brs, 1H, NH), 4.99 (s, 1H), 4.10 (m, 4H), 2.33 (s, 6H), 1.22 (t, 6H); **^{13}C NMR (75MHz, $CDCl_3$) δ:** 167.7, 147.7, 144.0, 127.9, 127.7, 126.0, 103.9, 59.7, 39.5, 19.4, 14.2; **MS**: m/z: 329 (M^+); **Anal. Calcd. for** $C_{19}H_{23}NO_4$: C, 69.28; H, 7.04; N, 4.25; **Found**: C, 68.99; H, 7.01; N, 4.18.

2.4.2. Diethyl 4-(4-nitrophenyl)-2,6-dimethyl-1,4-dihydropyridine-3,5-dicarboxylate (4b)
FT- IR (KBr) V_{max} cm^{-1}: 3341, 2989, 1656, 1344, 1141, 702; **^{1}H NMR ($CDCl_3$, 300 MHz, ppm) δ:** 8.09 (d, 2H), 7.46 (d, 2H), 5.64 (brs, 1H, NH), 5.10 (s, 1H), 4.05-4.15 (m, 4H), 2.32 (s, 6H), 1.22 (t, J=7.2 Hz, 6H); **^{13}C NMR (75MHz, $CDCl_3$) δ:** 168.1, 147.5, 144.7, 131.5, 130.1, 120.4, 104.3, 60.4, 39.9, 20.2, 14.8; **MS**: m/z: 374 (M^+); **Anal. Calcd. for** $C_{19}H_{22}N_2O_6$: C, 60.95; H, 5.92; N, 7.48; **Found**: C, 60.89; H, 5.81; N, 7.39.

2.4.3. Diethyl 4-(4-chlorophenyl)-2,6-dimethyl-1,4-dihydropyridine-3,5-dicarboxylate (4c)
FT- IR (KBr) V_{max} cm^{-1}: 3350, 2986, 1693, 1647, 1112, 822; **^{1}H NMR ($CDCl_3$, 300 MHz, ppm) δ:** 8.91 (s, 1H), 7.11 (d, J=8.1Hz, 2H), 7.11 (d, J=8.4 Hz, 2H), 4.99 (s, 1H, NH), 3.90 (d, J=8.7 Hz, 4H), 2.13 (s, 6H), 1.06 (t, J=7.0 Hz, 6H); **^{13}C NMR (75MHz, $CDCl_3$) δ:** 167.8, 146.21, 144.21, 129.51, 129.23, 126.90, 117.80, 101.59, 59.17, 40.11, 18.31, 14.28; **MS**: m/z: 363 (M^+); **Anal. Calcd. for** $C_{19}H_{22}ClNO_4$: C, 62.72; H, 6.09 N, 3.85; **Found**: C, 62.69; H, 6.01; N, 3.79.

2.4.4. Diethyl 4-(4-methoxyphenyl)-2,6-dimethyl-1,4-dihydropyridine-3,5-dicarboxylate (4d)
FT- IR (KBr) V_{max} cm^{-1}: 3340, 2981, 1690, 1651, 1211, 1129, 753; **^{1}H NMR ($CDCl_3$, 300 MHz, ppm) δ:** 7.23 (d, J=8.6Hz, 2H), 6.76 (d, J=8.6 Hz, 2H), 6.13 (s, 1H), 4.95 (s, 1H, NH), 4.12 (q, J=7.2 Hz, 4H), 3.76 (s, 3H), 2.31 (s, 6H), 1.25 (t, J=7.2 Hz, 6H); **^{13}C NMR (75MHz, $CDCl_3$) δ:** 167.6, 157.90, 143.47, 140.32, 128.95, 113.20, 104.45, 59.68, 55.14, 38.76, 19.58, 14.27; **MS:** m/z: 359 (M^+); **Anal. Calcd. for** $C_{20}H_{25}NO_5$: C, 66.83; H, 7.01 N, 3.90; **Found**: C, 66.78; H, 7.67; N, 3.85.

2.4.5. Diethyl 4-(p-toly)-2,6-dimethyl-1,4-dihydropyridine-3,5-dicarboxylate (4e)
FT- IR (KBr) V_{max} cm^{-1}: 3349, 1655, 1490, 1201, 1115, 741; **^{1}H NMR ($CDCl_3$, 300 MHz, ppm) δ:** 7.51 (m, 4H), 5.60 (brs, 1H, NH), 4.89 (s, 1H), 3.98 (m, 4H), 2.30 (s, 6H), 2.19 (s, 3H), 1.27 (s, 6H); **^{13}C NMR (75MHz, $CDCl_3$) δ**: 168.4, 146.4, 145.1, 127.8, 126.9, 126.0, 103.8, 60.1, 39.8, 19.4, 14.9, 14.2; **MS:** m/z: 343 (M^+); **Anal. Calcd. for** $C_{20}H_{25}NO_4$: C, 69.95; H, 7.34 N, 4.08; **Found**: C, 69.88; H, 7.27; N, 4.05.

2.4.6. 3,3,6,6-tetramethyl-9-phenyl-3,4,6,7,9,10-hexahydroacridinne-1,8 (2H, 5H)-dione (6a)
FT- IR (KBr) V_{max} cm^{-1}: 3431, 3269, 2956, 2875, 1614, 1479, 1366, 1224, 1154; **^{1}H NMR (DMSO-d_6, 300 MHz, ppm)**: 9.37 (brs, 1H, NH), 7.15-7.23 (m, 5H), 4.81 (s, 1H), 2.42 (d, J= 16.2 Hz, 2H), 2.39 (d, J= 16.2 Hz, 2H), 2.28 (d, J=16.2 Hz, 2H), 2.18 (d, J=16.2 Hz, 2H), 1.01 (s, 6H), 0.96 (s, 6H); **^{13}C NMR (75MHz, DMSO-d_6) δ**: 111.7, 50.4, 40.6, 33.1, 32.3, 29.3, 26.6. **MS: m/z:** 349 (M^+); **Anal. Calcd. for** $C_{23}H_{27}NO_2$: C, 70.03; H, 6.64; N, 7.10; **Found**: C, 70.00; H, 6.57; N, 7.05.

2.4.7.3,3,6,6-tetramethyl-9-(4-nitrophenyl)-3,4,6,7,9,10-hexahydroacridinne-1,8(2H,5H)-dione (6b)
FT-IR (KBr) V_{max} cm^{-1}: 3427, 3176, 2969, 2871, 1604, 1463, 1222, 1090; **^{1}H NMR (DMSO-d_6, 300 MHz, ppm):** 9.25 (brs, 1H, NH), 7.21-7.30 (m, 4H), 4.78 (s, 1H), 2.43 (d, 2H), 2.40 (d, 2H), 2.30 (d, 2H), 2.15 (d, 2H), 1.21 (s, 6H), 1.01 (s, 6H); **^{13}C NMR (75MHz, DMSO-d_6) δ**: 196.2, 150.0, 148.3, 127.4, 120.8, 111.7, 50.4, 41,8, 34.1, 32.9, 29.5, 29.4, 26.4; **MS: m/z**: 394 (M^+); **Anal. Calcd. for** $C_{23}H_{26}N_2O_4$: C, 70.03; H, 6.64 N, 7.10; **Found**: C, 70.00; H, 6.57; N, 7.05.

2.4.8.3,3,6,6-tetramethyl-9-(4-chlorophenyl)-3,4,6,7,9,10-hexahydroacridinne-1,8 (2H,5H)-dione (6c)
FT- IR (KBr) V_{max} cm^{-1}: 3387, 3320, 3208, 3173, 3029, 2196, 1677, 1605, 1459, 1360, 1221, 1144; **^{1}H NMR (DMSO-d_6, 300 MHz, ppm)** δ: 8.5 (brs, 1H, NH), 7.28 (d, 2H), 6.79 (d, 2H), 5.05 (s, 1H), 2.35 (d, 2H), 2.24 (d, 2H), 2.22 (d, 2H), 2.15 (d, 2H), 1.01 (s, 6H), 0.96 (s, 6H); **^{13}C NMR (75MHz, DMSO-d_6) δ:** 196.3, 150.0, 145.5, 131.6, 129.6, 128.2, 112.7, 50.9, 40.5, 33.5, 32.7, 29.7, 27.1; **MS:** m/z: 383 (M^+); **Anal. Calcd. for** $C_{23}H_{26}ClNO_2$: C, 71.96; H, 6.83 N, 3.65; **Found**: C, 71.80; H, 6.77; N, 3.55.

2.4.9.3,3,6,6-tetramethyl-9-(4-methoxyphenyl)-3,4,6,7,9,10-hexahydroacridinne-1,8(2H,5H)-dione (6d)
FT- IR (KBr) V_{max} cm^{-1}: 3418, 3268, 3152, 2750, 1645, 1608, 1447, 1350, 1218, 1140; **^{1}H NMR (DMSO-d_6, 300 MHz, ppm)** δ: 8.58 (brs, 1H, NH), 7.35 (d, 2H ArH), 6.64 (d, 2H), 4.95 (s, 1H), 3.84 (s, 3H), 2.30 (d, 2H), 2.25 (d, 2H), 2.20 (d, 2H), 2.13 (d, 2H, CH_2), 1.27 (s, 6H, CH_3), 1.01 (s, 6H, CH_3); **^{13}C NMR (75MHz, DMSO-d_6) δ:** 196.7, 157.6, 149.6, 140.4, 129.9, 113.5, 113.1, 54.9, 51.9, 40.5, 32.7, 31.1, 29.5, 28.1; **MS:** m/z: 379 (M^+); **Anal. Calcd. for** $C_{24}H_{29}NO_3$: C, 75.96; H, 7.79 N, 3.69; **Found**: C, 75.80; H, 7.74; N, 3.58.

2.4.10. 3,3,6,6-tetramethyl-9-(p-toly)-3,4,6,7,9,10-hexahydroacridinne-1,8(2H,5H)-dione (6e)
FT-IR (KBr) V_{max} cm^{-1}: 3371, 3322, 3197, 2950, 1644, 1618, 1466, 1364, 1213, 1160; **^{1}H NMR (DMSO-d_6, 300 MHz, ppm)** δ **:** 9.37 (brs, 1H, NH), 7.15-7.23 (m, 4H), 3.94 (s, 1H), 2.60 (d, 2H), 2.51 (d, 2H), 2.44 (d, 2H), 2.38 (d, 2H), 2.32 (s, 3H), 1.34 (s, 6H), 1.20 (s, 6H, CH_3); **^{13}C NMR (75MHz, DMSO-d_6) δ:** 195.6, 148.7, 146.5, 135.9, 129.4, 128.0, 125.4.1, 114.3, 51.4, 50.7, 40.4, 39.3, 32.3, 29.4, 26.7, 18.3; **MS:** m/z: 363 (M^+); **Anal. Calcd. for** $C_{24}H_{29}NO_2$: C, 79.30; H, 8.04 N, 3.85; **Found**: C, 79.26; H, 8.00; N, 3.81.

2.4.11. Ethyl2,7,7-trimethyl-5-oxo-4-phenyl-1,4,5,6,7,8-hexahydroquinoline-3-carboxylate (7a)
FT-IR (KBr) V_{max} cm^{-1}: 3301, 2933, 1709, 1694, 1614, 1425, 1349, 1180, 1024, 766; **^{1}H NMR (DMSO-d_6, 400 MHz) δ:** 9.44 (brs, 1H, NH), 7.08-7.05 (m, 2H), 6.71-6.70 (m, 3H), 4.82 (s, 1H), 3.56 (s, 3H), 3.34 (s, 3H), 2.50 (s, 5H), 2.22-2.19 (q, 2H), 1.92 (s, 2H), 1.78 (t, 3H); **^{13}C NMR (100MHz, DMSO-d_6) δ:** 194.9, 166.7, 159.6, 151.6, 146.6, 141.5, 126.9, 128.4, 113.9, 113.3, 113.1, 59.6, 55.8, 39.5, 31.8, 26.4, 18.6, 14.6; **MS**: m/z: 339 (M^+); **Anal. Calcd. For** $C_{21}H_{25}NO_3$: C, 74.31; H, 7.42 N, 4.13; **Found**: C, 74.26; H, 7.33; N, 4.11.

2.4.12. Ethyl2,7,7-trimethyl-(4-nitrophenyl)-5-oxo-1,4,5,6,7,8-hexahydroquinoline-3-carboxylate (7b)
FT- IR (KBr) V_{max} cm^{-1}: 3293, 2928, 1695, 1656, 1433, 1341 1100, 1029, 779; **^{1}H NMR (DMSO-d_6, 400 MHz) δ:** 9.78 (brs, 1H, NH),7.09-7.15 (m, 3H),6.73-6.68 (m, 3H), 4.47 (s, 1H), 3.46 (s, 2H), 3.31 (s, 4H), 2.53 (s, 2H), 2.22 (m, 3H), 1.98 (d, 2H), 1.87 (t, 3H); **^{13}C NMR** (100MHz, DMSO-d_6) δ: 195.1, 167.7, 157.5, 151.7, 140.3, 128.6, 128.7, 113.55, 113.5, 113.4, 59.2, 55.2, 39.7, 31.4, 26.6, 18.4, 14.4; **MS**: m/z: 384 (M^+); **Anal. Calcd. for** $C_{21}H_{24}N_2O_4$: C, 65.61; H, 6.29 N, 7.29; **Found**: C, 65.53; H, 6.13; N, 7.20.

2.4.13. Ethyl2,7,7-trimethyl-(4-chlorophenyl)-5-oxo-1,4,5,6,7,8-hexahydroquinoline-3-carboxylate (7c)
FT- IR (KBr) V_{max} cm^{-1}: 3418, 2956, 1692, 1677, 1414, 1369, 1155, 1024, 773; **^{1}H NMR (DMSO-d_6, 400 MHz) δ:** 9.47 (brs, 1H, NH), 7.37-7.22 (q, 4H), 4.68 (s, 1H), 3.60 (s, 3H), 3.17 (s, 3H), 2.32 (s, 5H), 2.36 (m, 2H), 1.88 (d, 2H), 1.69 (t, 3H); **^{13}C NMR (100MHz, DMSO-d_6)** δ: 195.5, 167.5, 157.3, 151.7, 140.4, 128.3, 128.1, 113.2, 113.3, 113.4, 59.2, 55.0, 39.1, 31.5, 26.1, 18.2, 14.5; **MS**: m/z: 373 (M^+); **Anal. Calcd. for**$C_{21}H_{24}ClNO_3$: C, 67.46; H, 6.47 N, 3.75; **Found**: C, 67.43; H, 6.38; N, 3.60.

2.4.14. Ethyl-2,7,7-trimethyl-(4-methoxyphenyl)-5-oxo-1,4,5,6,7,8-hexahydroquinoline-3-carboxylate (7d)
FT- IR (KBr) V_{max} cm^{-1}: 3412, 2963, 1690, 1677, 1426, 1360, 1150, 1028, 783; **^{1}H NMR (DMSO-d_6, 400 MHz) δ:** 9.35 (brs, 1H, NH), 7.26-7.23 (q, 4H), 4.59 (s, 1H), 3.83 (s, 3H, OCH_3), 3.61 (s, 3H), 3.24 (s, 3H), 2.34 (s, 5H), 2.38 (m, 2H), 1.87 (d, 2H), 1.77 (t, 3H); **^{13}C NMR (100MHz, DMSO-d_6) δ:** 195.3, 167.4, 157.4, 151.6,

140.7, 128.3, 128.0, 113.3, 113.1, 113.0, 59.1, 55.4, 39.6, 31.5, 26.1, 18.2, 14.1; **MS**: m/z: 369 (M^+); **Anal. Calcd. for** $C_{22}H_{27}NO_4$: C, 71.52; H, 7.37 N, 3.79; **Found**: C, 71.43; H, 7.32; N, 3.61.

2.4.15. Ethyl2,7,7-trimethyl-5-oxo-4-(p-toly)-1,4,5,6,7,8-hexahydroquinoline-3-carboxylate (7e)
FT-IR (KBr) V_{max} cm^{-1}: 3430, 2951, 1691, 1680, 1414, 1369, 1150, 1024, 760; **^{1}H NMR (DMSO-d_6, 400 MHz) δ:** 9.49 (brs, 1H, NH),7.24-7.21 (q, 4H), 4.66 (s, 1H), 3.72 (s, 3H, OCH_3), 3.45 (s, 3H), 3.32 (s, 3H), 2.31 (s, 5H), 2.30 (m, 2H), 1.89 (d, 2H), 1.84 (t, 3H); **^{13}C NMR (100MHz, DMSO-d_6) δ**: 195.2, 167.2, 157.2, 151.5, 140.1, 128.2, 128.2, 113.3, 113.24, 113.1, 59.1, 55.1, 39.5, 31.4, 26.1, 18.19 14.6; **MS**: m/z: 353 (M^+); **Anal. Calcd. for** $C_{22}H_{27}NO_3$: C, 74.76; H, 7.70 N, 3.96; **Found**: C, 74.63; H, 7.62; N, 3.81.

3. RESULTS AND DISCUSSION

In the present investigation we report the efficient synthesis of Hantzsch 1,4 Dihydropyridines by reacting various aromatic aldehydes (1a) with ethylacetoacetate (2a) and ammonium acetate (3a) in the presence of Phenol-formaldehyde liquid resin (PF-Liquid Resin) as medium and catalyst at 115-120oC to afford the corresponding 1,4 Dihydropyridines (4a–e) in high yields. The reaction is illustrated in Scheme 1.

Scheme 1

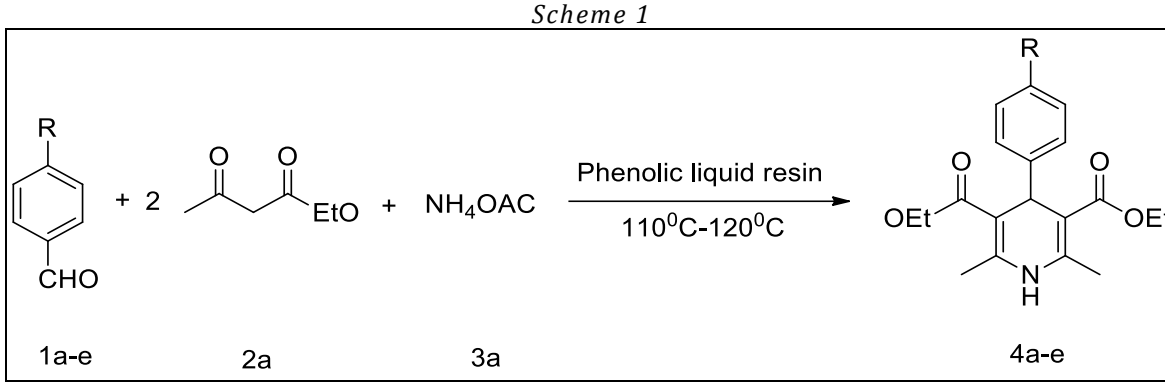

3.1. Effect of temperature and catalyst loading on 1,4 Dihydropyridine synthesis

The reaction of benzaldehyde (1a) with ethylacetoacetate (2a) and ammonium acetate (3a) in the presence of Phenol-formaldehyde liquid resin as medium and catalyst was chosen as a model reaction for studying the effect of temperature and catalyst loading on 1, 4 Dihydropyridine synthesis; the results are shown in Table 1. We have observed that in the absence of phenol-formaldehyde liquid resin the reaction did not progress. Using phenol-formaldehyde liquid resin as medium and catalyst caused a dramatic increase in yield and decreased the time considerably over conventional thermal heating procedures. The reaction did not progress to completion when smaller amounts of Phenol-formaldehyde liquid resin (<10.0g) and lower temperatures (<115^{0}C) were employed. Optimal yields and shortest reaction times were obtained at 115-120°C using 10.0g of Phenol-formaldehyde liquid resin for 0.0045moles of substrate namely benzaldehyde. The results of the reaction are depicted in Table.1 illustrated below. The Diethyl 2,6-dimethyl-4-phenyl-1,4-dihydropyridine-3,5-dicarboxylate (4a) was synthesized in 94.0% yield by reacting benzaldehyde (1a) with ethylacetoacetate (2a) and ammonium acetate (3a) in the presence of Phenol-formaldehyde liquid resin as medium and catalyst at 115-120°C. The product (4a) was thoroughly characterized by ^{1}H-NMR, ^{13}C-NMR, FT-IR, Mass spectral and CHN analysis.

Table 1 Effect of temperature on Hantzsch 1,4 dihydropyridine synthesis

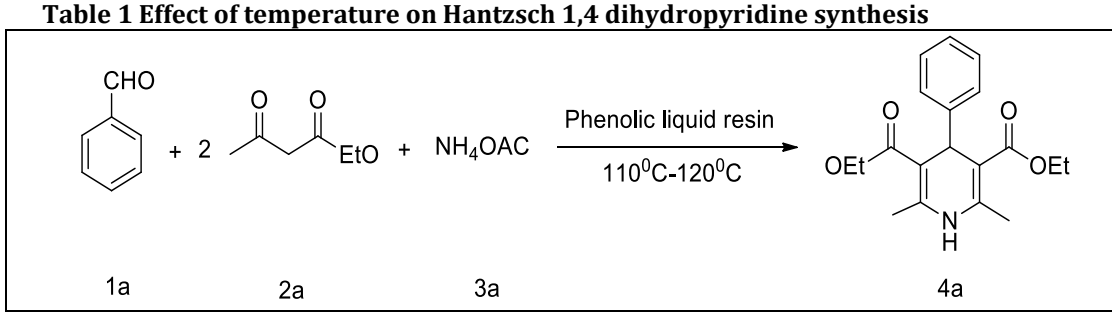

S.No	Catalyst Loading (g)	Temperature(°C)	Time (h)	Yield[a] (%)
1	5.0	25-27 °C	8.0 h	No reaction
2	5.0	60-70 °C	8.0 h	10.0
3	8.0	25-27 °C	8.0 h	No reaction
4	8.0	80-90 °C	8.0 h	No reaction
5	10.0	25-27 °C	8.0 h	Incomplete
6	10.0	80-82 °C	8.0 h	65.0
7	10.0	100-105 °C	5.0 h	80.0
8	10.0	115-120 °C	3.0 h	94.0

[a] Isolated yield after purification.

3.3. The effect of substituent's on 1, 4 dihydropyridine synthesis

After having optimized the reaction conditions, in order to demonstrate the efficiency of this protocol, we explored the generality of our methodology by reacting various other aldehydes with ethylacetoacetate (2a) and ammonium acetate (3a) in the presence of Phenol-formaldehyde liquid resin as medium and catalyst. For all the studied examples, Hantzsch 1,4 dihydropyridines were obtained in good to excellent yields. The effect of electron deficiency and the nature of substituent's on the aromatic ring of aldehydes showed some effect on this conversion. The aromatic aldehydes with electron donating groups such as methoxy, methyl and chloro-substituted aryl aldehydes required longer times to produce comparable yields than those of their simple electron-deficient counterparts which took shorter reaction times to give good yields. The results summarized in Table 2 clearly indicate the scope of the reaction with respect to various substituted aldehydes catalysed by Phenol-formaldehyde resin.

Table 2. Effect of substituents on Hantzsch 1,4 Dihydropyridine synthesis

S.No	Aldehyde	Time[a] (h/min)	Yield[b] (%)	Hantzsch 1,4 Dihydropyridines[c]
1	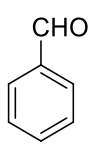	3.0 h	94.0	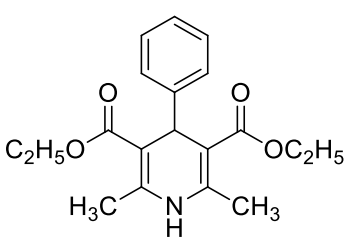 **(4a)**
2	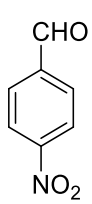	4.0 h	96.0	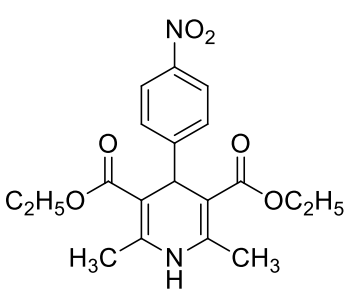 **(4b)**

3	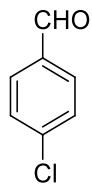	5.0 h	93.0	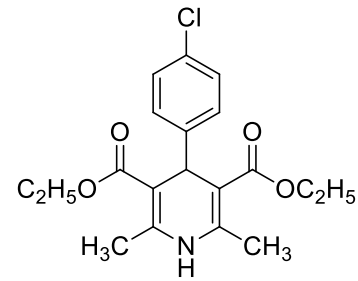 **(4c)**
4	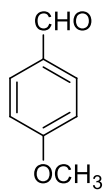	7.0 h	92.0	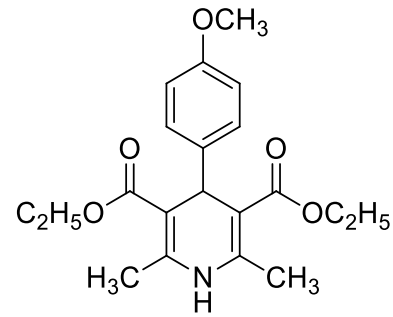 **(4d)**
5	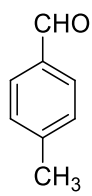	6.0 h	89.0	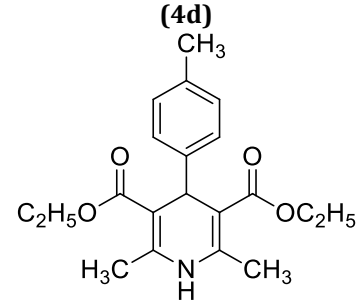 **(4e)**

[a] All the reactions were carried out according to typical experimental procedure (A).
[b] Isolated yield after purification.
[c] All the products were characterized by ^{1}H-NMR, ^{13}C-NMR, FT-IR and Mass spectral studies.

3.4. Synthesis of 1,8 dioxodecahydroacridine derivatives

The catalyst is also effective for the synthesis of a new class of 1,8 dioxodecahydroacridine (6a-e) in good yields. The reaction is illustrated in scheme 2. The results of the reactions are summarized in Table 3. Aromatic aldehydes containing both electron-withdrawing and electron donating groups afforded the product acridine derivatives in high yields.

Scheme-II

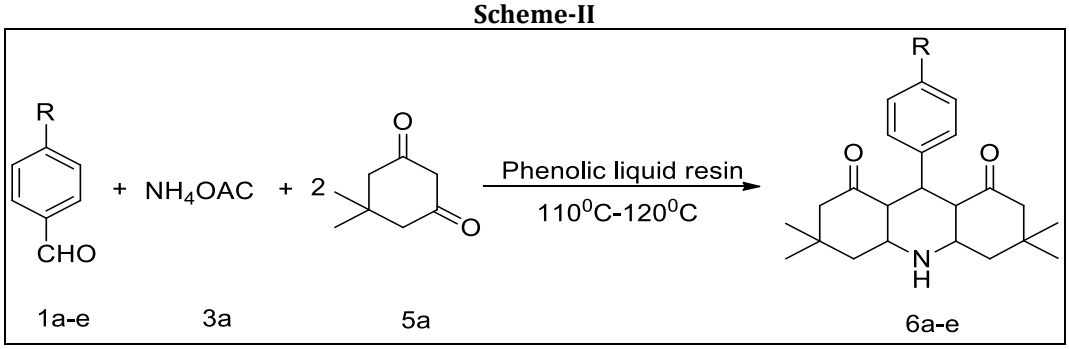

Table 3 Effect of Substituents on 1,8 Dioxodecahydroacridine Synthesis

S.No	Aldehyde	Time[a] (h)	Yield[b] (%)	1,8 Dioxodecahydroacridine[c]
1	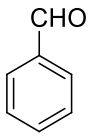	6.0 h	88.0	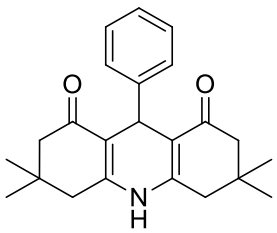 **(6a)**
2	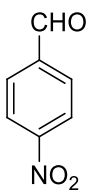	7.0 h	84.0	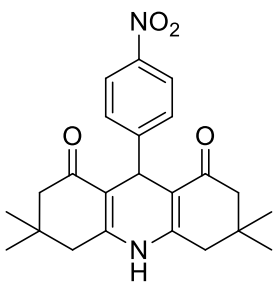 **(6b)**
3	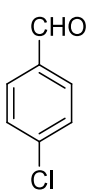	8.0 h	86.0	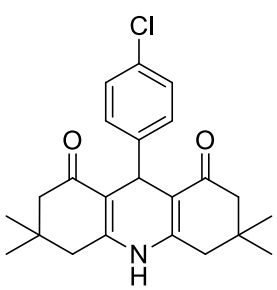 **(6c)**
4	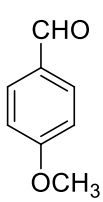	9.0 h	83.0	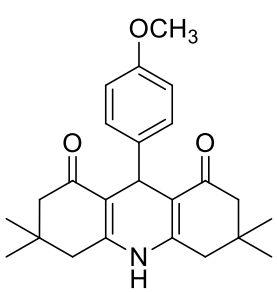 **(6d)**
5	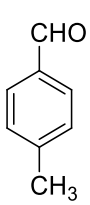	7.0 h	84.0	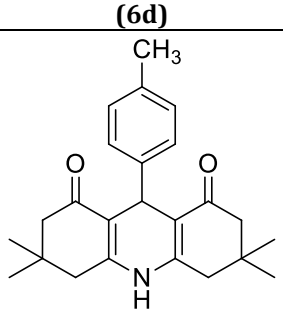 **(6e)**

[a] All the reactions were carried out according to typical experimental procedure (B).
[b] Isolated yield after purification.
[c] All the products were characterized by ^{1}H-NMR, ^{13}C-NMR, FT-IR and mass spectra studies.

3.5. Synthesis of Polyhydroquinolines derivatives

Polyhydroquinolines are an important class of compounds exhibiting potential applications as antimicrobial agents [28], antihyperglycemic and lipid modulating agents [29]. After successfully employing phenolic liquid resin for the efficient synthesis of 1,4 DHP's and acridine derivatives, we focussed our attention on the synthesis of the biologically important polyhydroquinoline derivatives by coupling reaction of dimedone, aldehyde, ethylacetoacetate and ammonium acetate in the presence of phenolic liquid resin (Scheme-III & table-IV) towards the formation of PHQ derivatives, via four component hantzsch coupling reaction. It is remarkable to mention that, different kind of structural aldehyde and substitutents on the aromatic ring did not show any effect on this PHQ derivatives.

Scheme-III

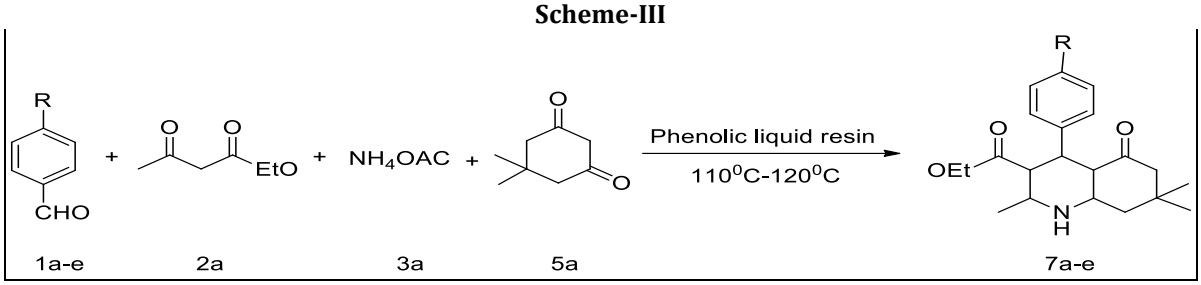

Table 4 Effect of substituents on Polyhydroxyquinoline synthesis

S.No	Aldehyde	Time[a] (h)	Yield[b] (%)	Polyhydroxyquinolines[c]
1	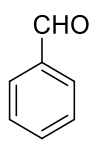	3.0 h	87	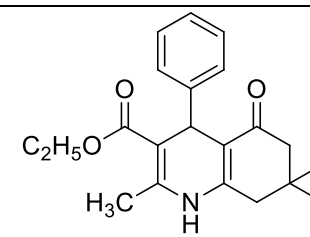 **(7a)**
2	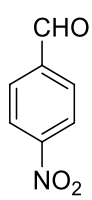	4.0 h	83	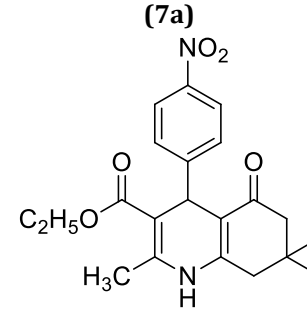 **(7b)**
3	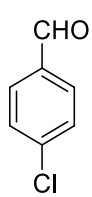	5.0 h	88	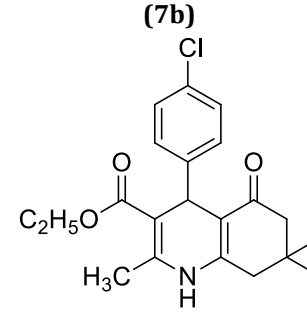 **(7c)**

4	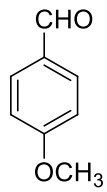	7.0 h	90	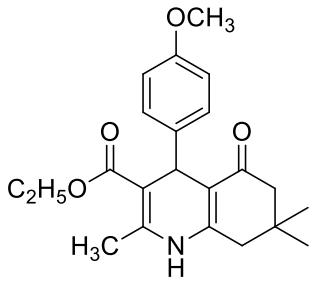 **(7d)**
5	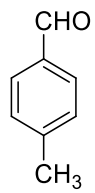	6.0 h	89	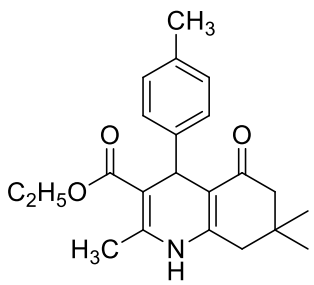 **(7e)**

[a] All the reactions were carried out according to typical experimental procedure (C).
[b] Isolated yield after purification.
[c] All the products were characterized by ^{1}H-NMR, ^{13}C-NMR, FT-IR and Mass spectra studies.

3.6. Plausible mechanism

The reaction of benzaldehydes with ethylacetoacetate (2a) and ammonium acetate (3a) in the presence of Phenol-formaldehyde liquid resin proceeded through the successive intermediates such as knoevenegal adduct (1) and Enamine (II). The catalyst phenol-formaldehyde liquid resin acts as medium and catalyst by aiding the Michael addition reaction between knoevenegal adduct (1) and Enamine (II) to give Hantzsch 1,4 Dihydropyridine (III, Scheme 3). The complete recovery of the catalyst without loss of activity and the high yields of the products lends support to the suggested mechanism. A plausible mechanism for the typical reaction of aromatic aldehydes with ethylacetoacetate (2a) and ammonium acetate (3a) in the presence of Phenol-formaldehyde liquid resin is given in scheme 3.

Scheme 3

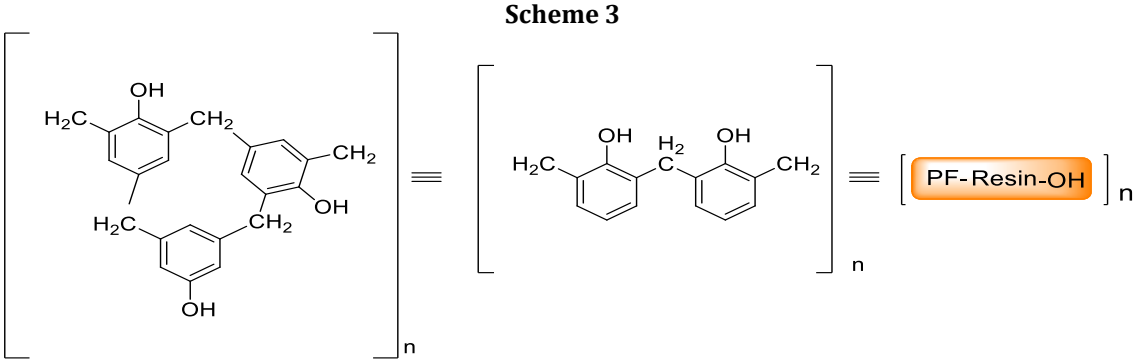

Phenol Formaldehyde Liquid Resin

STEP 1

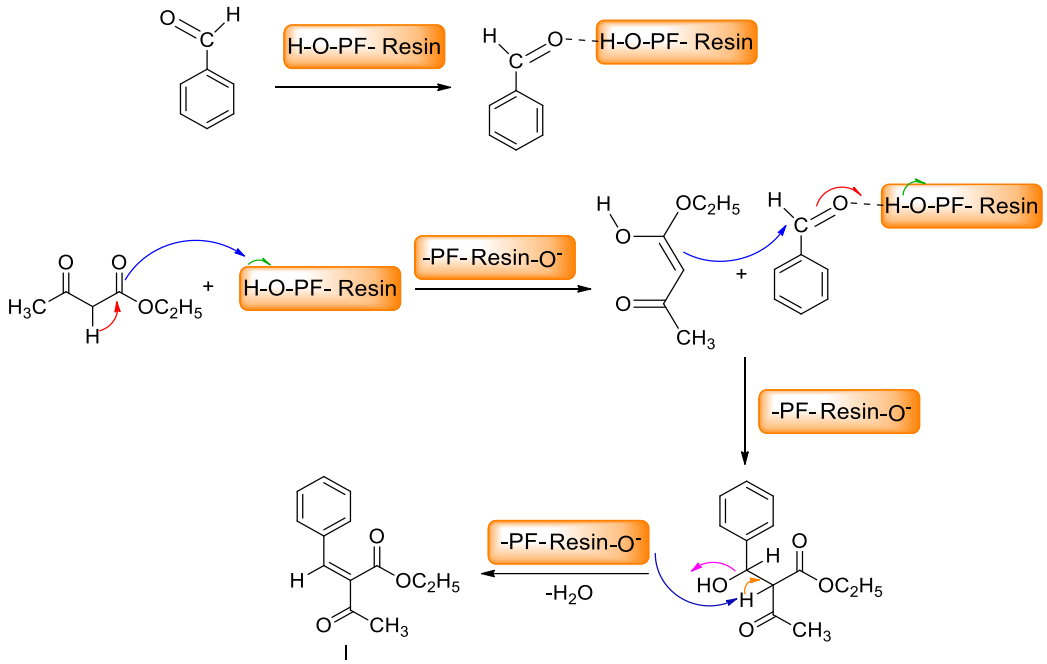

I

STEP 2

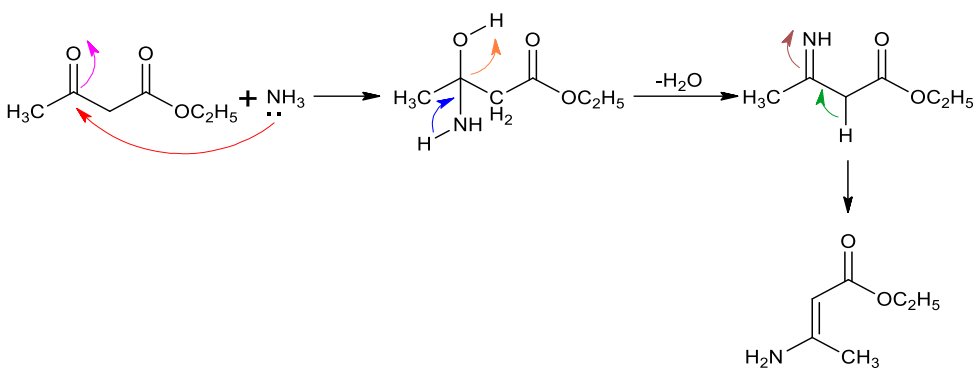

ENAMINE II

STEP 3

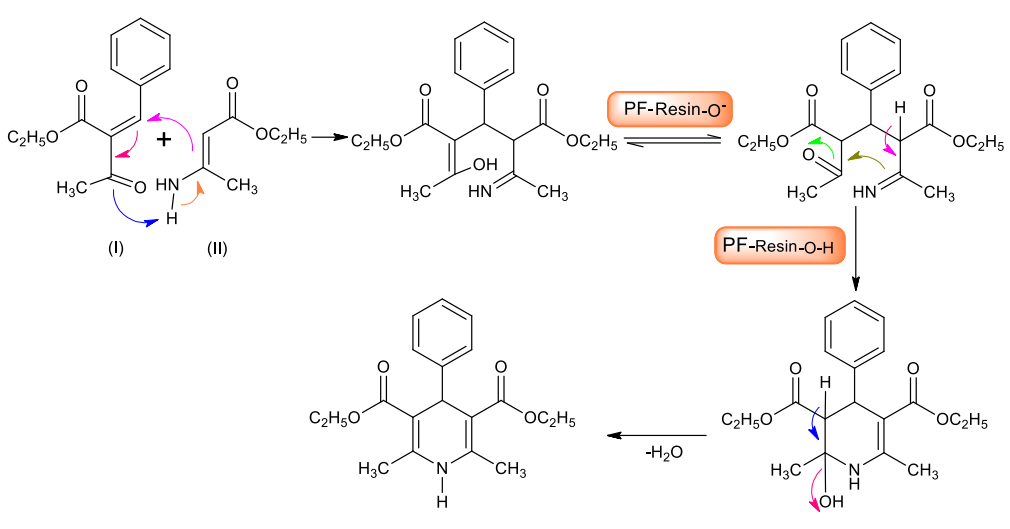

(I) (II) (III)

4. CONCLUSION

In the present investigation we report the efficient synthesis of 1,4 Hantzsch Dihydropyridines and 1,8 dioxodecahydroacridinein the presence of Phenol-formaldehyde liquid resin as medium and catalyst at ambient temperatures. In conclusion we have described, a novel and highly efficient procedure for the preparation of 1,4 Hantzsch Dihydropyridines and 1, 8 dioxodecahydroacridines in good yields. The procedure offers several advantages. The catalyst was used repeatedly without loss of activity. This procedure does not require the use of anhydrous solvents and inert atmosphere. A mechanism for the catalytic activity is proposed. The effect of temperature, the effect of substituents, the influence of mole ratio, and the recyclable use of the catalyst were investigated. A plausible mechanism for the reaction was also proposed. Moreover, the procedure offers mild reaction conditions, cleaner reactions, economically cheap alternative, short reaction times, highly efficient reaction with no side products, as well as simple experimental and isolation procedures. These advantages make it a useful and attractive process for the synthesis of these compounds.

Reference

1.
   (a) Mauzeral D, Westheimer FH, J.Am. Chem. Soc., 1955;77: 2261.
   (b) Baraldi PG. Chiarini A. Budriesi R. Roberti M. Casolar A. Manfredini S. Simoni, D.; Zanirato V, Varani K, Borea PA, Drug Des. Deliv.1989;5:13.
   (c) Baraldi PG, Budriesi R, Cacciari B, Chiarini A, Garuti L, Giovanninetti G, Leoni A, Roberti M, Collect. Czech. Chem. Commun., 1992, 169;
   (d) Di Stilo A, Visentin S, Clara C, Gasco AM, Ermondi G, Gasco A, J. Med. Chem., 1998;41:5393.
   (e) Kawase M, Shah A, Gaveriya H, Motohashi N, Sakagami H, Varga A, Molnar JJ. Bioorg. Chem., 2002;10:1051.
   (f) Suarez M, Verdecia Y, Illescas B, Martinez-Alvarez R, Avarez A, Ochoa E, Seoane C, Kayali N, Martin N, Tetrahedron, 2003;59:9179.
   (g) Shan R, Velazquez C, Knaus EE, J. Med. Chem., 2004;47:254.
   (h) Sawada Y, Kayakiri H, Abe Y, Mizutani T, Inamura N, Asano M, Hatori C, Arsmori I, Oku T, Tanaka H, J. Med. Chem., 2004;47:2853.
2.
   (a) Klusa V, Drugs Future, 1995;20:135.
   (b) Bretzel RG, Bollen CC, Maeser E, Federlin KF, Am. J. Kidney Dis., 1993;21: 54.
   (c) Bretzel RG, Bollen CC, Maeser E, Federlin KF, Drug Future, 1992;17: 465.
   (d) Boer R, Gekeler V, Drug Future, 1995; 20: 499-509.
   (e) Davis HL, Davis TE, Cancer Treat. Rep., 1979; 63(5): 809-815.
3. Pastan I, Gottesman MMN, Engl. J. Med., 1987; 316:1388, DOI:10.1056/ NEJM198705283162207
4. Tilak BD, Ayyangar NR, Chem. Heterocycl. Comp., 1973; 9:579-613.
5. Albert A. The Acridines, Edward Arnold Publications Ltd. London. 1966.
6. Srividya N, Ramamurthy P, Shanmugasundaram P, Ramakrishnan VT. Synthesis, J. Org. Chem., 1996; 61: 5083-5089, DOI:10.1021/jo9600316
7. Dolle F, Hinnen F, Valette H, Fuseau C, Duval R, Peglion J, Crouzel C, Bioorg. Med. Chem., 1997; 5: 749-764, DOI: 10.1016/S0968-0896(97)00024-2.
8. Hernandez-Gallegos Z, Lehman PAF, Hong E, Posadas F, Hernandez-Gallegos E, Eur. J. Med. Chem., 1995; 30:355-364, DOI: 10.1016/0223-5234(96)88245-6.
9. Ko S, Sastry MNV, Lin C, Yao CF, Tetrahedron Lett., 2005; 46: 5771-5774, DOI: 10.1016/j.tetlet.2005.05.148
10. Ji SJ, Jiang ZQ, Lu J, Loh TP, Synlett. 2004; 831-835, DOI: 10.1055/s-2004-820035
11. Donelson JL, Gibbs RA, De SK, J. Mol. Catal. Chem., 2006; 256: 309-311, DOI: 10.1016/j.molcata.2006.03.079
12. Maheswara M, Siddaiah V, Damu GLV, Rao CV, Arkivioc, 2006; 201-206.
13. Das B, Ravikanth B, Ramu R, Rao BV, Chem. Pharm. Bull., 2006; 54: 1044-1045, DOI: 10.1248/cpb.54.1044.
14. Sabitha G, Reddy GSKK, Reddy CS, Yadav JS, Tetrahedron Lett., 2003; 44: 4129-4131, DOI: 10.1016/S0040-4039(03)00813-X
15. Ko S, Yao CF, Tetrahedron, 2006; 62:7293-7299, DOI: 10.1016/j.tet.2006.05.037
16. Kumar S, Sharma P, Kapoor KK, Hundal MS, Tetrahedron, 2008;64(3):536-542. DOI: 10.1016/j.tet.2007.11.008
17. Kumar A, Maurya RA, Synlett, 2008;883, DOI: 10.1055/s-2008-1042908
18. Brietenbucher JG, Figliozzi G, Tetrahedron Lett., 2000; 41: 4311-4315, DOI: 10.1016 /S0040-4039(00)00660-2
19. Evans CG, Gestwicki J.E, Org. Lett., 2009; 11: 2957, DOI: 10.1021/ol901114f
20. Mekheimer RA, Hameed AA, Sadek KU, Green Chem., 2008; 10: 592, DOI: 10.1039/ B715126H
21. Debache A, Ghalem W, Boulcina R, Belfaitah A, Rhouati S, Carboni B, Tetrahedron Lett. 2009; 50: 5248, DOI: 10.1016/j.tetlet.2009.07.018.

22. Das B, Thirupathi P, Mahender I, Reddy VS, Rao YK, J. Mol. Catal. A. Chem., 2006; 247: 233-239, DOI: 10.1016/j. molcata.2005.11.048
23. Karthikeyana G, Pandurangana A, J. Mol. Catal - A. Chem., 2009; 311:36-45, DOI: 10.1016/j.molcata.2009.06.020
24. Kumar D, Sandhu JS, Synth. Commun., 2010; 40:510-517, DOI: 10.1080/ 00397910902987792
25. Rostamizadeh S, Amani AM, Mahdavinia GH, Amiri G, Sepehrian H, Ultrason.Sonochem. 2010; 17: 306-309, DOI: 10.1016/j.ultsonch.2009.10.004
26. Li G., Wang L.J *et al* 2002 Study on the synthesis and the performance of water soluble phenol-formaldehyde resin *Journal of Hebei University of Tchnology* **31** 37-41
27. Parthiban D. Joel Karunakaran, Magesh C.J, International research journal of pure and applied chemistry, 2018, 16(1) : 1-10.
28. Ladani N. K, Mungra D.C, Patel M.P, Patel R.G, Chinese chemical letters, 2011, 22, 1407
29. Kumar A, Sharma S, Tripathi V.D, Maurya R.A, Sivastava S.P, Bhatia G, Tamrakar A.K, Srivastava A.K, Bioorganic and medicinal chemistry letters, 2010, 18, 41-38.

SYNTHESIS AND CHARACTERIZATION OF HYDROGEL BEADS BY USING SODIUM ALGINATE

Bhavani Perumal[1], CT.Ravichandran[1], G. Saranya[1] & Bama Perumal[2]
[1]Arignar Anna Govt. Arts College, Cheyyar, Thiruvannamalai dist., Tamilnadu- 604 40, India
[2]Institute for Future Transport and Cities, Coventry University, Coventry, CV1 5FB, United Kingdom

ABSTRACT: *Hydrogels are one of the upcoming classes of polymer-based controlled-release drug delivery systems. Besides exhibiting swelling-controlled drug release, hydrogels also show stimuli-responsive changes in their structural network and hence, the drug release. Because of large variations in physiological pH at various body sites in normal as well as pathological conditions, pH-responsive polymeric networks have been extensively studied. In recent years, the hydrogel technology has been an integral part of human health care. The pharmaceutical industry has been developing hydrogel based drug delivery system in an advanced manner by tuning the structure, shape and surface modifications of the biopolymers. There has been considerable research interest into the possible use of hydrogels in agriculture but limited study on characterisation of hydrogel beads using Sodium alginate. The present work has been carried out to highlights the role of hydrogels in Agricultural Industry. This superabsorbent hydrogel polymers can in principle influence soil permeability, density, and structure, texture, evaporation and infiltration rates of water through soils. They can also allow pesticides to be released slowly over a long period, increasing effectiveness and reducing side-effects such as pesticide runoff. Therefore, an attempt has been made to study a state of–art on the hydrogel, its synthesis and characterisation of hydrogel beads by using sodium alginate. An innovated combination of new generation hydrogel was investigated and presented in detail*

Keywords: *Hydrogels; Drug delivery; sodium Alginate; X-ray Diffraction; Fourier-transform infrared spectroscopy.*

1. Introduction

Three-dimensional, hydrophilic, polymeric network proficient in absorbing a great amount of water or biological fluids. Owing to their high-water content, porosity and soft consistency, they intently simulate natural living tissue, more so than any other category of synthetic biomaterial. Hydrogel is a polymeric material that exhibits the ability to swell and retain a significant fraction of water within a structure but will not dissolve in the water. Hydrogels are also known as “reversible” or “physical” gels. This can either be chemically durable or they may eventually disintegrate and dissolve (poppas et al., 2000). Hydrogel have received considerable attention in the past 50 years, due to their exceptional promise in wide range of applications [1-2]. Physical gels are often rescindable and it is achievable to dissolve them by altering the environmental conditions, such as pH and the ionic strength of solution or temperature. In permanent or chemical gels, the linkage of covalent bonds linking distinct macromolecular chains can be attained by cross-linking polymers in the dry state or in solution (Hoffmann, 2012). These gels may be either “charged” or “non-charged” dependent on the behaviour of functional groups existing in their structure [3-4]. Site-specific and temporal control of drug delivery have recently been of great interest in both basic and applied biomedical fields as a new approach to achieve improved drug therapies. The utilization of polymeric materials as delivery matrices is promising to achieve these drug delivery strategies. We have been investigating stimuli-responsive 'intelligent' polymers for drug delivery systems to achieve either pulsatile or auto-feedback type drug release patterns.

Continued progresses in many fields of biotechnology have produced numerous kinds of engineered peptides and proteins as novel therapeutic drugs. Development of delivery formulations for these bioactive compounds has been recognized as a key technology to achieve successful therapeutic effect in clinical medicine because these bioactive materials are metabolized quickly when administered in vivo, sometimes showing undesirable side-effects due to their high bioactivity.

Hydrogels are used for various industrial applications in pharmaceutical, biomedical, personal care products and in ago-allied industries. A large percentage of the hydrogels are prepared from synthetic polymers such as polyacrylate, polyacrylamide and polymethacrylates which are form fossil resources. The gel-like behaviour of xanthan was investigated as a function of temperature and $CaCl_2$ concentration. Solutions passed through states of maximum and minimum gel-like character at 100% and 200% stoichiometric equivalence of Ca^{2+}, which were ascribed to the partial replacement of intermolecular site binding of calcium ions by binding to individual carboxyl groups, maximizing the degree of complexation

and network formation [5-6].

Hydrogels are hydrophilic cross-linked polymers that form three-dimensional molecular networks which can absorb and hold great amounts of water [7-8]. Different type of hydrogels in agriculture. Commonhydrogel agriculture'singredient is potassium polyacrylate orsodiumpolyacrylate. As a superabsorbent material, it can absorb plenty water and turn water gel to storewater. Hydrogel agriculture technology uses insoluble gel-forming polymers to improve thewater holding properties of different soils, such as clays and sandy loams [10-12]. This can increase water-holding and water use (up to 85% for sand), improve soil permeability, reduce the need forirrigation, reduce compaction, soil erosion, leaching and improve plant growing. Desertification and lack of water threaten agriculture in many arid and semi-arid regions of theworld; these may be mitigated with hydrogels.

1.1 SCOPE AND OBJECTIVES OF THE WORK.

Sodium alginategels have been used in both drug delivery and agriculture applications in the bead form usually produced by dripping sodium alginate solution into a $CaCl_2$ bath. Hydrogels are used to make soft contact lenses, nappies, wound dressings and drug delivery systems. A wound dressing is put over a cut in the skin to help the skin heal. The hydrogel is applied as a thin layer which is moist and soothing. Hydrogels - Water Absorbing Polymers. Soft contact lenses, disposable nappies, hair gel and plant water crystals all make use of substances called hydrogels. These are polymers which have the unusual property of being able to absorb huge quantities of water. The water is absorbed because the hydrogel has many negative charges on it molecules. Water molecules are polar (they have small charges on them) so they are attracted to the negative charges on the hydrogel polymer.

2. Materials and Methods:

2.1 Materials:

Sodium alginate (Aldrich)
Calcium chloride (Merck)
Ferric chloride (Merck)
Paracetamol (as per pharmaceutical grade)
Solvents: Distilled water

2.2 Preparation of hydrogel beads

Sodium alginate solution 2%w/v in water was prepared by soaking the powder in distilled water for 3 hours. 4 grams of calcium chloride were added drop by drop in petridishat room temperature in the sodium alginate viscous solution. The petridish contained 100 ml of calcium chloride of 4% w/v solution. The formed beads were separated, washed with distilled water and dried at 100 ^{0}C in the hot air oven. Same procedure was used for preparation of hydrogel beads by using Ferric chloride, Aluminum sulphate and paracetamol.

2.3. Loading of the beads with the drug

A plain sodium alginate beads were produced as described in method of preparation. The beads were left to dry at room temperature then they were soaked 0.5%w/v of paracetamol for different periods of time. Beads were separated, washed with distilled water and the drug content was determined.

2.4. Water Absorption

The amount of solvent intake by the beads was studied. The wet beads were weighed and dried in oven and allowed to get 24 hours. The dried beads were then quickly weighed after blotting the surface water and the values noted. The swelling degree using the formula.

Weight of wet beads – weights of dry beads X 100% Weight of dry beads

3. Instrumentation

3.1 XRD (X-ray Diffraction)

XRD permits the identification of crystalline structures in samples. The analysis of the patterns can lead to the determination of other structural parameters such as strain state, crystallite size, phase composition and preferential growth of the crystals. In XRD, a filtered X-ray beam is directed on the sample and the beam is diffracted when it interact with a plane in the crystalline structure, for detect diffracted beams signal of different planes, is necessary that the diffracted beam are in phase with respect to another

one, in other case the beams cancel. The interplanar distance'd' can be calculated using Bragg's equation and the average crystallite size by using Scherrer's equation.(Diffractometer X 'Pert proanalytica).

3. 2 FTIR (Fourier-transform infrared spectroscopy)

The technique works on the fact that bonds and groups of bonds vibrate at characteristic frequencies. A molecule that is exposed to infrared rays absorbs infrared energy at frequencies, which are characteristic to that molecule. During FTIR analysis, a spot on the specimen was subjected to a modulated IR beam. The specimen's transmittance and reflectance of the infrared rays at different frequencies was translated into an IR absorption plot consisting of reverse peaks (Perkin Elmer FT-IR spectroscopy) The resulting FTIR spectral pattern was then analysed and compared with known signatures of identified materials in the FTIR library.

3.3 SEM (Scanning Electron Microscope) and EDAX (compositional analysis)

The surface morphology of the beads were analysed using SEM (Hitachi S -3400 N). The samples were cut into sufficient size and sputter coated with gold to make the samples. The SEM image reveals the dispersion of the paracetamol drug and any phase separation in the case of beads. It is an instrument for obtaining micro structural images using scanning electron beam. In the SEM, a small electron beam spot usually circa 1μm) is scanned over the surface area of the sample. SEM possesses a few advantages, such as producing more realistic images, deep focusing easy to use and ease of specimen preparation. The micrographs produced show the surface topography and chemical contrast at the shortest time.

4. Results and discussion

4.1 Water Absorption of various hydrogel beads

Water absorption results are given in table 1 and table 2. Water absorption of calcium chloride ($CaCl_2$) hydrogel beads are highly hydrophilic in nature compare with aluminium sulphate $Al_2(S0_4)_3$ and ferric chloride ($FeCl_2$). For this work, calcium chloride is used for the preparation of hydrogel beads along with sodium alginate. Here, sodium alginate is acting like a super water absorbent gel. It absorb more than 100 times compare to other compounds. Various weight percentage of the hydrogel beads were prepared with calcium chloride. As expected, the water uptake values increased with increase with weight fraction of $CaCl_2$ in the hydrogel beads (HB). Water uptake is an important parameter in HB. Because the water that resist in the hydrophilic domains facilities in the agriculture. Hydrogel beads are usually contain water it is used in potting plants and use in gardens to save water.

Name of the compound	Water absorption percentage
$CaCl_2$	0.283
$Al_2(S0_4)_2$	0.257
$FeCl_3$	0.255

Tabel 1. Water absorption percentage

Weight of the $CaCl_2$	Water absorption percentage
2g	0.26
4g	0.274
6g	0.263
8g	0.287
10g	0.35

Table 2. Weight of the $CaCl_2$ and Water absorption percentage

4.2 Drug content Determination

Different weight proportion of dried calcium chloride beads were prepared. There means content of paracetamol was loaded. Generally, the drug compressing 50% of the total dried beads weight. Concertation of Sodium alginate or calcium chloride had no effect on the entrapped amount of paracetamol. The reproducibility of paracetamol content in the system may be attributed to the insoluble of the paracetamol in the calcium chloride solution or organic solvent. However when the beads were exhausted by soaking for 10 hours in 0.5 N hydrochloric acid the released paracetamol was found 65% of the embodied quantity indicating that the remained amount is strongly trapped in the beads body.

4.3. FTIR behaviour of Paracetamol-Sodium alginate-$CaCl_2$

The FTIR spectrum of **Paracetamol/Sodiumalginate/$CaCl_2$**, shown in Figure1, showed the -OH stretching vibration at 3286 cm^{-1} as a broad band. The -CH_3 and alginate C-H stretching vibrations were clearly seen at 2918 and 2850cm^{-1}. The -C=N vibration is shifted to 1597cm^{-1}. Its broadening indicates overlapping of aromatic ring skeletal vibration (1600cm^{-1}) with it. The Ca-O vibration occurred below 800cm^{-1}. So, the features are nearly same as the previous spectra. So, all the three spectra, it is confirmed presence of paracetamol, alginate and the corresponding metal ion.

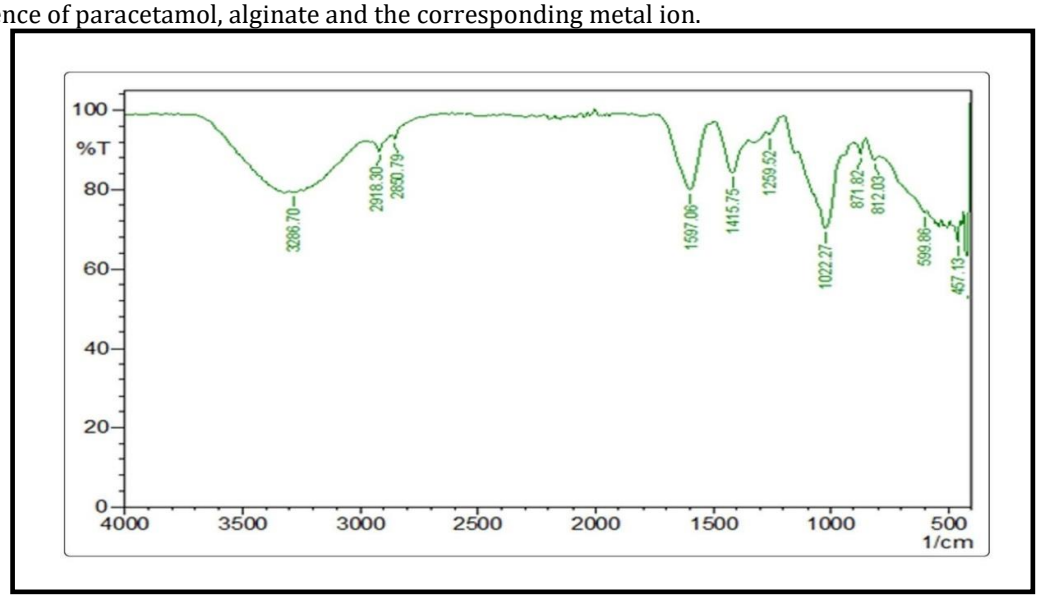

FIGURE 1:FTIR behaviour of the Paracetamol-Sodium alginate-$CaCl_2$

4.4. FTIR behaviour of /sodium alginate/ $FeCl_2$

The FTIR spectrum of sodium alginate-FeCl in Figure.2 showed a broad intense absorption in the high energy region around 3269cm^{-1}. It includes -OH stretching vibration of alginate. The C-H stretching vibration of the aromatic ring (just above 3000cm^{-1}). But the -CH stretching vibration of the methyl group of alginate occurred as a group of peaks at 2931CM-1. The peak at 1612cm^{-1}, due to C=N- vibration confirms it. It is little broadened due to overlapping of the peak due to aromatic ring skeletal vibration which generally occurs around 1600cm^{-1}. The peak at 1429cm^{-1} is due to -CH_3 bending mode and the aromatic ring skeletal vibration. The phenolic C-O vibration occurred at 1300 cm^{-1}, and the alcoholic C-O vibration at 1026cm^{-1}. The intense broad band below 800 $cm^{-1}$is due to Fe-O vibration. SO, the FTIR spectrum confirms the presence of alginate and Fe in the material.

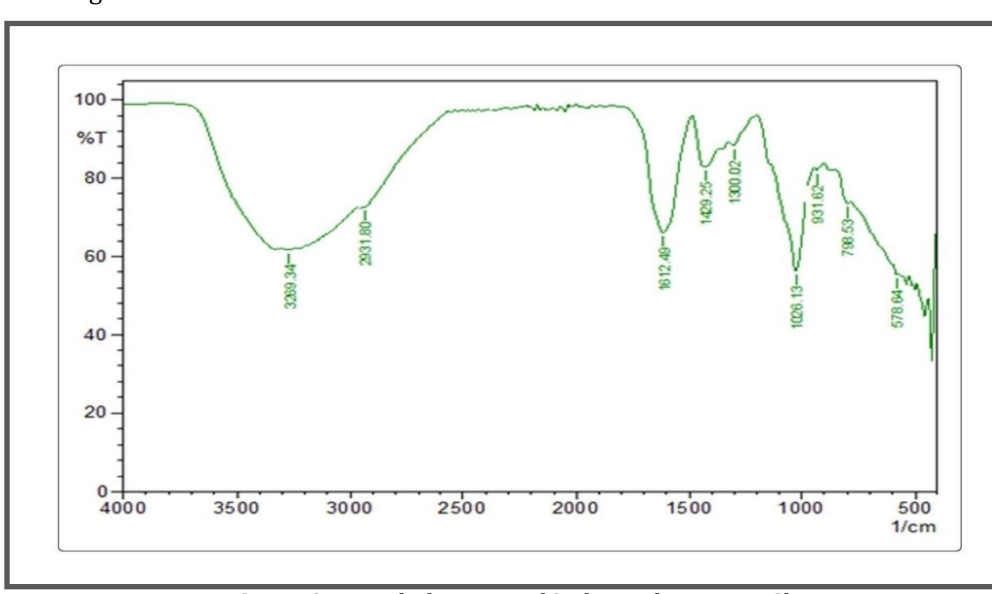

FIGURE 2: FTIR behaviour of Sodium alginate-$FeCl_3$

4.5. FTIR behaviour of sodium alginate-$Al_2(SO_4)_3$:

The FTIR spectrum of **sodium alginate/**$Al_2(SO_4)_3$ is shown in Figure 3. It showed similar features as that of Figure.1. But the -OH stretching vibration is shifted to lower wave number. The peak maximum occurs at 2920$cm^{-1}$where the alkyl -C-H stretching generally occurs. The -C=N- vibration and that of -C-O are shifted to higher energy. So, such bonds are strengthened when iron is replaced with aluminium. The Al-O bond stretching occurred below 800cm^{-1}.

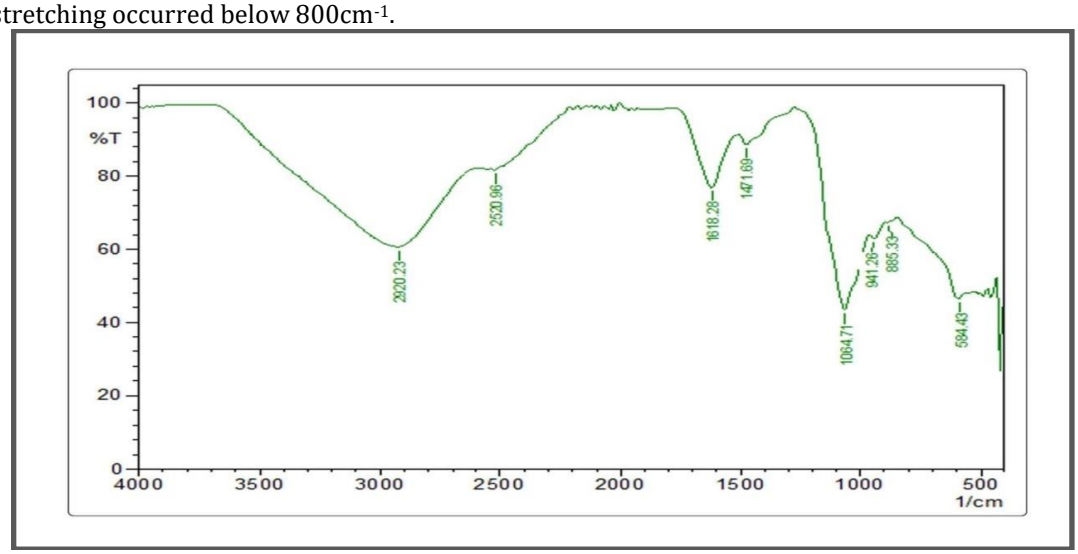

FIGURE 3: FTIR behaviour of Sodium alginate-$Al_2(SO_4)_3$

4.6 XRD Pattern of Paracetamol-Sodium alginate-$CaCl_2$

In Figures 4, the reflections at 29.0° and 48.13° (2 theta) were present. The spectrum did not have any evidence for sodium alginate and paracetamol crystallites. Hence, both were not crystallized during drying of the beads. As the bead is a highly cross-linked network derived from viscous aqueous sodium alginate, paracetamol might not be free enough to crystallize inside the bead. As Ca^{2+} is used to cross-link alginate, the excess $CaCl_2$trapped in the bead during its formation might have crystallized. So, its characteristic reflections were observed.

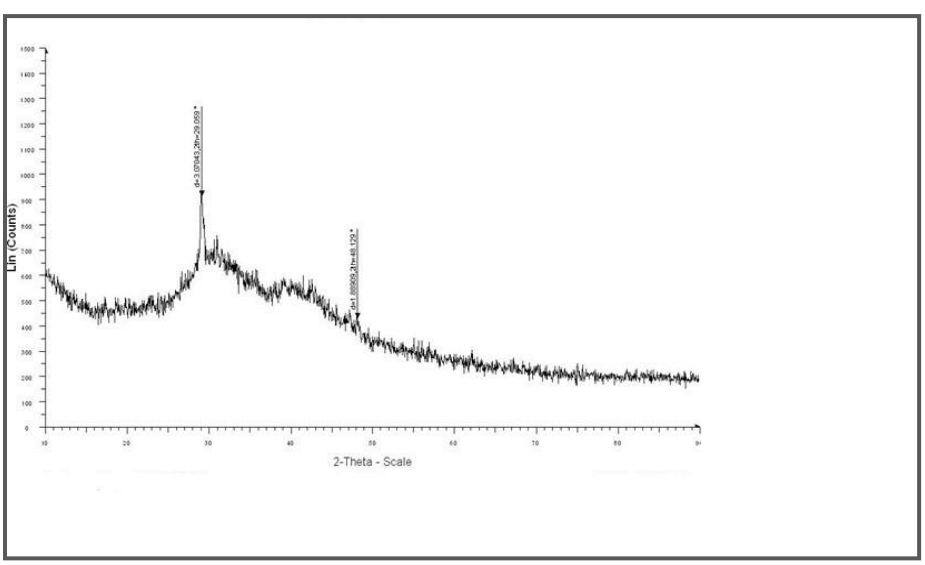

Figure 4: XRD pattern of Paracetamol-Sodium alginate-$CaCl_2$

4.7 XRD pattern of $CaCl_2$

The XRD pattern, Figure 5, confirms largely amorphous nature of $CaCl_2$. The two reflections occurred at 29.3° and 47.2° (2 theta) are assigned to existence of crystalline phase of $CaCl_2$. Both are assigned to reflections from (101) and (104), respectively.

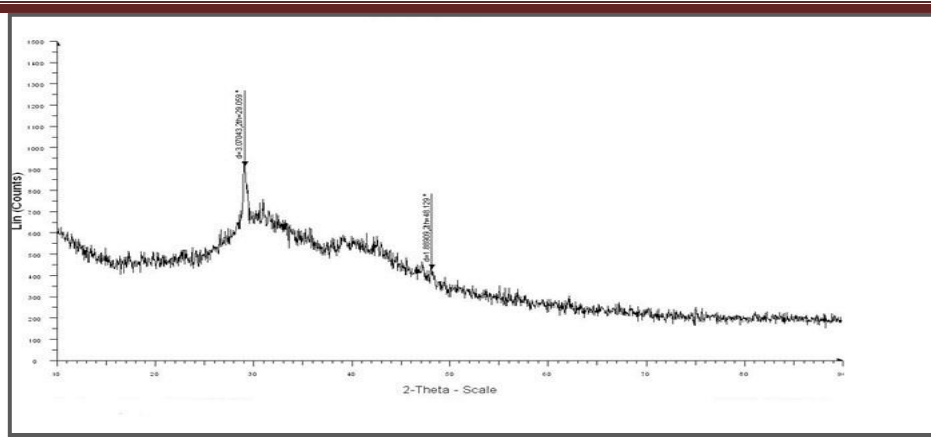

Figure 5: XRD Pattern of CaCl2

4.7. SEM and EDAX Analysis

The SEM image of paracetamol-sodium alginate-$CaCl_2$ is shown in Figures 6 & 7. Although the bead was initially spherical before drying, it was completely changed after drying. It is due to the difference in crosslink density at different regions of the bead. The tiny white particles are due to crystallized $CaCl_2$ as evidenced from XRD. The presence of tiny rods on the surface may be due to paracetamol.

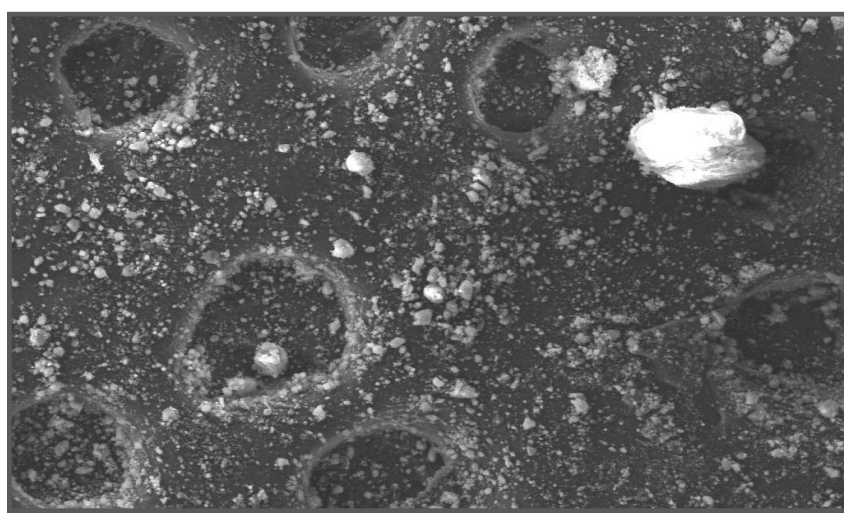

Figure 6: SEM Analysis of Paracetamol-Sodium alginate-$CaCl_2$

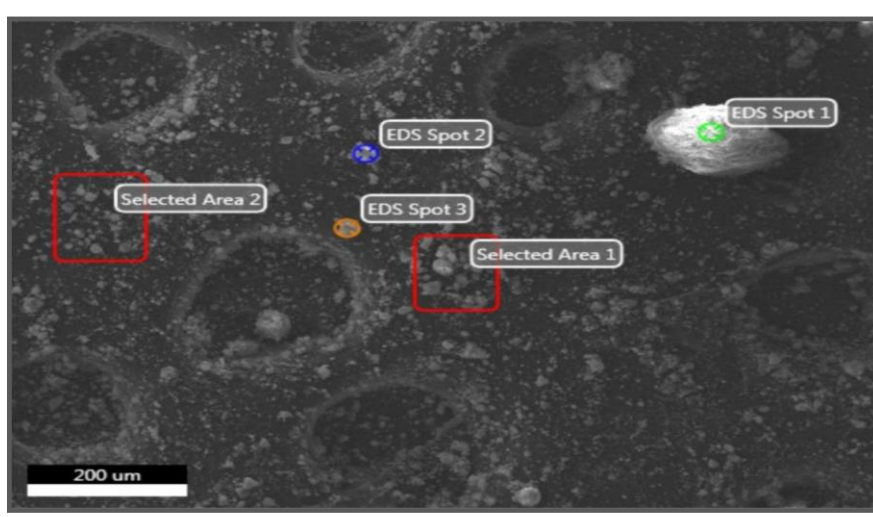

Figure 7: EDAX analysis of Paracetamol-Sodium alginate

The presence of chlorine accounts for crystallization of $CaCl_2$, as evidenced by XRD. The presence of little amount of sodium indicates, the entire sodium alginate in the bead is not completely converted into calcium salt. Because of diffusion problem, the sodium alginate near the surface can be completely used up for cross-linking, but those in the bulk portion of the bead cannot be completely converted, as calcium ions may not be inaccessible.

5.CONCLUSION

In conclusion, this study shows that water absorption of sodium alginate and calcium chloride beads are appreciable for in the field of agriculture. Especially potting plants and use in gardens to save water. This unique property can potentially be exploited in the development of fast and high water uptake hydrogels for a variety of pharmaceutical biomedical and industrial applications.

Different weight proportion of dried calcium chloride beads were prepared. There means content of paracetamol was loaded. When the beads were exhausted by soaking for 10 hours in 0.5 N hydrochloric acid the released paracetamol was found 65% of the embodied quantity indicating that the remained amount is strongly trapped in the beads body. Finally, it can be concluded that the hydrogel beads with sodium alginate with paracetamol drug exhibits more stability and bears potential for being used as oral drug releasing system.

The FTIR spectra showed the -OH stretching vibration at 3286 cm^{-1} as a broad band. The CH_3 and alginate -C-H stretching vibrations were clearly seen at 2918 and 2850cm^{-1}. The C=N vibration is shifted to 1597cm^{-1}. Its broadening indicates overlapping of aromatic ring skeletal vibration (1600cm^{-1}) with it. The Ca-O vibration occurred below 800cm^{-1} and the features are nearly same as the previous spectra. The resultant FTIR spectra shows the presence of paracetamol, alginate and the corresponding metal ion.

The XRD pattern showed the bead is a highly cross-linked network derived from viscous aqueous sodium alginate, p-acetamol might not be free enough to crystallize inside the bead. As Ca^{2+} is used to cross-link alginate, the excess $CaCl_2$ trapped in the bead during its formation might have crystallized. So, its characteristic reflections were observed. Confirms largely amorphous nature of $CaCl_2$. The two reflections occurred at 29.3° and 47.2° (2 theta) are assigned to existence of crystalline phase of $CaCl_2$. Both are assigned to reflections from (101) and (104), respectively. The surface morphology of hydrogel beads with drug were studied by SEM. The bead was initially spherical before drying, it was completely changed after drying. It is due to difference in crosslink density at different regions of the bead. The tiny white particles are due to crystallized.

The EDAX results, showed all the elements present in the dried bead. As expected, the percentage of carbon and oxygen was higher than the other elements. The presence of chlorine accounts for crystallization of CaCl2, as evidenced by XRD. From the current research, it may be concluded that the hydrogel beads are suitable for both in agriculture and drug releasing system.

REFERENCE

1. Vundavallia, Ramesh (2015). "Biodegradable Nano-Hydrogels in Agricultural Farming.
2. Alternative Source for Water Resources". Procedia Materials Science. **10**: 548–554.
3. Ahmed, Enas M. (2015). "Hydrogel: Preparation, characterization, and applications: A review". Journal of Advanced Research. **6** (2): 105–121. Doi:10.1016/j.jare.2013.07.006.
4. Jyothi, A.N. (2010). "Starch Graft Copolymers: Novel Applications in Industry". Composite Interfaces. **17**.
5. Narjari, Bhaskar; Aggarwal, Pramila; Kumar, Satyendra; M.D, Meena (2013). "Significance of Hydrogel and its application in agriculture". Indian Farming. **62** (10): 15–17.
6. L. O., Ekebafe; Ogbeifun, D. E.; Okieimen, F. E. (2011)."Polymer Applications inAgricultur "Biokemistri. **23**: 81–89.
7. Puoci, Francesco; et al. (2008)."Polymer in Agriculture: A Review"(PDF). American Journal of Agricultural and Biological Sciences. **3** (1): 299–314.
8. Rudzinski, W. E.; et al. (2002). "Hydrogels as controlled release devices in agriculture: Review". Designed Monomers and Polymers. 5 (1): 39–65.
9. Suruchinit, J.; Kaith, Balbir Singh; Jindal, Rajeev; Kapur, G. S.; Kumar, Vaneet (2014). "Synthesis, characterization and evaluation of Gum tragacanth and acrylic acid based hydrogel for sustained calcium chloride release – enhancement of water holding capacity of soil". Journal of the Chinese Advanced Materials Society. 2 (1). doi:10.1080/22243682.2014.893412.
10. George Pasparakis, Nikolaos Bouropoulos, Swelling, 24 May 2006.
11. A.D.SEZER and J.AKBUGA,chiston, 8101, Haydarpasa-Istanbul, Turkey.
12. Akihiko Kikuchi,"Minako Kawabuchi, Masayasu Sugihara, Yasuhisa Sakurai,

DNA binding and biological activity of cobalt(III) complex containing 2, 2'-bipyridyl and Schiff base

S. Dhakshanamoorthy[1], N. Sri Gayathrai Devi[1], M. Murali Krishnan[2] & M.N. Arumugham[1]
[1]Department of Chemistry, Thiruvalluvar University, Vellore – 632115. Tamilnadu, India
[2]Department of Chemistry, Bannari Amman Institute of Technology, Sathyamangalam-638401, Tamilnadu, India

ABSTRACT: *Cobalt complex of type $[Co(Bipy)_2(SB)](ClO_4)_2$ [Bipy = 2,2'-bipyridyl, SB = schiff base) has been synthesized and characterized by elemental analyses, NMR, UV-visible, infrared spectral studies. DNA binding properties of this metal complex was investigated using absorption spectroscopy, fluorescence spectroscopy, viscosity measurements and cyclic voltammetry. The experimental results indicate that the complex bind to DNA through an intercalative mode. The complex tested for biological activity and it has good antibacterial and antifungal activity on comparing with standard drugs.*

Keywords: *DNA binding, cobalt(III) complex, antimicrobial activity, schiff base*

Introduction

Recently, the interaction of transition metal polypyridyl coordination compounds with DNA has been extensively studied. Due to the unusual binding properties and general photoactivity, these coordination compounds are suitable candidates as DNA secondary structure probe, photocleavers and antitumor drugs[1, 2]. The effects of size, shape, hydrophobicity, and the charge on the binding of the complex to DNA have been studied by changing the type of heteroaromatic ligand or metal centre[3, 4]. The vast majority of such studies have been focused on complexes of Ru(II)[5–7], but to a far lesser extent, on other metal complexes. Barton has reported that chiral bipyridal–cobalt (III) complexes recognize different local structures of DNA. In the previous work, they have synthesized many cobalt (III) complexes and investigate their DNA-binding properties[8–10]. The ligands, 1,10-phenanthroline and 2,2'-bipyridyl are strong field bidentate ligands that form more stable chelates with many transition metals. These ligands, as well as some of their derived complexes, do exhibit antimicrobial properties[11-13].

Schiff bases are important class of compounds in medicinal and pharmaceutical field. They show biological applications including antibacterial, antifungal and antitumor activity[14,15]. Aniline Salicylaldimine schiff bases and their complexes have been used as biological models to understand the structures of biomolecules and biological processes[16-17]. The interaction of metal complexes containing N, O Schiff base ligands has been thoroughly considered[18-20]. DNA binding is the critical step for DNA activity. To design effective chemotherapeutic agents and better anticancer drugs, it is essential to explore the interactions of metal complexes with DNA. Recently, there has been tremendous interest in studies related to the interaction of transition metal ions with nucleic acid because of their relevance in the development of new reagents for biotechnology and medicine [21]. These studies are also important to understand the toxicity of drugs containing metal ions. Cobalt complexes have gained importance for their applicability in the biological field. Recently, our group focused on DNA binding activity of important amino acid containing copper(II) complexes are really interested, copper(II) complexes of the type amino acid-Cu-heterocyclic base show efficient DNA binding, cleavage and cytotoxicity[22-25].

In this paper, we synthesized and characterization of complex of cobalt (III) containing a ligand with 2, 2'-bipyridyl and Schiff bases, were done by elemental analysis, conductivity measurement, IR and NMR spectral studies. DNA binding properties were studied using absorption spectroscopy, fluorescence spectroscopy, cyclic voltammetry and viscosity measurements. The results should be of value in understanding the binding mode of the complex to DNA. The cobalt (III) complex show good activity against gram positive, gram negative bacteria as well as fungus.

Experimental Section

Synthesis of $[Co(Bipy)_2Cl_2]Cl$ [26]

Cobaltus chloride ($CoCl_2.6H_2O$), 1.185 g (5 mmol) was dissolved in 12 mL of water and 0.780 g (5 mmol) of 2, 2-bipyridyl was added. It was heated in a round bottomed flask until solution became partly

and it was cooled rapidly with constant strring to yield fine pink crystal $CoCl_2$ 2 bipy. $3H_2O$, chlorine gas was passed into this mixture with frequent stacking and it was gradually converted into dirty violet paste, oxidation being complete in 1-1/2 hours. The product was separated by sucking an glass filter washed several times with 2 M HCl and dried in air. To purify the product, 30 mL of hot water was added, the cherry red solution was treated with 25 mL of Con.HCl and the mixture was heated on the water bath. Dark violet crystal with grayish tinge in the forms of prism ending in elongated pyramids gradually separated, more than 90% of the product was recrystallised in this way.

Synthesis of $[Co(Bipy)_2(SB)](ClO_4)_2$ (1)

2.380 g (5 mmol) of $[Co(Bipy)_2Cl_2]Cl$ complex was dissolved in (25ml) ethanol and stirred well. About 0.985 g (5 mmol) of Schiff bases was dissolved in 25 ml of ethanol. Then this solution was added to the above solution the mixture was refluxed for 5 hours in the water bath. On cooling the solution to ambient temperature, an aqueous solution of sodium perchlorate 1.2245 g (10 mmol) was added to the above mixture and then refluxed for 30 minutes. A yellowish green colored substance was separated out, which was filtered and dried.

Results and Discussion

General Aspects

The elemental analysis data of the cobalt (III) complex (Table 1) agree with the theoretical values. The synthetic strategy of the complex is outlined in Scheme-1.

The molar conductance measurement revealed[27]that the cobalt (III) complex 1 behave as 1:2 electrolyte in aqueous medium.

Table 1: The Elemental Analysis, Molar conductivity of cobalt (III) complex

Complexes	Carbon	Hydrogen	Nitrogen	Molar Conductance (Sm^2mol^{-1})
$[Co(Bipy)_2(SB)](ClO_4)_2$	51.65 (51.58)	3.55 (3.52)	9.13 (9.06)	218

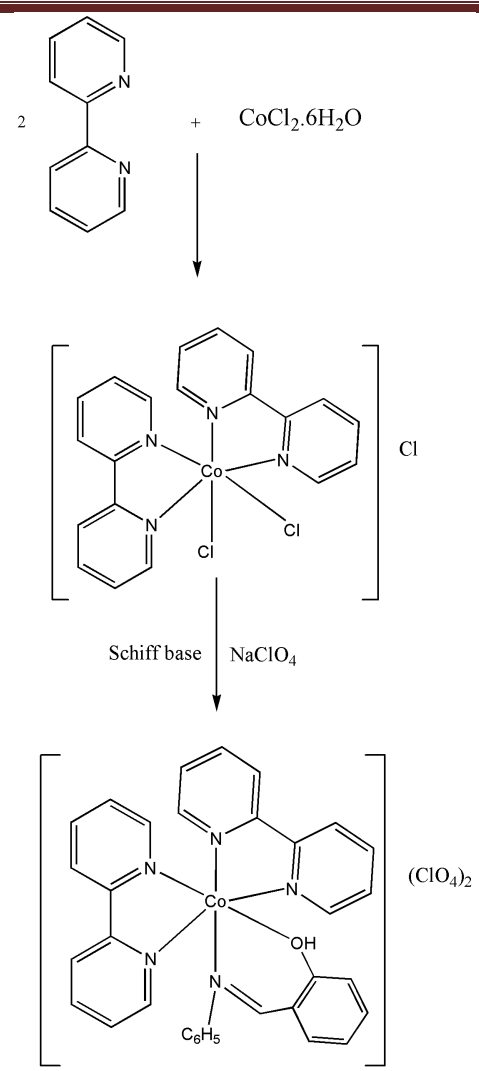

Scheme 1: Synthesis of complex $[Co(Bipy)_2(SB)](ClO_4)_2$ (1)

Electronic Spectra

Electronic spectra were recorded in water. The bands were near 300 nm due to intraligand π—π* transitions of bipyridyl ligands (Figure 1).

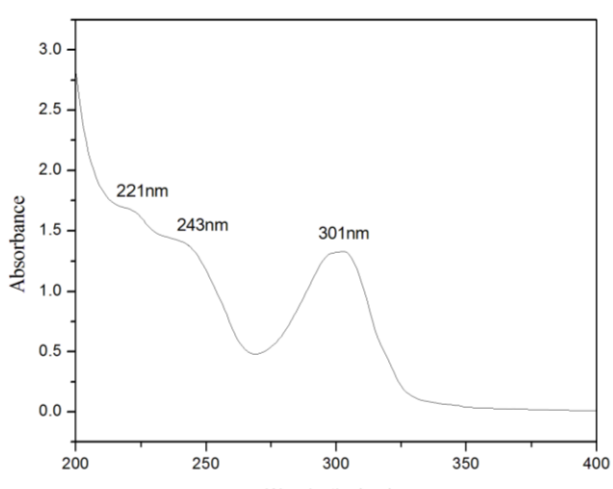

Figure 1: Electronic Spectrum of $[Co(Bipy)_2(SB)](ClO_4)_2$

Infrared spectra

Infrared spectrum of the complex was shown in Figure 2. The characteristic out-of-plane hydrogen bending modes of free bipy observed at 853, 738 cm^{-1}, are red shifted to 842 and 715 cm^{-1}(**1**) 842 and 722 cm^{-1} (**2**) upon metal complexation. This shift can be explained on the basis of the fact that the nitrogen atoms of bipyridine ligand donate a pair of electrons each to the central cobalt metal, forming a coordinate covalent bond. Besides, it is also confirmed by the shift of ν(C–N) of bipyridine from about 1670 cm^{-1} in the free ligand to 1625 cm^{-1} after coordination. The broad band observed around 3425 is assigned to the ν(O-H) is stretching of Schiff bases. However, the strong band at ca. 1617 cm^{-1} is assigned to *ν*(C=N) of the Schiff base ligand[28] which shifts approximately 11 cm^{-1} to the lower wave numbers upon coordination to metal[29]. The coordination of the nitrogen and oxygen atoms is confirmed with the presence of new bands at ca. 526 and 460 cm^{-1}, assignable to *ν*(Co-N) and *ν*(Co-O), respectively[30]. Furthermore, the appearance of two new bands around 1098 and 636 cm^{-1} is indicative of uncoordinated perchlorate ions.

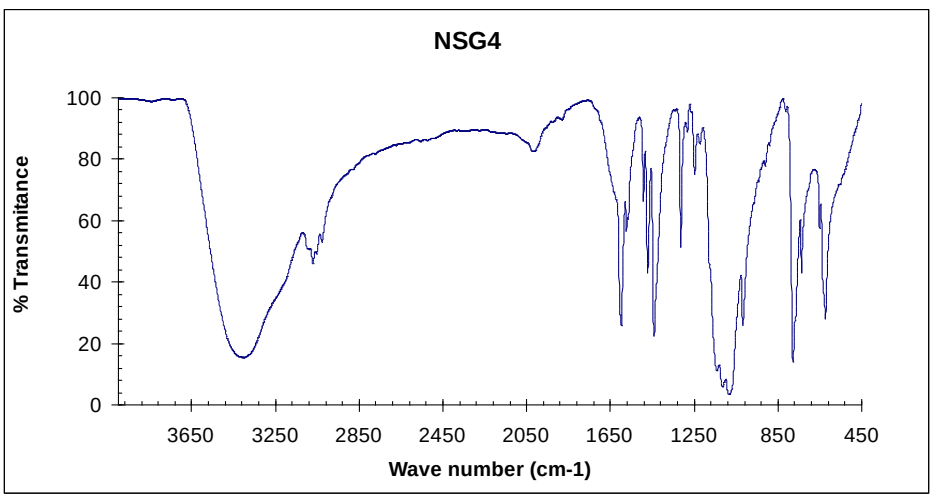

Figure 2: Infrared spectrum of $[Co(Bipy)_2(SB)](ClO_4)_2$

NMR Studies

The electronic environment of many aromatic hydrogen atoms is similar and hence their ^1H NMR signals appear in a narrow chemical shift range. In fact the aromatic regions of the spectra of this complex complicated due to the overlapping of several signals, which have precluded the identification of individual resonance. However, from the direct comparison of the intensity of the aromatic protons with that of the observable bipyridyl proton the number of aromatic protons expected 1H NMR (DMSO-d6) s (3.36 ppm): 7.71 (s, 1H), 7.26 (s, 1H), 8.45 (s, 1H), 8.15 (s, 1H), for these complex was confirmed (Figure 3a, 4b).

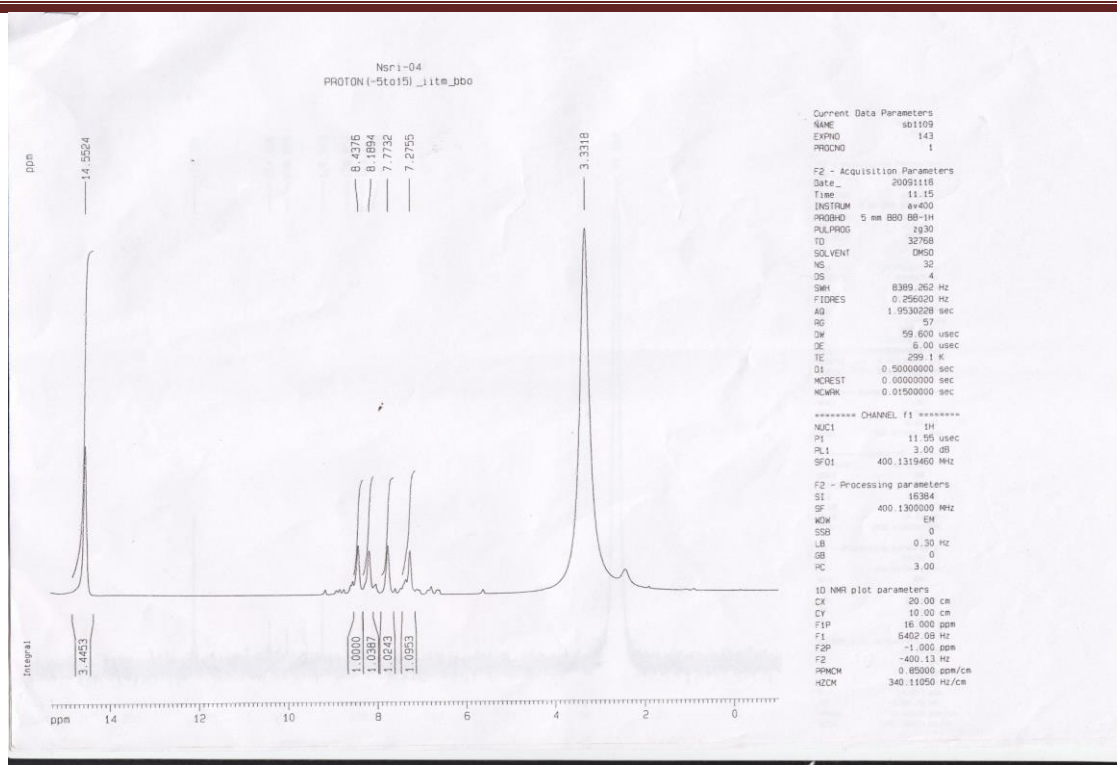

Figure 3: ^{1}H NMR

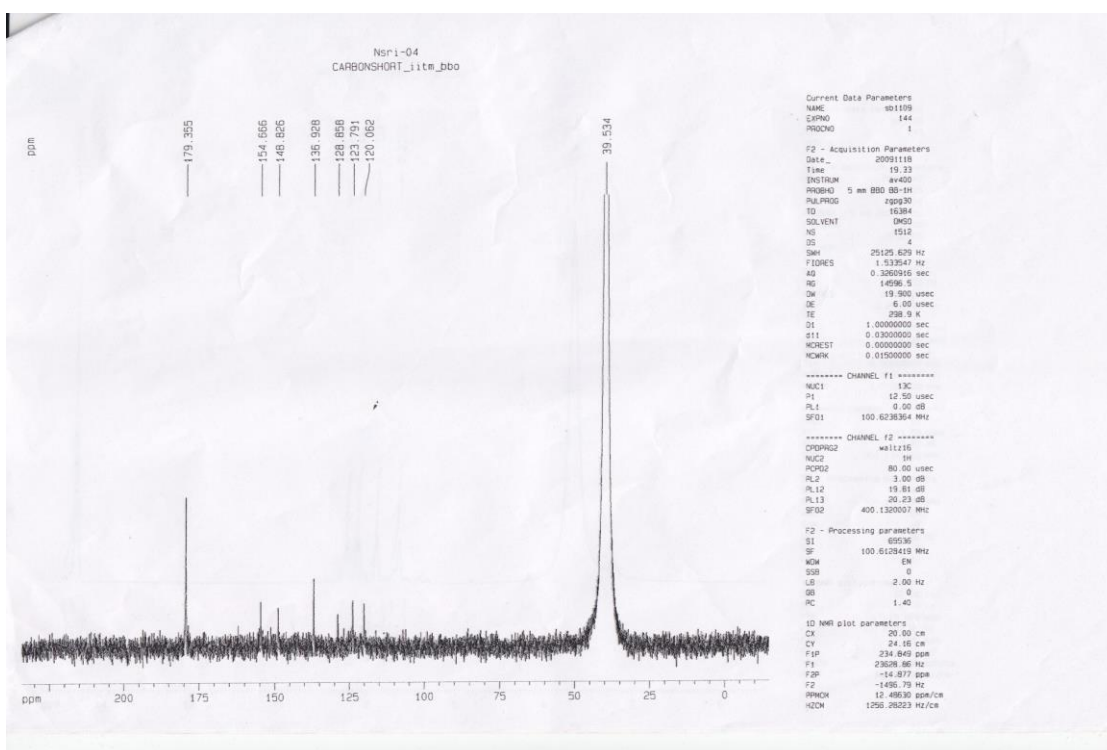

Figure 4: ^{13}C NMR

DNA binding studies

UV-Vis absorption spectra

Electronic absorption spectra were initially employed to study the binding of cobalt (III) complex with CT-DNA. The absorption spectra in aqueous buffer media of cobalt (III) complex in the absence and in

the presence of CT DNA are given in Figure 5.

In the UV region, the complex presented bands at 243, 301 for complex which can be attributed to π→π* transition of the coordinated bipyridine ligand.

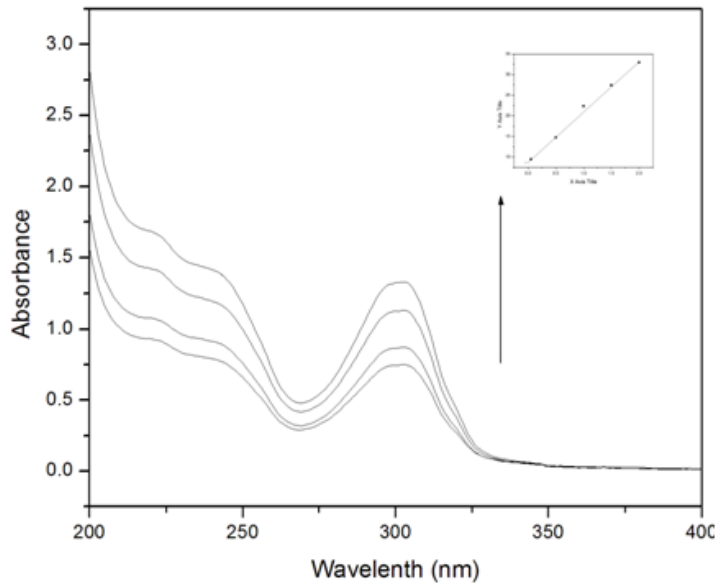

Figure 5: Electronic spectra of $5.0x10^{-5}$M complex $[Co(Bipy)_2(SB)](ClO_4)_3$ in the absence (---) and presence (—) of increasing amount of CT DNA at the ratio r = 0.3, 0.5, 0.7, 1.0. Arrow (↑) shows the absorbance changes upon increasing DNA concentration. Inset: linear plot for the calculation of the intrinsic DNA binding constant. K_b.

The absorption intensity of the complex increased (hyperchromism) evidently after the addition of DNA, which indicated the interactions between DNA and the complex. A similarly hyperchromism has been observed for the soret bands of certain porphyrins when interacted with DNA but has not yet been clearly explained[31, 32]. On the other hand, since DNA possesses several hydrogen bonding sites which are accessible both in minor and major grooves, it is likely that the amine groups Schiff bases forms hydrogen bonds with N-3 of adenine or O_2^- of thymine in the DNA, which may contribute to the hyperchromism observed in the absorption spectra. The hyperchromic effect may also be due to the groove binding interaction between positively charged complex and the negatively charged phosphate backbone at the periphery of the double helix CT-DNA[33]. Structurally, intercalation to DNA may be one of the binding patterns, since the cobalt(III) complexes contains bipyridine ligands which should provide aromatic moiety extending from the metal center through which overlapping occurs with base pairs of DNA by an intercalative mode[34]. The intrinsic binding constant (K_b), was determined from the following equation:

$$[DNA]/(\varepsilon_a-\varepsilon_f) = [DNA]/(\varepsilon_b-\varepsilon_f) + 1/K_b(\varepsilon_b-\varepsilon_f)$$

The 'enarappat' extinction coefficient (ε_a) was obtained by calculating $A_{obsd}/[Co]$. The terms ε_f and ε_b correspond to the extinction coefficients of free (unbound) and fully bound complex, respectively. A plot of $[DNA]/(\varepsilon_a-\varepsilon_f)$ vs. [DNA] will give a slope $1/(\varepsilon_b-\varepsilon_f)$ and an intercept $1/K_b$ $(\varepsilon_b-\varepsilon_f)$. K_b is the ratio of the slope and the intercept[35]. The intrinsic binding constant (K_b) for the association of the complexes with C-T DNA (inset of Figure 5) can be calculated using the absorption at 272 nm respectively. The K_b value is three order of magnitude lower than that observed for classical intercalators such as ethidum bromide (K_b,$1.23x10^6$ M^{-1}) in 25mM Tris-HCl/40 mM NaCl buffer,(pH 7.9)[36]. This indicates the complex have a very low binding affinity to DNA.

Fluorescence spectra

Competitive binding studies using DNA with bound ethidium bromide (EtBr) was carried out. The extent of fluorescence quenching of ethidium bromide (EB) by competitive displacement from DNA is a measure of the strength of interaction between the second molecule and DNA. The results in Figure 6 showed that the fluorescence intensity of CT-DNA-EB decreased remarkably with the addition of cobalt complex, which indicated that the complex can bind to DNA and replace EB from the CT-DNA-EB system[37]. The above data was analyzed by means of the Stern-Volmer equation[38]. The quenching plots (inset of Figure

6) illustrates that the fluorescence quenching of EB bound to DNA by the complex is in linear agreement with the Stern-Volmer relationship, which corroborates that the complex bind to DNA. In the plot of I_o/I vs. [complex]/[DNA], K_{sq} value for the complex are 0.043.

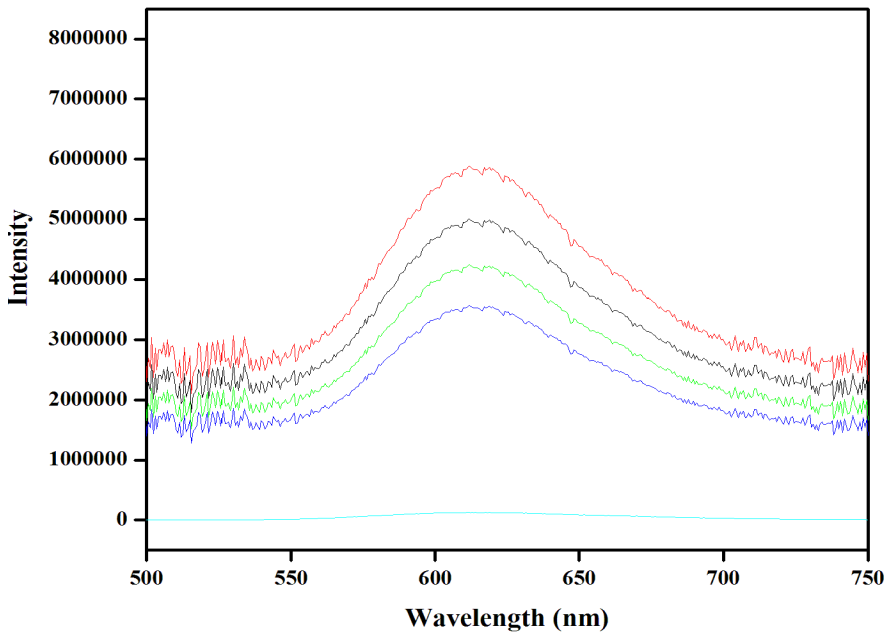

Figure 6: Emission spectra of EB bound to DNA. $[Co(Bipy)_2(SB)](ClO_4)_2$ [EB]= 40 µM, [DNA] = 40 µM, [Complex] = (0-50 µM). Arrow (↓) shows the intensity changes upon increasing the concentration of the complex. Inset: Stern-Volmer quenching curves.

Viscosity measurement.

Mode of interaction between the metal complex and DNA was clarified by viscosity measurements. Hydrodynamic measurements are sensitive to length change (i.e., viscosity and sedimentation) are regarded as the least ambiguous and the most critical test of binding in solution. A classical intercalation mode demands that the DNA helix lengthens as base pairs are separated to accommodate the bound ligand, leading to the increase of DNA viscosity. In contrast, a partial non-classical intercalation of ligand could bend (or kink) the DNA helix, reduce its effective length and concomitantly its viscosity[39].

Effect of the complexes on the viscosity of rod like DNA is shown in the (Figure 7). The viscosity of DNA is increased with the increase of the concentration of the complex in contrast to that of proven DNA intercalator. Based on the viscosity results, it was observed that these complex bind with DNA through intercalation binding[40].

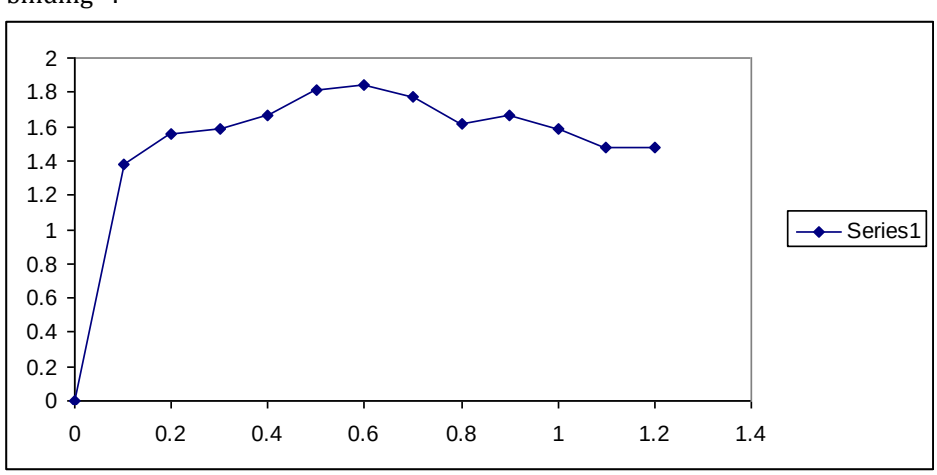

Figure 7: Effects of increasing amounts of complex on the relative viscosities of CT DNA at 25 ^{0}C $[Co(Bipy)_2(SB)](ClO_4)_2$.

Cyclic voltammetry studies

Cyclic Voltammetric (CV) response for complex in Tris-HCl buffer (pH 7.28) in the presence and absence of CT DNA is shown in (Figure 8). In the forward scan, a single cathodic peak was observed, which corresponds to the reduction of complex. In the reverse scan, no anodic peak was observed, which indicates that the process is irreversible. When CT-DNA is added to a solution of complex, marked decrease in the peak current and potential values were observed. The cyclic voltammetric behavior were not affected by the addition of very large excess of DNA, indicating that the decrease of peak current of complexes after the addition of DNA due to the binding of $[Co(Bipy)_2(SB)](ClO_4)_2$ complex to the DNA[41]. When the concentration of DNA increased, the changes in peak current and potential become slow. This reveals that the complex were interact with CT-DNA.

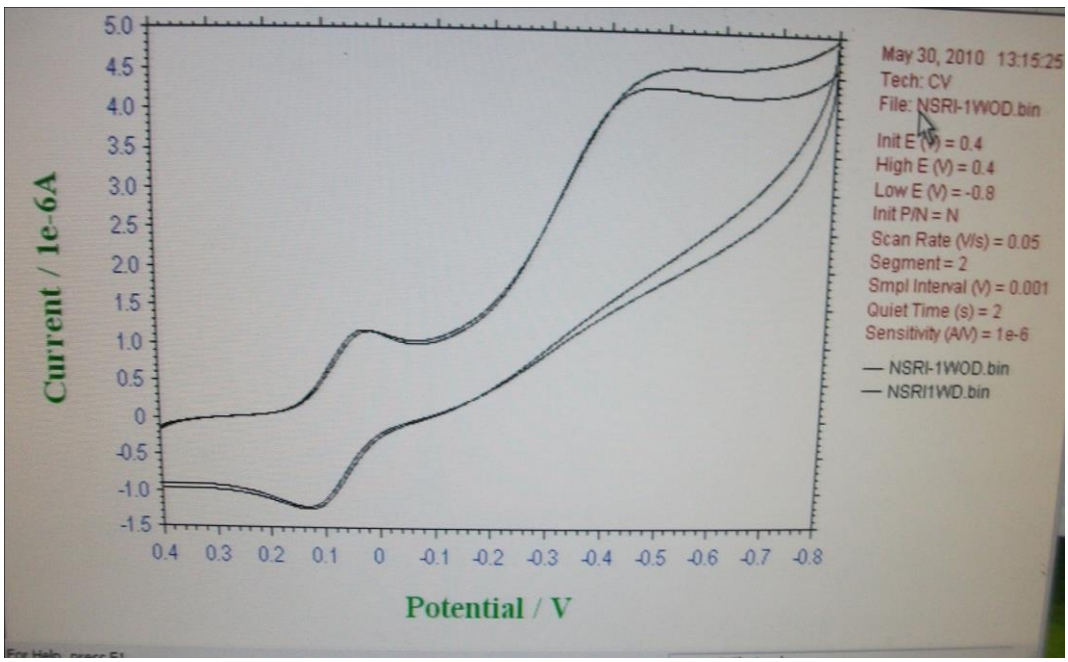

Figure 8: Cyclic voltammogram of 0.5 mM complex $[Co(Bipy)_2(SB)](ClO_4)_2$ in the absence (–) and presence (---) of 2.5 mM DNA.

Antimicrobial screening

The cobalt (III) complexes were screened *in vitro* for its antibacterial activity against certain pathogenic bacteria and fungi species using disc diffusion method. These complex were found to reveal considerable activity against Gram +ve, Gram -ve bacteria and fungi.

The test solutions were prepared in sterile distilled water and the results of the antimicrobial activities are summarized in Table 2. The complexes were found to reveal considerable activity against Gram +ve, Gram –ve bacteria and fungi. The results of the antimicrobial activities are summarized in Table 2. The complex showed greater extent of inhibition to the growth of bacteria. This may be due to the possible mode of increased toxicity of the cobalt complexes. Chelation considerably reduces the polarity of the metal ion because of partial sharing of its positive charge with donor groups and possible π–electron delocalization over the whole chelate ring. Such a chelation could enhance the lipophilic character of the central metal atom, which subsequently favours it permeation through lipid layers of cell membrane and blocking the metal binding sides on enzymes of microorganism. Either the variation in the effectiveness of different compound against different organisms depends on the impermeability of the cells of the microbes or differences in Ribosome's of microbial cells[42, 43].

Table 2: Antimicrobial activity of complexes $[Co(Bipy)_2(SB)](ClO_4)_2$

Name of the test organism	Cobalt complex
Gram +ve	
Staphylococcus aureus	10
Micrococcus luteus	14
Bacillus cereus	11
Gram -ve	
Escherichia coli	15
Klebsiella pneumonia	15
Pseudomonas aeruginosa	-
Fungi	
Aspergillus niger	16
Aspergillus flaves	18
Candida albicans	16

Conclusion

We described here one cobalt (III) complex. Further characterization of the complexes was achieved through physico-chemical and spectroscopic methods. The effectiveness of the binding of the complexes is being confirmed by means of hyperchromism in the electronic spectral studies and change in intensity of emission in the case of emission spectral studies. Besides, the effect of binding is also confirmed by the viscometric and cyclic voltammetric studies. This shows that the complex interact with DNA base pairs effectively. The cobalt (III) complex has exhibit good antimicrobial activities.

References

1. J.K. Barton, A.T. Danishefsky, J.M. Goldberg, *J. Am. Chem. Soc*., 1984, **106,** 2172–2176.
2. B. Nordn, P. Lincoln, B. Akerman, E. Tuite, in: A. Sigel, H. Sigel (Eds.), *Metal Ions in Biological Systems,* 1996, **33**, 177.
3. S. Baskaran, M. Murali Krishnan, M.N. Arumugham, *Inorg. Met. Chem,* 2017, **47**, 269-267.
4. S.Dhakshanamoorthy, M.Murali Krishnan, M.N. Arumugham, *Ind. J. Adv. Chem. Sci*, 2018, **6**, 53-58.
5. V. Aranyos, A. Hagfeldt, H. Grennberg, E. Figgemeier, *Polyhedron,* 2004**, 23**, 589–598.
6. L.F. Tan, H. Chao, Y.J. Liu, H. Li, B. Sun, L.N. Ji, *Inorg. Chim. Acta*, 2005, **358**, 2191–2198.
7. Q.L. Zhang, J.G. Liu, H. Xu, H. Li, J.Z Liu, H. Zhou, L.H. Qu, L.N. Ji, *Polyhedron,* 2001, **20**, 3049–3055.
8. X.L. Wang, H. Chao, H. Li, X.L. Hong, Y.J. Liu, L.F. Tan, L.N. Ji, *J. Inorg. Biochem.,* 2004, **98,** 1143–1150.
9. Q.L. Zhang, J.G. Liu, J.Z. Liu, H. Li, Y. Yang, H. Xu, H. Chao, L.N. Ji, *Inorg. Chim. Acta,* 2002, **339,** 34–40.
10. A.A.A. Abu-Hussen, *J. Coord. Chem.,* 2006**, 59,** 157-176.
11. B.Coyle, K.Kavannagh, M. McCann, M. Devereux, M. Geraghty, *Biotals*, 2003, **16**, 321-329.
12. S. Baskaran, M. Murali Krishnan, M.N. Arumugham, Rakesh Kumar, *J. Coord. Chem,* 2015, **68**, 4395-4407.
13. S. Baskaran, M. Murali Krishnan, M.N. Arumugham, Rakesh Kumar, *J. Mol. Liq,* 2016, **221**, 1045-1053.
14. R. Mladenova, M. Ignatova, N. Manolova, T. Petrova, I. Rashkov, *Eur. J. Polym.,* 2002, **38**, 989-999.
15. O.M. Walsh, M.J. Meegan, R.M. Prendergast, T.A. Nakib, *Eur. J. Med. Chem*., 1996, **31**, 989-1000.
16. J.E. Kovacic, *Spectrochim. Acta,* 1967, **23**, 183-187.
17. R. Atkins, G. Brewer, E. Kokot, G.M. Mockler, E. Sinn, *Inorg. Chem*., 1985, **24**, 127-134.
18. A. Sigel, in: H. Sigel (Ed.), *Metal ions in biological systems*, 1996, 32.
19. K.E. Erkkila, D.T. Odom, J.K. Barton, *Chem. Rev.,* 1999, **99**, 2777-2796.
20. C. Metcalfe, J.A. Thomas, *Chem. Soc. Rev*., 2003, **32,** 215-224.
21. V. Uma, V.G. Vaidyanathan, B.U. Nair, *Bull. Chem. Soc. Jpn***.,** 2005, **78**, 845-850.
22. S.Dhakshanamoorthy, M.Murali Krishnan, M.N. Arumugham, *Asian. J. Res. Chem*, 2017, **10**, 312-318.
23. D. Ezhilarasan, M. Murali Krishnan, M.N. Arumugham, *J. Chem. Chem Sci*, 2017, **7**, 477-485.
24. S.Dhakshanamoorthy, M.Murali Krishnan, M.N. Arumugham, *Int. J. Chem. Phy. Sci*, 2017, **6**, 39-47.
25. H. Gopinathan, N. Komathi, M.N. Arumugham, *Inorg. Chem. Acta*, 2014, **416**, 93-101.
26. A V. Ablou, *Russion J. Inorg.chem.*, 1961, **6**, 157.
27. J.K. Nath, J.B. Baruah, *Polyhedron*, 2012, **36**, 1-5.
28. B.A. Uzoukwu, K. Gloe, H. Duddeck, *Inorg. Met. Org. Chem*., 1998, **28**, 819-831.

29. N. Shahabadi, S. Kashanian, F. Darabi, *DNA Cell Biol*., 2009, **28**, 1-8.
30. N. Saha, S. Sinha, *Indian J. Chem*., 1990, **29**, 292.
31. R. F. Pasternack, E. J. Gibbs, J.J. Villafranca, *Biochemistry,* 1983, **22**, 2406.
32. C.L. Liu, J.Y. Zhou, Q.X. Li, l.J. Wang, Z.R. Lia, H.B. Xu, *J. Inorg. Biochem*.**,** 1999, **75,** 233.
33. R. Senthil Kumar, S. Arunachalam, V. S. Periasamy, C.P. Preethy, A. Riyasdeen, M.A. Akbarsha, *Polyhedron,* 2008, **27,** 1111.
34. Z.H. Xu, F.J. Chen, P.X. Xi, X.H. Liu, Z.Z. Zeng, *J. Photochem. Photobiol. A Chem*., 2008**, 196,** 77.
35. A.M. Pyle, J.P. Rehmann, R. Meshoyrer, C.V. Kumar, N.J. Turro, J.K. Barton*, J. Am. Chem. Soc.*, 1989, **111,** 3051.
36. W.D. Wilson, L. Ratmeyer, M. Zhao, L. Strekowski, D. Boykin, *Biochemistry,* 1993, **32**, 4098.
37. R. Senthil Kumar, S. Arunachalam, V. S. Periasamy, C.P. Preethy, A. Riyasdeen, M.A. Akbarsha, *J. Inorg. Biochem*., 2009**, 103**, 117.
38. J.R. Lakowicz, G. Webber, *Biochemistry,* 1973**, 12**, 4161.
39. S. Satyanarayana, J.C. Dabrowiak, J.B. Chaires, *Biochemistry*, 1993, **32**, 2573.
40. L.S. Kumar, H.D. Revanaslddappa, *J. Coord. Chem*., 2011, **64**, 699.
41. M. C. Prabahkara, H.S.b. Naik, *Biometals,* 2008, **21**, 675.
42. P.C. Saravanan, M. Murali Krishnan, M.N. Arumugham, *Ind. J. Adv. Chem. Sci*, 2017, **5**, 1-6
43. S. Dhakshanamoorthy, M.Murali Krishnan, S.Baskaran, M.N. Arumugham, *Int. J. App. Adv. Sci. Res*, 2016, 2, 87-93.

Adsorption, biosorption and discolouration on tannery effluents using Ferrous chloride and Ferric chloride Nano particles by using rose petal extract form collected near tannery industry

E. Revathi[1], A. Thaminum Ansari[1], S. Ulaganathan[2] & CT. Ravichandran[2]
[1]Department of Chemistry, Muthurangam Government Arts College (Autonomous), Vellore, Tamilnadu
[2]Department of Chemistry, Arignar Anna Government Arts College Cheyyar, Tamilnadu

ABSTRACT: *The development of reliable, eco-friendly processes for the synthesis of nano scale materials is an important aspect of nanotechnology. Ferrous chloride ($FeCl_2.4H_2O$), ferric chloride ($FeCl_3.6H_2O$) nano particles have been known to have Adsorption, biosorption and discolouration. In the present study ferrous chloride and Ferric chloride nano particles by using Rose petal extract. Nano particles of Ferrous chloride and Ferric Chloride has been synthesized by simple chemical precipitation method and characterized by UV-Vis, XRD and SEM analysis. In future, combination of both may be the best option for purifications. The aim of the project is to analyze the tannery effluents purification using the nano particles. Ferrous chloride and Ferric chloride nano particles were also applied with tannery effluents for estimation Colour, pH, Turbidity, TDS, Alkalinity, COD, BOD, Chloride, Residual free Chlorine, Sulphate, Sulphide, Nitrate, Nitrite and also color removal efficiencies.*

Keywords: *Ferrous chloride and Ferric chloride nanoparticles, UV-spectroscopy, X-ray diffraction*

1.INTRODUCTION

In the area of water purification, nanotechnology offers the possibility of an efficient removal of pollutants and germs. Since early in history, people have dumped sewage into waterways, relying on natural purification by dilution and by natural bacterial breakdown. Population increases resulted in greater volume of domestic and industrial wastewater, requiring that we give nature a helping hand. Basic wastewater treatment facilities reduce organic and suspended solids to limit pollution to the environment. Advancement in needs and technology has necessitated the evolving of treatment processes that remove dissolved matter and toxic substances. Currently, the advancement of scientific knowledge and moral awareness has led to a reduction of discharges through pollution prevention and recycling, with the noble goal of zero discharge of pollutants. Main pollution in tannery effluents came from tannery finishing processes.

These processes require the input of a wide range of chemicals and dyestuffs, which generally are organic compounds. Because all of them are not contained in the final product, became waste and caused disposal problems. Major pollutants in tannery effluents are high suspended solids, chemical oxygen demand, heat, colour, acidity, and other soluble substances.

Synthesis of nanoparticles, a number of chemical methods exist in the literature (Waghmode and Dagade, 2013). Thus, researchers in the field of nano scale material synthesis and assembly have been eagerly looking at eco-friendly methods of synthesis as an alternative (Sreekanth and Nagajyothi, 2013).

It is well known that extracts of adsorption have the ability to synthesize nanoparticles from the metal salt solutions of the respective metals and also retain their stability in the nanosize by acting as capping agents and preventing them from precipitating for a reasonably long duration of time. These natural extracts like Garlic extract, Wheat grass extract, Rose petal extract play an important role in remediation of toxic metals through reduction of metal ions and act as interesting nanofactories.

Metal nanoparticles have been studied extensively because of their unique physicochemical characteristics. Among metal nanoparticles Ferrous chloride ($FeCl_2.4H_2O$) and ferric chloride ($FeCl_3.6H_2O$) nanoparticles have been known adsorption and biosorption effects.

As seen above nanoparticles of different metals have proven to be a boon in medical as well as chemical researches and for this reason, the present work has been focused on the development of natural and green method of synthesis of nanoparticles (Baghayeri and Namadchian, 2013) of Ferrous chloride and ferric chloride.

2. EXPERIMENTAL METHODS

2.1MATERIALS

The roses were obtained from the local flower shop each time. Ferrous chloride ($FeCl_2.4H_2O$) and ferric chloride ($FeCl_3.6H_2O$) were obtained from galaxy vellore (SDS make) and used as received.

2.2 EXPERIMENTS

2.2.1 Source of Rose petals:

The roses were obtained from the same local florist each time the extract was prepared and confirmed to be of the same species i.e. Rosa petal. Also called as Dublin ray roses, they were easily available at any local florist (Fig. 1).

Fig. 1: Rose flowers used for extract

2.2.2 Rose petal extract preparation method

Rose petals were first given a wash of distilled water and were crushed using the mixer-blender apparatus thereafter. These shredded rose petals were then subjected to boiling for 5min in distilled water (0.5g rose petals per 1ml distilled water). This solution was then filtered using a filter paper and the filtrate was used as the extract while residue was discarded.

2.2.3Synthesis of Ferrous chloride and ferric chloride Nanoparticles:

In 250ml flasks, 4.5g of ferrous chloride ($FeCl_2.4H_2O$) and 4.5g of ferric chloride ($FeCl_3.6H_2O$) then 100 ml rose petal extract was added to it. Immediately after this addition the flasks were stirred for 6 hours at a temperature of 60^oC. After 6 hours the above mixture was visual observation of colour change of the solution. Initially colour change was observed from light pink to dark brown which indicated formation of nanoparticles. This was done just for the preliminary detection. These samples were then subjected to optical measurements, which were carried out by using a UV-Visible spectrophotometer and nanoparticles was checked by SEM and Xray Diffraction (XRD) using an X-ray diffractometer.

3.RESULTS AND DISCUSSIONS

3.1Characterization of Ferrous chloride and ferric chloride Nanoparticles:

In the present study, natural synthesis of ferrous chloride ($FeCl_2.4H_2O$) and ferric chloride ($FeCl_3.6H_2O$), nanoparticles using rose petal extract were studied. Visual observations show colour change in the ferrous chloride and ferric chloride solutions after extract additions. The colour changes to brown after formation of ferrous chloride and ferric chloride noparticles which was further characterized by using UV-visible, XRD and SEM analysis.

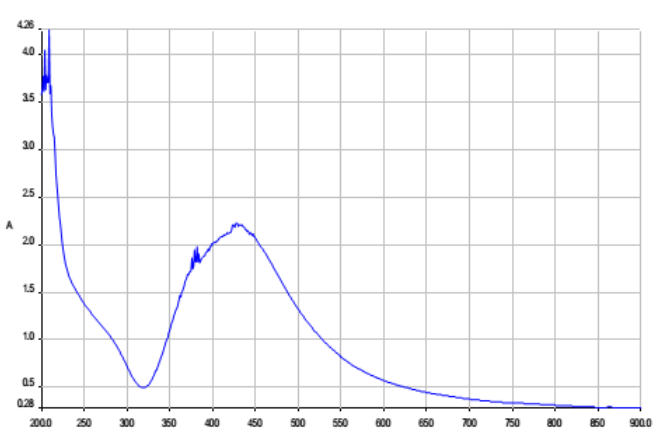

Fig.2: UV-Visible spectra of ferrous chloride and ferric chloride Nanoparticles

Figure 2 show the UV-visible spectrum of ferrous chloride ($FeCl_2.4H_2O$), ferric chloride ($FeCl_3.6H_2O$) nanoparticles by using green synthesis of rose petal extract which acts as capping as well as stabilizing agents. The stability of these nanoparticles we have checked after three months. The Ferrous chloride and ferric chloride nanoparticles show absorption of $FeCl_2$ and $FeCl_3$ in visible region, the absorption at 422nm which is due to ferrous chloride and ferric chloride. Due to the free electrons present in the ferrous chloride ($FeCl_2.4H_2O$), ferric chloride ($FeCl_3.6H_2O$) Fe nanoparticles, this free electron gives the surface absorption band at 422 nm.

3.2 XRD of Ferrous chloride and Ferric chloride nanoparticles:

The phase purity of as synthesized ferrous chloride and ferric chloride nanoparticles was examined by using powder X-ray diffraction.

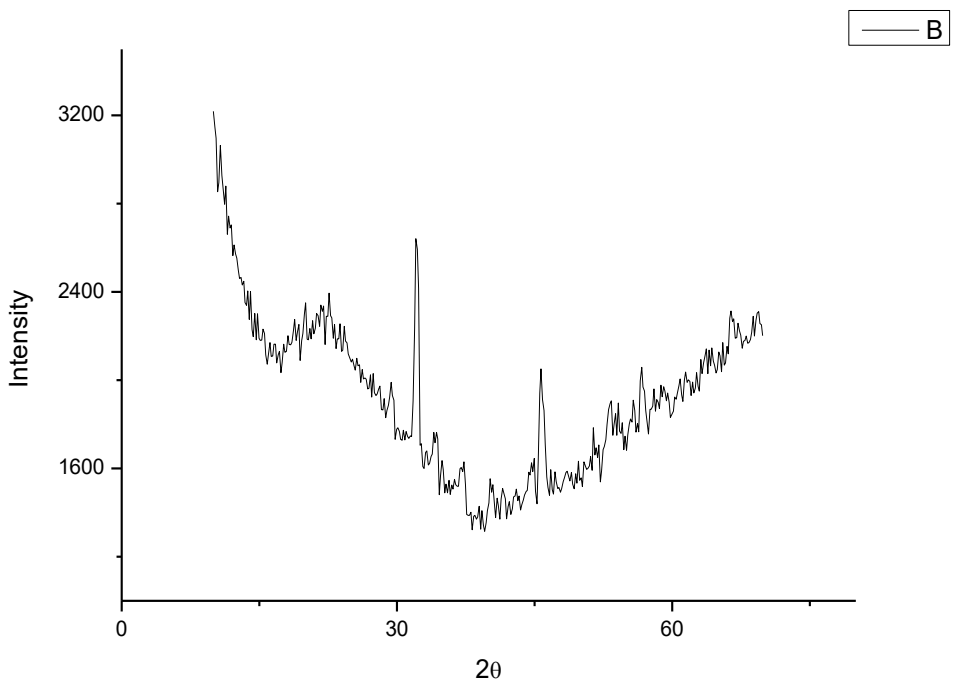

Fig.3: XRD patteren of ferrous chloride and Ferric chloride nanoparticles

The X-ray diffraction Figure 3 shows two intense peaks at 28.54°, 45.52° corresponds to planes (111) and plane (220) for Ferrous chloride ($FeCl_2.4H_2O$), ferric chloride ($FeCl_3.6H_2O$) nanoparticles with further diffraction peaks at 28.54, 46 , 54.9, 57.3, 68 and 77 which confirms formation of ferrous chloride and ferric chloride nanoparticles with face centered cubic structure.

3.3 SEM of Ferrous chloride and Ferric chloride nanoparticles:

The SEM analysis provided information about size and shape of resulting ferrous chloride and Ferric chloride nanoparticles Obtained micrographs are shown in Fig. 4. It was observed, that the nanoparticles of all prepared samples have particle sizes below 200 nm. Bigger particles were obtained in the case of molar ratio Fe2+:Fe3+ =1:1 However, the difference was not too significant. The change in particle sizes before and after was also almost negligible. The roduced nanoparticles were generally spherical in the shape and both types tend to form agglomerates, as can be seen in the Fig. 4.

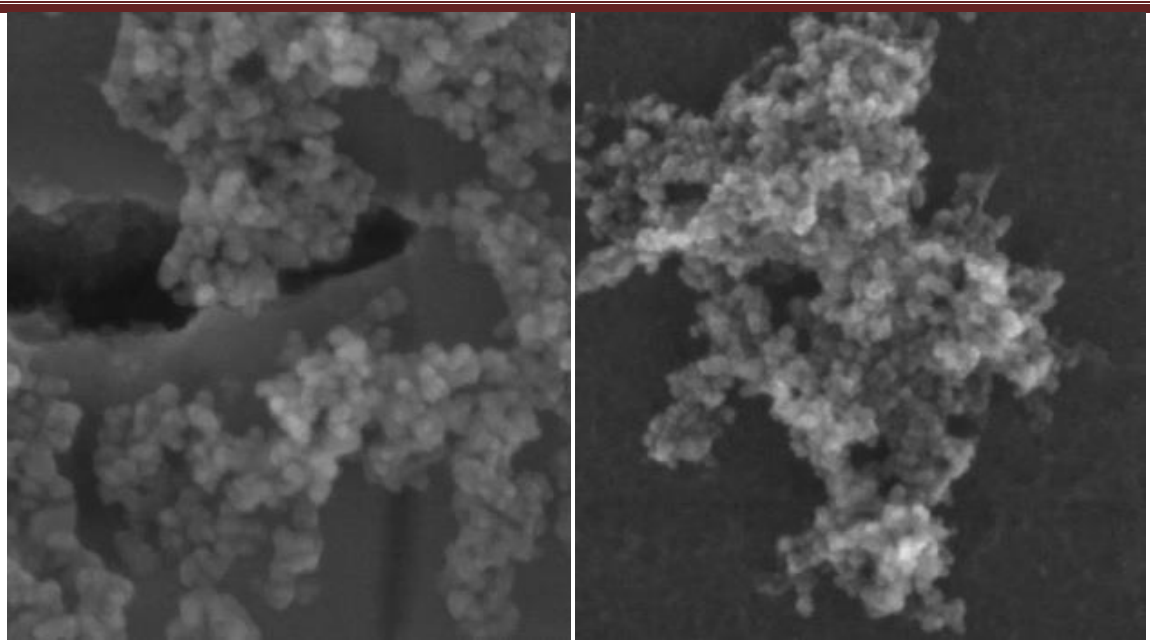

Fig. 4 SEM micrographs of produced ferrous chloride and ferric chloride nanoparticles

Water sample collected near tannery industry reservoir at a depth of one feet using polyethylene bottles of two liter capacity. The collected water samples were immediately bought to the laboratory and analyzed. All the physico-chemical parameters like turbidity, dissolved solids, conductivity, pH, carbonate alkalinity, bicarbonate alkalinity, alkalinity, hardness, calcium, magnesium, ammonia, nitrite, chloride, sulphate and phosphate were carried out as per the standard methods. The parameters of the experiment are shown in Table 1.

Table-1 Variation of physiochemical properties of tannery effluent on adding ferrous chloride and ferric chloride nanoparticles

S.No	TEST NAME	Unit	Adsorbant dosage				
			1g	2g	3g	4g	5g
1	COLOUR	TCU	15.42	11.32	8.42	7.48	6.62
2	COD	Mg/Lit	470	424	346	335	316
3	BOD	Mg/Lit	240	215	185	172	156
4	TDS	Mg/Lit	5,250	4325	3,752	3230	2,754
5	PH		9.72	9.36	8.72	8.53	7.65
6	ALKALINITY	Mg/Lit	1958	1876	1,736	1364	960
7	Chloride	Mg/Lit	2488	2152	1,685	1430	1236
8	Residual Free Chlorine	Mg/Lit	742	632	560	468	346
9	Sulphate	Mg/Lit	862	732	592	480	366
10	Barium	Mg/Lit	188	161	136	128	108
11	Copper	Mg/Lit	84	73	62	52	43
12	Iron	Mg/Lit	92	86	77	64	53
13	Manganese	Mg/Lit	77	63	43	37	28
14	Nitrate	Mg/Lit	626	530	432	395	363
15	Nitrite	Mg/Lit	143	131	118	107	96
16	Zinc	Mg/Lit	128	110	93	79	66
17	Al	Mg/Lit	398	321	243	221	197
18	Ca	Mg/Lit	1622	1524	1122	1028	978

19	Mg	Mg/Lit	384	324	246	198	166
20	sulphide	Mg/Lit	86	74	62	51	43
21	Sodium	Mg/Lit	790	682	563	469	377
22	Potassium	Mg/Lit	836	638	432	348	268
23	Phosphate	Mg/Lit	163	147	128	102	75
24	Turbidity	NTU	16.62	15.58	12.68	10.74	9.30

4.CONCLUSION

A simple, one step green approach was developed for synthesis of ferrous chloride ($FeCl_2.4H_2O$), ferric chloride ($FeCl_3.6H_2O$) nanoparticles using rose flower extract acts as adsorption agent. The XRD spectrum of as synthesized sample shows the presence of ferrous chloride and ferric chloride nanoparticles. The SEM analysis shows the nanostructure nature of the sample with the average particle size of 35-45 nm and polydispersed. The green synthesized ferrous chloride ($FeCl_2.4H_2O$), ferric chloride ($FeCl_3.6H_2O$) shows good Adsorption, biosorption and discolouration agent.

The present study suggested that most of the all the physico-chemical parameters addition of equimolar concentrations of ferrous chloride, ferric chloride nanoparticles reduced the removal of turbidity, dissolved solids, conductivity, pH, carbonate alkalinity, bicarbonate alkalinity, alkalinity, hardness, calcium, magnesium, ammonia, nitrite, chloride, sulphate and phosphate hardly influenced the removal.

REFERENCE

1. Shobha Waghmode, P. Chavan, V. Kalyankar, and S. Dagade, Synthesis of Silver Nanoparticles Using Triticum aestivum and Its Effect on Peroxide Catalytic Activity and Toxicology, J. Chem., Article ID 265864 (2013)
2. Sreekanth, T.V.M., C. Nagajyothi, P., Prasad, T.N.V.K.V., Duk Lee, Kap, Green Synthesis of Silver Nanoparticles Using Citrus Reticulata Juice and Evaluation of their Antibacterial Activity and Cytotoxicity Against MelanomaB16/F10 Cells, Current Nanoscience, 9(4) 457-462 (2013).
3. Baghayeri M., M. Namadchian, H. KarimiMaleh and H. Beitollahi, Determination of nifedipine using nanostructured electrochemical sensor based on simple synthesis of Ag nanoparticles at the surface of glassy carbon electrode: application to the analysis of some real samples, J. Electroanalytical Chemistry, 697, 53-59 (2013).
4. Robinson, T.; Chandran, B.; Nigam, P. Studies on desorption of individual textile dyes and a synthetic dye effluent from dye-adsorbed agricultural residues using solvents. *Bioresour. Technol.* **2002**, *84*, 299–301.
5. Robinson, T.; Chandran, B.; Nigam, P. Removal of dyes from a synthetic textile dye effluent by biosorption on apple pomace and wheat straw. *Water Res.* **2002**, *36*, 2824–2830.
6. Babel, S.; Kurniawan, T.A. Low-cost adsorbents for heavy metals uptake from contaminated water: A review. *J. Hazard. Mater.* **2003**, *97*, 219–243.
7. Ramakrishna, K.R.; Viraraghavan, T. Dye removal using low cost adsorbents. *Water Sci. Technol.***1997**, *36*, 189–196.
8. BIS 10500: Bureau of Indian Standard, Drinking water specification second revision, Drinking water sectional committee, New Delhi (2012).
9. Namasivayam, C.; Kavitha, D. Removal of Congo Red from water by adsorption onto activated carbon prepared from coir pith, an agricultural solid waste. *Dye. Pigment.* **2002**, *54*, 47–58.
10. BIS 10500: Bureau of Indian Standard, Drinking water specification second revision, Drinking water sectional committee, New Delhi (2012)
11. APHA: Standard Methods for the estimation of water and waste water, American public health association, American waste water Association and water pollution control federation, Washington (1995)
12. Robinson, T.; Chandran, B.; Nigam, P. Studies on desorption of individual textile dyes and a synthetic dye effluent from dye-adsorbed agricultural residues using solvents. Bioresour. Technol.2002, 84, 299–301.
13. Babel, S.; Kurniawan, T.A. Low-cost adsorbents for heavy metals uptake from contaminated water: A review. J. Hazard. Mater. 2003, 97, 219–243.
14. Purkait, M.K.; DasGupta, S.; De, S. Adsorption of eosin dye on activated carbon and its surfactant based desorption. J. Environ. Manag. 2005, 76, 135–142.
15. Ramakrishna, K.R.; Viraraghavan, T. Dye removal using low cost adsorbents. Water Sci. Technol. 1997, 36, 189–196.
16. Robinson, T.; Chandran, B.; Nigam, P. Removal of dyes from a synthetic textile dye effluent by biosorption on apple pomace and wheat straw. Water Res. 2002, 36, 2824–2830

Adsorption, biosorption and discolouration on Vat dye effluents using Ferrous chloride and Ferric chloride Nano particles by using rose petal extract form collected near textile dye industry

S. Ulaganathan[1], A. Thaminum Ansari[2], E. Revathi[2] & CT. Ravichandran[1]
[1]Department of Chemistry, Arignar Anna Government Arts College Cheyyar, Tamilnadu
[2]Department of Chemistry, Muthurangam Government Arts College (Autonomous), Vellore, Tamilnadu

ABSTRACT: *The development of reliable, eco-friendly processes for the synthesis of nano scale materials is an important aspect of nanotechnology. Ferrous chloride ($FeCl_2.4H_2O$), ferric chloride ($FeCl_3.6H_2O$) nano particles have been known to have Adsorption, biosorption and discolouration. In the present study ferrous chloride and Ferric chloride nano particles by using Rose petal extract. Nano particles of Ferrous chloride and Ferric Chloride has been synthesized by simple chemical precipitation method and characterized by UV-Vis, XRD and SEM analysis. In future, combination of both may be the best option for purifications. The aim of the project is to analyze the textile waste water purification using the nano particles. Ferrous chloride and Ferric chloride nano particles were also applied with textile wastewater for estimation Colour, pH, Turbidity, TDS, Alkalinity, COD, BOD, Chloride, Residual free Chlorine, Sulphate, Sulphide, Nitrate, Nitrite and also color removal efficiencies.*

Keywords: *Ferrous chloride and Ferric chloride nanoparticles, UV-spectroscopy, X-ray diffraction*

1.INTRODUCTION

In the area of water purification, nanotechnology offers the possibility of an efficient removal of pollutants and germs. Since early in history, people have dumped sewage into waterways, relying on natural purification by dilution and by natural bacterial breakdown. Population increases resulted in greater volume of domestic and industrial wastewater, requiring that we give nature a helping hand. Basic wastewater treatment facilities reduce organic and suspended solids to limit pollution to the environment. Advancement in needs and technology has necessitated the evolving of treatment processes that remove dissolved matter and toxic substances. Currently, the advancement of scientific knowledge and moral awareness has led to a reduction of discharges through pollution prevention and recycling, with the noble goal of zero discharge of pollutants. Main pollution in textile wastewater came from dyeing and finishing processes.

These processes require the input of a wide range of chemicals and dyestuffs, which generally are organic compounds of complex structure. Because all of them are not contained in the final product, became waste and caused disposal problems. Major pollutants in textile wastewaters are high suspended solids, chemical oxygen demand, heat, colour, acidity, and other soluble substances.

Synthesis of nanoparticles, a number of chemical methods exist in the literature (Waghmode and Dagade, 2013). Thus, researchers in the field of nanoscale material synthesis and assembly have been eagerly looking at eco-friendly methods of synthesis as an alternative (Sreekanth and Nagajyothi, 2013).

It is well known that extracts of adsorption have the ability to synthesize nanoparticles from the metal salt solutions of the respective metals and also retain their stability in the nanosize by acting as capping agents and preventing them from precipitating for a reasonably long duration of time. These natural extracts like Garlic extract, Wheat grass extract, Rose petal extract play an important role in remediation of toxic metals through reduction of metal ions and act as interesting nanofactories.

Metal nanoparticles have been studied extensively because of their unique physicochemical characteristics. Among metal nanoparticles Ferrous chloride ($FeCl_2.4H_2O$) and ferric chloride ($FeCl_3.6H_2O$) nanoparticles have been known adsorption and biosorption effects.

As seen above nanoparticles of different metals have proven to be a boon in medical as well as chemical researches and for this reason, the present work has been focused on the development of natural and green method of synthesis of nanoparticles (Baghayeri and Namadchian, 2013) of Ferrous chloride and ferric chloride.

2. EXPERIMENTAL METHODS

2.1MATERIALS

The roses were obtained from the local flower shop each time. Ferrous chloride ($FeCl_2.4H_2O$) and

ferric chloride ($FeCl_3.6H_2O$) were obtained from galaxy vellore (SDS make) and used as received.

2.2 EXPERIMENTS

2.2.1 Source of Rose petals:

The roses were obtained from the same local florist each time the extract was prepared and confirmed to be of the same species i.e. Rosa petal. Also called as Dublin ray roses, they were easily available at any local florist (Fig. 1).

Fig. 1: Rose flowers used for extract

2.2.2 Rose petal extract preparation method

Rose petals were first given a wash of distilled water and were crushed using the mixer-blender apparatus thereafter. These shredded rose petals were then subjected to boiling for 5min in distilled water (0.5g rose petals per 1ml distilled water). This solution was then filtered using a filter paper and the filtrate was used as the extract while residue was discarded.

2.2.3Synthesis of Ferrous chloride and ferric chloride Nanoparticles:

In 250ml flasks, 4.5g of ferrous chloride ($FeCl_2.4H_2O$) and 4.5g of ferric chloride ($FeCl_3.6H_2O$) then 100 ml rose petal extract was added to it. Immediately after this addition the flasks were stirred for 6 hours at a temperature of 60°C. After 6 hours the above mixture was visual observation of colour change of the solution. Initially colour change was observed from light pink to dark brown which indicated formation of nanoparticles. This was done just for the preliminary detection. These samples were then subjected to optical measurements, which were carried out by using a UV-Visible spectrophotometer and nanoparticles was checked by SEM and Xray Diffraction (XRD) using an X-ray diffractometer.

3. RESULTS AND DISCUSSIONS

3.1Characterization of Ferrous chloride and ferric chloride Nanoparticles:

In the present study, natural synthesis of ferrous chloride ($FeCl_2.4H_2O$) and ferric chloride ($FeCl_3.6H_2O$), nanoparticles using rose petal extract were studied. Visual observations show colour change in the ferrous chloride and ferric chloride solutions after extract additions. The colour changes to brown after formation of ferrous chloride and ferric chloride noparticles which was further characterized by using UV-visible, XRD and SEM analysis.

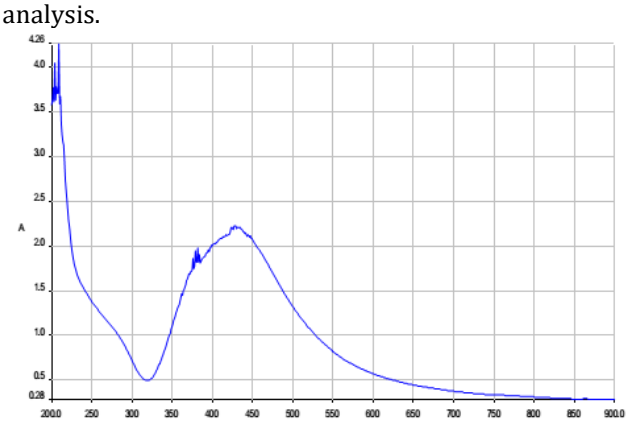

Fig.2: UV-Visible spectra of ferrous chloride and ferric chloride Nanoparticles

Figure 2 show the UV-visible spectrum of ferrous chloride ($FeCl_2.4H_2O$), ferric chloride ($FeCl_3.6H_2O$) nanoparticles by using green synthesis of rose petal extract which acts as capping as well as stabilizing agents. The stability of these nanoparticles we have checked after three months. The Ferrous chloride and ferric chloride nanoparticles show absorption of $FeCl_2$ and $FeCl_3$ in visible region, the absorption at 422nm which is due to ferrous chloride and ferric chloride. Due to the free electrons present in the ferrous chloride ($FeCl_2.4H_2O$), ferric chloride ($FeCl_3.6H_2O$) Fe nanoparticles, this free electron gives the surface absorption band at 422 nm.

3.2 XRD of Ferrous chloride and Ferric chloride nanoparticles:

The phase purity of as synthesized ferrous chloride and ferric chloride nanoparticles was examined by using powder X-ray diffraction.

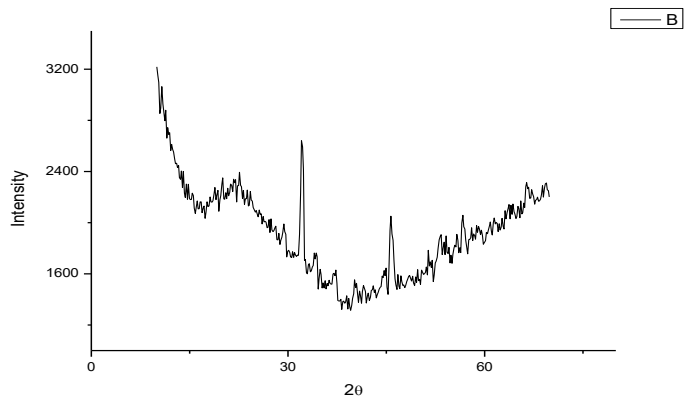

Fig.3: XRD patteren of ferrous chloride and Ferric chloride nanoparticles

The X-ray diffraction Figure 3 shows two intense peaks at 28.54˚, 45.52˚ corresponds to planes (111) and plane (220) for Ferrous chloride ($FeCl_2.4H_2O$), ferric chloride ($FeCl_3.6H_2O$) nanoparticles with further diffraction peaks at 28.54, 46 , 54.9, 57.3, 68 and 77 which confirms formation of ferrous chloride and ferric chloride nanoparticles with face centered cubic structure.

3.3 SEM of Ferrous chloride and Ferric chloride nanoparticles:

The SEM analysis provided information about size and shape of resulting ferrous chloride and Ferric chloride nanoparticles Obtained micrographs are shown in Fig. 4. It was observed, that the nanoparticles of all prepared samples have particle sizes below 200 nm. Bigger particles were obtained in the case of molar ratio Fe2+:Fe3+ =1:1 However, the difference was not too significant. The change in particle sizes before and after was also almost negligible. The roduced nanoparticles were generally spherical in the shape and both types tend to form agglomerates, as can be seen in the Fig. 4.

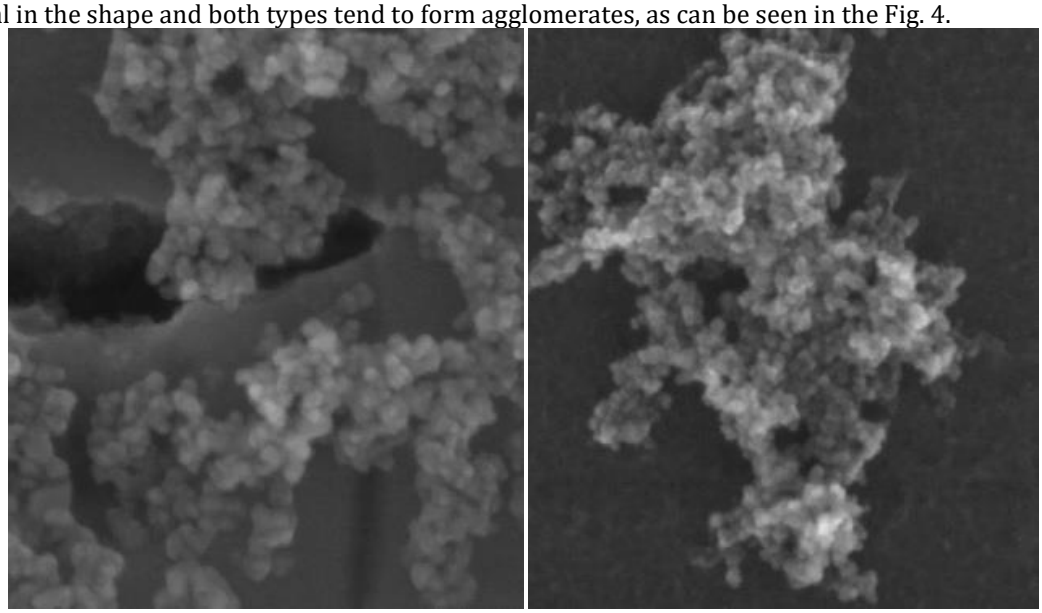

Fig. 4 SEM micrographs of produced ferrous chloride and ferric chloride nanoparticles

Water sample collected near tannery industry reservoir at a depth of one feet using polyethylene bottles of two liter capacity. The collected water samples were immediately bought to the laboratory and analyzed. All the physico-chemical parameters like turbidity, dissolved solids, conductivity, pH, carbonate alkalinity, bicarbonate alkalinity, alkalinity, hardness, calcium, magnesium, ammonia, nitrite, chloride, sulphate and phosphate were carried out as per the standard methods. The parameters of the experiment are shown in Table 1.

Table-1 Variation of physiochemical properties of dye effluent on adding ferrous chloride and ferric chloride nanoparticles

S.No	TEST NAME	Unit	Adsorbant dosage				
			1g	2g	3g	4g	5g
1	COLOUR	TCU	13.62	10.52	8.32	7.48	6.62
2	COD	Mg/Lit	446	414	386	355	322
3	BOD	Mg/Lit	238	217	198	178	156
4	TDS	Mg/Lit	5,652	4568	3,436	3152	2,868
5	PH		9.82	9.46	8.52	8.12	7.98
6	ALKALINITY	Mg/Lit	1852	1612	1,342	1124	960
7	Chloride	Mg/Lit	2362	2142	1,870	1630	1236
8	Residual Free Chlorine	Mg/Lit	742	632	560	468	346
9	Sulphate	Mg/Lit	862	732	592	480	366
10	Barium	Mg/Lit	188	161	136	128	108
11	Copper	Mg/Lit	84	73	62	52	43
12	Iron	Mg/Lit	92	86	77	64	53
13	Manganese	Mg/Lit	77	63	43	37	28
14	Nitrate	Mg/Lit	626	530	432	395	363
15	Nitrite	Mg/Lit	143	131	118	107	96
16	Zinc	Mg/Lit	128	110	93	79	66
17	Al	Mg/Lit	398	321	243	221	197
18	Ca	Mg/Lit	1738	1634	1542	1386	1236
19	Mg	Mg/Lit	396	319	242	206	168
20	sulphide	Mg/Lit	86	74	62	51	43
21	Sodium	Mg/Lit	790	682	563	469	377
22	Potassium	Mg/Lit	836	638	432	348	268
23	Phosphate	Mg/Lit	163	147	128	102	75
24	Turbidity	NTU	17.62	15.58	13.68	11.72	10.32

4.CONCLUSION

A simple, one step green approach was developed for synthesis of ferrous chloride ($FeCl_2.4H_2O$), ferric chloride ($FeCl_3.6H_2O$) nanoparticles using rose flower extract acts as adsorption agent. The XRD spectrum of as synthesized sample shows the presence of ferrous chloride and ferric chloride nanoparticles. The SEM analysis shows the nanostructure nature of the sample with the average particle size of 35-45 nm and polydispersed. The green synthesized ferrous chloride ($FeCl_2.4H_2O$), ferric chloride ($FeCl_3.6H_2O$) shows good Adsorption, biosorption and discolouration agent.

The present study suggested that most of the all the physico-chemical parameters addition of equimolar concentrations of ferrous chloride, ferric chloride nanoparticles reduced the removal of turbidity, dissolved solids, conductivity, pH, carbonate alkalinity, bicarbonate alkalinity, alkalinity, hardness, calcium, magnesium, ammonia, nitrite, chloride, sulphate and phosphate hardly influenced the removal.

REFERENCE

1. Shobha Waghmode, P. Chavan, V. Kalyankar, and S. Dagade, Synthesis of Silver Nanoparticles Using Triticum aestivum and Its Effect on Peroxide Catalytic Activity and Toxicology, J. Chem., Article ID 265864 (2013)
2. Sreekanth, T.V.M., C. Nagajyothi, P., Prasad, T.N.V.K.V., Duk Lee, Kap, Green Synthesis of Silver Nanoparticles Using Citrus Reticulata Juice and Evaluation of their Antibacterial Activity and Cytotoxicity Against MelanomaB16/F10 Cells, Current Nanoscience, 9(4) 457-462 (2013).
3. Baghayeri M., M. Namadchian, H. KarimiMaleh and H. Beitollahi, Determination of nifedipine using nanostructured electrochemical sensor based on simple synthesis of Ag nanoparticles at the surface of glassy carbon electrode: application to the analysis of some real samples, J. Electroanalytical Chemistry, 697, 53-59 (2013).
4. Robinson, T.; Chandran, B.; Nigam, P. Studies on desorption of individual textile dyes and a synthetic dye effluent from dye-adsorbed agricultural residues using solvents. *Bioresour. Technol.* **2002**, *84*, 299–301.
5. Robinson, T.; Chandran, B.; Nigam, P. Removal of dyes from a synthetic textile dye effluent by biosorption on apple pomace and wheat straw. *Water Res.* **2002**, *36*, 2824–2830.
6. Babel, S.; Kurniawan, T.A. Low-cost adsorbents for heavy metals uptake from contaminated water: A review. *J. Hazard. Mater.* **2003**, *97*, 219–243.
7. Ramakrishna, K.R.; Viraraghavan, T. Dye removal using low cost adsorbents. *Water Sci. Technol.***1997**, *36*, 189–196.
8. BIS 10500: Bureau of Indian Standard, Drinking water specification second revision, Drinking water sectional committee, New Delhi (2012).
9. Namasivayam, C.; Kavitha, D. Removal of Congo Red from water by adsorption onto activated carbon prepared from coir pith, an agricultural solid waste. *Dye. Pigment.* **2002**, *54*, 47–58.
10. BIS 10500: Bureau of Indian Standard, Drinking water specification second revision, Drinking water sectional committee, New Delhi (2012)
11. APHA: Standard Methods for the estimation of water and waste water, American public health association, American waste water Association and water pollution control federation, Washington (1995)
12. Robinson, T.; Chandran, B.; Nigam, P. Studies on desorption of individual textile dyes and a synthetic dye effluent from dye-adsorbed agricultural residues using solvents. Bioresour. Technol.2002, 84, 299–301.
13. Babel, S.; Kurniawan, T.A. Low-cost adsorbents for heavy metals uptake from contaminated water: A review. J. Hazard. Mater. 2003, 97, 219–243.
14. Purkait, M.K.; DasGupta, S.; De, S. Adsorption of eosin dye on activated carbon and its surfactant based desorption. J. Environ. Manag. 2005, 76, 135–142.
15. Ramakrishna, K.R.; Viraraghavan, T. Dye removal using low cost adsorbents. Water Sci. Technol. 1997, 36, 189–196.
16. Robinson, T.; Chandran, B.; Nigam, P. Removal of dyes from a synthetic textile dye effluent by biosorption on apple pomace and wheat straw. Water Res. 2002, 36, 2824–2830.

ELECTROCHEMICAL DETERMINATION OF CEFTRIAXONE ON GRAPHENE OXIDE MODIFIED GLASSY CARBON ELECTRODE USING DIFFERENTIAL PULSE VOLTAMMETRY

K. Boobalan, S. Nithya, S. Shreedevi & CT Ravichandran
Department of Chemistry, Arignar Anna Government Arts College, Cheyyar-604 407,
Tiruvannamalai (Dt.), Tamil Nadu, India

ABSTRACT: *Electrochemical behaviour of ceftriaxone was studied in detail and an electro analytical procedure was developed. In Cyclic voltammetry, the study on the influence of pH on the redox behaviour of ceftriaxone revealed maximum peak current at pH 1.0. This could be explained due to faster electron transfer rate and easier redox behaviour of ceftriaxone at this pH. The results from this study at GCE suggested the selection of pH 1.0 for the electrochemical studies. Hence pH 1.0 was chosen as optimum medium for further electrochemical studies with GO modified GCE. Controlled potential coulometry was carried out to determine the number of electrons involved in the oxidation. It resulted as one electron transfer duringanodic scan and a probable reaction mechanism is proposed.Electrochemical studies of ceftriaxone were also studied in pH 1.0 using GO/GCE modified working electrode to develop Differential Pulse stripping voltammetric procedure for trace level determination. In DPSVoptimum experimental conditions were arrived by varying the parameters such as accumulation potential, accumulation time, initial potential, pulse height, pulse width and scan increment. The peak current was measured under optimum conditions at various concentrations. The concentrations were directly proportional to the stripping peak current. The i_p and concentration were correlated and the result was a straight line. The calibration plot was arrived at and used for the determination of ceftriaxone. The analytical characteristics are found out and presented.The lower limit of detection was 1 ppm.*

1.0 Introduction

Since the mid-19th century, pharmaceuticals have moved from the periphery to thecenter of health care. In the course of that transition, a new industry sector expanded to globalscope, the field of medicinal chemistry rose to its current prominence, and governmentsadopted dual roles of supporting basic research and regulating drug safety and efficacy. We are all patients at various points in life and for patients drugs have taken on newmedical roles and value. In recent years especially, it has become common for people to takedrugs for years, even decades, to reduce risks of disease and increase life span. Taking drugsfor life has intensified a long-standing hybrid of scientific, emotional, and policy issuesaround side effects and widespread resentment of companies that profit from drug inventionand marketingIt is therefore of interest to have methodologies that allow for the determination ofdrug-albumin affinity constants while simultaneously providing information on the locationof the drug binding site. Analyses of drugs in post-ingestion for select studies which providestructural, spectral, and/or analytical data above and beyond routine toxicological "screening"techniques. The forensic analysis of illicit drugs has been the subject of a number of minorreview articles and monographs over the past 10 years (1,2). In addition, several articles havegiven more general overviews of the field (3). Systematic approaches to substanceidentification have also been presented (4), and a number of scientific working groups arecurrently establishing national/international standards for forensic analysis of illicit drugs (5).

The assay analysis is essential and important in all the pharmaceutical industries and quality control laboratories. Newer improved procedure for the determination of pharmaceutical samples becomes inevitable.

Currently, the most widely used methods in analysis of drugs are separation-based techniques. Examples are variants of chromatography and electrophoresis. These techniques are excellent, when dealing with complex samples like urine or when following the products of drug metabolism. In analyses of tablets or injection solutions, in particular of samples containing a single physiologically active component, electroanalytical techniques can, in some instances, offer some advantages, among them are simple sample handling, speed of analysis, high sensitivity, comparable or better accuracy, cheaper instrumentation and lower cost of chemicals used and limited use of environmentally unfriendly organic solvents.

These voltammetric methods are applied in organic analysis most frequently in pharmaceutical

chemistry and pharmacology, in polymer chemistry, in the foodstuff industry, in criminology and more recently in environmental research [6].Hence electroanalytical techniques are applicable to a very large number of organiccompounds encountered in many fields. The literature survey for the last 25 years shows thatpolarography and voltammetry have been used in the organic field, particularly in thepharmaceutical and biological fields [[7. Meites and Zuman have listed the polarographicbehaviour of a large number of substances [[8. Many compounds that are neither reducednor oxidized in the available potential range or for which the signals acquired are not suitablefor analytical purposes can be converted into electroactive substances via chemical orelectrochemical methods and then they can be analysed [9,10].

Ceftriaxone is a third-generation cephalosporin antibiotic. Like other third-generation cephalosporins, it has broad-spectrum activity against Gram-positive and Gram-negative bacteria. In most cases, it is considered to be equivalent to cefotaxime in terms of safety and efficacy. Ceftriaxone sodium is marketed by Hoffmann-La Roche under the trade name Rocephin.

Ceftriaxone is often used (in combination, but not direct, with macrolide and/or aminoglycoside antibiotics) for the treatment of community-acquired or mild to moderate health care-associated pneumonia. It is also a choice drug for treatment of bacterial meningitis. In pediatrics, it is commonly used in febrile infants between 4 and 8 weeks of age who are admitted to the hospital to exclude sepsis. The dosage for acute ear infection in the very young is 50 mg/kg IM, one dose daily up to three days. It has also been used in the treatment of Lyme disease, typhoid fever, and gonorrhea [11].Intravenous dosages may be adjusted for body mass in younger patients and is administered every 12–24 hours, at a dose that depends on the type and severity of the infection. Hypoprothrombinaemia and bleeding are specific side-effects. Haemolysis is reported. Biliary sludging is another known though rare adverse effect that occurs primarily in neonates [12, 13].Electrochemical studies of ceftriaxoneassume importance because of the presence of electroactive thio and amine group. Among various antibiotic drugsceftriaxoneis important because of its utility in the field of pharmaceuticals.

This work is aimed at developing a simple and sensitive electro-analytical method for the determination of ceftriaxone on GO/ GCmodified electrode using Differential Pulse Stripping Voltammetry (DPSV).

2.0 Material and Methods

2.1 Apparatus and Reagents

All the voltammetric measurements were carried out using a single-compartment three electrode cell setup with nanostructured polyaniline modified glassy carbon electrode as the working electrode, Ag/AgCl as the reference electrode and platinum wire as an auxiliary electrode. Differential Pulse Stripping Voltammetry (DPSV) and Cyclic Voltammetry (CV) experiments were carried out using an CH Instruments Electrochemical Workstation (model CH 650C). All potentials given are with respect to the potential of the reference electrode. The pH measurements were performed with a Hanna instrument pH/ORP meter using a combination glass electrode. Surface analysis done by the Nanosurf Easy scan 2 AFM under the following conditions: scan direction – up, Time/Line – 206 ms, Tip voltage -1.0 V, Vibration frequency – 169.969 KHz, Measurement environment – air and Operating mode – Dynamic force. Ceftriaxonewas obtained and 0.1M solution was prepared by dissolving the compound in Millipore water. Supporting electrolytes such as 0.1 M H_2SO_4 (pH 1.0), B.R Buffer (pH 4.0), 0.1 M KCl (pH 7.0), B.R Buffer (pH9.2) and 0.1 M NaOH (pH 13.0) were prepared.

2.2 Preparation of GO/ GC modified electrode

1 mg GO (sigma) was dispersed in 10 ml water using an ultrasonicator to give black suspensions. Cast films were prepared by placing 2 □ L of the GO suspensions on GCE and then evaporating at 40 ºC.

3.0 Results and discussions

3.1 Characterization of electrode surfaces

The AFM studies depending on the optimal conditions. The GO and compound adsorption on GO are dispersed in water by sonication for 10 min and coated evenly on a glass plate, dried and used for AFM analysis. The original solution is also analyzed to compare the surface morphology of drug molecule on GCE. To better understand the morphology of a surface a quantitative description of the surface topography must be carried out. The topography matrix data should be treated in each profile line (2D) or over all profiles extending the analysis to surface (3D) (Fig 1 &2).

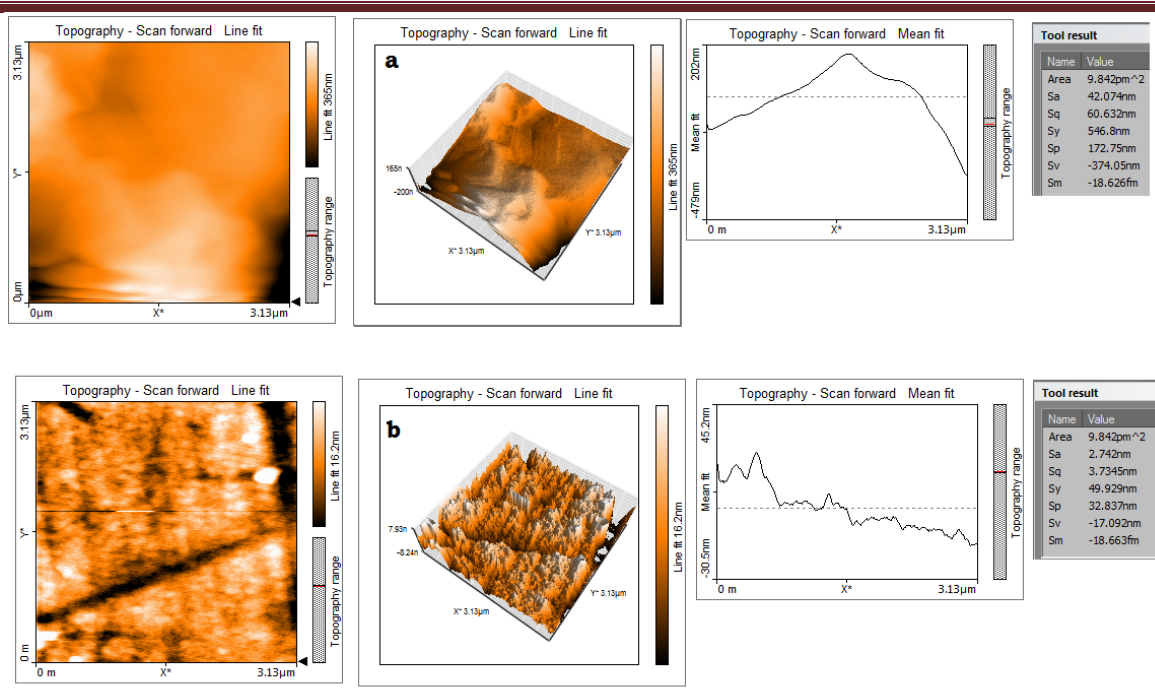

Fig 1. AFM behavior of a) Glassy Carbon Electrode b) Compound on GCE

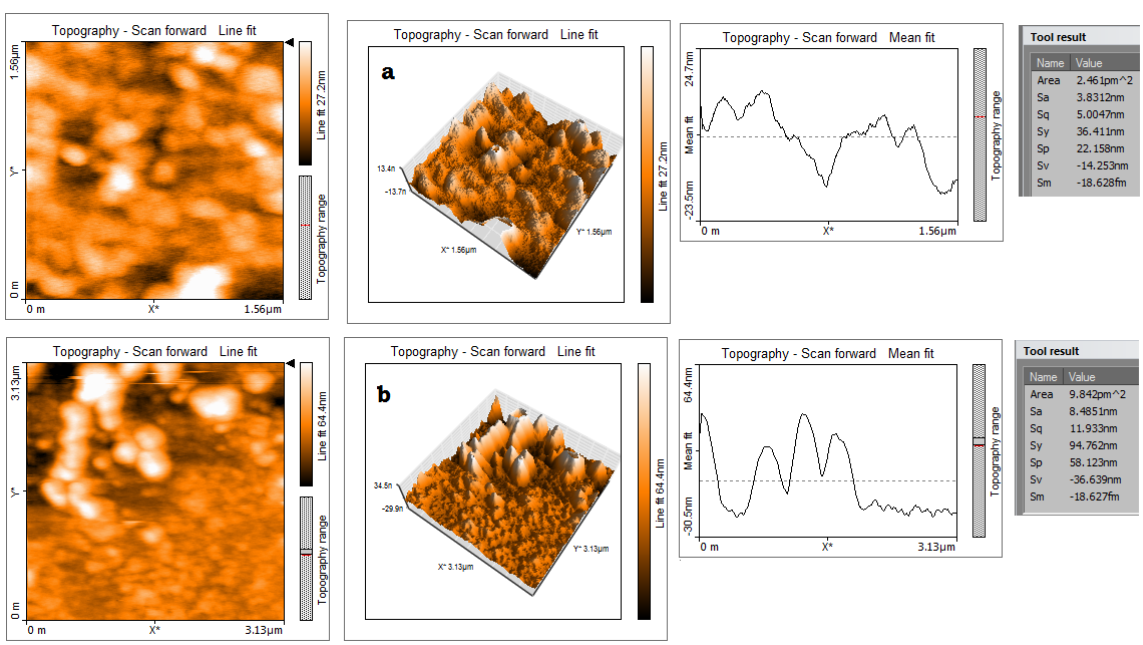

Fig 2. AFM behavior of a) Graphene Oxide b) Compound on GO/GCE

3.2 Effect of pH

Ceftriaxoneis soluble in aqueous medium. Hence, the electrochemical behavior of ceftriaxonewas examined in aqueous medium using GCE andgraphene oxide (GO) modified GCE. Detailed investigations were carried out at pH 1.0, 4.0, 7.0, 9.2 and 13.0.The cyclic voltammogram observed at pH 1.0 of 250 ppm ceftriaxone for the scan rate 100 mVs^{-1} is presented in figure 3. It showed one anodic and cathodic peak with good peak current in the potential around 965 and 760 mV. The peak current may be due to oxidation of the nitrogen group. In the reverse scan, characteristic peak observed. The typical cyclic voltammogram at pH 4.0 (Fig. 4) exhibited a same trend as previous pH medium.The figure 5 represents the cyclic voltammogram of ceftriaxoneat pH 7.0. The voltammetric behavior observed was same as in the above mentioned pH

conditions. The cyclic voltammogram of ceftriaxone obtained at pH 9.2 is presented in figure 6. One anodic and cathodic peak was observed. They were found to be lower sharp as in pH 4.0.A typical cyclic voltammogram of ceftriaxone obtained at pH 13.0 is presented in figure 7. Here also only one anodic peak was observed at 642 mV.

The cyclic voltammetric studies at 1.0 to 13.0 pHs revealed electroactive nature of ceftriaxone and the observation of one oxidation and one reduction behavior were discussed. Among the all pHs studied, in pH 1 ceftriaxone exhibited well sharp oxidation peaks with high current response with GC electrode. Hence pH 1 was selected for further studies with GO/GC modified electrode.

3.3 Effect of scan rate

It was studied by varying the scan rate from 25 to 500 mVs^{-1} at a concentration of 250 ppm ceftriaxone. The peak current values were plotted against the scan rate. A straight line was obtained with good correlation ($R^2 = 0.9896$) . It showed that peak current increased with increase in scan rate. The plot of peak current vs. square root of sweep rate resulted in straight line but correlation value was lower compared to previous. Log peak current correlated with the log of scan rate also resulted in straight line with a slope value of 0.665. All these facts confirmed adsorption-controlled oxidation. The cathodic peak not fulfilling the criteria for reversibility with the anodic peak was observed in the reverse scan. Hence, the oxidation was irreversible. The fractional αn value (0.211) calculated from the slope obtained in the plot Ep vs. log ν also confirmed that the electron transfer was irreversible.

3.4 Effect of concentration

Cyclic voltammetric studies were carried out by varying the concentration from 100 to 300 ppm at 100 mVs^{-1}. The peak currents increased linearly with increase in concentration and the peak potential shifted anodically.

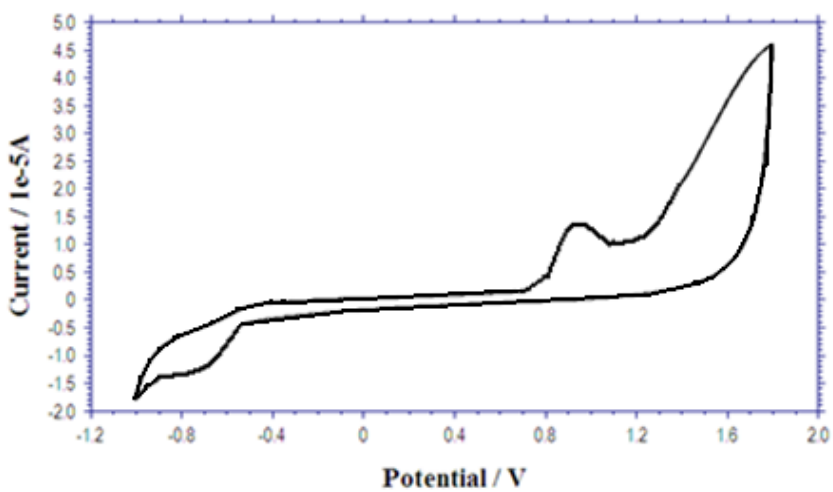

Fig.3. Cyclic voltammetricbehaviuor of ceftriaxoneon GCE at pH 1.0

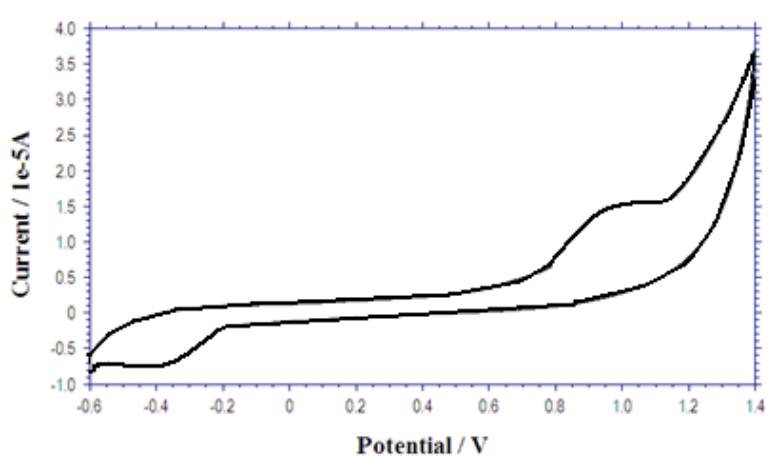

Fig.4. Cyclic voltammetricbehaviuor of ceftriaxoneon GCE at pH 4.0

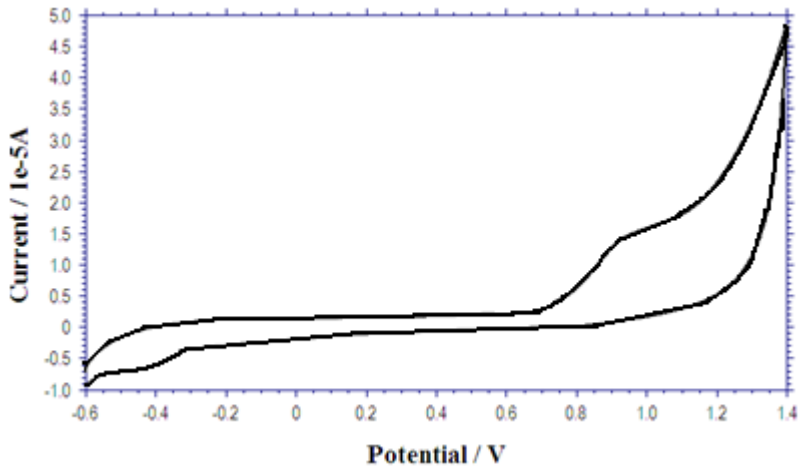

Fig.5. Cyclic voltammetricbehaviuor of ceftriaxoneon GCE at pH 7.0

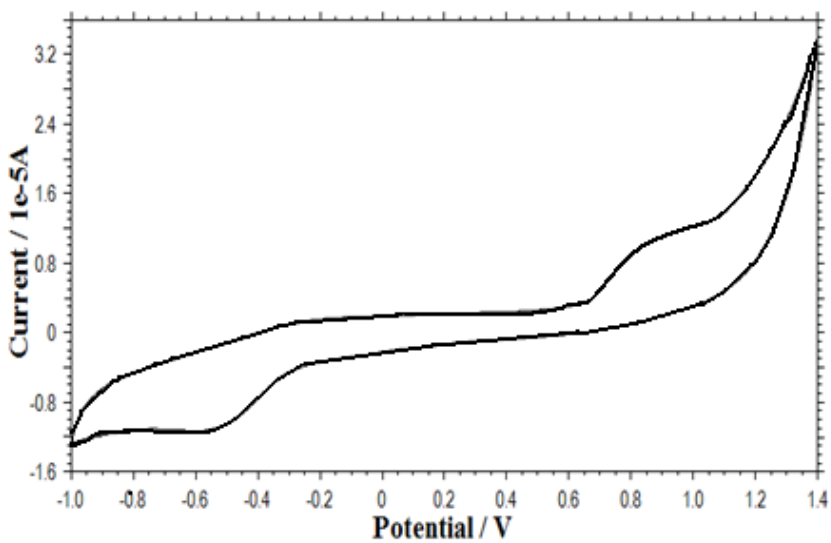

Fig.6 Cyclic voltammetricbehaviuor of ceftriaxoneon GCE at pH 9.2

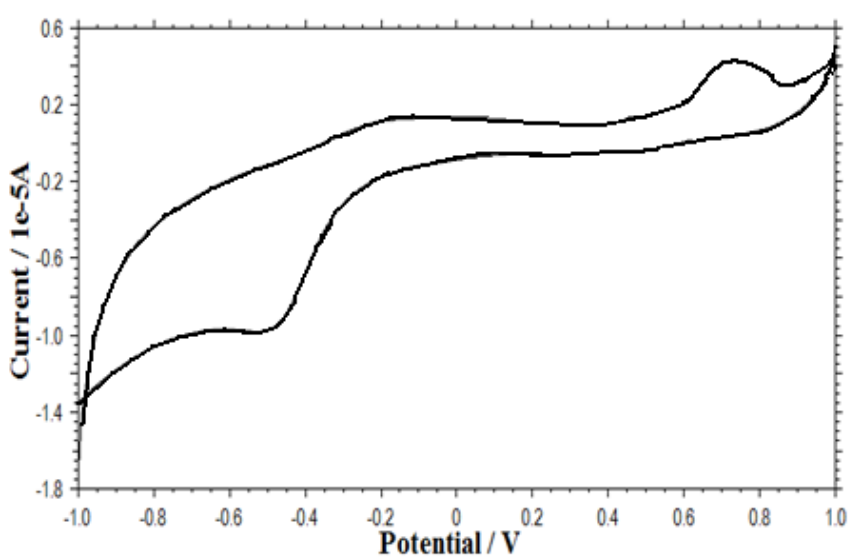

Fig.7. Cyclic voltammetricbehaviuor of ceftriaxoneon GCE at pH 13.0

3.5. Cyclic Voltammetric Studies of ceftriaxoneon GO/GCE Modified Electrode

The cyclic voltammogram observed at pH 1.0 of 250 ppm ceftriaxone on GO/GCE for the scan rate 100 mVs^{-1} is presented in figure 8. It showed one well defined anodic peak and cathodic peak with good peak current in the potential around 965 and 260 mV. The peak current may be due to oxidation of the nitrogen group. In the reverse scan, characteristic peak observed. For detailed discussion, the anodic peak was considered. Under identical conditions the cyclic voltammograms of ceftriaxone is recorded at pH 1.0 at different scan rate between 25 to 500 mVs^{-1}. The concentration studies were also done at the various concentration from 100 ppm to 300 ppm at a fixed scan rate of 250 mVs^{-1} .The correlations were made for the well-shaped anodic oxidation peaks observed in the forward scan. The peak current increased linearly with sweep rate with good correlation. A non-linear plot of peak current vs square root of scan rate and log ip vs log scan rate revealed that the voltammetric redox process was diffusion-controlled and irreversible.

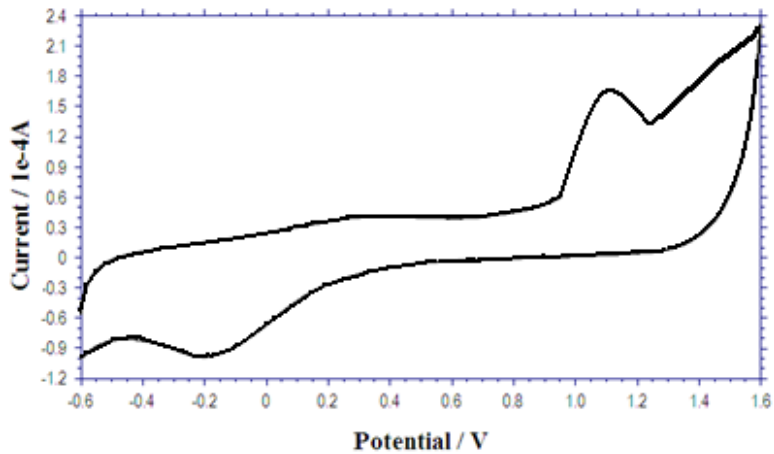

Fig.8. Cyclic voltammetricbehaviuor of ceftriaxoneon GO modified GCE at pH 1.0;

3.6. CONTROLLED POTENTIAL COULOMETRIC STUDIES

The number of electrons transferred was calculated from controlled potential coulometric studies. The controlled potential coulometry of ceftriaxone was carried out at the appropriate potential using the GCE at pH 1.0 in order to find out the number electron transfer in anodic peak. The potential at which controlled potential coulometry carried out, the charge consumed and the number of electrons calculated the value is 1. Based on this the following mechanism was proposed.

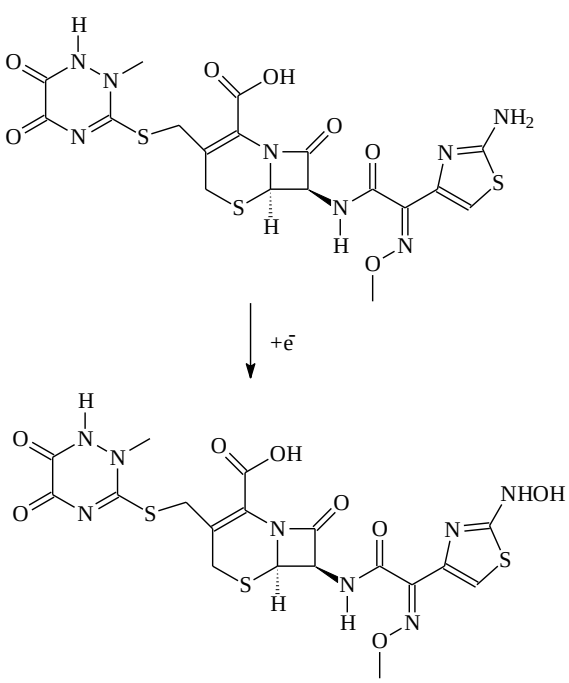

3.7 Differential pulse stripping analysis of Ceftriaxone

Differential pulse stripping voltammetry (DPSV) is one of the most useful and convenient method for sample identification. By employing this technique parts per billion (ppb) range of a compound can be determined. The voltammetric behaviour of ceftriaxonedrug allowed employing stripping analysis for the simultaneous determination using modified GO / GCE.Cyclic voltammetric results revealed the adsorption controlled of the substrate modified GO / GCE at pH 1.0. It was expected that ceftriaxone would be adsorbed on the electrode during the accumulation step and stripped off easily in the stripping step. Hence, ceftriaxone was considered as a suitable substrate for the adsorptive stripping voltammetric studies. Thus the stripping voltammetric studies of ceftriaxonewere done at modified GO/GCE in aqueous medium pH 1.0 using differential pulse stripping voltammetric method. The drug exhibits a very good stripping signal. A systematic study of various instrumental parameters that affect the stripping response has been carried out with 33.3 ppm concentration of drug to establish the optimum conditions.

Hence optimization of the accumulation potential was done as the first part for this study. This potential was varied from 0.2 to 0.8 V at an accumulation time of 15s. Maximum peak current was observed at 0.4 V and it was fixed as the optimum accumulation potential.By varying the deposition time from 5 to 15s, the effect of deposition time was studied after fixing the deposition potential at 0.4 V. It reveals highest current is observed at 10s deposition time. Hence this is taken for the further consideration.The initial scanning potential is another important parameter as it confirms the non-faradaic nature of the preconcentration step. It also controls both the peak potential and peak current in the stripping voltammogram. The influence of the initial potential on the peak current was studied by varying the initial scan potential from 0 to 0.8 V. The peak current is affected by this initial potential in a different way. Better response ie, high peak current with better resolution was observed at 0 V. Hence 0 V was fixed as initial scanning potential and the reproducibility of the method was determined by making successive measurements.

Effect of pulse height was studied by varying from 10 to 75 mV. The sharp peak current was observed at the pulse height of 50mV. Similar to pulse height, pulse width also studied by varying from 25 to 100ms. The sharp peak nature with higher current was observed at pulse width of 50 ms. Hence the pulse width of 50 ms was chosen as optimum value.The scan increment was varied between 2 to 10 mV and maximum peak current response was obtained at 4 mV scan increment.A study on the effect of pulse period in the range between 1to5 s was carried out. The stripping voltammetric signal showed the maximum peak current at 2 s. The optimum conditions that resulted in good peak response were used to study the effect of analyte concentration.

All the experimental parameters are optimized as discussed above. The DPSV response of ceftriaxone is given in Fig 9 under optimum conditions.

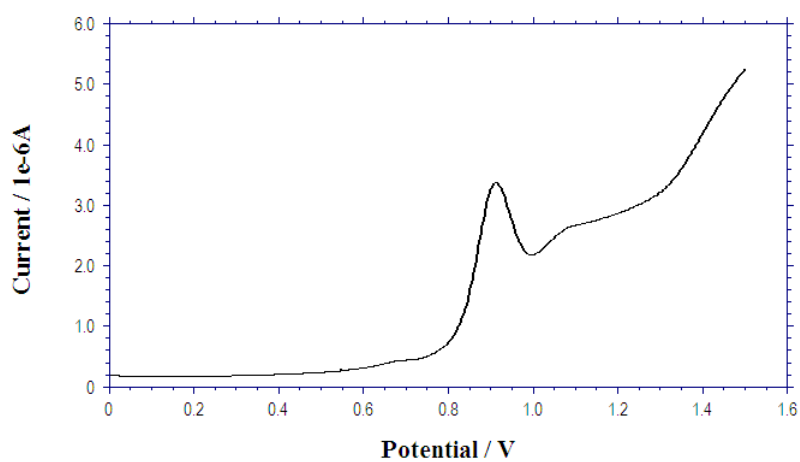

Fig.9. DPSVbehavior ofceftriaxone on GO modified GCE under Optimum Conditions

3.8 Analytical characteristic

Under optimum experimental conditions, the influence of concentration on the stripping signal was studied. The experimental results showed that the peak current increased with the increase in concentration of ceftriaxone. A calibration was made, which indicated the linear dependence of peak current

with concentration (fig 10). The range of determination was found in between 1 to 3.3 ppm. The lower limit of detection was 1 ppm.

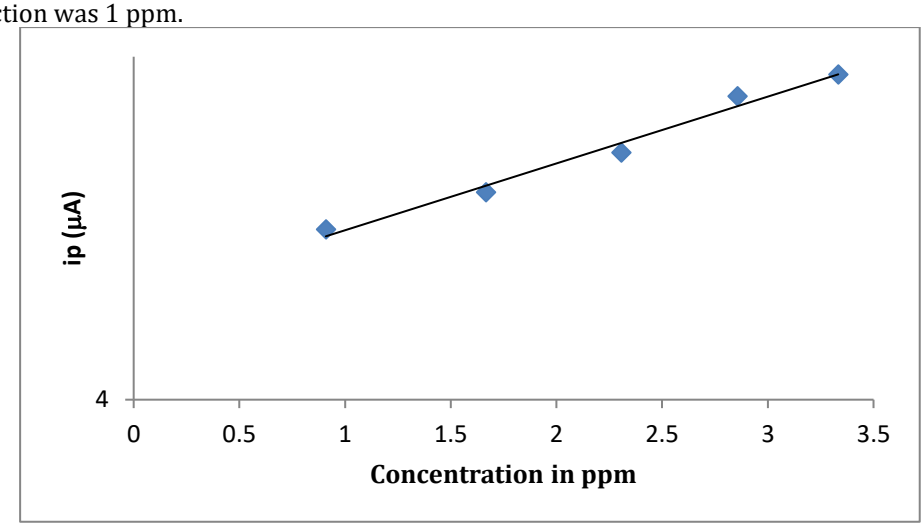

Fig. 10. Calibration plot of DPSV under optimum experimental conditions

4.0 Conclusion

The Graphene Oxide was used to modify the GCE for the electrochemical detection of **Ceftriaxone**. Electrochemical behavior of ceftriaxone was studied in detail and an electro analytical procedure was developed. In Cyclic voltammetry, the study on the influence of pH on the redox behaviour of ceftriaxone revealed maximum peak current at pH 1.0. Electrochemical studies of ceftriaxone were also studied in pH 1.0 using GO/GCE modified working electrode to develop Differential Pulse stripping voltammetric procedure for trace level determination. In DPSVoptimum experimental conditions were arrived by varying the parameters and the peak current was measured under optimum conditions at various concentrations. The concentrations were directly proportional to the stripping peak current. The i_p and concentration were correlated and the result was a straight line. The calibration plot was arrived at and used for the determination of ceftriaxone. The analytical characteristics are found out and presented.The lower limit of detection was 1 ppm. Due to the electrode's simple fabrication procedure, wide linear range, low detection limit for detection was achieved. The simple fabrication procedure, high analysis speed, reproducibility, structural stability, wide linear dynamic range and high sensitivity, suggest that the proposed sensor is an attractive candidate for the practical applications.

5.0 Reference

1. K. D. Trigathi, Essentials of Medical Pharmacology, Jaypee Brothers' Medical Publishers, New Delhi, India, 5th edition, 2003.
2. J. N. Delgado and W. A. Remers, Textbook of Organic Medicinal and Pharmaceutical Chemistry, Lippincott-Raven, Philadelphia, Pa, USA, 10th edition, 1998.
3. V. T. Andriole, in Proceedings of the 7th Mediterranean Congress on Chemotherapy, Barcelona, Spain, 1990.
4. L. E. Bermudez, C. Inderlied, and L. S. Young, Antimicrobial Agents and Chemotherapy, vol. 35, no. 12, pp. 2625–2629, 1991. View at Scopus
5. J. Elks and C. R. Ganellin, Dictionary of Drugs, Chapman and Hall, London, UK, 1991.
6. M. Trojanowicz, M. Szewczynska, Trends Anal. Chem. 2005, 24, 92.
7. J. J Gooding, Electrochim. Acta 2005, 50, 3049.
8. A. Merkoci, M. Pumera, X. Llopis, B. Pe´ rez, M. del Valle, S. Alegret, Trends Anal. Chem. 2005, 24, 826.
9. J. Wang, Electroanalysis 2005, 17, 7.
10. G. Rivas, M. D. Rubianes, M. C. Rodrguez, N. Ferreyra, G. L. Luque, M. L. Pedano, C. Parrado, Talanta 2007, 74, 291.
11. L.A. Knackstedt, R.I. Melendez, P.W. Kalivas,Biol Psychiatry,2009, **67** (1): 81.
12. Mir Reza Majidi, Karim Asadpour-Zeynali and Behnam Hafezi, **Anal.Methods,** 2011,**3**, 646
13. A.R. Guru Prasad, and V.S. Rao,Res Pharm Sci. 2010,5(1) 57.

MICROWAVE-ASSISTED SYNTHESIS OF HETEROCYCLIC COMPOUNDS BINDING WITH CHALCONE NUCLUES CONTAINING THIAZOLE MOIETY

R. SUMATHI
SRI BHARATHI WOMENS ARTS AND SCIENCE COLLEGE, KUNNATHUR, ARNI-632301

ABSTRACT: *Thiazole compounds can be synthesized by mico-wave using piperidone and thiosemicarbazide. It is well known that thiazole derivatives are important compounds in medicinal chemistry due to their broad range of biological activities This type of heterocycles has shown a wide variety of pharmacoactive properties as antiinflammatory, antitubercular, antibacterial, fungicidal, local anaesthetic tranquilizers, insecticides, antimicrobial, antitumor and diuretic. Considerable efforts have been devoted to the synthesis of this type of compounds.*

Keywords: *Piperidone, chalcones, Thiosemicarbazide, Varioussubstituted phenacylbromides.*

INTODUCTION

Heterocyclic chemistry is the basis of life and society. Heterocyclic compounds are widely prevalent in animals as well as in the field of plant kingdom and they play a vital role in the metabolism of all the living cells [1-5]. Recently, heterocyclic compounds analogues and their derivatives have attracted strong interest in medicinal chemistry due to their biological and pharmacological propertieA thiazole ring is found naturally in the essential vitamin B_1. Thiazole derivatives find a variety of applications ranging from bacteriostatics, antibiotics, and CNS regulates of high selling diuretics. Chalcones and their derivatives are an attractive molecular scaffold for the search of new biologically active molecules. The chemistry of chalcones generated intensive scientific studies throughout the world, especially interesting for their biological and industrial applications [6-7]. Chalcones are coloured compounds because of the presence of the chromophore and auxochromes. They are known as benzalacetophenones or benzylidene acetophenones. Kostanecki and Tambor gave the name chalcone. Chalcones are characterized by their possession of a structure in which two aromatic rings are linked by an aliphatic three carbon chain. Studies reveal that incorporation of pyrazole moiety into various heterocyclic ring systems gives worthwhile molecules from the biological point of view. Several pharmaceutical drugs, including celecoxib and rimonabantutilize the pyrazole as their core molecular entity. Many pyrazole derivatives are reported to have a broad spectrum of biological activities, such as antiinflammatory, antifungal, herbicidal, antiviral, Aadenosine receptor antagonists, etc. On the otherhand, chalcones or 1,3diaryl /heteroaryl-2-propene-1-ones, have been recently subject of great interest due to their interesting pharmacological activities including antioxidant, antibacterial, antileishmanial, anticancer, antiangiogenic, antiinfective, antiinflammatory, nitricoxide inhibition, antifungal, tyrosinase inhibition, etc. Among the various derivatives of chalcones, synthesis of pyrazolines has engrossed substantial attention from organic and medicinal chemists because of their pronounced biological activities such as tranquillizing, muscle relaxant, psychoanaleptic, antidepressant, antimicrobial, etc. Keeping in view the potential biological activities of pyrazoles, chalcones and pyrazolines, it was perceived that the synergistic effect of heterocyclic moieties in single nucleus might result in the formation of some worthwhile molecules from the biological point of view [8-10].

MATERIALS AND METHODS

All reagents were purchased from Sigma Aldrich and used as received. Ethanol was supplied by Spectrochem. Visualization of spots on TLC plates was effected by UV illumination, exposure to iodine vapour and heating the plates dipped in $KMnO_4$ stain [11- 15].

The NMR spectra of all the synthesized compounds were recorded using Bruker ASCEND 400 and Bruker DPX 300 instrument with 5 mm PABBO BB-1H tubes. ^{1}H NMR spectra recorded in d_6-DMSO, $CDCl_3$ at 400 and 300MHz with TMS as internal reference. ^{13}C NMR spectra were recorded in d_6-DMSO, $CDCl_3$ at 100 and 300 MHz with TMS as internal reference. The IR spectra were recorded in the solid state, using KBr pellets by Perkin- Elmer spectrum 100 series FT-IR spectrometer. Melting points were determined by Toshniwal apparatus. LCMS were obtained using Agilent 1200 series LC and Micromass ZQ spectrometer.

The elemental analysis has been obtained using a Flash VarioEL III elemental analyzer. Microwave experiments were carried out using an LG domestic microwave system [16-20].

.

SYNTHESIS

General procedure for the synthesis of compounds

Several substituted thiazole derivatives containing pyrazoline derivatives were efficiently synthesized by three step process. As depicted in the Scheme-1, the reaction between the commercially available 2-acetyl piperazine **1**, and piperonal **2** with sodium hydroxide in absolute ethanol provided chalcones **3** in quantitative yield of 90%. The isolated compound 3 was treated with thiosemicarbazide with potassium hydroxide in absolute ethanol at reflux condition for three hours. Then ethanol was evaporated to dryness, filtered the solid washed with water and dried to get the 1-thiocarbamoyl-3,5-diaryl-2-pyrazoline [21-25].

This intermediate treated with various phenacyl bromide in absolute ethanol was placed in a pyrex vial and irradiated with 200W for 10 min at 150^{0}C (final temperature). The reaction was monitored by TLC, after the completion of the reaction; the reaction mixture was cooled to room temperature and concentrated. The solid obtained was washed with little amount of hexane, filtered and dried under reduced pressure to give the product [26].

PROCEDURE FOR THE SYNTHESIS OF

GENERAL PROCEDURE FOR THE SYNTHESIS OF (Z)-3-(benzo[*d*][1,3]dioxol-5-yl)-1-(pyrazin-2-yl)prop-2-en-1-one (3):

A mixture of 2-acetylpiperazine (0.04 mol) (**1**), piperonal (0.04 mol) (**2**) and 10% aqueous sodium hydroxide (10 ml) in abs.ethanol (30 ml) was stirred at room temperature for about 3 h. The resulting solid was washed, dried and recrystallized from ethanol.

5-(benzo[d][1,3]dioxol-5-yl)-3-(pyrazin-2-yl)-4,5-dihydro-1H-pyrazole-1-arbothioamide(4):

To a suspension of chalcone derivative (**3**) (0.01 mol) and potassium hydroxide (1g, 0.025 mol) in abs.ethanol (50 ml), thiosemicarbazide (0.012 mol) was added. The mixture was refluxed for 3h. The products were poured into crushed ice and the solid mass which separated out was filtered, dried and recrystallized from ethanol.

PROCEDURE FOR THE SYNTHESIS OF

2-(5-(benzo[d][1,3]dioxol-5-yl)-3-(pyrazin-2-yl)-4,5-dihydro-1H-pyrazol-1-yl)-4-phenylthiazole (5a-g):

To a suspension of compound (**4**) (0.01 mol) in ethanol (15ml) phenacyl bromide derivatives (0.01 mol) were placed in a pyrex vial and irradiated with 200W for 10 min at 150°C (final temperature). The reaction was monitored by TLC, after the completion of the reaction, the reaction mixture was cooled to room temperature and concentrated. The solid obtained was washed with little amount of hexane, filtered and dried under reduced pressure to give the desired product.

Synthesis of 5-(benzo[d][1,3]dioxol-5-yl)-3-(pyrazin-2-yl)-4, 5-dihydro-1H-pyrazole-1-carbothioamide

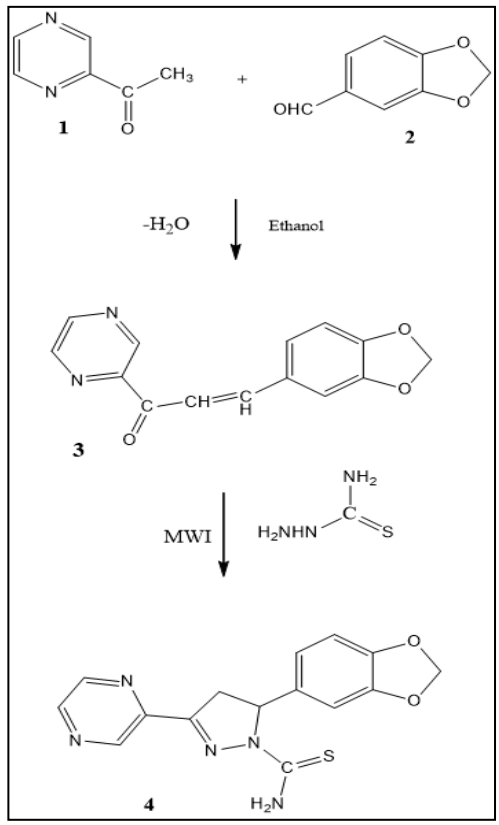

Synthesis of 2-(5-(benzo[d][1,3]dioxol-5-yl)-3-(pyrazin-2-yl)-4,5-dihydro-1H-pyrazol-1-yl)-4-phenylthiazole(5a-g):

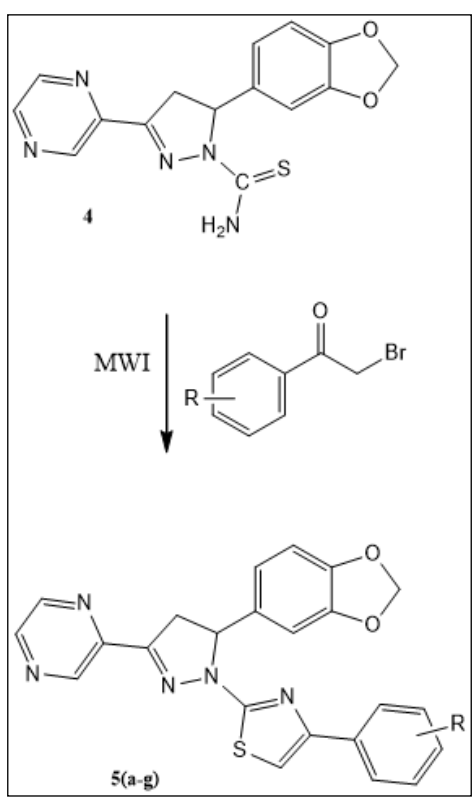

S. No.	R
a	3-Cl
b	4-F
c	4-CH_3
d	4-Cl
e	H
f	4-CN
g	4-Cl,2-F

RESULT AND DISCUSSION

ANTIBACTERIAL ACTIVITY OF THIAZOLE DERIVATIVES CONTAINING CHALCONE NUCLEUS:

The synthesized thiazole derivatives were investigated for their antibacterial *Streptococcus faecalis, Bacillus subtilis, Pseudomonas aeruginosa* bacterial strains by disc diffusion method. Results of antibacterial activity of above synthesized compounds are given in the Table-1&3. The synthesized compounds compared with the standard ciprofloxacin and DMSO is used as a control [27-28].

Among the synthesized thiazole compounds, containing pyrazoline nucleus,compounds C2 and C3, showed good activity against all the microbial strains,because fluro substituents increases the activity. C5 showed moderate activity in staphylococcus aureus and Escherichia coli. Compound C3 showed good activity in pseudomonas aeruginosa.compound C5 and C6 showed moderate activity in Bacillus subtilis.

ANTIMICROBIAL ACTIVITY

An antibacterial is a substance that kills or inhibits the growth of bacteria. Bacteria are unicellular microorganisms. Typically a few micrometers in length, bacteria have a wide range of shapes, ranging from spheres to rods to spirals. In general, any compound or a drug which inhibits the growth or causes the death of bacterias are known as antibacterial agents. Any drug which inhibits the growth of bacteria is said to possess bacteriostatic activity. If it kills the bacteria, it is said to possess bactericidal activity [29].

The large number of antibacterial molecules that are used as therapeutic agents, target the bacterial metabolic machinery. Interestingly, most of these molecules have been isolated from microorganisms. Several potent antibiotics have complex chemical structures with several chiral sites whose correct stereochemistry is essential for activity. They are synthesized on multi-enzyme complexes. While tremendous success has been achieved in treating bacterial infections, over the years, bacteria have evolved mechanisms to counter these antibiotics [30-33].

NAME OF THE SYNTHESIZED THIAZOLE COMPOUNDS CONTAINING CHALCONE NUCLEUS:

- 4-(2-(5-(benzo[d][1,3]dioxol-5-yl)-3-(pyrazin-2-yl)-4,5-dihydro-1H-pyrazol-1-yl)thiazol-4-yl)benzonitrile(C**1**).
- 2-(5-(benzo[d][1,3]dioxol-5-yl)-3-(pyrazin-2-yl)-4,5-dihydro-1H-pyrazol -1-yl)-4-(4-fluorophenyl)thiazole(C**2**).
- 2-(5-(benzo[d][1,3]dioxol-5-yl)-3-(pyrazin-2-yl)-4,5-dihydro-1H-pyrazol -1-yl)-4-(4-chloro-2-fluorophenyl)thiazole(C**3**).
- 2-(5-(benzo[d][1,3]dioxol-5-yl)-3-(pyrazin-2-yl)-4,5-dihydro-1H-pyrazol -1-yl)-4-phenylthiazole(C**4**).
- 2-(5-(benzo[d][1,3]dioxol-5-yl)-3-(pyrazin-2-yl)-4,5-dihydro-1H-pyrazol -1-yl)-4-(p-tolyl)thiazole(C**5**).
- 2-(5-(benzo[d][1,3]dioxol-5-yl)-3-(pyrazin-2-yl)-4,5-dihydro-1H-pyrazol -1-yl)-4-(4-nitrophenyl)thiazole(C**6**).

Antimicrobial activity of thiazole compounds containing chalcone nucleus:

Antibacterial activity of newly synthesized compound (zone of inhibition in mm)

Table 1

Compd	*Klebsiella pneumoni a (mm)*	*Staphylococcus aureus (mm)*	*Escherihiacoli (mm)*	*Streptococcusfaecalis (mm)*	*Bacillus subtilism (mm)*	*Pseudomonas aeruginosa (mm)*
C1	7	16	20	10	10	10
C2	8	15	18	20	15	14
C3	9	20	22	8	13	30
C4	-	-	-	-	-	**7**
C5	-	10	10	6	5	5
C6	-	-	-	-	-	-
Ciprofloxacin (mm)	20	20	24	26	24	15
Control (DMSO)	-	-	-	-	-	-

Note: - No zone of inhibition

8.3.2 Antifungal activity of newly synthesized compound(zone of inhibition in mm)

Table 2

Compound	*Candida albicans (mm)*	*Aspergillus niger(mm)*	*Aspergillus fumigates (mm)*	*Rhizopus sps(mm)*	*Penicillium sps(mm)*	*Mucor Sps (mm)*
C1	34	45	32	20	25	40
C2	45	50	52	45	41	54
C3	32	30	40	22	32	42
C4	20	11	22	23	19	27
C5	23	19	36	11	23	25
C6	32	15	25	29	30	38
Ketoconazole (mm)	30	13	20	26	17	20
Control (DMSO)	-	-	-	-	-	-

Note: - No zone of inhibition

SUMMARY

The screening of compounds is an alternative approach to high throughput screening for identification of leads for therapeutic targets. The main aim of the present study is to synthesize and investigate the antimicrobial activity of the heterocyclic derivatives containing piperidone, chalcone, and thiazole moieties with the hope of discovering new structures serving as potential broad spectrum antimicrobial agents. A series of novel thiazole and pyrazoline derivatives were synthesized and evaluated for their antibacterial and antifungal activity. All the derivatives were efficiently synthesized by two or three step process. In this study, thiazole derivatives were more active against antimicrobial activity. The structure of the newly synthesized compounds was elucidated by their ^{1}H NMR, ^{13}C NMR, LC-MS/MS, IR spectral data and elemental analysis.

In conclusion, we have successfully synthesized a new series of thiazole and chalcone derivatives and moreover, some of compounds contains bioactive heterocyclic moiety.

The antimicrobial screening suggests that all the newly synthesized compounds showed moderate to good activity against the tested organisms. According to structure – activity relationships (SAR), it can be concluded that chalcone, and thiazole moieties are essential for the antimicrobial activity. Basically introduction of piperidone, chalcone moiety in the structure of the final compound has increased the antifungal activity compare to the other. From the study, it can be concluded that all the synthesized compounds demonstrated potential antimicrobial activity

REFERENCES

1. Abbe, G.L.; Luyten, I.; Toppet, S.; *J. Heterocycl.Chem.* **1992**, *29*, 713-17.
2. AbdulBhat, R.; FareedaAthar.; AmirAzam. *Eur.J. Med. Chem.* **2009**, *44*, 426-431.
3. Ahmed, R.; Eman,Ali, R.; El-Bendary.; MariamGhaly, A.; Ihsan, A.; Shehata. *Eur. J. Med. Chem.* **2014**, *75*, 492–500.
4. AhmetOzdemir,; GülhanTuranZitouni,; ZaferAsımKaplancıklı, Gilbert Revial,; KıymetGuven. *Eur. J. Med. Chem.* **2007,** *42*, 403–409.
5. Albert Lévai,; and JózsefJek. *ARKIVOC* **2009**, *6*, 63-70.
6. Alvarez-Ibarra, C.; Davila, E.; Mateo, A.; Ortiz, P.; Quiroga, M.L. **1987,** *28*, 6667–6670.
7. BadriNarayanAcharya.;DeepikaSaraswat.;MugdhaTiwari.;AsishKumarShrivastava.;RamaraoGhorpade.;SarojBapne.;MahabirParshadKaushik. *Eur. J. Med Chem*. **2010**, *45*, 430-438.
8. Bakr.F.; Abdel-Wahab.; Hatem Abdel-Aziz,A.; Essam Ahmed,M. *Eur. J. Med. Chem.* **2008,** 543**,** 1–4.
9. Burger, A. *Comprehensive Med. Chem*. by Hansch C. Pergamon Press publishing company, NewYork. **1998,** *1*, 25-30.
10. Carmen Alcaraz.; Ma Dolores Fernández.; Ma Pilar de Frutos.; L.Joseé Marco.; Manuel Bernabé.; Concepción Foces-Foces.; Félix H. Cano. *Tetrahedron,* **1994,** *50*,12443–12456.
11. Chattopadhyay, G.; Lahiri,S. *J. Ind. Chem. Soc*. **1998,** *75*, 427-29.
12. Chinnaraja, D.; Rajalakshmi .R. *J. of. Saudi Chem.* Soc. **2014,** *12*, 2094.
13. Closs, G.L.; Heyn, H. *Tetrahedron*. **1996,** *22*, 463–471.
14. Cukurovali, A.; Yilmaz, I.; Gur, S.; Kazaz, C. *Eur. J. Med. Chem*. **2006**, *41*, 201-07.
15. Das, B.; Reddy,V.S.; Ramu, R. *Chem. Abst. J Mole Catalysis A: Chemical,* **2006**, *252*, *12*,235-37.
16. El-Subbagh, H.E.; Al-Obaid, A.A. *Eur. J. Med. Chem.* **1996**, *31*,12, 1017-21.
17. Fadi Awadallah, M.; Gary Piazza, G.; Bernard Gary, D.; Adam Keeton, B.; Joshua Canzoneri, C. *Eur. J. Med. Chem.* **2013**, *70*, 273–279.
18. Kumar, P.V.; Reddy, R.V.; Rao, V.R. *Ind. J. Chem* .**2003**, *42*, 1738-41.
19. Magdy, A.H.; Zahran.; Hanan Salama, F.; Yasmin Abdin, G.; and Amira, M.; Gamal-Eldeen. *J. Chem. Soc*. **2010**, *122*, 587-595.
20. Mane, R.A.; Ingle, D.B. *Ind. J. Chem.* **1983**, *22*, 81-82.
21. Marchesini, G.; Gazz.; Chim. Ital, **1894**, *24*, 65.
22. Noller,C. R .; Balaiah,V.J. *J. Am.Chem. Soc.* **1948**, *70*, 3853.
23. Norbert de Kimpe.; Mark Boelens.; Jean-Paul Declercq. *Tetrahedron*. **1993,** *49*, 3411–3424.
24. Palaska, E.; Erol, D.; Demirdamar, R. *Eur. J. Med. Chem*. **1996**, *31*, 43 -47.
25. Panhekar, Y.D.; Ghiya, B.J. *Ind. J. Heterocycl.Chem.* **1995**, *5*, 159-60.
26. Parameshwar Makam.; Ramakrishna Kankanala.; Amresh Prakash. *Eur. J. Med. Chem.* **2013**, *69*, 564-576.
27. Rao, G.K.; Chakraborthy, S.; Pai, S.P.N.; and Murthy, S.M. *Asian. J. Chem*. **2005**, *17*, *3*, 2010-2012.
28. RatnadeepJoshi, S.; Priyanka, G.; Mandhane.; Santosh Diwakar, D.; Sanjay Dabhade, K.; Charansingh Gill, H. *Bioorg. Med. Chem. Lett*. **2010**, *20*, 3721-3725.
29. Ravizza, S.A.; Netherlands Appl. No. 6 508 138; *Chem. Abstr.* **1966**, *64*, 17611A.
30. RaziehFazaeli.; Hamid Aliyan.; Maryam Bordbar and Esmaeel Mohammadi.; Beilstein. *J. Org. Chem*. **2007**, *3*,1186/1860-5397-3-13.
31. Robert Roper.; Ma ,T.S. Netherlands Appl. No. 6 508 138; *Chem. Abstr.* **1966**, *64*,17611A.
32. Ryabinin, V.A.; Zakharova, O.D.; Yurchenko, E.Y.; Timofeeva, O.A,; Martyanov, I.V.; Tokarev, A.A. *Bioorg. Med. Chem*. **2000**, *8*, 985-93.
33. Salimon, J.; Salih, N.; Yousif, E. *E. J. King Saud University. (Science)* **2010**, *10*, doi: 10, 1016.